BLAST VIBRATION MODELING USING IMPROVED SIGNATURE HOLE TECHNIQUE FOR BENCH BLAST

DISSERTATION

A dissertation submitted in partial fulfillment of the
requirements for the degree of Doctor of Philosophy in the
College of Engineering at the
University of Kentucky

By

Jhon Jairo Silva-Castro

Lexington, Kentucky

Director: Dr. Braden T. Lusk, Associate Professor of Mining Engineering

Lexington, Kentucky

2012

Copyright © Jhon Jairo Silva-Castro 2012

ABSTRACT OF DISSERTATION

BLAST VIBRATION MODELING USING IMPROVED SIGNATURE HOLE TECHNIQUE FOR BENCH BLAST

Mining blast vibration prediction is a complex task due to the complexity of the variables involved in the problem. The lack of consistency in the blast parameters such as the geometry of the blastholes, the composition of the explosives, and the geology in mining operations make each blast a unique event. Despite the technological advances in the application of blasting, the design and the prediction of the results is based on empirical equations, or in best cases statistical information, with a limited or no theoretical support.

The objective of this research was to improve signature hole technique with a new methodology. The scatter in the initiation system, the geology, the consistency of the explosives, the changes in the vibration path between the source and the monitoring point and the geometry of blastholes are considered in the methodology. Parameters including the initiation timing, the traveling time of the vibration waves, and the vibration waveform generated by each hole are assigned a random behavior. To randomize the vibration waveform for each hole, one equation was developed base on Fourier series. An equation called the Silva-Lusk equation captures the main properties of the vibration waveform for the location where blast vibrations are under study. Every time a hole is blasted, the methodology generates a complete random vibration waveform for such hole using random normal distributions for the amplitude of the signal, the frequency content and the attenuation of the signal. In the proposed methodology, to superpose the random signals of each blasthole and assess the complete vibration waveform, a Monte Carlo scheme is used. Using this technique, a series of likely waveforms are generated. When all the likely outputs are plotted, an envelope waveform is generated containing the actual vibration for the blast. Along with the envelope, a peak particle velocity histogram is generated, providing an opportunity to assess the vibration levels measuring the percentage of confidence in the final result. The validation of the proposed methodology was achieved through several field blasting tests performed in a surface coal mine in West Virginia. Recommendations and future work are provided to improve the methodology.

KEYWORDS: Electronic detonators, Waveform, Signature hole, Fourier Series, Blast vibration.

_____
Student's Signature

_____
Date

BLAST VIBRATION MODELING USING IMPROVED SIGNATURE HOLE TECHNIQUE FOR BENCH BLAST

By

Jhon Jairo Silva-Castro

_____
Director of Dissertation

_____
Director of Graduate Studies

_____

.

"*Quasi nanos gigantum humeris insidentes" Bernard of Chartres*

This dissertation is dedicated to the people who were, are and always will be part of my life. Thanks to my parents, Trinidad and Pedro, for my being, for all your love, and all the life lessons that you are still giving me. To my brothers, Henry and Daniel, who always believed in my capabilities and for whom I have been trying to be a role model. To Trinidad Melo, thanks for all her support and encouragement. To Eduardo Torres, my mentor, who guided me into the mining industry, thanks for his advice and friendship. To Edmundo, who started the spark that made all this possible. Without his encouragement and the support of his lovely family I would be in another world, now…I am glad to be where I am. To Isabel, who I have the privilege to call my friend, thanks for her support, and the technical and philosophical discussions through all this time. To my friends and mentors Braden and Shannon for all their support and encouragement during my studies. I would like to thank my fellow graduate students: Kumar, Todor, Josh and Gosh.

Finally, thanks to Sandra my lovely wife who has always been there for me. Thanks for her support and encouragement, thanks for your patience and understanding along the way to achieve this goal; without her and the baby we are expecting, this accomplishment would not have any meaning. Sandra, you are giving a beautiful meaning to all this effort, I love you, a thousand thanks.

ACKNOWLEDGEMENTS

Thanks to the entire faculty and staff of the Mining Engineering Department here at The University of Kentucky. Special thanks to those who served on my committee; Dr. Bryson, Dr. Honaker, Dr. Wala, Dr. Perry and Dr. Kalinski. The comments you provided on my dissertation where very valuable and improved a lot this work, thank you.

Thank you to Rick Townsend of Nelson Brothers. You helped me setup many of the seismographs and collect the information. Another especial thanks goes to Ken Eltschlager of OSM you provide valuable comments during this research.

Finally thanks Dr. Lusk, you have been the perfect mentor for me, thanks for your support, encouragement and guidance.

TABLE OF CONTENTS

ACKNOWLEDGEMENTS iii

TABLE OF CONTENTS iv

LIST OF TABLES viii

LIST OF FIGURES ix

Chapter 1 1

INTRODUCTION 1

1.1 Background 1

1.2 Fundamentals of blast vibration 2

1.2.1 Characteristics of the explosive 4

1.2.2 Initiation system used 4

1.2.3 Shot Geometry and Timing 5

1.2.4 Distance source monitoring point 5

1.2.5 Geology 5

Chapter 2 7

BLAST VIBRATION 7

2.1 Blast vibration characteristics 7

2.2 Blast vibration measurement 9

2.3 Blast vibration prediction 11

2.3.1 Scaled distance estimation 11

2.3.2 Analytical and numerical approaches 14

2.3.3 Signature hole technique 18

Chapter 3 26

DETAILED DISCUSSION OF CURRENT SIGNATURE HOLE TECHNIQUE 26

3.1 Introduction 26

3.2 Blast vibration energy 26

3.3 Seed waveform 27

3.4 Explosion sequence 31

3.5 Linear superposition 34

Chapter 4 37

MODEL DEVELOPMENT 37
4.1 Introduction 37
4.2 Monte Carlo scheme 37
4.2.1 Discrete Random Variables 37
4.2.2 General Scheme of the Monte Carlo Method 41
4.2.3 Pseudorandom numbers generation 42
4.3 Seed waveform variability 42
4.3.1 Modeling of changes in signature waveform 45
4.3.1.1 Signature waveform comparison 48
4.3.1.2 Fourier series and Signature Waveform 51
4.3.1.3 Signature Waveform approach based on Fourier series 55
4.3.1.4 Numerical example random signature waveform generation 65
4.4 Wave arrival time distribution and time sequence 67
4.4.1 Wave arrival time 67
4.4.2 Blasting time sequence 70
4.4.2.1 Experimental setup 70
4.4.2.2 Non-electric detonators results 76
4.4.2.1 Electronic detonators results 80
4.5 Linear superposition and discrete convolution 84
4.5.1 Practical example 89
Chapter 5 95
IMPROVED SIGNATURE HOLE TECHNIQUE VALIDATION 95
5.1 Introduction 95
5.2 Field Experiments 95
5.2.1 Instrumentation and data collection 95
5.2.1.1 Site description 95
5.2.1.2 Instrumentation 96
5.3 Test's description 102
5.4 Analysis and results of the models using improved signature hole technique 107
5.4.1 Model 1. Airblast modeling (test No.5) 107

5.4.1.1 Signature test No.5 108
5.4.1.2 Synthetic signature signals 109
5.4.1.3 Timing sequence 110
5.4.1.4 Results Model 1 111
5.4.2 Model 2. Particle Velocity (test No.10) 116
5.4.2.1 Signature test No.10 117
5.4.2.2 Synthetic signature signals 118
5.4.2.3 Timing sequence 119
5.4.2.4 Results Model 2 120
5.4.3 Model 3. Particle Velocity (test No.12) 123
5.4.3.1 Signature test No.12 125
5.4.3.2 Synthetic signature signals 126
5.4.3.3 Timing sequence 127
5.4.3.4 Results Model 3 (test No.12) 128
5.4.4 Model 4 Pyrotechnic initiation (test No.14) 131
5.4.4.1 Signature test No.14 133
5.4.4.2 Synthetic signature signals 134
5.4.4.3 Timing sequence 135
5.4.4.4 Results Model 4 (test No.14) 136
5.4.5 Model 5 electronic initiation system (test No.15) 139
5.4.5.1 Signature test No.15 140
5.4.5.2 Synthetic signature signals 140
5.4.5.3 Timing sequence 140
5.4.5.4 Results Model 5 (test No.15) 141
Chapter 6 143
DISCUSSION OF RESULTS AND FUTURE WORK RECOMMENDATIONS143
6.1 Discussion about the improved methodology and the validation results 143
6.1.1 Number of frequencies to model the signature signal 143
6.1.2 Decay factor 151
6.1.3 Initiation system, timing and blast vibration 151

Chapter 7 159
CONCLUSIONS AND FUTURE WORK 159
7.1.1 Conclusions 159
7.1.2 Novel contributions 161
7.1.3 Recommendations for Future Work 161
REFERENCES 163
VITA 170
APPENDIX A 171
Blasting log reports from the mine 171
APPENDIX B 199
Plan Layout of tests performed in 2011 199
APPENDIX C 206
Vibration records for events recorded in 2011 206

LIST OF TABLES

Table 2-1 Range of typical blast parameters (after Dowding, 1985)..... 7
Table 4-1 Statistical parameters to modeling random signals 66
Table 4-2 Typical rock velocities (from Bourbié, Coussy, and Zinszner, Acoustics of Porous Media)..... 69
Table 4-3 Detonator Matrix 74
Table 4-4 Summary of Results for Non-Electric Validation Example 76
Table 4-5 Summary non-electric detonator results..... 78
Table 4-6 Summary of Results for Electronic Validation Example 80
Table 4-7 Summary statistics electronic system..... 81
Table 4-8 Blast test parameters..... 89
Table 5-1 Seismograph location and their characteristics 98
Table 5-2 Seismograph's triggering parameters..... 100
Table 5-3 Triggering levels used in the second round of test..... 102
Table 5-4 Tests including signature hole..... 103
Table 5-5 Blast test parameters test No.5 107
Table 5-6 Blast test parameters test No.10 116
Table 5-7 Blast test parameters test No.12 123
Table 5-8 Blast test parameters test No.14 131
Table 5-9 Blast test parameters test No.15 139
Table 6-1 Comparison results according to the number of frequencies used..... 145
Table 6-2 Decay factor signature waveforms at 3599 seismograph location..... 151
Table 6-3 Results test 14 and 15 particle velocity peak values (actual readings)153
Table 6-4 Delay timing and initiation system simulation far seismographs (beyond 1440ft)..... 155
Table 6-5 Modeling results for seismograph 4906 (Pyrotechnic vs electronic) Radial component 156

LIST OF FIGURES

Figure 1.1 Waveform idealization in a blast event (Adapted from Dowding, 1985). 3
Figure 1.2 Types of Detonators (After Miller, D., Drew, M. 2007) 4
Figure 1.3 Factors affecting ground vibration (after Khandelwal, M and Singh, T. 2006) 6
Figure 2.1 Typical earthquake and blast waveforms 8
Figure 2.2 Blast vibration recommended regulation Z curve. Safe level blasting criteria from USBM RI 8507 (After Siskind, 2000) 9
Figure 2.3 Scaled distance law, analysis for different components (Lusk, Silva, Eltschlager, Hoffman, 2010) 14
Figure 2.4 Main components of rock fracturing modeling process (Adapted from Saharan, Mitri and Jethwa, 2006) 15
Figure 2.5 pressure pulse shape A. Ideal detonation. B. Non-ideal detonation (Aimone, 1992., Olsson et al., 2001) 16
Figure 2.6 Sketch of a system with continuous and discrete signals. 18
Figure 2.7 Time Invariant systems single input - single output (Adapted from "Signal and Systems" 3th edition) 19
Figure 2.8 **SI-SO, C, L, TI** systems (Adapted from "Signal and Systems" 3th edition) 20
Figure 2.9 Systems Theory and Signature Hole Technique similarity. 21
Figure 2.10 Finite impulse response from one hole blasted 22
Figure 2.11 Summary of the most common signature hole techniques currently available (After Spathis, 2010) 25
Figure 3.1 Particle velocity spectra for single charge shots of short column weight (After Crenwelge 1988) 28
Figure 3.2 Particle velocity spectra for single charge shots of tall column weight (After Crenwelge 1988) 29
Figure 3.3 Particle velocity spectra for single charge shots (a) short column weight (b) tall column weight (Crenwelge 1988) 29
Figure 3.4 Seismograms recorded for three different charge weights and two locations (After M. Sakamoto, et al., 1989) 30
Figure 3.5 Seismograms recorded for three different charge weights (After Bonner, et al., 2008) 30
Figure 3.6 Spectral analysis for three different charge weights (After Bonner, et al., 2008) 31
Figure 3.7 Explosion sequence function 32
Figure 3.8 Graphical representation of Equation 3.7 32
Figure 3.9 System's homogeneity property 34
Figure 3.10 Numerical homogeneity concept between the quantity of explosive and the particle velocity. 35
Figure 3.11 Additivity concept for signature hole technique 36
Figure 4.1 Histogram for the $randn$ function in Matlab®. 42
Figure 4.2 Signature hole reproducibility (adapted from Blair 1999) 43
Figure 4.3 General view of the tested area 45
Figure 4.4 Test plan layout 46

Figure 4.5 Seismograph network at Guyan mine..... 47
Figure 4.6 Complete signature waveform three components 47
Figure 4.7 Complete waveform, Radial component Seismograph 01 48
Figure 4.8 Signature waveform comparison..... 49
Figure 4.9 Frequency content of the signals and four frequency zones..... 50
Figure 4.10 Signature 1 Isolated from complete record (Radial component)..... 52
Figure 4.11 Magnitude coefficients from Fourier series 53
Figure 4.12 FFT and magnitude coefficients from Fourier series 54
Figure 4.13 Fourier series and signature 1 54
Figure 4.14 Measured signal Vs base equation 58
Figure 4.15 Exponential decay calculation..... 59
Figure 4.16 Measured signal Vs base equation including exponential decay factor 60
Figure 4.17 Measured signal Vs final approach 61
Figure 4.18 Frequency domain comparison..... 62
Figure 4.19 Frequency parameter for Equation 4.48 64
Figure 4.20 Numerical example frequencies signature 1 test 01 65
Figure 4.21 Random generated signatures using Silva-Lusk equation..... 66
Figure 4.22 Signature signals measured vs Generated using one and three signals 67
Figure 4.23 Delay times involved in the signature analysis 68
Figure 4.24 Illustration of Interaction between Break Wire and Counter 71
Figure 4.25: Blasting Machine Counter Interaction 71
Figure 4.26: Bunch Block Configuration..... 72
Figure 4.27: Graphical User Interface test setup 73
Figure 4.28 Test Cells..... 74
Figure 4.29 Break Wire Placement..... 75
Figure 4.30 Detonators Awaiting Test..... 75
Figure 4.31: Electronics Break Out Box..... 76
Figure 4.32 Frame grabs from non-electric sample showing detonation sequence 77
Figure 4.33 Normal distribution, density function, non-electric detonators tested. 78
Figure 4.34 Normal distribution, density function, non-electric detonators at 9, 25 and 100 ms nominal delays..... 79
Figure 4.35 Normal distribution, density function for nominal delays, non-electric detonators at 700, 1000 and 1400 ms..... 79
Figure 4.36: Frame grabs from electronic sample showing detonation sequence 80
Figure 4.37 Normal distribution, density function, electronic detonators tested.. 81
Figure 4.38 Normal distribution, density function, electronic detonators at 10ms nominal delays. 82
Figure 4.39 Normal distribution, density function, electronic detonators at 1000ms nominal delays. 82
Figure 4.40 Normal distribution, density function, electronic detonators at 8000ms nominal delays. 83

Figure 4.41 comparison 9ms and 10ms nominal delay (non-electric Vs electronic) 83
Figure 4.42 Pair impulse – signature waveform 85
Figure 4.43 Three holes numerical example 85
Figure 4.44 Result of three holes detonation mathematical convolution..... 86
Figure 4.45 Implementation of convolution in VB®..... 87
Figure 4.46 Convolution in Matlab®..... 87
Figure 4.47 Convolution using Matlab 87
Figure 4.48 Convolution results using matlab and a more discretized signal. 88
Figure 4.49 Shifted signals to perform the sum. 88
Figure 4.50 Vibration record for test blast 4 holes detonated at the same time... 90
Figure 4.51 Plan view from the blast report for the test 90
Figure 4.52. Radial signature (seed) waveform 91
Figure 4.53 Matlab command to load signature and timing vectors..... 91
Figure 4.54 Convolution for radial component..... 92
Figure 4.55 Graphical procedure to calculate vibration waveform in test..... 92
Figure 4.56 Final waveform after sum 17 signals using graphical procedure 93
Figure 4.57 Final waveform simulation using commercial software Apha-Blast® 93
Figure 4.58 Complete waveform comparison using different methodologies..... 94
Figure 5.1 Location of the mine where the field experiments were conducted.... 95
Figure 5.2 Drill Hole GY 9411, stratigraphic column 96
Figure 5.3 Case for the seismograph setup 97
Figure 5.4 Seismographs location 99
Figure 5.5 Seismographs location for second round of test. (Summer 2011)..... 101
Figure 5.6 NOMIS® 5400 System used to collect blast vibrations and airblast 102
Figure 5.7 Plan layout test 06/24/2011 104
Figure 5.8 Vibration record for test No.12, seismograph 4906 (approx. 767ft from source)..... 104
Figure 5.9 Radial vibration component for test No.12 and all the seismographs in summer 2011..... 105
Figure 5.10 Airblast records for test No.12 and all the seismographs in summer 2011..... 106
Figure 5.11 Airblast record for Test No.5 (Four holes signature) 107
Figure 5.12 Plan view from the blast report for the test No.5 108
Figure 5.13. Airblast signature waveform test No.5 108
Figure 5.14 Airblast signature waveform and synthetic waveform (approach).. 109
Figure 5.15 Frequency interval and scale factor for test No.5 110
Figure 5.16 Random airblast signature waveform signals test No.5 110
Figure 5.17 Delay time series for test No.5 111
Figure 5.18 Time function for test No.5. Zero and 1ms standard deviation in detonator 111
Figure 5.19 Results using one iteration and zero delay standard deviation..... 112
Figure 5.20 Variables involved in the prediction test No.5 using improved signature technique. 112
Figure 5.21 Monte Carlo result using initial parameters for test No.5 113

Figure 5.22 Monte Carlo results using 3Hz frequency as main frequency in test No.5 114
Figure 5.23 Histogram absolute maximum calculated values 115
Figure 5.24 Convergence plot for test No.5 115
Figure 5.25 Test No.10, plan view from survey 116
Figure 5.26 Vibration record seismograph 3599 test No.10 116
Figure 5.27. Ground vibration signature waveform test No.10 117
Figure 5.28 Signature waveform and synthetic waveform (approach) test No.10. 118
Figure 5.29 Frequency interval and scale factor for test No.10 118
Figure 5.30 Random ground vibration signature waveform signals test No.10 119
Figure 5.31 Time series for test No.10 119
Figure 5.32 Time function for test No.10. Including both timing parameters... 120
Figure 5.33 Results using one iteration for test No.10 120
Figure 5.34 Variables involved in the prediction test No.10 using improved signature technique. 121
Figure 5.35 Monte Carlo result using fixed parameters for test No.10 122
Figure 5.36 Histogram absolute maximum calculated values test No.10..... 122
Figure 5.37 Convergence plot for test No.10..... 123
Figure 5.38 Test No.12, plan view from survey 124
Figure 5.39 Vibration record seismograph 3599 test No.12 124
Figure 5.40. Ground vibration signature waveform test No.12 125
Figure 5.41 Signature waveform and synthetic waveform (approach) test No.12. 126
Figure 5.42 Frequency interval and scale factor for test No.12 126
Figure 5.43 Random ground vibration signature waveform signals test No.12 127
Figure 5.44 Time series for test No.12 127
Figure 5.45 Time function for test No.12. Including both timing parameters... 128
Figure 5.46 Results using one iteration for test No.12 128
Figure 5.47 Variables involved in the prediction test No.12 using improved signature technique. 129
Figure 5.48 Monte Carlo result using fixed parameters for test No.12 130
Figure 5.49 Histogram absolute maximum calculated values test No.12..... 130
Figure 5.50 Convergence plot for test No.10..... 131
Figure 5.51 Test No.14, plan view from survey 132
Figure 5.52 Vibration record seismograph 3599 test No.14 132
Figure 5.53 Signature waveform for test No.14 133
Figure 5.54. Ground vibration signature waveform test No.14 133
Figure 5.55 Signature waveform and synthetic waveform (approach) test No.14. 134
Figure 5.56 Frequency interval and scale factor for test No.14 135
Figure 5.57 Random ground vibration signature waveform signals test No.14 135
Figure 5.58 Time series for test No.14 136
Figure 5.59 Time function for test No.14. Including both timing parameters... 136
Figure 5.60 Results using one iteration for test No.14 137

Figure 5.61 Variables involved in the prediction test No.14 using improved signature technique. 137
Figure 5.62 Monte Carlo result using fixed parameters for test No.14 138
Figure 5.63 Histogram and convergence plot of the prediction for test No.14 .. 138
Figure 5.64 Test No.15, plan view from survey 139
Figure 5.65 Vibration record seismograph 3599 test No.15 140
Figure 5.66 Results using one iteration for test No.15 141
Figure 5.67 Monte Carlo result using fixed parameters for test No.15 141
Figure 5.68 Histogram and convergence plot of the prediction for test No.14 .. 142
Figure 6.1 Signature signal test No.5 using five frequencies 143
Figure 6.2 Random airblast signature waveform signals test No.5 using 25 frequencies. 144
Figure 6.3 Final prediction for airblast using 25 frequencies and amplification factor of 2.2 for main frequency (3Hz). 145
Figure 6.4 Results comparison using four and twenty five frequencies for model 02, test No.10. 146
Figure 6.5 Results comparison using four and twenty five frequencies for model 03, test No.12. 147
Figure 6.6 Results comparison using four and twenty five frequencies for model 04, test No.14. 148
Figure 6.7 Results comparison using four and twenty five frequencies for model 05, test No.15. 149
Figure 6.8 Synthetic signal for test No.14 before apply decay factor..... 150
Figure 6.9 Accuracy and precision electronic vs non-electric system..... 151
Figure 6.10 Waveform comparison test No.14 vs test No.15 transversal component (seismograph 3599)..... 152
Figure 6.11 Frequency domain comparison test No14 vs test No.15 (seismograph 3599) 153
Figure 6.12 Test No.15 simulating both initiation systems and including only time delay due to initiation sequence. 154
Figure 6.13 Signature used to model Tests No.14 and 15 (average) in seismograph 4906 location..... 156
Figure 6.14 Modeling results test No.14 seismograph 4906 (Pyrotechnic)..... 158
Figure 6.15 Modeling results test No.15 seismograph 4906 (Electronic) 158

Chapter 1

INTRODUCTION

1.1 Background

Vibrations as a result of blasting practices in mining engineering are complex phenomena controlled by many variables. Mining blast vibration modeling and prediction are becoming more important as a consequence of the general negative perception of the public to mining activity. Many communities (all over the world) that are close to mines complain about airblast and vibrations as a consequence of mine blasting activity. It is important for the mining industry to have tools and understandable methodologies to model and predict blast vibration.

There are several approaches to model and assess blasting vibration levels. They range from the scaled distance methodologies to very complex and elaborate numerical models. The scaled distance methodologies used a power law relationship between the peak particle velocity (*PPV*) and the scaled distance to the specific point under study. These methodologies demand statistical estimations of the main parameters involved in the problem, so they are reliable after a good database of events is available.

Numerical models range from models that use the physical properties of the rock and elastic solutions to simulate the propagation waves in a continuous medium to more elaborate proposals. According to the computational developments, numerical models for continuous medium are capable of including a large number of variables in the simulation, but are not able to reproduce exactly the geology where the blasting takes place and how the vibration propagates. As a consequence, the results of numerical simulations of blasting vibrations are just models of the real phenomena. More advanced numerical approaches are related to the analysis of block systems (Mortazavi A., Katsabanis P.D., 2001). In such models, systems of simultaneous equations are formulated and solved minimizing the energy of the system to bring the system into equilibrium.

Usually, the blast phenomenon that occurs in the hole (the explosion) is simulated using cavity expansion and propagation crack theories around the blast hole. The numerical techniques used to solve the wave propagation depend on the assumptions regarding the medium. If the medium is considered as a continuum where the influence of the rock mass joint system is neglected or simulated as interfaces, the most common methods to use are finite element models (FEM), and boundary element methods (BEM). On the other hand, if the presence of the discontinuities is taken into account and large displacements and rotating blocks are allowed in the discontinuities, methods as distinct element method (DEM), discontinuous deformation analysis (DDA) or bounded particle method (BPM) are used (A. Bobet et al., 2009).

DEM is one of the most successful techniques used to simulate the media subjected to vibrations (rock mass) as a discontinuous medium composed by an assemblage of discrete blocks. The internal discontinuities are treated as boundary

conditions between blocks; large displacements along such discontinuities and rotations are allowed, the individual blocks are modeled as rigid or deformable solids in accordance with the properties of the rock and rock mass to be modeled (Wang et al., 2009). These methodologies require significant computational time, parameters or physical properties for the media to simulate that, in some cases, are difficult to evaluate by field or laboratory testing, and highly-trained personnel capable of modeling and interpreting the results. Due to this, modeling processes using these types of techniques sometimes are not practical or become very expensive.

A technique based on the use of seismic analysis, waveform interpretations and signal and systems theories has become used more often in mining applications. Using this methodology, it is possible to model the complete waveform of a mining production blast for a critical site where vibration monitoring or control is needed. In this approach, one seismic signal from one blasthole is recorded in the site under study and using signal and systems procedures that involve mathematical convolution of signals, the waveforms from each blasthole can be superposed to model the complete vibration waveform for the production blast. One of the outputs of this technique is the initiation timing between charges to reach given vibrations levels (usually the minimum vibration level for a production blast). Due to that reason, waveform superposition technique is becoming increasingly popular with the use of electronic detonators since their use provides better control over the initiation timing pattern (in other words less scatter initiation timing). Improvements in fragmentation, vibration levels and air blast have been reported in the literature through the use of both electronic detonators and waveform superposition (Chistopherson, and Papillon, 2008).

The areas of study of this research were:

- Background behind the vibration modeling using waveform superposition;
- Waveform superposition methodologies;
- Analysis of the major assumptions in the waveform superposition methodologies;
- New approach to improve these methodologies in order to obtain more reliable and accurate results when vibration levels are assessed.

1.2 Fundamentals of blast vibration

In the literature, there are different approaches to explain and model the physical process when a buried charge of explosives is detonated. In general, if a classification according to the strain-stress behavior of the blasted material is made, it is possible to distinguish two different zones, i.e., the inelastic and elastic zones. In the inelastic zone, the energy contained in the explosive is released through a chemical reaction. In the inelastic zone, tremendous pressure and high temperatures are developed due to the chemical reaction. As result, the solid medium is subject to inelastic phenomena such as breaking, shearing and crushing of the rock mass. Also, large strains are developed within this zone (Enescu et al., 1973; Bollinger, 1980; Saharan et al., 2006). A fundamental discussion of the inelastic process within the inelastic zone in an explosion can be found in Cook (1958) or in Langefors and Kihlstrom (1963). At some distance

from the explosive reaction, the behavior is more elastic. In this zone, the disturbance due to the energy released during the explosion propagates as seismic waves. The behavior in this zone is considered as elastic because it is commonly assumed that the solid medium returns to its initial state after passage of the seismic disturbance.

The seismic waves propagating through the earth media can be divided in two major categories: body waves and surface waves. Body waves propagate through the solid medium (soil or rock) and surface waves travel along the surface. The main surface wave is the Rayleigh wave denoted by R-wave. Body waves can be subdivided into compressive waves (P-waves) and shear waves (S-waves).

Explosions produce mainly body waves (P and S) at small distances while R-waves become important at larger transmission distances (Dowding, 1985). The waveforms can be idealized for far and close distances according to the location of the recording site. The two idealized waveforms are explained using Figure 1.1

If the strain, pressure, or particle velocity (PV) is measured at Point A (close-in explosion), the shape of the idealized wave will be a single-spiked pulse. This is because at Point A, only direct-transmission of the waves generated by the explosion is measured. On the other hand, if the recording site is located at Point B (far explosion), the idealized waveform of the strain, pressure or particle velocity will be more like a sinusoidal shape. At Point B the sinusoidal waveform will be a combination of direct-transmission, reflection and refraction waves (Silva et al., 2011).

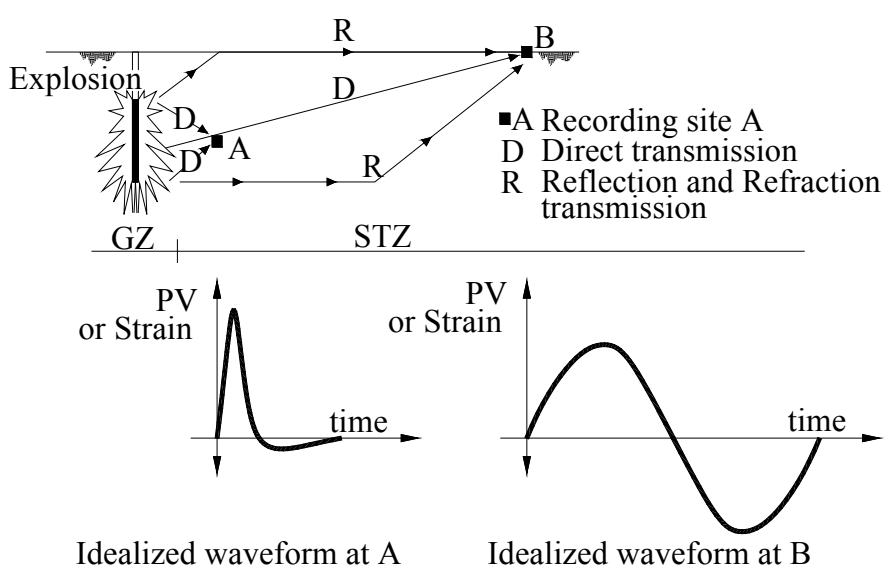

Figure 1.1 Waveform idealization in a blast event (Adapted from Dowding, 1985).

In the blast vibration phenomena, there are several factors involved in the process. These factors are explained briefly in the following sections.

1.2.1 *Characteristics of the explosive*

It has been documented that the type of explosive used in mine blasting influences the blast vibration (Hossain and Sen, 2004; Hunter et al., 1993; Harries and Gribble, 1993). There are two broad categories of explosives according to the type of detonation generated, non-ideal and ideal detonations. Non-ideal detonation occurs when the rise time for the peak blast hole is longer and the post peak pressure drop is much slower when compared to ideal detonation. On the other hand, in the ideal detonations, the peak pressure rise time is very short and the post peak pressure drop is steep (Saharan, M.R., Mitri, H.S. 2008). In their research, Hunter et al., (1993) reported that explosives with lower density and lower detonation velocity (non-ideal detonation) produced lower ground vibration levels when compared to ideal detonation.

1.2.2 *Initiation system used*

Safety fuses were developed to improve the safety in the blasting operations. These devices introduced a delay before the detonations occurred, which gave the blaster enough time to move away from the blast site. After the introduction of the safety fuse, the electric detonator was introduced at the beginning of the 20th century to increase performance in blasting. Electric means that there is a bridge wire in the detonator that matches with the initiation system (electricity). In the 1960s and 1970s, Dyno Nobel introduced the non-electric (nonel) detonator. In the nonel detonator, as well in the electric detonator, the time delay is given by the length of the pyrotechnic element; therefore, varying the length of this element varies the time delays. Due to the chemical nature of the delay element (pyrotechnic), the accuracy is relatively low when compared to electronic and high compared to safety fuse. Through the 21st century, scatter in the detonation time has decreased. Since 1950 to '80s, improvements in the pyrotechnic elements have increased the accuracy to levels of 1.5% to 2.5 % of the total time delay (Larsson et al., 1988). Despite this effort to reduce the scattering of time delays, the pyrotechnic delay still gives low accuracy in some situations. With longer delays, the delay inaccuracy can potentially cause overlap and holes firing out of sequence affecting the vibrations and performance of the blast (Lusk, et al., 2012).

Shock tube or non-electric detonators (nonel), electric and electronic detonators are the major delay systems currently used. The basic differences between the three types of detonators are the type of delay element used to produce the time delay and the igniter. Figure 1.2 adapted from Miller and Drew (2007) shows the major differences between the three systems.

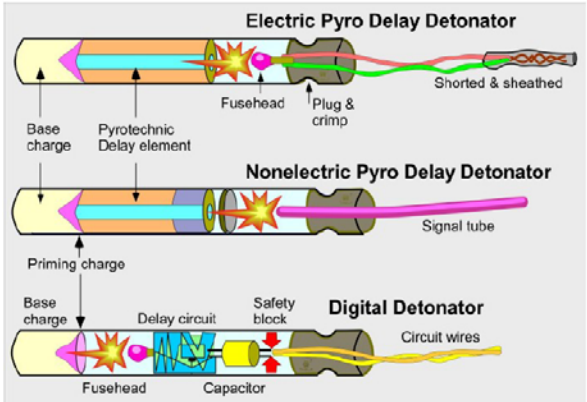

Figure 1.2 Types of Detonators (After Miller, D., Drew, M. 2007)

In a traditional pyrotechnic detonator (nonel or electric), the delay element is composed of a pyrotechnic device (chemical delay) while, in electronic, the time delay is controlled by an electronic circuit and a bridge wire.

1.2.3 *Shot Geometry and Timing*

The shot geometry take into account six variables involved in the problem: diameter of the hole, burden, spacing, length, stemming and sub-drilling (Ash, 1973). The relationship between these variables determines the performance of the explosive forces and whether or not the mining blast behaves as expected. From the blast vibration point of view, the shot geometry affects the degree of confinement of the charges which affects the level of the seismic waves generated in the mine blasting process. It is commonly assumed that high degree of confinement will generate higher vibration levels than with a one less confined blast pattern. Regarding timing the use of electronic initiation systems, the 8 ms rule to control blast vibration levels is under analysis (Reiz, et al., 2006). Current researchers are trying to explore the advantages of short timing delay (under 8ms) to diminish the total time of exposure under blast vibration that a structure under control is subject when a long timing delay is used in a mining blast.

1.2.4 *Distance source monitoring point*

The distance from the blast pattern to the monitoring point is one of the most important parameters in blast vibration. As vibration waves travel away from the source, they spread out meaning longer duration and lower frequency. Additionally, some of the energy is absorbed by the materials they travel through. As consequences of the spreading out of the waves with the distance, the waves change their characteristics, including their amplitude and frequency. The spreading of energy with distance is related to the type of waves. In the case of body waves (p and s waves), the amplitude decreases according to the relation ($\mathbf{1/R}$) where $\boldsymbol{R}$ is the distance source-measurement point. For surface waves (Rayleigh waves) the decrement relation is ($\mathbf{1/R^{0.5}}$). Additionally as consequence of the energy absorption of the materials, the ground motion amplitude decrease exponentially with $\boldsymbol{R}$ (Kramer, S.L., 1996).

1.2.5 *Geology*

The geologic discontinuities and joints act as boundaries in the medium. The waves are reflected and or refracted every time they hit a boundary. Also, the lithology introduces changes (amplitude and frequency changes) in the waves because the different dynamic properties of the materials the waves travel through. Geology creates new type of waves when original P and S waves hit an inclined boundary producing, for example, reflected and refracted P-and SV –waves. The path to reach one specific monitoring point that the vibration energy follows coming from each hole in a blasting pattern change according to the geological features the waves hit while they are traveling towards the monitoring point. Figure 1.3 shows the main factors affecting ground vibrations due to mining blasting for a single shot.

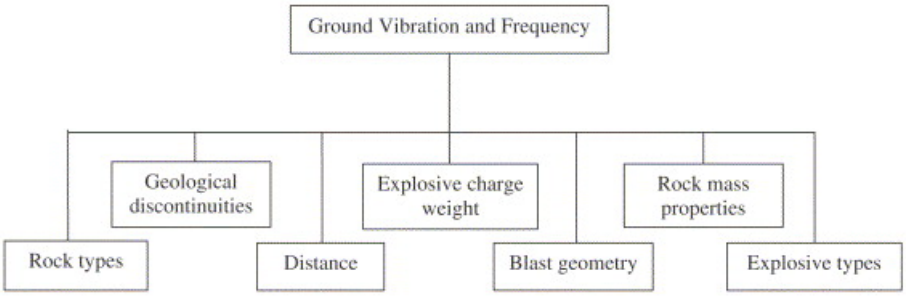

Figure 1.3 Factors affecting ground vibration (after Khandelwal and Singh,. 2006)

BLAST VIBRATION

2.1 Blast vibration characteristics

Ground vibrations from blasting are the result of energy release from chemical explosives during an explosion in a blast hole. In the detonation process, the solid mass of explosive is converted nearly instantaneously into gaseous products. The change in the pressure of the gas occurring during the explosion generates a rapid change in the initial stress state of the medium (rock) which crushes the rock near the hole and displaces the rock in to a muck of pile (Saharan et al., 2006). Beyond the hole at some distance related to the initial hole diameter, the stress deforms the rocks elastically and part of the energy released during detonation travels as a stress wave or a seismic wave through the medium generating vibrations (Sally and Daemen, 1983).

Seismic waves can travel considerable distances (Frantti. G.E., 1963). In a production blast, several holes are detonated at varying times generating different pulses and seismic waves. The interaction of the seismic waves in a constructive or destructive manner produces a complex vibration pattern which is recorded at a specific site. The vibration waveform recorded in a blast event usually consists of three orthogonal components: radial, longitudinal and vertical. Generally, the radial and longitudinal components are in a horizontal plane while vertical component is perpendicular to the other two. This arrangement is due to the construction of the geophone.

Most vibrations from surface mine blasting have a frequency content less than 200 Hz while underground mining blasts tend to produce much higher frequencies (Spathis, 2010). Particle velocity is commonly used to measure or establish the permitted levels of ground vibrations. This parameter was chosen over displacement or acceleration from the research of Langefors, et al., (1958), Edwards and Northwood (1960) and Duvall and Fogelson (1961) among others. In these studies, the particle velocity was established as the best criterion to assess the structural damage due to blast vibrations. Most current regulations stipulate particle velocity to establish maximum vibration levels from a mining blast; however, to choose which vibration parameter to measure (displacement, velocity or acceleration) it is necessary to assess the frequency content of the vibration (Dowding, 1985). Table 2-1 contains the range of the main parameters of blast vibration.

Table 2-1 Range of typical blast parameters (after Dowding, 1985)

Parameter	Typical range
Particle displacement	10^{-4} to 10 mm
Particle velocity	10^{-4} to 10^{3} mm/s
Particle acceleration	10 to 10^{5} mm/s/s
Pulse duration	0.5 to 2 s
Wavelength	30 to 1500 m
Frequency	0.5 to 200 Hz
Strain	3 to 5000 microstrain

In general, the waveform of ground vibrations from blasting has a lower particle velocity and higher dominant frequencies comparatively to the waveform of ground vibrations from earthquakes (Siskind 1993). The total duration of both types of events (earthquake and blast) in a typical production blast differ considerably. Figure 2.1 shows a typical earthquake wave form recorded by the Kentucky Seismic Network and a blast vibration signal from a production blast. Figure 2.1a shows the comparison in time domain between a signal recorded form an earthquake versus a mining blast. Earthquake record is bigger and longer than blasting record. Figure 2.1b shows how the main frequency is higher when compared to blast vibration signal.

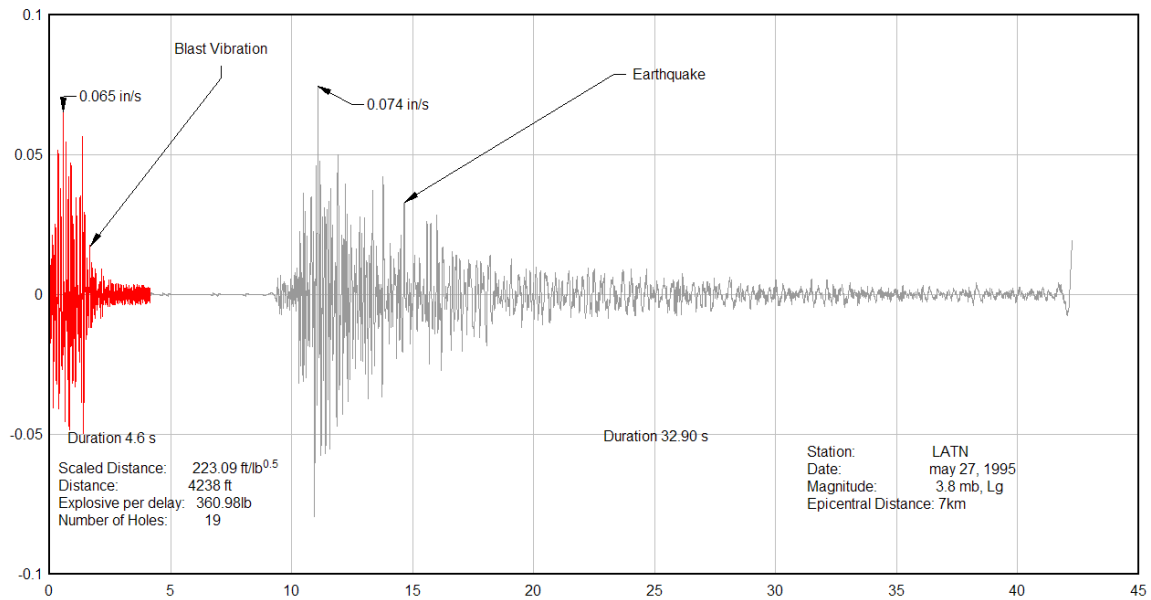

a) Time series comparison (Blast Event – Earthquake)

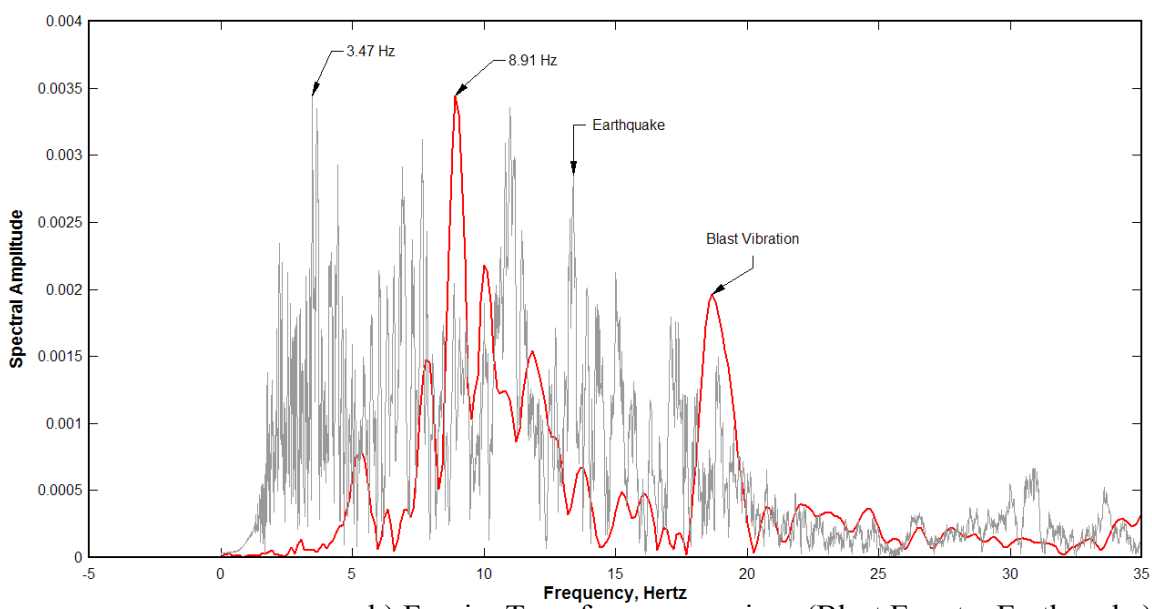

b) Fourier Transform comparison (Blast Event – Earthquake)

Figure 2.1 Typical earthquake and blast waveforms

After the vibration guidelines published by the United States Department of Interior's Bureau of Mines (USBM), (Siskind et al., 1980), most of the blast vibration regulations are based on particle velocity and frequency content. The USBM study was based on damage due to blast vibrations of houses ranging from modern houses with drywall interiors to older houses with plaster or wood lath interiors. The damage was categorized as threshold, minor and major damage. In this study, around 200 blast where included.

Graphically, USBM blast vibration recommended regulation is expressed using the so-called Z curve presented in Figure 2.2.

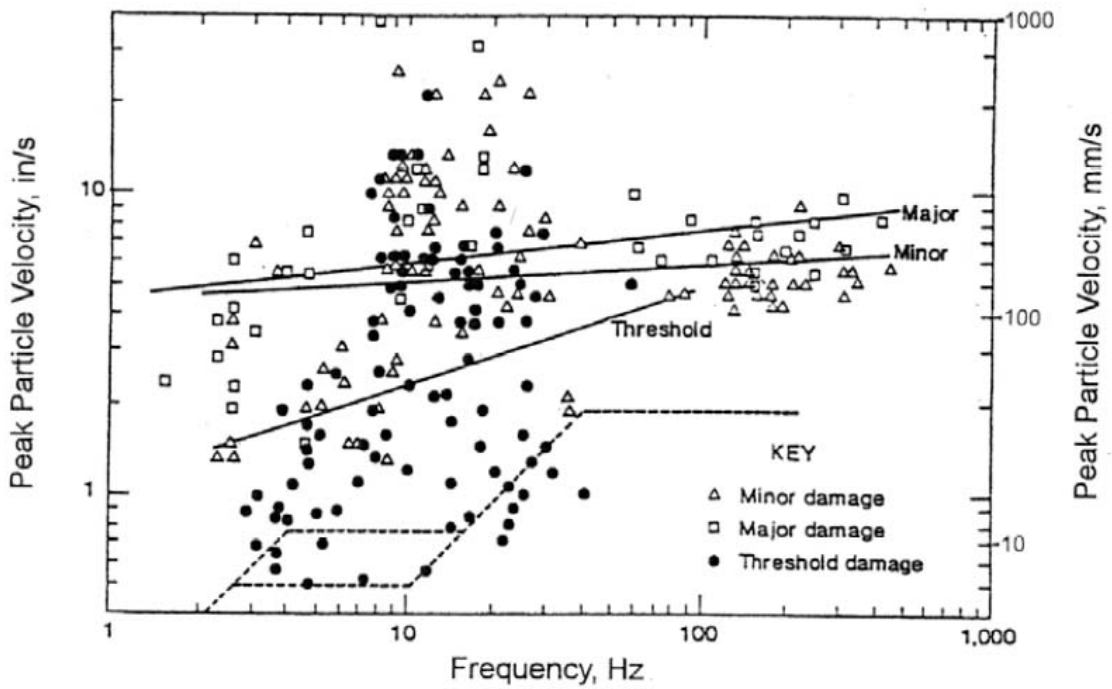

Figure 2.2 Blast vibration recommended regulation Z curve. Safe level blasting criteria from USBM RI 8507 (After Siskind, 2000)

In Figure 2.2, dashed lines define USBM recommended safe limits (Z curve). Symbols shown are positive damage observations in the houses under study.

2.2 Blast vibration measurement

The objective of the measurement of blast vibration is to describe the behavior at a point in the ground due to the vibratory motion produced by a mining blast. From the physics point of view, it is possible to measure displacement, velocity or acceleration. However, as explained previously, the research of Duvall and Fogelson (1961) found that particle velocity is better to use to describe and control vibrations levels.

To describe completely the dynamic behavior of a point in the ground due to the mining blast, it is necessary to measure three orthogonal components of any of the physical quantities given by the displacement, velocity or acceleration as a function of time (t). The relationships of these three physical quantities are given by:

$$a = \frac{dv}{dt} = \frac{d^2x}{dt^2}$$

[2.1]

Where:
a: acceleration
v: velocity
x: displacement
t: time

In principle, the measurement of one of the physical quantities allows the determination of the other two through integration or derivation.

The devices to measure blast vibrations are mainly composed of four components; a transducer, a recorder, a timing system, and a storage system. There are many types of transducers. One of the most basic transducers is composed by a magnet suspended inside a coil. When the magnet experiences a movement, the relative movement between the magnet and the coil generates a current. The output current is proportional to the movement of the magnet and in turn the movement of the magnet is proportional to the displacement, particle velocity or acceleration in the ground. Most of the devices currently in operation use electronic transducers composed by piezoelectric materials. Those materials when subject to transient forces generate electrical currents proportional to accelerations, velocity or displacements. This current is calibrated to a specific range of motion. Regardless of the type of transducer, the controlling factor in the blast vibration measurement is the natural frequency of the instrument and the ground vibration frequency to measure. (Bollinger, 1980).

Initial ground motion instruments record the motion in an analog form on paper or photographic film (Kramer 1996). Due to the computational development in technology, analog signals are transformed into digital signals. Analog signals are also called continuous-time signals (CT). By definition, a CT signal is defined at every time instant in a time interval of interest and its amplitude can assume any value in a continuous range. On the other hand, a digital signal or discrete-time signal (DT) is defined only at discrete time instants, and its amplitude can assume any value in a continuous range (Cheng, C.T., 2004).

Many devices commonly used in mining to measure blast vibrations use a sample rate of 1024 samples per second (although many are capable of 2048 samples per second), for a total recording time of 12 seconds. That means that the sampling period (T) is given by:

$$T = \frac{sampling\ time * 1\ sample}{number\ of\ samples\ in\ sampling\ time} = \frac{1\ s * 1 samples}{1024\ samples} = 0.0009765s$$

[2.2]

Many of the records used to analyze and predict blast vibrations using waveform superposition have a precision close to one millisecond (0.97 ms). In other words, the

time step between two consecutive values in the signal is one millisecond. If the time step of one millisecond in the signal is compared against the fact that when electronic initiation systems are used, the standard deviation in the timing of the initiation system for short periods is sometimes below one millisecond (Lusk, B., et.al 2012), a disadvantage arises when waveform superposition is performed using the conventional time sampling given by the devices used commonly to monitoring mine blast vibrations.

2.3 Blast vibration prediction

There are, in the literature, many approaches to assess the vibration levels from a mining blast. Those methods can be categorized into five approaches (Spathis, 2010)

- historical data review;
- charge weight scaling laws;
- waveform superposition;
- scaled charge weight superposition;
- analytical and/or numerical methods.

In this document, only the most common methodologies are included giving a brief discussion about each approach.

2.3.1 *Scaled distance estimation*

Scaled distance approaches have been used in connection to small-scale modeling of nuclear explosions (Dowding, 1985). In this research, commonly the empirical expressions for particle velocity due to blast deducted from ground shock data have the general form given by (Drake and Little, 1983):

$$V_o = f * A * B^{-n} \left(\frac{R}{W^{1/3}} \right)^{-n}$$

[2.3]

where:

V_o:	peak particle velocity
f:	coupling factor for near surface detonations
R:	distance to the explosion
A, B:	constants
n:	attenuation coefficient
W:	explosive charge mass. It is proportional to the energy release during detonation

Those equations are derived from the Buckingham Pi theory of dimensionless analysis (Buckingham, 1915). The Pi theorem states that any of the parameters may be considered to be a function of another, and that the parameters may be raised to any power. In the case of the particle velocity, the dimensionless group is given by (Ambraseys and Hendron, 1968):

$$\frac{V}{c} = g_2 \left[\frac{tc}{R}, \frac{W}{\rho c^2 R^3} \right]$$

[2.4]

Where:

V:	particle velocity	$[LT^{-1}]$
c:	seismic velocity of rock mass	$[LT^{-1}]$
t:	time	$[T]$
R:	distance from explosion (range)	$[L]$
W:	energy released by explosion	$[FL]$
ρ:	density of the rock mass	$[FT^2L^{-4}]$
g_2:	unknown function of the dimensionless group	

Assuming that the density ρ and the seismic velocity of the media c are relatively constants when compared to the distance to the explosion R and the energy released by the explosion W, they are sometimes dropped from the dimensionless terms. Since the parameters may also be raised to any power, V can be plotted against $(W)^{1/3}/R$ or $R/(W)^{1/3}$, those parameters produce consistent relationships according to Ambraseys and Hendron (1968) and Dowding (1985) and others (Villano, Charlie, 1993).

It was in Bulletin 656 of the Bureau of Mines (Nicholls, et al., 1971) data analysis from 171 blasts at 26 quarries where the form of the equation given by Equation 2.5 was proposed:

$$V_i = H_i \left(\frac{D}{W^{\alpha}}\right)^{\beta_i} \qquad [2.5]$$

where:

V_i:	particle velocity in i direction
H_i:	particle velocity in i direction intercept
D:	shot to gage distance
W:	charge weight
α:	exponent
β_i:	slope or decay factor in i direction
i:	denotes component, radial, vertical, or transverse

In the case of the Equation 2.5, it was determined that using a value of $\alpha = \frac{1}{2}$, for the data of such project that when a log-log plot is made between particle velocity V and $D/W^{\frac{1}{2}}$ a significant reduction in the spread of the data was achieved.

If Equation 2.5 is written in the traditional form, using square root of the charge instead of cube root of the energy released by explosion, the particle velocity is expressed by:

$$V_i = a * (SD)^{-b} \qquad [2.6]$$

where:

a and b:	adjustable parameters, dependent upon the local ground conditions
SD:	scaled distance defined by:

$$SD = \frac{R}{\sqrt[2]{W}} \qquad [2.7]$$

where:

R: distance from explosion

W: charge weight

Although Equation 2.7 is one of the equations most used in mining engineering to estimate and control vibrations from blasting, this equation has fundamental problems (Blair, 2004). The main problem about Equation 2.7 is regarding to units; if we assume that the units in Equation 2.7 are given by:

R:	length	[L]
W:	mass	[M]

Then, the units of scaled distance should be:

SD:	units of	$[LM^{-1/2}]$

That means that the "constant" a in Equation 2.6 should have dimension or units; for example if b=2, the units of a will be:

a:	units of	$[M^{-1}L^{3}T^{-1}]$

However if b=1 then:

a:	units of	$[M^{-1/2}L^{2}T^{-1}]$

If we consider that b is both, site and direction specific, then a unit's change continually and Equation 2.6 is not a fundamental equation for vibration prediction (Blair, 2004)

To predict vibrations, using scaled distance laws, it is necessary to collect information of vibration levels from a set of standard blast events that represent the conditions of blasting of the mine in the future. The main assumption besides the applicability of the scale distance law is that the future blasts are going to produce equal or similar vibration levels than the standard blasts. Figure 2.3 shows an example of data used to produce scaling law in different vibration components (Lusk, et al., 2010).

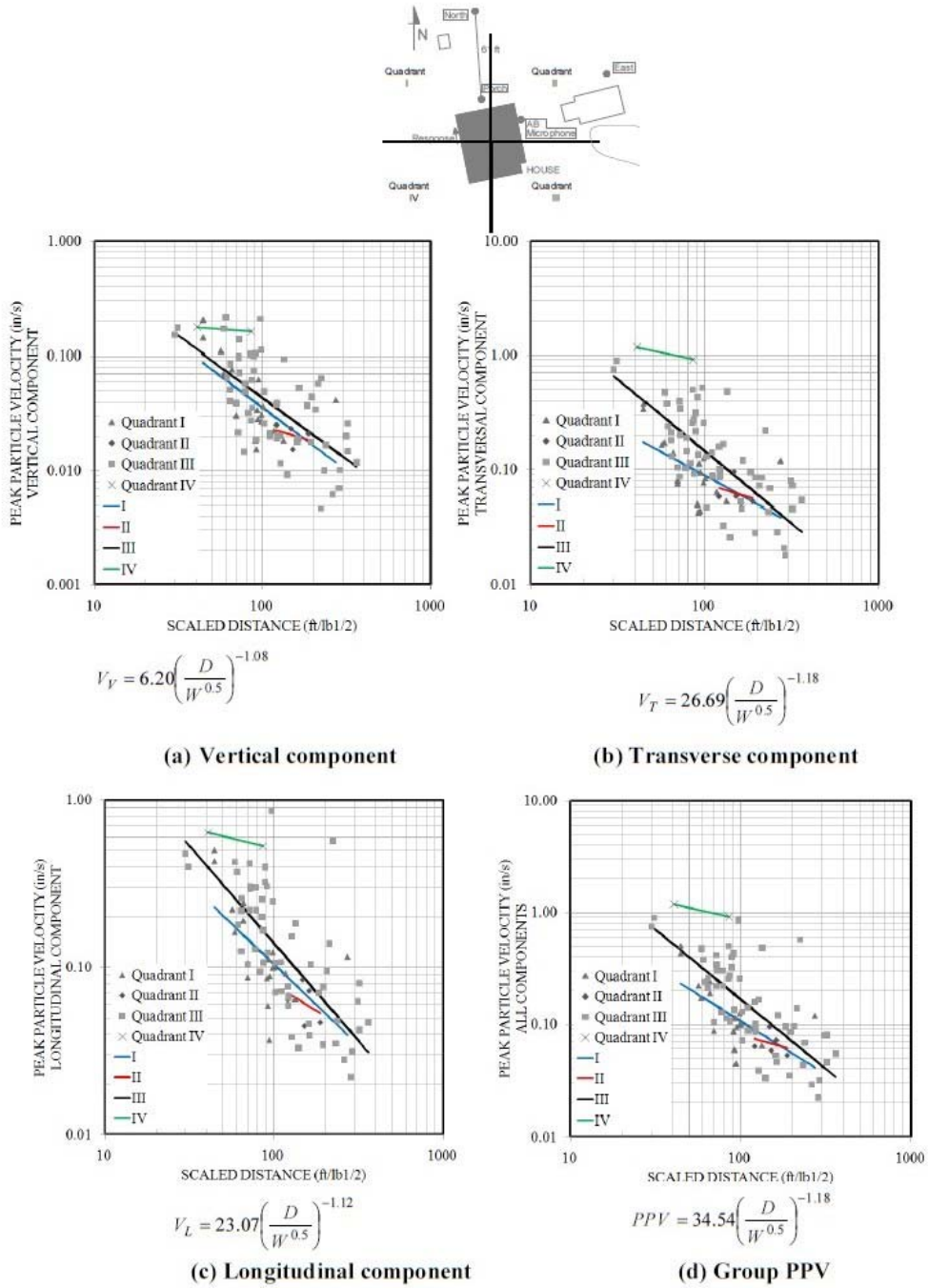

Figure 2.3 Scaled distance law, analysis for different components (Lusk, Silva, Eltschlager, Hoffman, 2010)

2.3.2 *Analytical and numerical approaches*

Currently most of the efforts to model mining blasts are more focused on the modeling of the fracture and fragmentation process than blast vibration prediction. The majority of numerical modeling research is focused in the study of the fragmentation process and the evaluation of the vibration levels is just some additional information. A

summary of the main assumptions, developments and considerations when blasting numerical modeling is performed are given next.

The components in the modeling of fracturing process can be grouped in three branches (Saharan, et al., 2006):

- Materials (Rock);
- Explosive;
- Boundary conditions.

From each branch there are more ramifications creating more sub-systems. Each branch is physically independent but they interact with each other to explain the fracturing process. Figure 2.4 adapted from (Saharan, et al., 2006) shows the main components to explain the fracturing process.

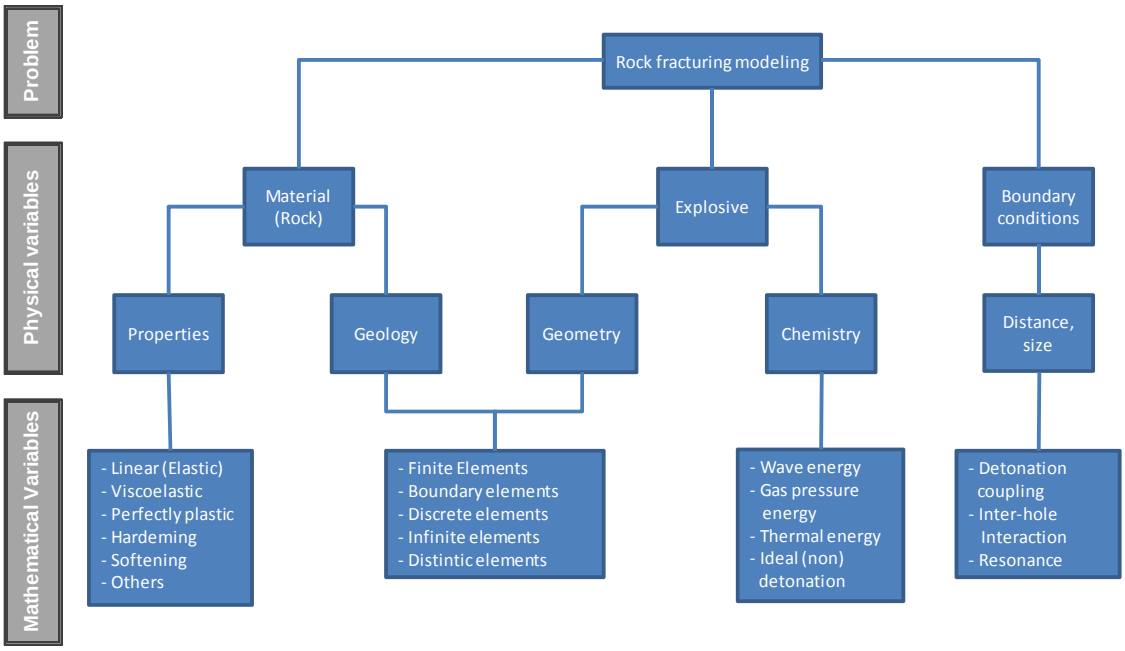

Figure 2.4 Main components of rock fracturing modeling process (Adapted from Saharan, Mitri and Jethwa, 2006)

The most common simplification in the fracturing model using analytical or numerical approaches is to assume elastic properties of the surrounding rock to the charged hole and a cylindrical geometry for the blast hole (Spathis, 2010). Other authors (Batzle et al., 1980, Blair and Cook, 1998, Kranz, 1983) suggest the tensile failure mode as the basic failure mechanism in rock. Under this failure mechanism, fractures generated radially from the blast hole grow by taking the path of least resistance, i.e. either that of least shear stress of the rock (usually the tensile strength) or the least confining stress (Saharan and Mitri, 2008). When detonation pressure, exceeding the tensile strength near the blast hole perimeter is overwhelming, and a crushing zone is developed. Beyond the crushing zone, blasting results in the formation of a discrete fracture networks. It is also common to assume the behavior of the material having a viscoelastic law ignoring the non-linear behavior that the blasting process implies.

Regarding the dynamic load, there are two different pressure pulse shapes. The form of the shape is related to the time the chemical compound reaches the peak pressure.

Those pulses explain the ideal and non-ideal detonation. In the ideal detonation, the rise in the peak pressure is reached in a very short time while the rise time for the peak in the non-ideal detonation is longer and the post peak pressure drop is much slower when compared to ideal detonation. Figure 2.5 show the two most used pressure pulses in fragmentation and blast vibration analytical and numerical modeling.

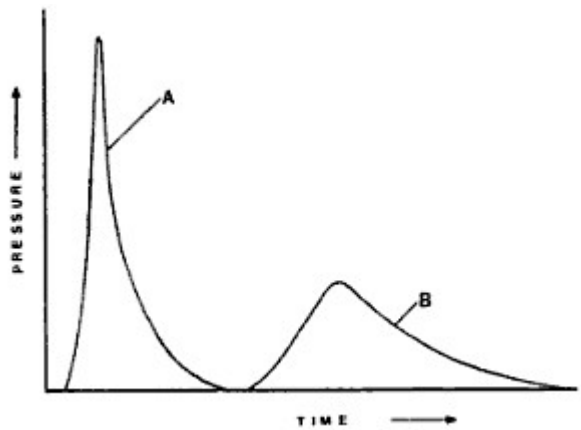

Figure 2.5 pressure pulse shape A. Ideal detonation. B. Non-ideal detonation (Aimone, 1992., Olsson et al., 2001)

Usually in the modeling process, it is assumed that the cylindrical hole is pressurized simultaneously over a section of its length. However, in production blastholes, this process may take several milliseconds.

Several analytical solution assuming elasticity and isotropy of the material can be found in the literature. In 1952 Blake derived the solution for the governing equation of the problem of the propagation of a spherical wave due to an impulsive pressure; the governing equation is given by:

$$\frac{\partial^2 \emptyset}{\partial t^2} = {C_p}^2 \nabla^2 \emptyset \qquad [2.8]$$

Where:

C_p: compressional wave velocity

t: time

$\emptyset$: a potential function

∇^2: Laplacian operator

If a pressure function is defined (pressure pulse shape) as:

$$p(t) = p_o e^{-\alpha t} \qquad \text{for } t \geq 0$$
$$p(t) = 0 \qquad \text{for } t < 0 \qquad [2.9]$$

Using $\alpha = 0$, the radial displacement at large distances ($r \gg a$) can be found as:

$$u_r = \frac{\partial \emptyset}{\partial r} = -\frac{p_o a^3 K}{\rho {C_p}^2 r^2}\left[-1 + \sqrt{2-2\vartheta} * e^{-\alpha_o \tau} * cos\left(\omega_o \tau - tan^{-1}\left\{\frac{1}{\sqrt{4K-1}}\right\}\right)\right]$$
$$+ \frac{p_o a^3 K}{\rho {C_p}^2 r}\left[\frac{\alpha_o}{C_p} + \sqrt{2-2\vartheta} * e^{-\alpha_o \tau} * cos\left(\omega_o \tau - tan^{-1}\left\{\frac{1}{\sqrt{4K-1}}\right\}\right)\right]$$
$$+ \left[\frac{\omega_o}{C_p} + \sqrt{2-2\vartheta} * e^{-\alpha_o \tau} * sin\left(\omega_o \tau - tan^{-1}\left\{\frac{1}{\sqrt{4K-1}}\right\}\right)\right]$$

[2.10]

Where:

a:		radius of the sphere
K:	$\frac{1-\vartheta}{2(1-2\vartheta)}$	Bulk module
ϑ:		Poisson's ratio
r:		radial coordinate
α_o:	$\frac{C_p}{2aK}$	radiation damping constant
τ:	$t - \frac{r-a}{C_p}$	time lag
ω_o:	$\frac{C_p}{2aK}\sqrt{4K-1}$	natural frequency

To calculate the particle velocity it is needed to differentiate Equation 2.10.

$$\dot{u}_r = \frac{\partial^2 \emptyset}{\partial r \partial t} = \frac{p_o a}{\rho C_p r}\left[\sqrt{2-2\vartheta} * e^{-\alpha_o \tau} * cos\left(\omega_o \tau + tan^{-1}\left\{\sqrt{1-2\vartheta}\right\}\right)\right]$$

[2.11]

This approach has the limitation that the source of the pressure is spherical and purely compressional modes of radiation are analyzed in the problem. A recent effort to develop a numerical model that represents the mechanism of rock blasting involving the detonation, fracturing and movement process has been conducted by an international collaboration project (The Hybrid Stress Model Project (HSBM)). The model proposed is named Hybrid Stress Blasting Model (Furtney et al., 2009). In this model, a numerical code simulating the non-ideal detonation process is coupled to a numerical model that simulates the behavior of a 3D rock mass. The model uses a combination of discrete and continuum numerical techniques to model the rock blasting behavior. In the near field, close to the blast hole, the rock mass is represented as a continuum grid. Such continuum grid is coupled to another continuum grid that represents the explosives and their behavior while detonation, (volume expansion, pressure and axial flow). The gas products are introduced also into the network of fractures, causing further expansion of the fractures and heave of the resulting rock fragments. The rock in the intermediate and far field is represented based on a lattice of nodes and springs. (Cundall, 2008).

Currently even using the most advanced computational technology, the run times for large models makes the day-to-day application of those methodologies impractical.

2.3.3 *Signature hole technique*

This technique is based on signals and system theories. It is well known that in a blast event, the vibration structure response is a function of the amplitude and frequency content of the ground vibration signal reaching the structure (Siskin et al., 1980b). It was in the 1980s when wave interference concept began to be introduced (Anderson, et al., 1985) and (Crenwelge et al., 1986) to control blast vibrations. Past researches had shown the benefits of the use of wave interference to reduce the ground vibration levels in a blast event (Lusk et al., 2006), (Christopherson and Papillon 2008), (Chiappetta, et al., 1985).

The basic concept behind the signature hole technique is similar to the principles applied in the signals and systems theories. In that branch of knowledge, a system is defined as an entity with a unique relationship between the excitation or input and the response or output (cause and effect) Figure 2.6 shows this similarity.

There are many types of systems. From an Input - Output point of view, they can be:

SISO: Single Input – Single Output
MIMO: Multiple Input Multiple Output
and his combinations:

MISO: Multiple Input – Single Output
SIMO: Single Input – Multiple Output

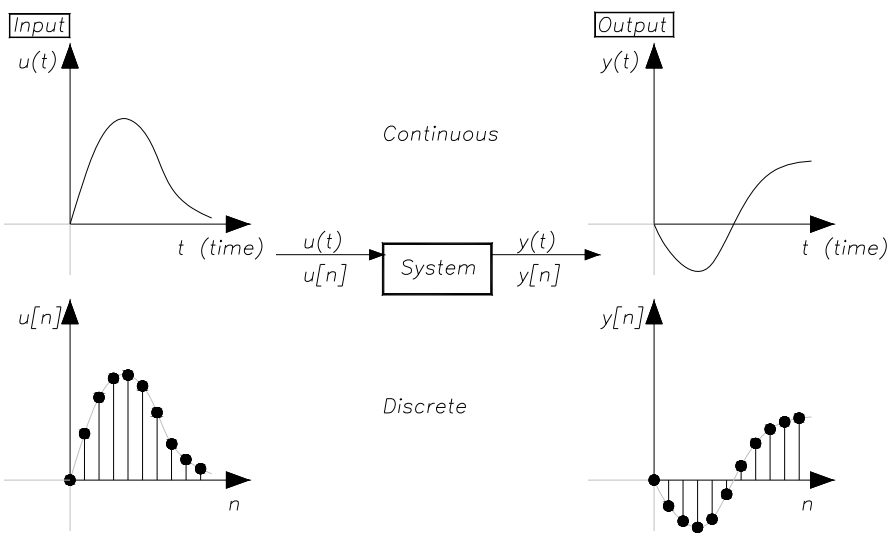

Figure 2.6 Sketch of a system with continuous and discrete signals.

The systems can also be classified according to the characteristics in causal or non-causal, lumped or distributed, linear or nonlinear and finally as time invariant or time varying.

Single-Input, causal, linear and time invariant systems are very useful in the "real world" because many physical phenomena can be modeled using the system theory

applicable to that type of systems. Figure 2.7 shows the basic concepts of the SI-SO, and time invariant systems.

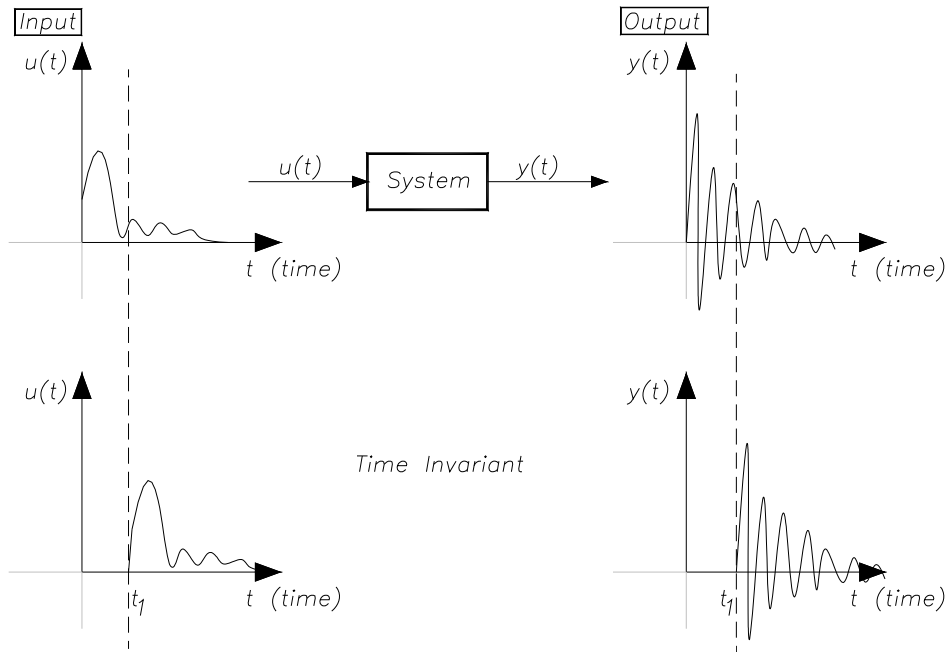

Figure 2.7 Time Invariant systems single input - single output (Adapted from "Signal and Systems" 3th edition)

Causality is related to the relationship between the Input- Output and the time. One system is causal if the current output is only related to the current input (the current response is not related to past or future inputs). On the other hand, linearity in the systems theory is related to the linear superposition of different actions to produce a response. Finally if the system does not change over time, this means that the system is time invariant, i.e., an input in current time, produces the same output that an input given to the system in the future.

All these concepts mean that if the system is Continuous (**C**) Linear (**L**) and Time Invariant (**TI**), by knowing a pair Input – Output signals, it is possible to predict the outputs for whatever Input signal. Figure 2.8 shows this concept in more detail.

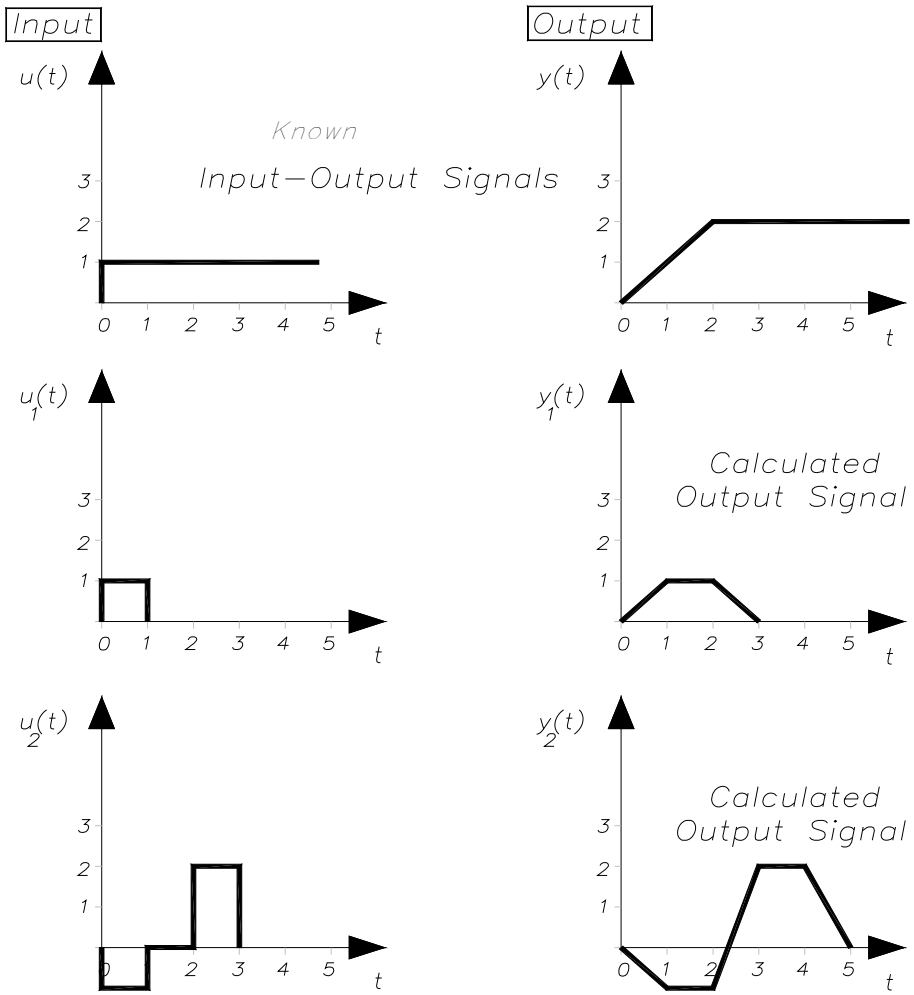

Figure 2.8 **SI-SO, C, L, TI** systems (Adapted from "Signal and Systems" 3th edition)

In blasting, the signature hole technique assumes that the vibrations generated as energy release in a blast, and transformed into elastic waves travelling within the rock, are a physical phenomenon developed in an SI-SO, C, L, TI system.

In such case, the system is the entity that wraps the site specific geological conditions between the event site and the point under study (joints, faults, lithology etc.,), and the path of the vibration waves, including reflections and refractions of waves propagating away from the event site. Figure 2.9 shows this concept.

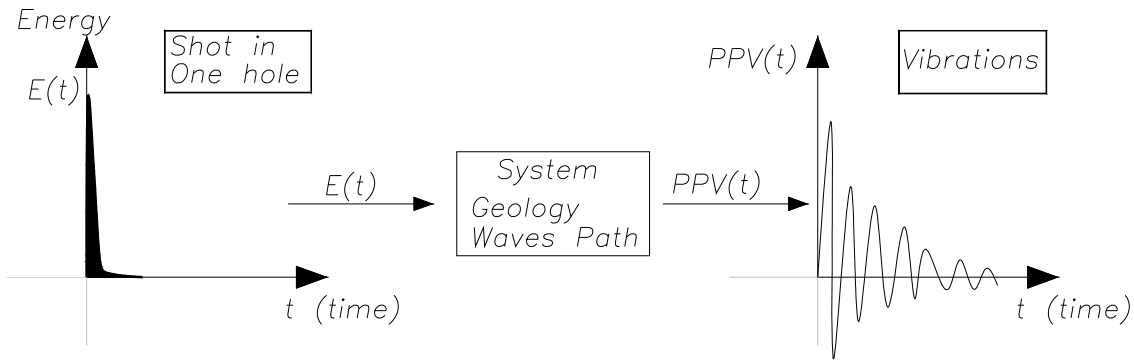

Figure 2.9 Systems Theory and Signature Hole Technique similarity.

Other assumptions to the signature hole technique are (after Anderson 2008):

- There is a need to control the vibrations in a specific location;
- All holes are detonated at the same location, so that the path traveled by the waves is identical;
- All holes have the same explosive charge type and weight. In others word, the quantity of energy converted into elastic waves each time a hole is blasted is the same;
- The phenomenon occurs in a system ideally SI-SO, C, L, and TI, so that all holes have the same explosive-rock interaction. That means that the source pulse (detonation) always generates the same response in the site under study (signature wave).

In the signature hole technique, assuming that all the assumptions are fulfilled, the signature wave recorded in a specific site (the signal recorded when a hole is blasted) can be expressed as a finite impulse response (FIR). This means an impulse response with finite nonzero entries, which can be expressed as:

$$h[n] \neq 0 \;\; for\; n = 0,1,2,\dots,N-1 \qquad [2.12]$$

with

$$h[N-1] \neq 0 \qquad [2.13]$$

and

$$h[n] = 0\; for\; n \geq N \qquad [2.14]$$

Graphically, it is represented in Figure 2.10. In this specific case, when the input signal is the impulse, (one blasted hole at t_o=0), it can be expressed as:

$$u[n] = \delta[n] \quad or$$

[2.15]

$$u[n] = A_i \delta[n]$$

[2.16]

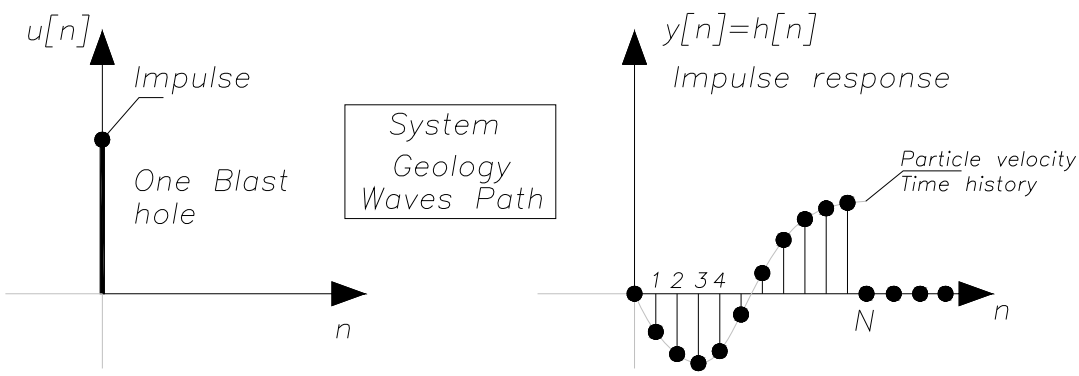

Figure 2.10 Finite impulse response from one hole blasted

Now, if we consider an arbitrary input sequence (production blast hole), it can be expressed as:

$$u[k] = A_i * \delta[t - m_i t_o]$$

[2.17]

and

$$u[n] = \sum_{k=0}^{\infty} u[k]\delta[n-k]$$

[2.18]

Assuming the system is linear and time-invariant, and using the shifting, homogeneity and additive properties of signals, the output *y[n]* excited by the input *u[n]*, for n≥0, can be given by:

$$y[n] = \sum_{k=0}^{n} h[n-k]u[k]$$

[2.19]

Or in a general form:

$$y[n] = \sum_{k=-\infty}^{\infty} h[n-k]u[k] := h[n] * u[n]$$

[2.20]

This algebraic equation is called a "discrete convolution". This equation relates the input and output of a system. Due to this relation, the convolution is also sometimes

called input-output description of the system. In this case, the description of the system (calculation of the output given an input) is developed without using any physical properties of the system and is based on signal-system properties as linearity, time invariance and causality.

In the signature hole technique, predicting the vibration levels of a production blast on the same monitoring point that the signature wave was recorded is achieved by using the recorded signature wave directly to calculate the blast vibration waveform of the production blast. On the other hand, if there is no signature waveforms available in the place where it is required to assess vibrations levels, some authors combine scaled distance estimations and transfer functions to get the signature waveform at the point of interest (Spathis, 2010).

In their methodology, Yang and Scovira (2010), use a set of signature waveform tests to estimate the amplitude attenuation of the vibration due to the distance from the source to the point of interest. Using the set of signature waveforms a graphical representation of Equation 2.6 and Equation 2.7 for the site under study is obtained. After calculating the maximum peak particle velocity for the point of interest according to Equations Equation 2.6 and Equation 2.7, the closest signature waveform is modified to match the peak particle velocity at the point of interest. It is well documented that not only is there a change in the amplitude of the vibration according to the distance, also when an acoustic pulse propagates, its frequency changes attenuating the higher frequencies (Kavetsky, et al., 1990). In order to model the change in frequency, the concept of an effective wavelength varying linearly with distance is introduced through the use of Kjartansson transfer function (Kjartansson, 1979). This transfer function may be used to propagate an arbitrary wave shape by Fourier transforming the convolution of the impulse response and the source wave. The Fourier transform of the propagated wave at the point of interest is given by:

$$W(\omega) = S(\omega)B(\omega) \qquad [2.21]$$

Where:

$W(\omega)$: Fourier transform of the propagated wave at point of interest

$S(\omega)$: Fourier transform of the source wave (closest signature waveform to the point of interest)

$B(\omega)$: Kjartansson transfer function

and the Kjartansson transfer function is given by:

$$B(\omega) = e^{\left\{-\frac{x*\omega_o}{c_o}\left|\frac{\omega}{\omega_o}\right|^{1-\gamma}\left[tan\left(\frac{\pi*\gamma}{2}\right)+i*sgn(\omega)\right]\right\}} \qquad [2.22]$$

Where:

x: distance from source wave to point of interest

ω_o: frequency of reference $\omega_o = \frac{1}{t_o}$; t_o: arbitrary reference time

c_o: phase velocity at the arbitrary reference frequency ω_o

$$c_o = \frac{\left(\frac{M_o}{\rho}\right)^{1/2}}{cos\left(\frac{\pi * \gamma}{2}\right)}$$

M_o: bulk modulus

ρ: density

γ: shear strain $\gamma = \frac{1}{\pi} tan^{-1}\left(\frac{1}{Q}\right) \approx \frac{1}{\pi * Q}$

Q: constant creep function (Rock quality factor)

$sgn(\omega) = 1$ $\omega > 0$

$sgn(\omega) = -1$ $\omega < 0$

Using this approach, bulk modulus, density and rock quality factor of the medium are required.

Finally, in their methodology, Yang and Scovira (2010), propose the waveform change as a function of screening effect of earlier firing holes. The screening effect assumes that there is a change in the amplitude and in the shape of the waveform due to the change in the medium where the blasting process is occurring. In other words, a previous hole blast affects the surrounding rock where the next blast hole takes place in the vibration path. The function proposed to change the seed waveform is a ratio between the quantity of explosive already blasted to the quantity of explosive that produce the waveform and is given by

$$s(\phi) = \lambda^{\phi} \qquad [2.23]$$

where

$$\phi = \frac{\omega_t}{\omega} \qquad [2.24]$$

ω_t total charge weight of earlier fired blast hole in the vibration path

ω charge weight of the presently firing charge, where $\lambda<1$

The limit conditions of this equation is given by

$$s(\phi) = \begin{cases} 1, & \phi \to 0 \\ 0, & \phi \to \infty \end{cases} \qquad [2.25]$$

Figure 2.11 summarizes the current signature hole technique methodologies.

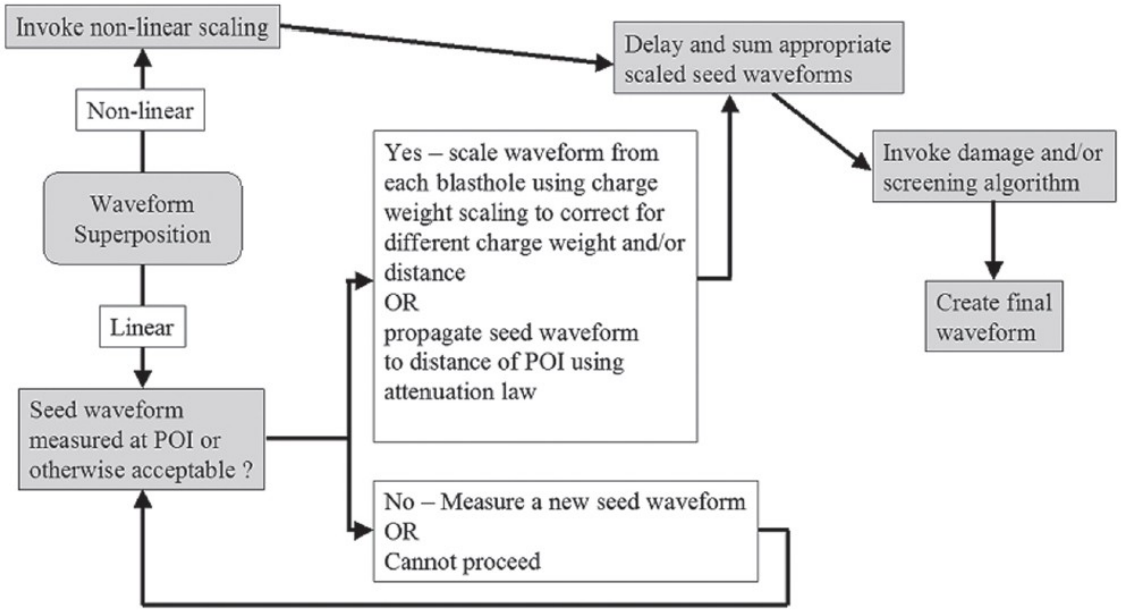

Figure 2.11 Summary of the most common signature hole techniques currently available (After Spathis, 2010)

The next chapter is a detailed discussion about the main assumptions in the current signature hole technique.

DETAILED DISCUSSION OF CURRENT SIGNATURE HOLE TECHNIQUE

3.1 Introduction

This chapter describes in detail the main aspects of the current signature hole technique. The description includes the major assumptions of the current signature hole technique as the seed waveform repeatability and the influence of the timing sequence in the waveform produced. Explanations about the linear superposition are given in two forms including the traditional one where convolution is used to calculate the total waveform and how to do the linear superposition using graphical techniques. Finally, results are included as comparison between the current prediction methodology and waveforms as a result of production blasts.

3.2 Blast vibration energy

The energy stored in the chemical components of explosives (ANFO, dynamite, Emulsions etc.) is released in a combined process of deflagration and detonation. Sanchidrián José et al., (2006), proposed that the major components of the released energy in a mining blasting process are composed by four parts: fragmentation, seismic, kinetic, and energy used in other types of work during the process. The equation that describes this behavior is given by:

$$E_E = E_F + E_S + E_K + E_{NM} \qquad [3.1]$$

Where:
E_E: Explosive energy in the chemical
E_F: Fragmentation energy
E_S: Seismic energy
E_K: Kinetic energy
E_{NM}: Not measurable energy

Not measurable energy includes the energy release as sound (airblast), heat, light and other phenomena that occurs in the explosion.

Using the energy flux concept defined as the power or rate of work per unit area, it is possible to relate the particle velocity of the ground to the dynamic stresses generated when the wave passes through a specific point as:

$$\Phi = \vec{\boldsymbol{t}}\,\vec{v} \qquad [3.2]$$

Where:
Φ: Energy flux
$\vec{\boldsymbol{t}}$: Stress vector
$\vec{\boldsymbol{v}}$: Particle velocity vector

Using stress tensors (Cauchy formula) and assuming that the energy transferred to the rock can be evaluated as the integral of the energy flow through a control surface at a given distance from the blast, it is possible to evaluate the seismic energy using the plane wave approximation as (Sanchidrián José, et al., 2006):

$$E_{Sis} = 4\pi r^2 \rho \left[c_L \int_0^\infty v_1^2 dt + c_T \int_0^\infty (v_2^2 + v_3^2)\, dt \right]$$

[3.3]

Where:

ρ:	rock density
c_L and c_T:	Longitudinal and Transverse rock wave velocity respectively.
r:	distance to the source
v_1, v_2, v_3:	Particle velocities radial, longitudinal and transverse respectively.

The signature hole technique assumes that each hole releases the same seismic energy under similar blasting conditions. In order to apply the technique, the seismic energy released by each hole can be analyzed as a pulse taking place at firing times, according to the delay sequence used in a blast. The previous statement implies that it is possible to use the delta function to mathematically represent the firing of each hole as:

$$Esis_i = A_i * \delta(t - m_i t_o)$$

[3.4]

Where:

$Esis_i$:	Seismic Energy release in the hole i
A_i:	Seismic Energy "Efficiency" in hole i
t:	time
$m_i t_o$:	Time delay for hole i

According to the signature hole assumptions, the seismic energy efficiency hole to hole ,$\mathbf{A_i}$, is equal to one (1).

3.3 Seed waveform

Many studies have shown how some parameters affect the characteristics of the seismic waves produced due to a mine blast. The main parameters involved in the blast–vibration phenomena can be summarized as follows (Aldas, 2010):

- Explosive-rock interaction;
- Blast-induced wave transmission property of a rock unit (i.e waves traveling along specific layers);
- Distance between blast location and measurement point;
- Geology of the propagation media (i.e faults, bedding planes, etc);
- Geology at the measurement point;

- Blasting parameters (i.e diameter, explosive type, borehole depth, spacing and burden, delays and free faces).

The first five of six elements involved in the wave generation are site specific and related to the geology. Despite the site specific nature of the phenomena, the assumption that each hole produces the same waveform in a specific measurement point is based on the fact that the frequency spectra for different blast single holes are similar according to Crenwelge (1988) findings.

In 1988, Crenwelge reported the typical spectra of seismic waves due to single blast hole. In addition, other variables like weight of explosives, the type explosive and the source distance – measurement point were studied to determine their influence on the spectra. Figure 3.1 shows the particle velocity spectra for single charge - shots of small column weight.

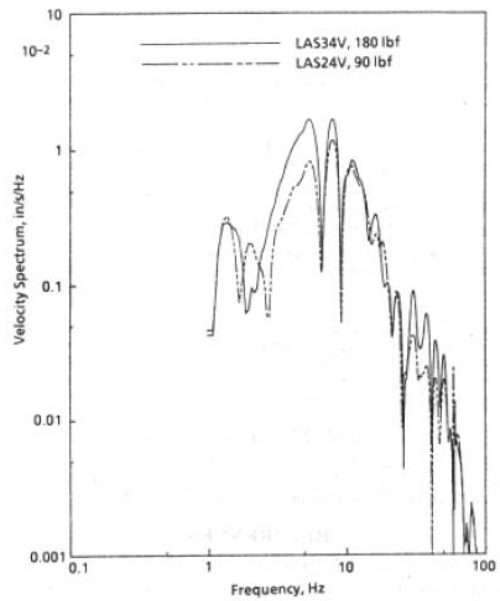

Figure 3.1 Particle velocity spectra for single charge shots of small column weight (Crenwelge, 1988)

In this case, the seismic waves were recorded at the same point of interest (geological conditions, distance to source – event and wave travel path are equal). The difference between both events is the quantity of explosive detonated (90 and 180 lbf) and no rock breakage influence between them. Despite the difference in the weight of explosives, in general terms, Figure 3.1 shows the similitude in the shape of the spectra of the two shots.

Similar results are obtained when the weight of explosives detonated is further increased in the hole. Figure 3.2 shows the seismic wave spectra for explosives with weights between 250 and 2,000 lbf.

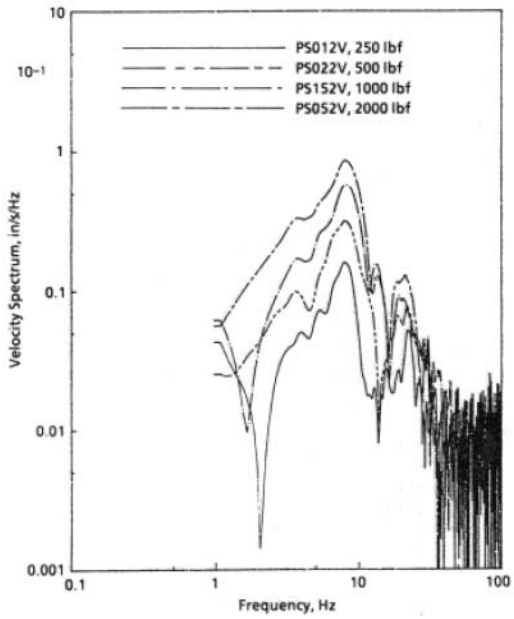

Figure 3.2 Particle velocity spectra for single charge shots of tall column weight (Crenwelge, 1988)

Different results are obtained in the frequency spectrum if the distance to the source-recording site changes. With the change in the distance, the geological conditions and travel path of the seismic waves change. Figure 3.3 shows how the shape of the spectra changes with the distance for both weights of explosives (small and high column weight).

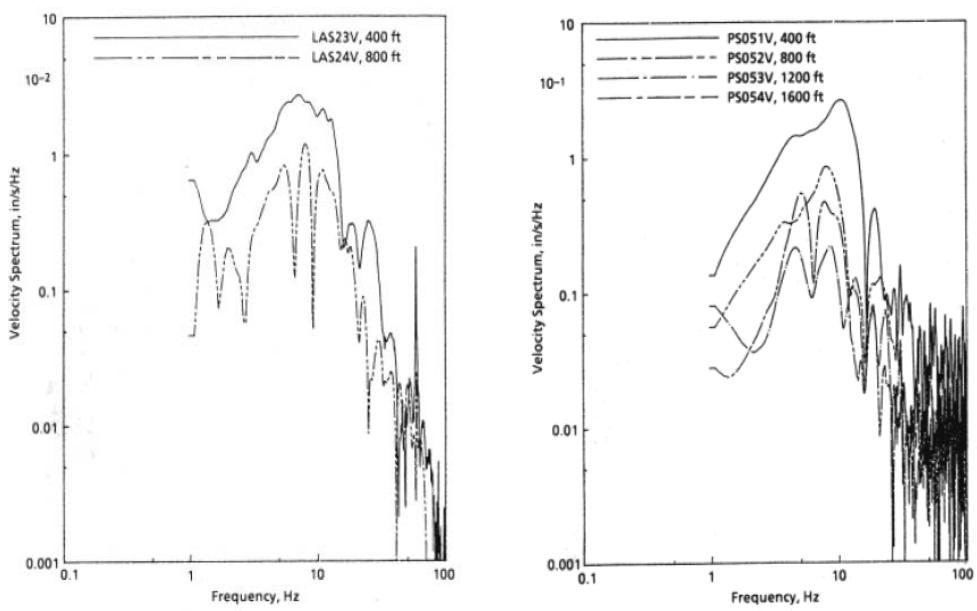

(a) (b)

Figure 3.3 Particle velocity spectra for single charge shots (a) short column weight (b) tall column weight (Crenwelge 1988)

These results show, as expected, that vibrations are site specific and the shape of the spectra is similar for the same site even if the weight of explosive is reduced or increased. Sakamoto et al (1989) in their study about the accuracy delay in detonators showed the signature waveform for two locations (100 and 150 meters) using three different weights of explosives in a limestone mine. As previously noticed with the spectrum, the signature waveforms are similar for three different loads. This is included in Figure 3.4

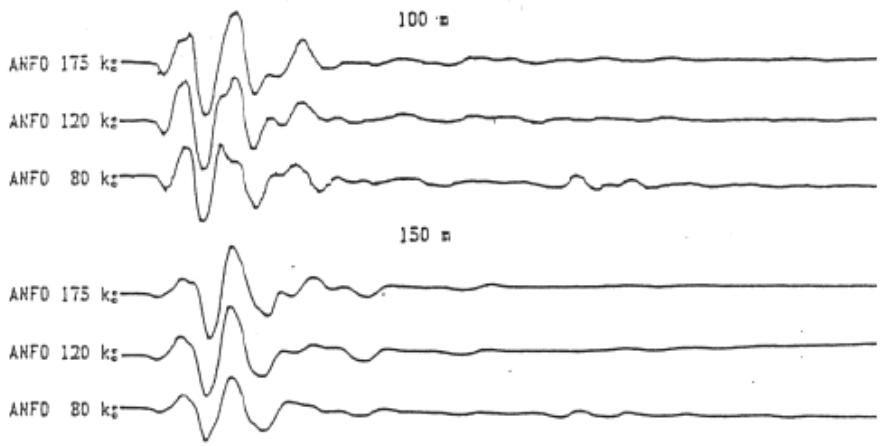

Figure 3.4 Seismograms recorded for three different charge weights and two locations (After M. Sakamoto, et al., 1989)

Similar results corresponding to waveform similitude were found by Bonner et al., 2008, where the effect of the explosive type in the rock damage and the source of shear wave generation were studied. Figure 3.5 shows the waveform similitude for a given fixed vibration recording station when different shots using different explosives where tested.

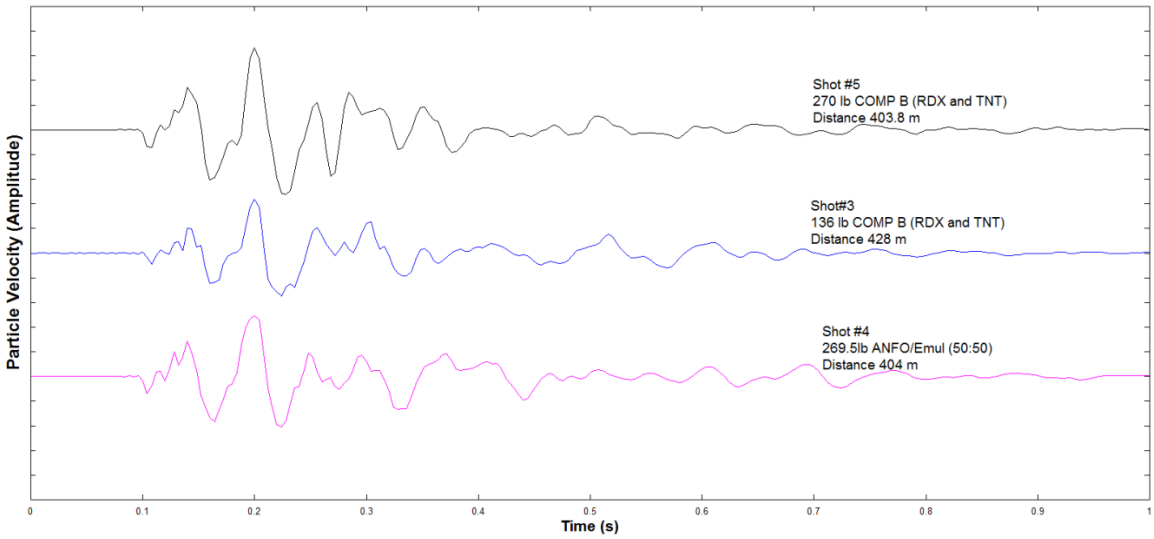

Figure 3.5 Seismograms recorded for three different charge weights (After Bonner, et al., 2008)

When a spectral analysis is done using those waveforms the vibration frequency content is between 1 and 22 HZ as shown in Figure 3.6.

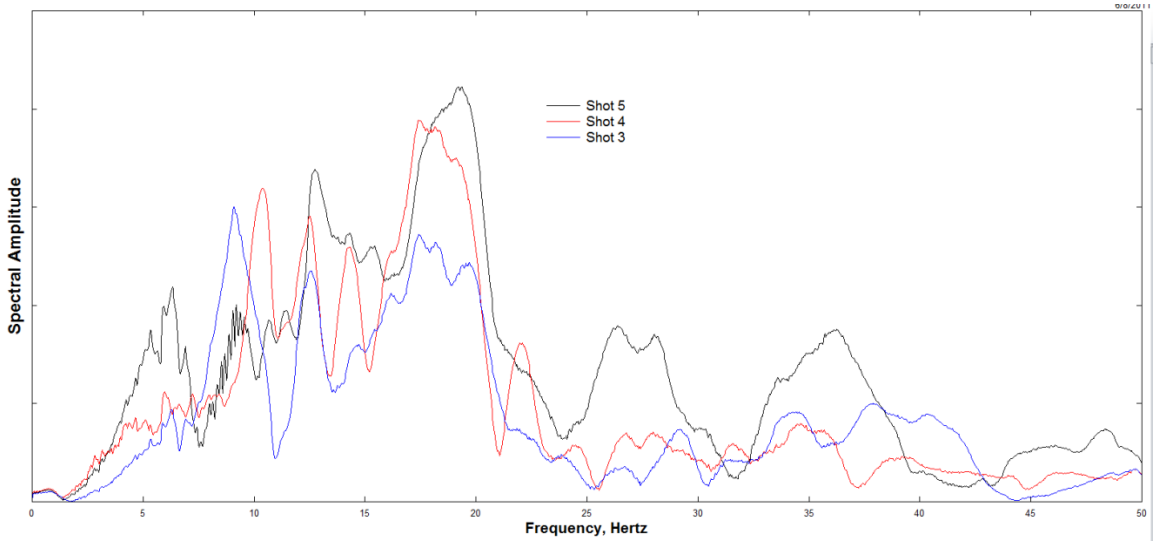

Figure 3.6 Spectral analysis for three different charge weights (Bonner, et al., 2008)

The original signature technique assumes the invariability in the waveform from different holes at the same station or measurement point. However, recently proposals recognize the waveform variability hole-to-hole in the signature hole methodology Aldas, (2010), Yang and Scovira (2010), Blair (1999), however the inclusion of the signature waveform variability in the methodology is not totally understood and the parameters used to change the waveform between holes are difficult to assess.

3.4 Explosion sequence

Based on signals and systems theories and assuming that the full-blast vibration record occurs in a casual, linear and invariant system and the phenomenon follows a linear superposition, the whole vibration record for the full-blast $y(t)$ can be mathematically expressed as the convolution of the signature waveform (impulse response-signature hole) $h(t)$ and a delta Dirac sequence (input sequence or blast timing sequence) $u(t)$. The relationship is given by:

$$y(t) = h(t) * u(t) = \int_{-\infty}^{\infty} h(\tau)u(t-\tau)d\tau \qquad [3.5]$$

In discrete terms Equation 3.5 can be expressed as

$$y[n] = \sum_{k=-\infty}^{\infty} h[k]u[n-k] \qquad [3.6]$$

The explosion sequence $u(t)$ or $u[k]$ is a function representing the energy released in each hole that is transformed into vibration and depends also of the time delay between holes.

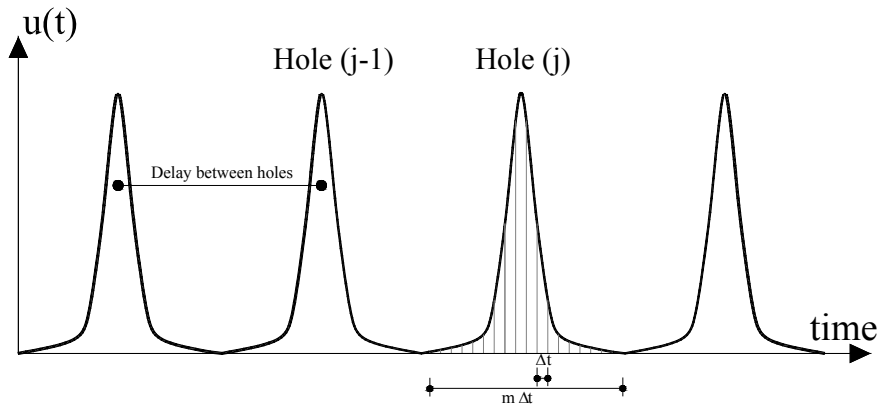

Figure 3.7 Explosion sequence function

The full-blast sequence function $u(t)$ can be approximated using a stair-step function given by:

$$u(t) = \sum_{n=0}^{\infty} u(nT) * [\ \delta_T(t - nT)]T \qquad [3.7]$$

Where:

$\delta_T(t - nT)$	pulse occurring at $t = nT$
$[\delta_T(t - nT)]T$	pulse height
T	pulse width
$u(nT)$	$u(t)$ evaluated in $t = nT$

The graphical representation of Equation 3.7 is shown in Figure 3.8.

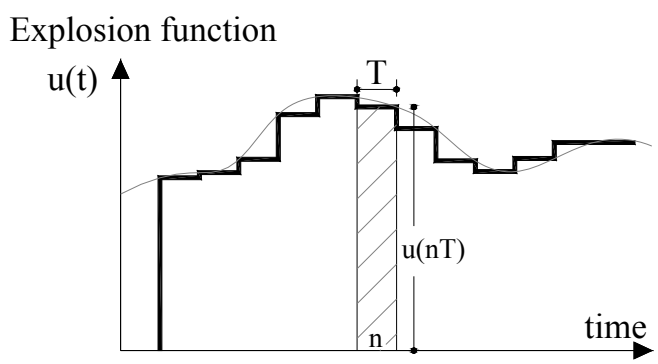

Figure 3.8 Graphical representation of Equation 3.7

If the vibration of the jth hole is isolated, the vibration component of the jth hole can be expressed as:

$$y_j(t) = h(t) * u_j(t) = \int_{-\infty}^{\infty} h(\tau) u_j(t-\tau) d\tau$$

[3.8]

Using Equation 3.7 and isolating from the full-blast function the explosion of the hole j, it is possible to express the explosion function for the jth hole as (Blair 1999):

$$u_j(t) = \sum_{k=1}^{m} A_{kj} * \ \delta(t - k\Delta t)$$

[3.9]

Where:

$u_j(t)$	explosion function for hole j (group of delta functions)
$m\Delta t$	duration of the Dirac sequence for the explosion in the hole j
A_{kj}	Amplitude of Dirac delta functions
Δt	time interval (pulse width in Equation 3.7)

In Equation 3.9, the amplitude of Dirac delta functions A_{kj} is constituted by two components; the first one is related to the relative amount of coherent energy in the waveform of the jth blasthole and the second represents the total amount of random energy.

In this sense and using Equation 3.8 and Equation 3.9, the vibration generated for the jth blasthole is given by

$$y_j(t) = (1 - R)h(t) + \frac{R}{R_j} \sum_{k=1}^{m} A_{kj} h(t - k\Delta t)$$

[3.10]

Where:

$y_j(t)$	vibration for the jth blasthole,
R	relative amount of random energy for each blasthole,
R_j	measurement of the total energy of the random component, evaluated using Parseval's Theorem as $R_j = \sum_{k=1}^{m} A_{kj}^2$,
A_{kj}	a random number in the range -1 to 1.

In Equation 3.10, if R=0, all blast hole waveforms are identical and there is not a random energy component exist in the full-blast. Notice that, if R=0, the vibration generated by the jth blasthole is equal to the signature waveform. On the other hand, if R=1, the waveform for each hole in a full-blast are totally different and there is no "correlation" between the signatures of any of the blast holes and the prediction of the complete waveform using signature technique is not possible. Field measurements reported by Blair (1993) suggest that a model based upon R=0.8 is reasonable.

The total vibration $y(t)$ for a sequence of delayed blast holes is given by:

$$y(t) = \sum_{j=1}^{N} y_j(t - d_j)$$

[3.11]

Where:

N:	total number of blastholes
d_j:	is the jth initiation delay time.
y_j:	vibration for hole j
t:	time

3.5 Linear superposition

The mathematical development behind signature hole technique requires that linear superposition to do the summation (convolution) of the signals be possible. A system is linear if the system satisfies two properties; homogeneity and additivity. A system is homogeneous if scaling the input the predicted output is going to be scaled by the same quantity (as it is illustrated in Figure 3.9). In other words:

$$\alpha u_1(t) \rightarrow \alpha y_1(t)$$

[3.12]

Where:

α:	real constant
$u_1(t)$:	input
$y_1(t)$:	output

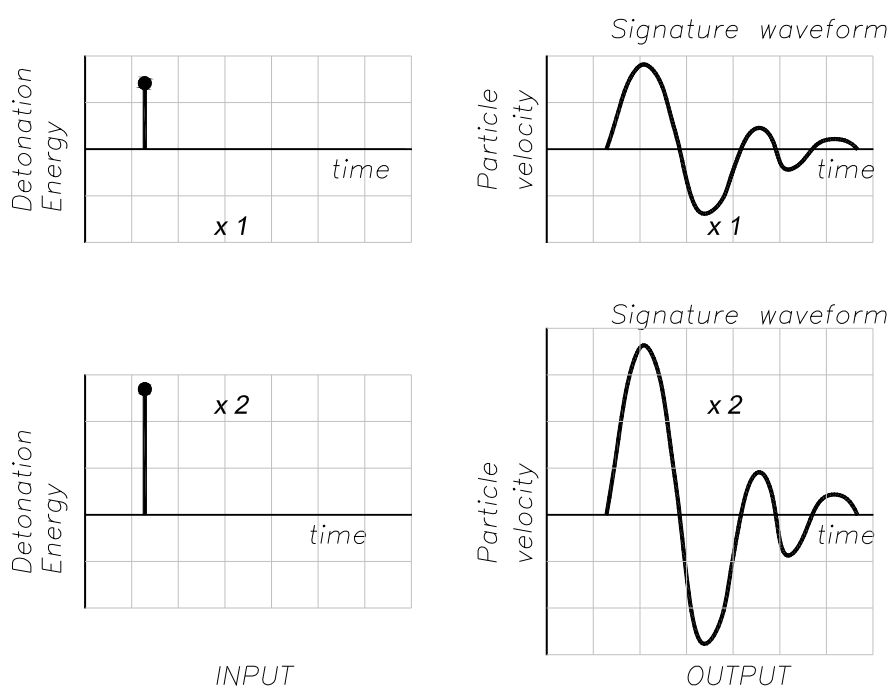

Figure 3.9 System's homogeneity property

Because α is a real constant, homogeneity is also called the scalar rule of a linear system. This property is not completely satisfied in a real production blast; however there is a relationship between the quantity of explosive used and the vibrations level generated. Using the scale law, despite all the inconsistencies previously mentioned, the relationship between the weight of explosive and the particle velocity in a given explosive weight interval can be assumed that the homogeneity property is satisfied. Figure 3.10 was elaborated using site constant values of: $a = 100$, $b = -1.5$ and $D = 100\ ft$.

The other property previously mentioned that a system should fulfill to be linear is additivity. The additivity concept (illustrated in Figure 3.11) is expressed for any pairs input output $\{u_i(t) \rightarrow y_i(t)\}$, for $i = 1, 2$ as:

$$u_1(t) + u_2(t) \rightarrow y_1(t) + y_2(t) \qquad [3.13]$$

Where:
$u_1(t), u_2(t)$: input 1 and 2
$y_1(t), y_2(t)$: output 1 and 2

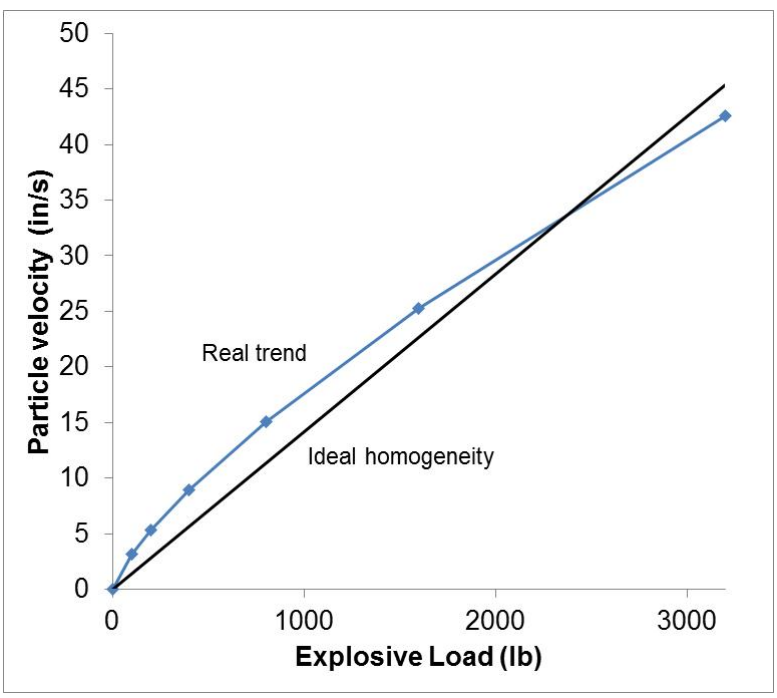

Figure 3.10 Numerical homogeneity concept between the quantity of explosive and the particle velocity.

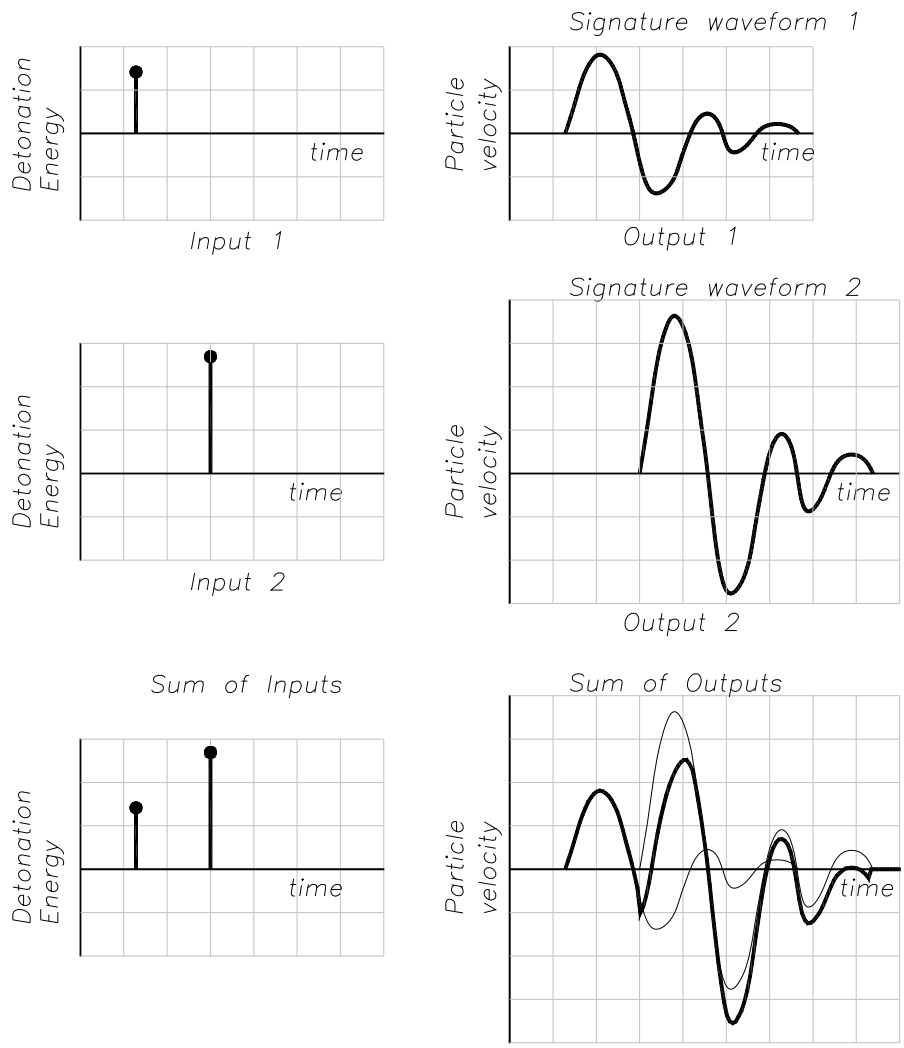

Figure 3.11 Additivity concept for signature hole technique

In the next chapter the Monte Carlo scheme is introduced in conjunction with the signature waveform methodology to improve the capability of blast vibration levels prediction.

MODEL DEVELOPMENT

4.1 Introduction

In this chapter, the Monte Carlo scheme is introduced to the signature hole technique. The probabilistic component for each stage of the methodology where it is possible to introduce this type of approach is discussed next.

4.2 Monte Carlo scheme

In a mining blast, the variables involved are related to geometry (e.g., depth of the holes, diameter, surface at the face etc). Quantity of explosives and geology are not constant hole-to-hole and they present some degree of uncertainty. This uncertainty makes it possible to treat some of the variables involved in the mining blast vibration phenomena as random variables within a given range.

Randomness sources in the blasting process come from different elements; those that are in situ such as the geology, the joint rock mass system, the underground seepage, etc., and those involving procedures of human activities like the drilling process, the loading of the holes with explosives and other blasting components like the detonation system.

Despite the high randomness involved in the mining blasting vibration phenomena, there are methodologies to study the problem using reasonable assumptions and approaches to obtain logical and meaningful results.

By solving blast vibration phenomenon as a random process, there is not a single answer or an exact prediction result. Most of the current deterministic methodologies to estimate the level of the particle velocity due to blasting are based on scaled distance.

Using a probabilistic approach like the Monte Carlo scheme, the result will be a probability distribution of peak particle velocity according to the probability distribution of the variables in the problem. To introduce the general idea about Monte Carlo scheme using signature hole technique, it is necessary to define some basic concepts.

4.2.1 *Discrete Random Variables*

According to probability theory, a random variable is a variable such that we do not know the value of this quantity in any given case, but we know what values it can assume and we know the probabilities with which it assumes these values Sobol, (1960).

A random variable X is called discrete if it can take any of a discrete set of values $\{x_1, x_2, \dots x_n\}$. So we can define X as given by Equation 4.1 Sobol, (1960)

$$X = \begin{pmatrix} x_1 & x_2 \dots & x_n \\ p_1 & p_2 \dots & p_n \end{pmatrix} \qquad [4.1]$$

Where:

$x_1, x_2, \dots\ x_n$	possible values of the variable X
$p_1, p_2, \dots\ p_n$	probabilities corresponding to possible values of the variable X

Equation 4.1 is called the distribution of the random variable X

The probability p_i that the random variable has the value x_i is denoted by:

$$P(X = x_i) = p_i \tag{4.2}$$

The values of the numbers $x_1, x_2, \dots x_n$ are arbitrary, however the probabilities $p_1, p_2, \dots\ p_n$ must satisfy the conditions given in Equation [4.3] and [4.4]:

$$p_i \geq 0 \tag{4.3}$$

and

$$p_1 + p_2 + \cdots + p_n = 1 \tag{4.4}$$

Last condition ([4.4) means that in every event X must assume one of the values $x_1, x_2, \dots x_n$.

The number given by:

$$E(X) = \sum_{i=1}^{n} x_i p_i \tag{4.5}$$

is called the expected value, or mathematical expectation, of the random variable X.

Some basic properties of mathematical expectation are given by:

$$E(X + c) = E(X) + c$$

$$E(cX) = cE(X)$$

and

$$E(X + Y) = E(X) + E(Y) \tag{4.6}$$

Where:

c:	is any constant
X, Y:	random variables

The variance defined as the mathematical expectation of the squared deviation of the random variable X from its average value $E(X)$ is given by:

$$Var(X) = E((X - E(X))^2)$$

or

$$Var(X) = E(X^2) - (E(X))^2$$

[4.7]

and is a measure of how far a set of numbers is spread out from the mean. As in the case of the mathematical expectation variance has some basic properties:

$$Var(X + c) = Var(X)$$

$$Var(cX) = c^2 Var(X)$$

[4.8]

Two random variables are independent when watching both variables, if the distribution of the variable X (Equation 4.1) does not change when the value which the variable Y assumes is known. If two random variables are independent the basic properties given by Equation 4.9 are satisfied:

$$E(XY) = E(X)E(Y)$$

and

$$Var(X + Y) = Var(X) + Var(Y)$$

[4.9]

To define the concept of probability density or density distribution of the random variable, it is necessary to assign a function to the probabilities of the possible values of the variable X in a given interval (a function for $p_1, p_2, \dots p_n$ in Equation 4.1). In other words, if a random variable X is defined in an interval of values $[a, b]$, (the interval of possible values $x_1, x_2, \dots x_n$) and a function $p(x)$ is assigned to these interval to represent the probabilities of those values $(p_1, p_2, \dots p_n)$, then $p(x)$ is called the probability density or density distribution of the random variable X. The significance of $p(x)$ is as follows: let (a', b') be an arbitrary interval contained in $[a, b]$. Then the probability that X lies in the interval (a', b') is equal to:

$$P(a' < X < b') = \int_{a'}^{b'} p(x)dx$$

[4.10]

The type of probability density to assign or to use for the random variable X depends of the physical process to represent. It has been seen that normal random variables are often encountered in nature.

A normal (Gaussian) random variable is a random variable Z defined on the whole axis $(-\infty, \infty)$ and having the density function given by:

$$p(x) = \frac{1}{\sigma\sqrt{2\pi}} e^{\left[-\frac{(x-a)^2}{2\sigma^2}\right]}$$

[4.11]

Where:

a, σ: numerical parameters where $\sigma > 0$.

In probability theory, it is possible to show that:

$$E(Z) = a \text{ and } Var(Z) = \sigma^2$$

[4.12]

One of the reasons or mathematical explanations why normal random variables are often encountered in nature is related to the concept of the central limit theorem of probability theory. Central limit theorem says that if there are N independent, identically distributed random variables (same function $p(x)$), their mathematical expectations and their variances also will coincide. Such theorem is expressed as:

$$E(X_1) = E(X_2) = \cdots = E(X_N) = m$$

and

$$Var(X_1) = Var(X_2) = \cdots = Var(X_N) = v^2$$

[4.13]

Also, if we denote the sum of all N variables by S_N:

$$S_N = X_1 + X_2 + \cdots + X_N$$

and

$$E(S_N) = E(X_1 + X_2 + \cdots + X_N) = Nm$$

$$Var(S_N) = Var(X_1 + X_2 + \cdots + X_N) = Nv^2$$

[4.14]

Now if there is a normal random variable Z_N with parameters

$$a = Nm \text{ and } \sigma^2 = Nv^2$$

[4.15]

By the theorem of the central limit "*The density of the sum S_N approaches the density of the normal variable Z_N in such a way that for every x,*

$$p\left(\frac{S_N - Nm}{v\sqrt{(N)}} < x\right) \approx p\left(\frac{Z_N - Nm}{v\sqrt{(N)}} < x\right)$$

for all large N.

[4.16]

the significance of this theorem is clear: The sum S_N of a large number of identical random variables is approximately normal, or:

$$p_{S_N}(x) \approx p_{Z_N}(x)$$

[4.17]

Using all previous probability concepts, next a brief explanation of the Monte Carlo scheme is given.

4.2.2 *General Scheme of the Monte Carlo Method*

Suppose we want to determine some unknown quantity m. Let us assume a random variable X that satisfies:

$$E(X) = m$$

and

$$Var(X) = v^2$$

[4.18]

Consider N independent random variables $X_1, X_{2,} \dots, X_N$ with distributions identical to that of X. If N is sufficiently large, then, according to the central limit theorem, the distribution of the sum $S_N = X_1 + X_2 + \cdots + X_N$ will be approximately normal with parameters $a = Nm$ and $\sigma^2 = Nv^2$.

In a normal distribution it is determined that:

$$\int_{a-3\sigma}^{a+3\sigma} p(x)dx = 0.997$$

[4.19]

Or in other words the probability that a random variable Z obtain a value differing from $E(Z) = a$ is less than 3σ, or:

$$P(a - 3\sigma < Z < a + 3\sigma) = 0.997$$

[4.20]

Using Equation 4.20 in the case of the sum S_N of random variables it is obtained:

$$P(Nm - 3v\sqrt{N} < S_N < Nm + 3v\sqrt{N}) \approx 0.997$$

[4.21]

Rearranging terms finally it is obtained:

$$P\left(\left|\frac{1}{N}\sum_{j=1}^{N} X_j - m\right| < \frac{3v}{\sqrt{N}}\right) \approx 0.997$$

[4.22]

Then if it is found N values of the random variable X, the arithmetic mean of these values will be approximately equal to m, the quantity that needs to be determined. Also the probability that the error of such approximation does not exceed the quantity $3v/\sqrt{N}$ is high and tends to zero when N increases.

4.2.3 *Pseudorandom numbers generation*

In this project, Matlab ® was used as an engine linked to Visual Basic ® to program the signature hole methodology including Monte Carlo method. In the programming stage, pseudorandom numbers were used to generate the random variables involved in the problem. Pseudorandom numbers differ from true random numbers in that they are generated by an algorithm, rather than a truly random process. However, the generated numbers are random in the sense that, on average, they pass statistical tests regarding their distribution and correlation. In this project, the function $randn$ was used to generate pseudorandom numbers from a normal distribution, using the algorithm called Mersenne Twister generator (Makoto Matsumoto., Takuji Nishiura., 1998).

By definition in Matlab®, the function $randn$ follows a normal distribution having a zero (0) mean and a variance equal to one (1). Figure 4.1 shows $randn$ function in Matlab®.

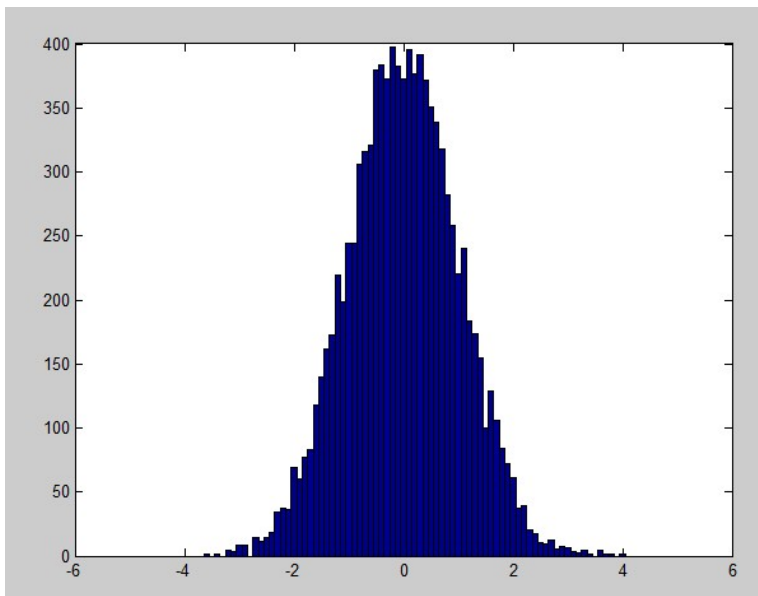

Figure 4.1 Histogram for the $randn$ function in Matlab®.

Next, a description about the introduction of the probabilistic approach in each of the stages of the signature waveform technique is given.

4.3 Seed waveform variability

As mentioned previously, all current methodologies using signature waveform technique assume that the signature wave does not change hole-to-hole. However, there are at least three reasons why the signature waveform hole-to-hole is not the same:

- Damage in the surrounding rock by previous holes;
- Difference in the distance and the path that vibration follows between the hole and the monitoring point;

- Variation in drilled hole, loading, contamination of explosives, priming effects, etc.

The first phenomena that affects the waveform hole-to-hole is related to the damage in the surrounding rock by previous holes. When a loaded hole is detonated, it changes the rock properties around the hole in a specific area. The extension of such area is a function of the initial conditions of the rock (i.e. rock joint system before detonation) as well as the geometry of the hole and the efficiency of the chemical energy transferred from the explosive to the rock. Accordingly, if the separation between holes S is enough to have no interference, the signature waveform from hole (i) will be equal to the signature waveform from hole (j) as show in Figure 4.2.

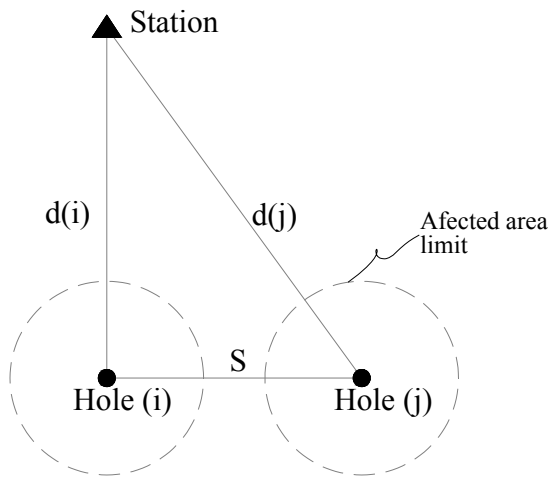

Figure 4.2 Signature hole reproducibility (adapted from Blair 1999)

If the affected area from hole (i) over lay or interfere with the affected area from hole (j), (i.e. the separation between holes S is such that affected areas interfere), there is a need to find a relationship to describe the nonlinear variation of the signature waveform hole-to-hole in a production blast event.

As previously mentioned, Yang and Scovira, (2009) propose the waveform's changes as a function of the ratio between the quantity of explosive already blasted to the quantity of explosive that produce the waveform:

$$s(\phi) = \lambda^{\phi} \qquad [4.23]$$

where

$$\phi = \frac{\omega_t}{\omega} \qquad [4.24]$$

ω_t total charge weight of earlier fired blast hole in the vibration path

ω charge weight of the presently firing charge, where $\lambda<1$

The limit conditions of this equation is given by

$$s(\phi) = \begin{cases} 1, & \phi \to 0 \\ 0, & \phi \to \infty \end{cases}$$

[4.25]

Field calibration of λ parameter and its the relation to the rock mass properties still is not well understood, despite the straightforward nature of Equation 4.23 and the intuitive correct meaning of the decrement in the amplitude of the vibration due to the detrimental quality of the rock mass as a result of previously blasted holes. Equations 4.23 to 4.25 are a good proposal to introduce a logical screening factor to reduce the amplitude of the waveform due to the damage of the rock mass. However such damage is considered only in the direction of the monitoring point and do not take into account that the cracks due to the explosion of previous holes should grow in all directions and the energy release by later holes can be affected by previous detonated holes, even if they are not in the vibration path.

The second reason why the waveform should change is due to the difference in the distance and the path that the vibrations follow between the hole and the station or monitoring point as shown in Figure 4.2 (i.e. the distances $d(i)$ and $d(j)$ are different for the full-blast situation). Blair (1999) proposed, using weight scaling laws, a methodology to take into account the change in the amplitude of the seed waveform, due to the variability of the distance between the holes and the specified monitoring vibration location point in a full-blast. According to the traditional weight scaling law, the vector peak particle velocity $vppv$ is given by the relation between distance d, charge weight W and the geology constants a and b as:

$$vppv = a(SD)^{-b}$$

[4.26]

Where SD is defined as:

$$SD = \frac{d}{\sqrt{W}}$$

[4.27]

As explained, despite of all limitations of Equation 4.26, this equation can be used to scale numerically the seed waveform for each blast hole in a full blast event. (Blair 1999).

To establish the proper values of the parameters a and b in Equation 4.26, it is recommended to develop a curve SD vs $vppv$ for signature holes. From these graphs, a and b coefficients can be established for a particular site. These correlated parameters will result in over estimation of the $vppv$ because isolated blast holes are usually fired in virgin ground (Blair, 1999) in contrast to ground previously affected by production blasting as in the real mining situation. For this reason, it is desirable to get the seed waveform in the most representative working conditions (along to one of the production shots). Finally, if there is information regarding signature holes, i.e. vibration records for a single blast hole, it is possible to use Monte Carlo schemes adjusting the values of a

and *b* and choosing the most representative value of these parameters for particular ground conditions.

4.3.1 *Modeling of changes in signature waveform*

In this research, a methodology for varying the signature waveform hole-to-hole was developed. This approach takes into account the change in both main parameters of the seed waveform amplitude and frequency. Notice that current methodologies only modify amplitude in the waveform hole-to-hole. The methodology is based on the main characteristics of any recorded signature waveform and the use of Fourier series to approach one equation to produce different waveforms for each hole in the vibration prediction process. Involving the change in amplitude and frequency of the waveforms, it is expected that changes in the surrounding material to the detonated hole, changes in the path from hole to monitoring point and variations in explosive output due to drilling and loading procedures be involved in the prediction process.

During the development of this research, several field blast tests were performed in order to study the variability of the signature waveform in a mining production blast event. Several tests were performed at the Guyan surface coal mine in West Virginia during the summer of 2011 for validation of models.

The rock mass is comprised of layers of sandstone and shales. It is possible to see in Figure 4.3 the geometrical arrangement used to do the test.

Figure 4.3 General view of the tested area

In total, 11 holes of 7.875 inch diameter were detonated. The depth of all holes was 42ft and the spacing and burden used was 15ft and 17ft, respectively. The main objective was to collect a series of signature holes combined with the detonation of two or more holes using delays with timing lower than 8ms. To have better control over the timing, electronic detonators were used. In this test, six holes were detonated using delay timing between holes of 5ms, followed by two signature holes. After the two signature holes, two holes using 5ms delay were detonated and finally a signature hole was detonated. In summary, in this test there are three signature holes and two sequences of

holes delayed by 5ms, the first sequence was composed by six holes while the second was composed by two holes.

Figure 4.4 shows the plan layout of the test indicating the signature holes, the sequence number and the timing used. The layout was generated using actual GPS surveyed locations for each hole.

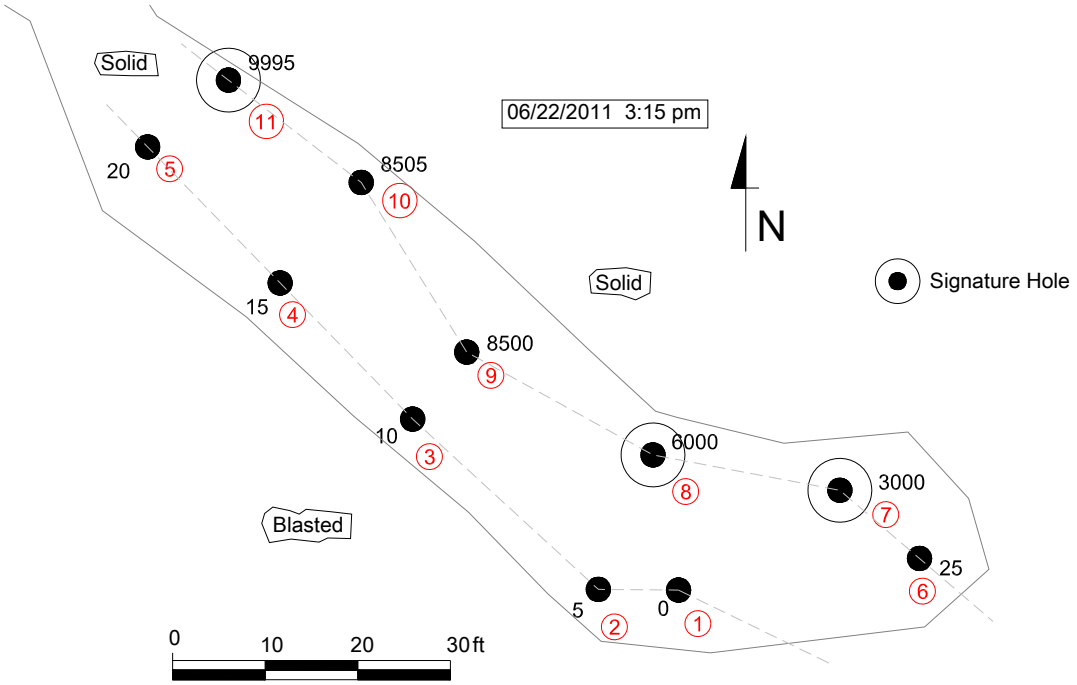

Figure 4.4 Test plan layout

Along with the blast test, a seismograph network was setup at the mine. Figure 4.5 shows the location of the seismographs and the area where the test was performed (blasting area summer 2011 in the map).

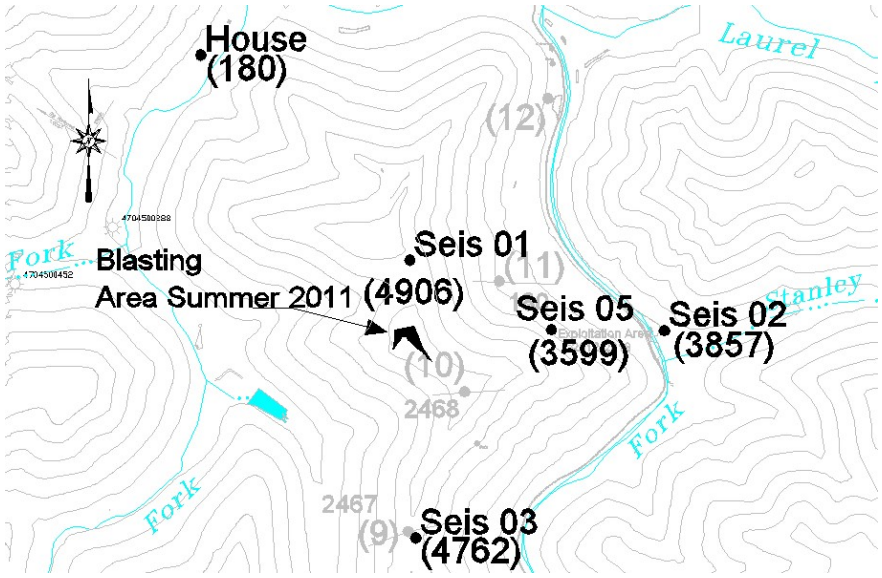

Figure 4.5 Seismograph network at Guyan mine

The detailed analysis of the signature waveform variability and modeling was performed for seismograph 01. However, this analysis is valid for any waveform. Seismograph 01 was located 210m (689 ft) from the blast area.

The complete waveform for the closest seismograph (seismograph 01) and three components (radial, traversal and vertical) are included in Figure 4.6.

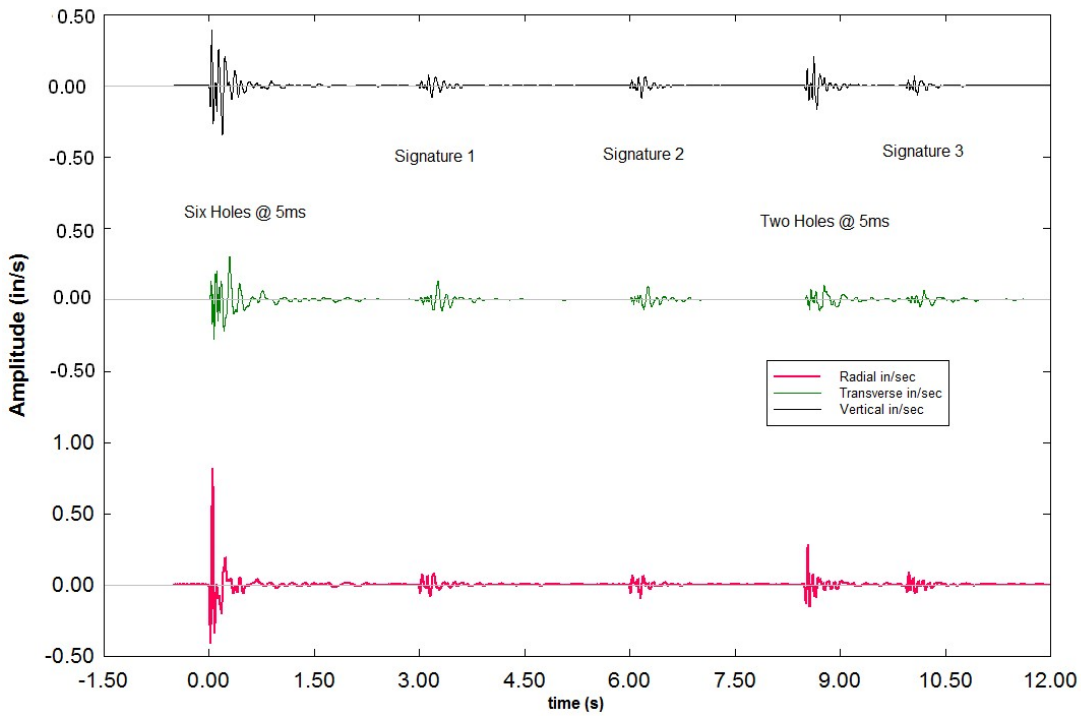

Figure 4.6 Complete signature waveform three components

Figure 4.6 shows clearly three signature waveforms and two other blast series. To develop the approach of simulating the signature waveform using Fourier series, the radial component was chosen; however this procedure can be used for any other vibration component (vertical or traverse).

First, a comparison between signature holes was performed. Such comparison was done in both time domain and frequency domain. Comparing the waveforms and the frequency content of the signatures it is possible to see how similar or dissimilar the signatures waveforms are. This also sheds light on the validity of the assumption regarding the invariability of the waveform used in the current signature hole vibration modeling techniques.

4.3.1.1 Signature waveform comparison

The radial component was used to develop the approach of simulating the signature waveform using Fourier series. Figure 4.7 shows the complete record for the test in this direction.

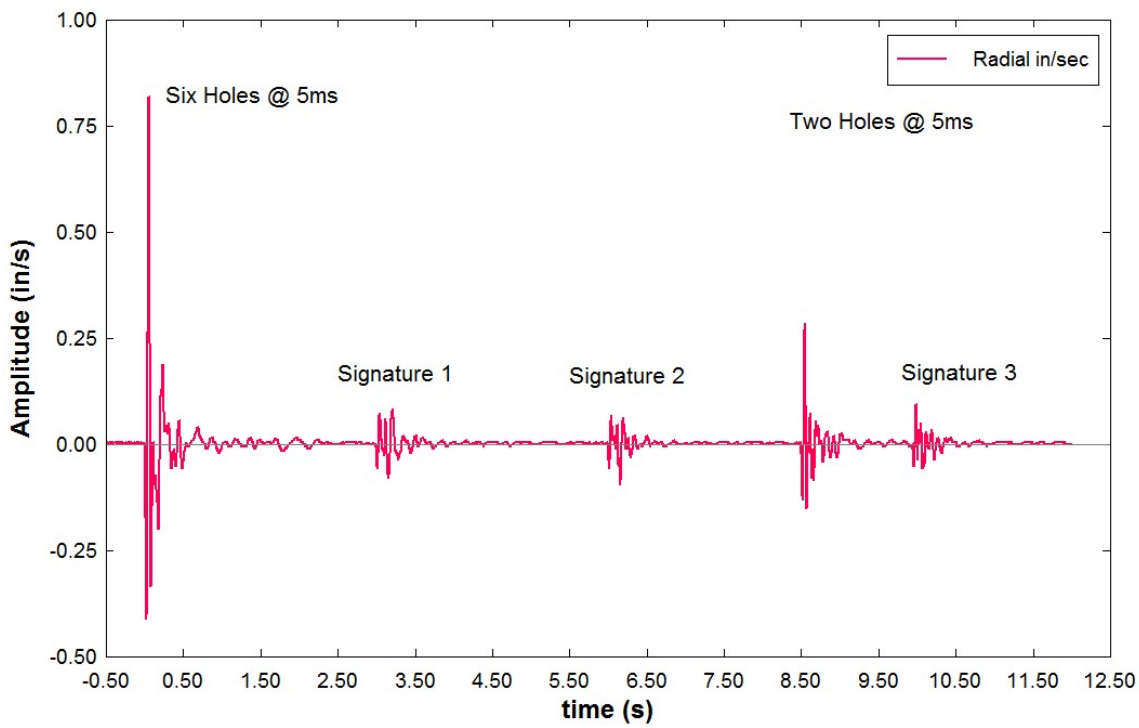

Figure 4.7 Complete waveform, Radial component Seismograph 01

Figure 4.8 is obtained when signature waveforms are isolated from the complete record and compared. They are placed on the same time domain to compare shapes and amplitudes.

It is possible to see in Figure 4.8 how the signatures waveforms change while the total blast is progressing. The maximum positive peak occurs for signature 3, after 10 holes have been detonated. In this test, the maximum positive peak is between 0.07 and 0.095 in/s (signature 2 and 3 respectively). For the positive peaks, the range is 0.025 in/s of variation. On the other hand, the maximum negative peak is reached in the signature 2 and the range for the negative amplitude is 0.04 in/s of variation.

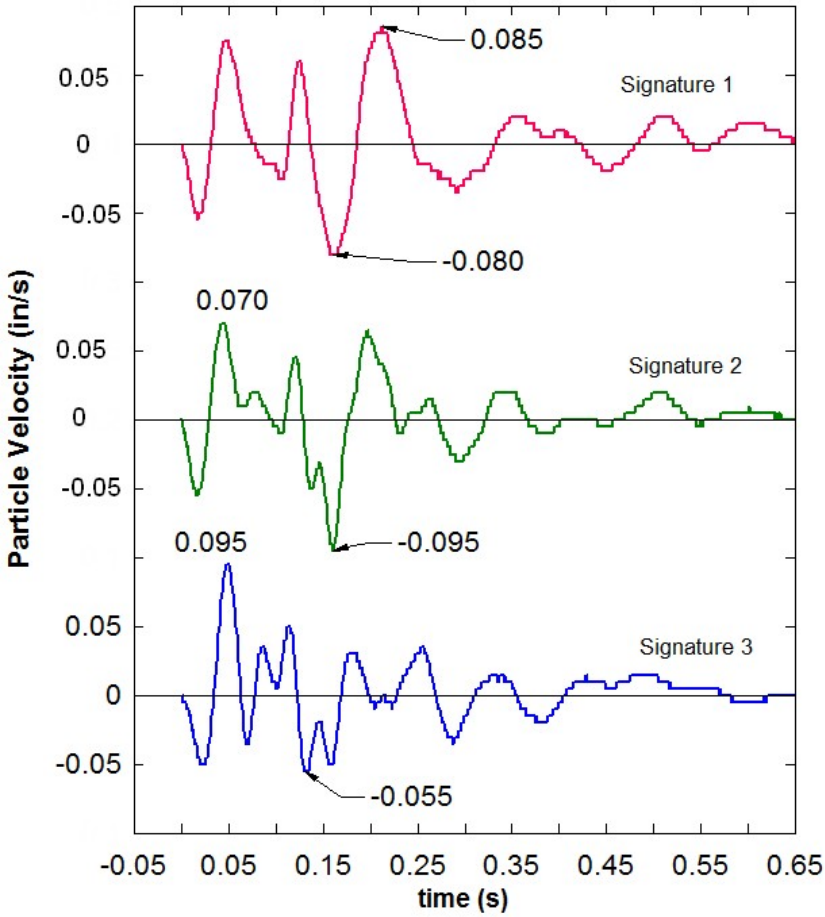

Figure 4.8 Signature waveform comparison

The maximum negative peaks are -0.095 and -0.055 in/s, presented in signature 2 and 3 respectively. In this test, the intermediate values for the amplitude of the waveform (positive and negative) are found in signature 1.

Signature 3 is characterized by the highest vibration output for many reasons. As shown in Figure 4.4, signature hole 3 (corresponding to hole 11) is the most confined and nearest hole to the monitoring point. Two factors (confinement and distance) result in the phenomenon that signature 3 produces the maximum vibration output in this test. Other factors that could have led to this outcome include different geologic paths from the source to the monitoring point and different energy output of each hole due to hole loading, explosive composition and/or contamination, priming etc. These factors result in

varying waveforms generated for each hole, making the waveform produced by each hole a somewhat random process within a given range.

Figure 4.9 shows the frequency content of the three signals. This representation of the signals reflects how the energy content of the signals (area under the curve) is diminishing while the blasting is progressing, meaning that the last blast (signature 3) applies lower energy to the ground than the other two signature holes. This behavior is expected because the energy applied by the explosion to the ground that becomes vibration is lower as the quality of the rock is also diminishing. Even though the three curves are not equal, it is possible to distinguish the same four frequency zones for the three spectrums. Such zones are defined as the zones where the spectral amplitude peaks are reached. The frequency limits for the zones are (Figure 4.9): between 0 and 9 Hz, from 9 to 12, from 12 to 17 and frequencies greater than 17 Hz.

The variation of the peak frequency content between the three curves inner to each zone is low for example for zone 1 the peak frequency is between 6.68 to 7.01 Hz, zone 2 between 10.70 to 10.74, zone 3 between 13.05 to 13.74 and in zone 4, where most variability in the peak frequency content is presented, ranging between 22.09 to 30.20 Hz.

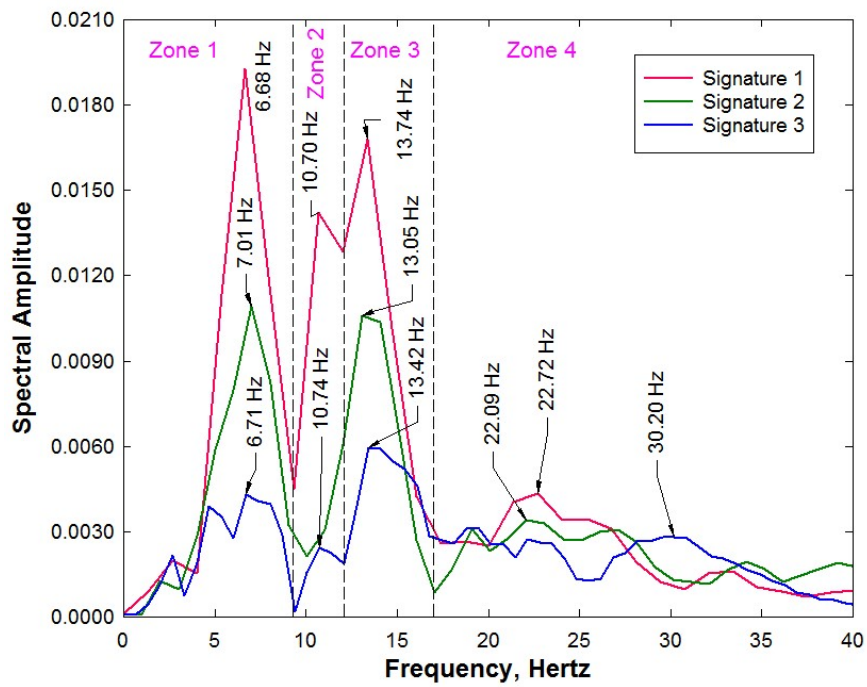

Figure 4.9 Frequency content of the signals and four frequency zones

After analyzing time vs particle velocity and the spectral content of the signals some conclusions about the data set can be drawn as follows:

a. There are some similarities between the three waveforms such as the time where peaks are reached in the time vs particle velocity curve.

b. Signature 1 and signature 2 are similar but signature 3 is different from the other two.

c. Energy content of signature 3 is the lowest but one of the highest particle velocity.

d. There are changes in the peak amplitude of the particle velocity between the three signals and there is not a clear trend in the values of the peaks while the blast is progressing.

e. For the three signals, it is possible to divide the curve frequency vs spectral amplitude in four zones.

Using the methodology proposed by Yang (2010), it is possible to reduce the amplitude of the particle velocity while the blast is progressing, but that trend is based on the assumption of lower values of particle velocity through the blasting process. Also in that proposal, the holes should be in the same vibration path, so in this particular case screening equations of Yang and Scovira (2010), are not useful. Finally, varying the amplitude without varying the frequency content between holes in a blast event may not provide optimized model simulations.

4.3.1.2 Fourier series and Signature Waveform

Using Fourier series, it is possible to express any arbitrary periodic function as a sum of sine and cosine terms. In other words, Fourier series can be used to express a function in terms of the frequencies (harmonics) that it is composed of. The representation of such function $f(t)$ is given by:

$$f(t) = c_o + \sum_{n=1}^{\infty} \left\{ a_n * sin\left(\frac{2\pi nt}{T}\right) + b_n * cos\left(\frac{2\pi nt}{T}\right) \right\}$$

[4.28]

Where:

$$c_o = \frac{1}{T}\int_0^T f(t) * dt$$

[4.29]

$$a_n = \frac{2}{T}\int_0^T f(t) * sin\left(\frac{2\pi nt}{T}\right) * dt$$

[4.30]

$$b_n = \frac{2}{T}\int_0^T f(t) * cos\left(\frac{2\pi nt}{T}\right) * dt$$

[4.31]

In order to express $f(t)$ in terms of sin function, from:

$$a * \sin(2\pi f t) + b * \cos(2\pi f t) = A * \sin(2\pi f t + \emptyset)$$

[4.32]

Where:

$$A = \sqrt{a^2 + b^2}$$

[4.33]

And

$$\emptyset = tan^{-1}\left(\frac{a}{b}\right)$$

[4.34]

Finally we can express the function $f(t)$ as:

$$f(t) = c_o + \sum_{n=1}^{\infty}\left\{A_n * sin\left(\frac{2\pi n t}{T} + \emptyset_n\right)\right\}$$

[4.35]

As an example, signature 1 is expressed using Fourier series. Figure 4.10 shows signature 1 isolated from the complete record.

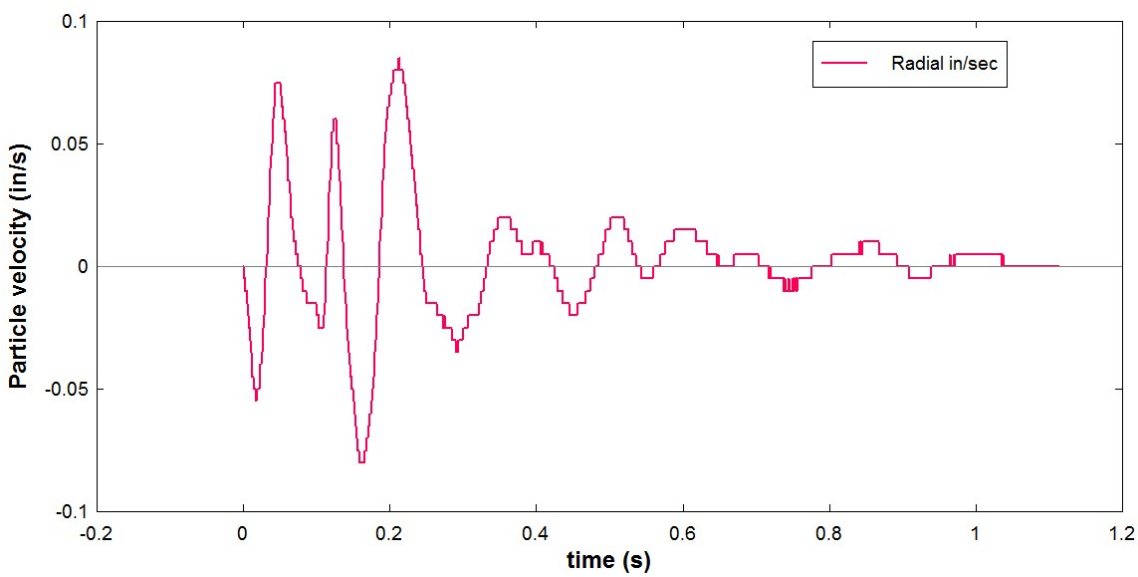

Figure 4.10 Signature 1 Isolated from complete record (Radial component)

Fourier series is used for periodic functions, however if we take a period T equal to 1 second for Figure 4.10, we will reproduce the complete waveform every second. After one second, the complete waveform will repeat itself in a periodic manner. Using Equation 4.28 to Equation 4.35, Figure 4.11 is the value of the amplitudes A_n (Equation 4.33) of the Fourier series coefficients (a_n, b_n) given by the Equation 4.30 and Equation 4.31 respectively. In Equation 4.28 the quantity of coefficients to calculate are infinite, however this example will use 25 coefficients to reproduce the signature 1 waveform.

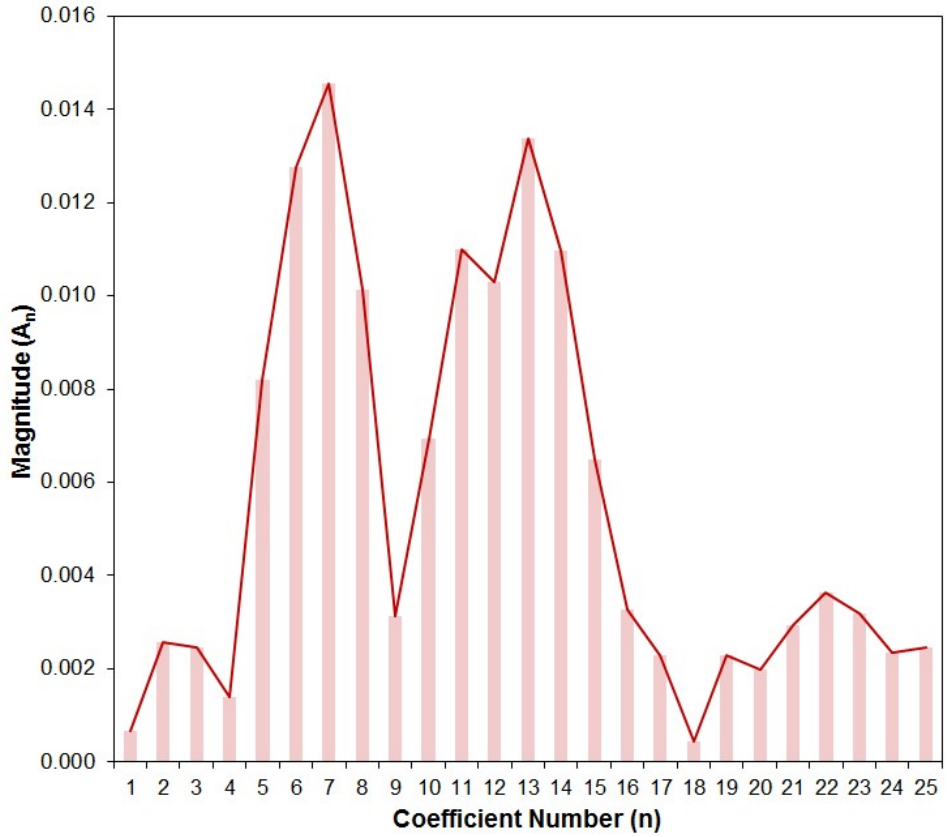

Figure 4.11 Magnitude coefficients from Fourier series

Figure 4.11 shows the amplitude calculated for each coefficient in the Fourier series, as mentioned before; the first 25 coefficients of the series were included. As expected, the shape of Figure 4.11 is similar to the Fourier Transform (FT) of the signal.

If the magnitude of the coefficients of the Fourier series is plotted in the same graph that the Fourier Transform, Figure 4.12 is obtained. In Figure 4.12 the two curves are not exactly the same because Equation 4.28 is an approximation to the "real" signal.

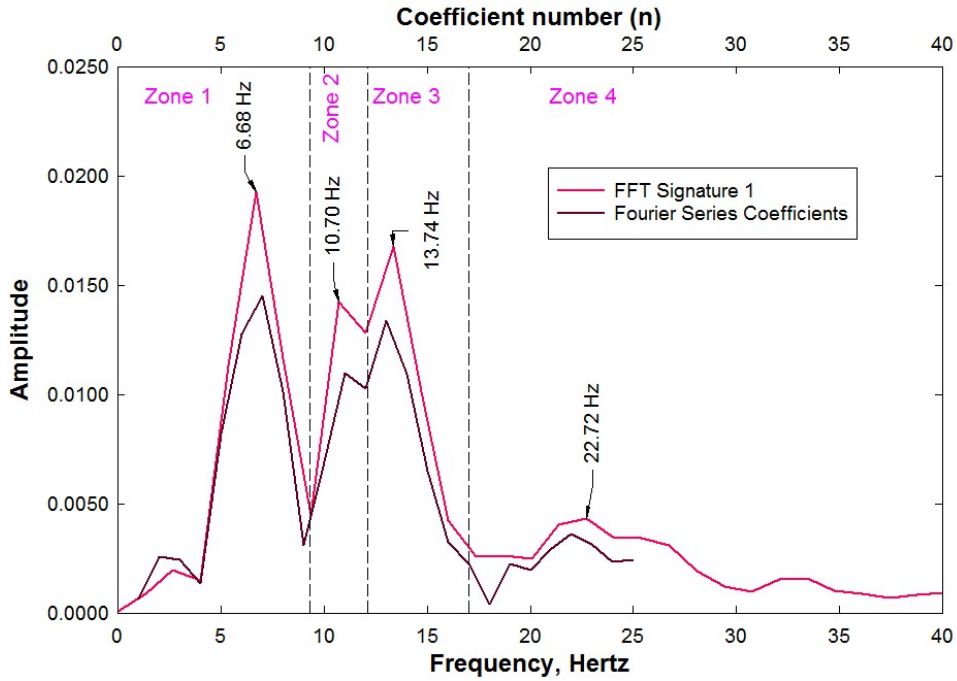

Figure 4.12 FFT and magnitude coefficients from Fourier series

Using Equation 4.28 and considering 25 coefficients in the series, for a period of two seconds we get the signal included in Figure 4.13.

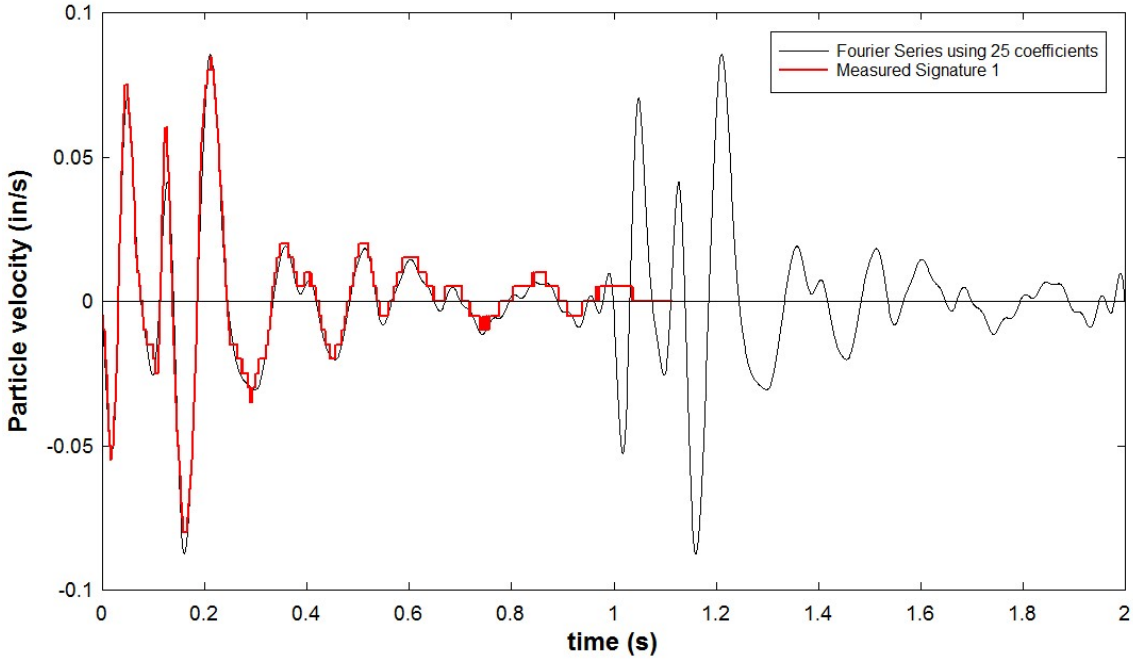

Figure 4.13 Fourier series and signature 1

Using Fourier series we have expressed the waveform of signature 1 using 25 terms in the Equation 4.28. Because this mathematical approach is for periodic signals, after 1 second the waveform repeats itself (same shape) and so on.

The objective in this research is to find the manner to reflect the changes in amplitude and frequency content of the signature waveform while the blast is progressing. Using Fourier series it is possible to find a mathematical expression for any wave form (in this case signature 1). The mathematical expression using 25 coefficients to reproduce signature waveform 1 is given as follows:

$$
\begin{aligned}
f(t)=&-0.000569014*\sin(2\pi*1*t)-0.000329002*\cos(2\pi*1*t)+0.002375264*\sin(2\pi*2*t)+0.000995719*\cos(2\pi*2*t)-\\
&0.002352615*\sin(2\pi*3*t)-0.000701881*\cos(2\pi*3*t)+0.001387061*\sin(2\pi*4*t)-\\
&0.000000666794*\cos(2\pi*4*t)+0.005975067*\sin(2\pi*5*t)+0.005620938*\cos(2\pi*5*t)+0.012204136*\sin(2\pi*6*t)-\\
&0.003749628*\cos(2\pi*6*t)-0.003956133*\sin(2\pi*7*t)-0.014002077*\cos(2\pi*7*t)-\\
&0.010074869*\sin(2\pi*8*t)+0.001179089*\cos(2\pi*8*t)-\\
&0.00125038*\sin(2\pi*9*t)+0.002866379*\cos(2\pi*9*t)+0.006366558*\sin(2\pi*10*t)+0.00276112*\cos(2\pi*10*t)+0.002\\
&493979*\sin(2\pi*11*t)-0.010698109*\cos(2\pi*11*t)-0.002414689*\sin(2\pi*12*t)-0.010005432*\cos(2\pi*12*t)-\\
&0.011576997*\sin(2\pi*13*t)-0.006731543*\cos(2\pi*13*t)-0.010293074*\sin(2\pi*14*t)+0.003760148*\cos(2\pi*14*t)-\\
&0.003702589*\sin(2\pi*15*t)+0.005326388*\cos(2\pi*15*t)-0.000832484*\sin(2\pi*16*t)+0.003166004*\cos(2\pi*16*t)-\\
&0.00101238*\sin(2\pi*17*t)+0.00204019*\cos(2\pi*17*t)-0.000367028*\sin(2\pi*18*t)+0.000253124*\cos(2\pi*18*t)-\\
&0.002068963*\sin(2\pi*19*t)+0.000968006*\cos(2\pi*19*t)-0.001672375*\sin(2\pi*20*t)+0.001087871*\cos(2\pi*20*t)-\\
&0.002401597*\sin(2\pi*21*t)+0.001691553*\cos(2\pi*21*t)-0.001971521*\sin(2\pi*22*t)+0.003042045*\cos(2\pi*22*t)-\\
&0.000515622*\sin(2\pi*23*t)+0.003129975*\cos(2\pi*23*t)+0.000724683*\sin(2\pi*24*t)+0.002240419*\cos(2\pi*24*t)+0\\
&.001364853*\sin(2\pi*25*t)+0.002051513*\cos(2\pi*25*t)
\end{aligned}
\qquad [4.36]
$$

Using software, it is possible to use any number coefficients in the Fourier Series to find the mathematical expression that represent any signature waveform. In order to simplify the mathematical development included in the next section, only four frequencies were used to find the approach equation.

4.3.1.3 Signature Waveform approach based on Fourier series

The main characteristics observed in the signatures waveforms from the field test are:

1. It is possible to determine for all signatures the zones where peak frequencies are presented. The main characteristic of those frequency zones is that they are the same for all signatures. The peaks frequencies within those zones for different signatures are similar. (Figure 4.9)
2. There is not a clear trend regarding the maximum amplitude of the signature waveform while the blast is progressing. However the peak values (positive and negative) are in a narrow range. (Figure 4.8)
3. It is a fact that after some time the blast vibration attenuate, in contrast to Fourier series where the waveform is repeated itself each period of time T.

Based on these characteristics, the general guidelines to approach a simplified function to represent the signature waveform are presented next.

a. Main frequency content of the signal and number of Fourier coefficients

From a mathematical point of view, it is possible to establish the number of coefficients in the Fourier series that are good enough to have a good simulation of a function. In that case, if $F(t)$ is a simulation of $f(t)$, the number of coefficients N in the simulation is such that the error between $F(t)$ and $f(t)$ is minimum. In other words:

$$F(t) = c_o + \sum_{n=1}^{N} \left\{ \alpha_n * sin\left(\frac{2\pi nt}{T}\right) + \beta_n * cos\left(\frac{2\pi nt}{T}\right) \right\}$$

[4.37]

and the error given by:

$$E = \frac{2}{T} \int_0^T (f(t) - F(t))^2 dt$$

[4.38]

should be minimum. In the current simulation, the proposal is to take the number of coefficients equal to the main frequencies of the signal (however it is possible to use a large number of frequencies if the shape of the waveform is complicated).

Following the assumptions, for example in the case of signature 1, the frequencies used to calculate their coefficients in the Fourier series are 6.68, 10.70, 13.74 and 22.72 Hz (Figure 4.12).

Calculations for the first frequency

The first frequency corresponds to 6.68 Hz. A time interval of 1 second is assumed in order to perform the integral for the coefficients so:

$c_o = \frac{1}{T} \int_0^T f(t) * dt$ = 0.002353

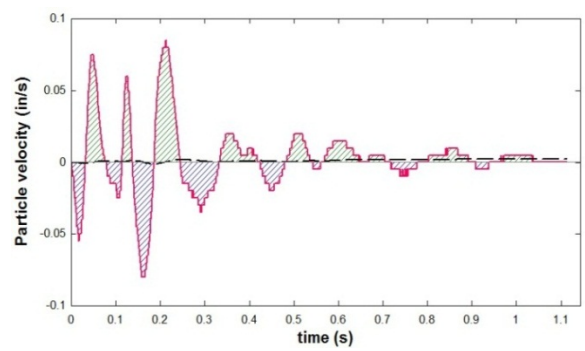

$$a_n = 2 \int_0^T f(t) * sin(2\pi 6.68t) * dt$$

=2* 0.0012836 = 0.0025672

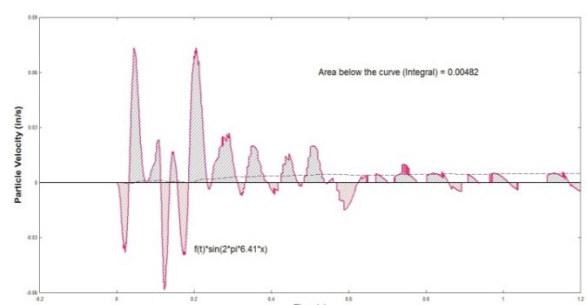

$$b_n = 2\int_0^T f(t) * cos(2\pi 6.68t) * dt$$

=2* - -0.008023 = -0.016046

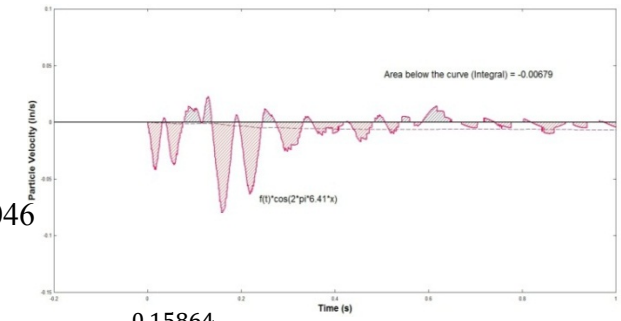

Phase calculation:

$\emptyset = tan^{-1}\left(\frac{0.0025672}{0.016046}\right) = 0.15864$; $\frac{0.15864}{\pi} = 0.05049$; $0.05049 - 0.5 = -0.4495 * \pi$

So the term for the frequency of 6.68 Hz is:

$$Term_{6.68\,Hz} = 0.01625 * \sin(2\pi * 6.68 * t - 0.4495\pi)$$

[4.39]

Equation 4.39 is the sin, cos component expressed using amplitude, A, and phase, $\emptyset$, from Equation 4.35 for the frequency at 6.68 Hz.

Calculations for the others frequencies

Following the same procedure, the results for the frequencies of 10.70, 13.74 and 22.72 Hz are presented next.

Frequency of 10.70 Hz

$a_n = 2 * 0.003646 \quad = \quad 0.007292$

$b_n = 2 * -0.004386 = -0.008772$

$\emptyset = tan^{-1}\left(\frac{0.007292}{0.008772}\right) = 0.69352$; $\frac{0.69352}{\pi} = 0.22075$; $0.22075 - 0.5 = -0.27924 * \pi$

$$Term_{10.70\,Hz} = 0.01140 * \sin(2\pi * 10.70 * t - 0.27924\pi)$$

[4.40]

Frequency of 13.74 Hz

$a_n = 2 * -0.00591 \quad = -0.01182$ -0.011631

$b_n = 2 * 0.0009114 = 0.0018228$ 0.0016649

$\emptyset = tan^{-1}\left(\frac{0.01182}{0.0018228}\right) = 1.4177$; $\frac{1.4177}{\pi} = 0.45129$; $0.45129 + 0.5 = 0.95129 * \pi$

$$Term_{13.74\,Hz} = 0.01196 * \sin(2\pi * 13.74 * t + 0.9513\pi)$$

[4.41]

Frequency of 22.72 Hz

$a_n = 2 * -0.0002039 \quad = -0.0004078$

$b_n = 2 * 0.0015031 = 0.0030062$

$$\emptyset = tan^{-1}\left(\frac{0.0004078}{0.0030062}\right) = 0.13483; \quad \frac{0.13483}{\pi} = 0.04291; \quad 0.04291 + 0.5 = 0.5429 * \pi$$

$$Term_{22.72\ Hz} = 0.003033 * \sin(2\pi * 22.72 * t + 0.5429\pi) \qquad [4.42]$$

When Equation 4.39 to Equation 4.42 are together, the base equation to represent the waveform of the signature 1 given by:

$$f(t) = 0.002353 + 0.01625 * \sin(2\pi * 6.68 * t - 0.4495\pi) + 0.01140 * \sin(2\pi * 10.70 * t - 0.27924\pi) + 0.01196 * \sin(2\pi * 13.74 * t + 0.9513\pi) + 0.003033 * \sin(2\pi * 22.72 * t + 0.5429\pi) \qquad [4.43]$$

When this equation is plotted against the signature waveform measured in the blast test, Figure 4.14 is obtained.

Different from a Fourier series using 25 coefficients (Equation 4.36), Equation 4.43 is a rough approximation to the measured waveform, so there is not a perfect match between two curves.

To improve the approximation, a decay factor is included to restrain the waveform to the duration time of the vibration (one second in this case) and one amplitude scale factors to match the amplitude of the waveform in the maximum peak.

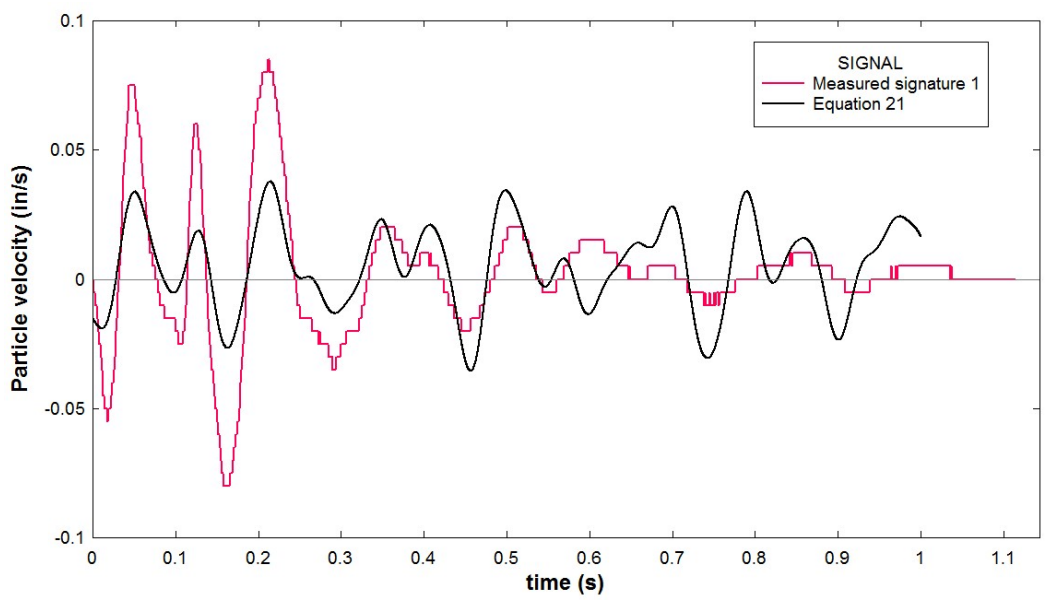

Figure 4.14 Measured signal Vs base equation

b. Decay factor calculation

As previously mentioned, after certain time, the blast vibration should decays to zero. However and due to the nature of the Fourier Series, using the mathematical expression, the signal repeats itself in a period T of time (see Figure 4.13). The decay factor is necessary to avoid that problem. To calculate the mathematical expression for decay, an exponential trend line is used to envelope the positive peaks of the waveform. Figure 4.15 show the signature 1 waveform, the envelope and the exponential decay trend line.

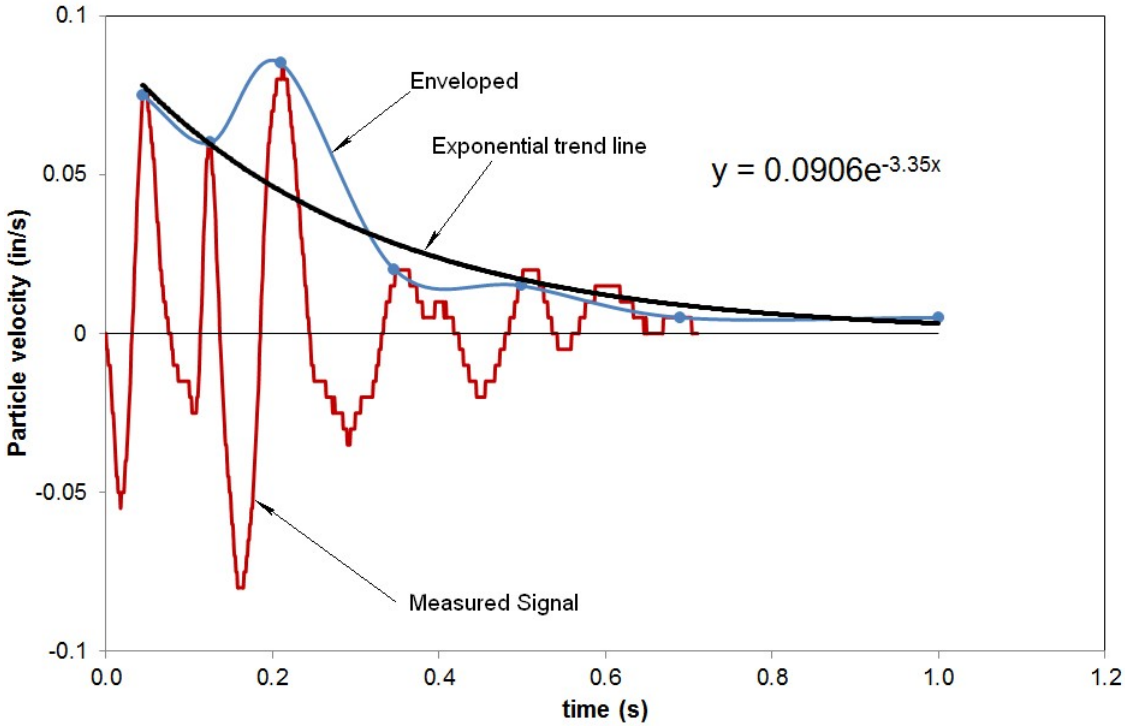

Figure 4.15 Exponential decay calculation

Figure 4.15 shows the decay factor, for signature 1 waveform the value of the decay exponent estimated is -3.35. Now a modification to Equation 4.43 is made, introducing the exponential decay, this results in Equation 4.44:

$$f(t) = (0.002353 + 0.01625 * \sin(2\pi * 6.68 * t - 0.4495\pi) + 0.01140 * \sin(2\pi * 10.70 * \mathrm{t} - 0.27924\pi) + 0.01196 * \sin(2\pi * 13.74 * \mathrm{t} + 0.9513\pi) + 0.003033 * \sin(2\pi * 22.72 * \mathrm{t} + 0.5429\pi)) * \boldsymbol{e}^{-3.35*t} \quad [4.44]$$

Figure 4.16 show Equation 4.44 when it is compared against to the measured signal.

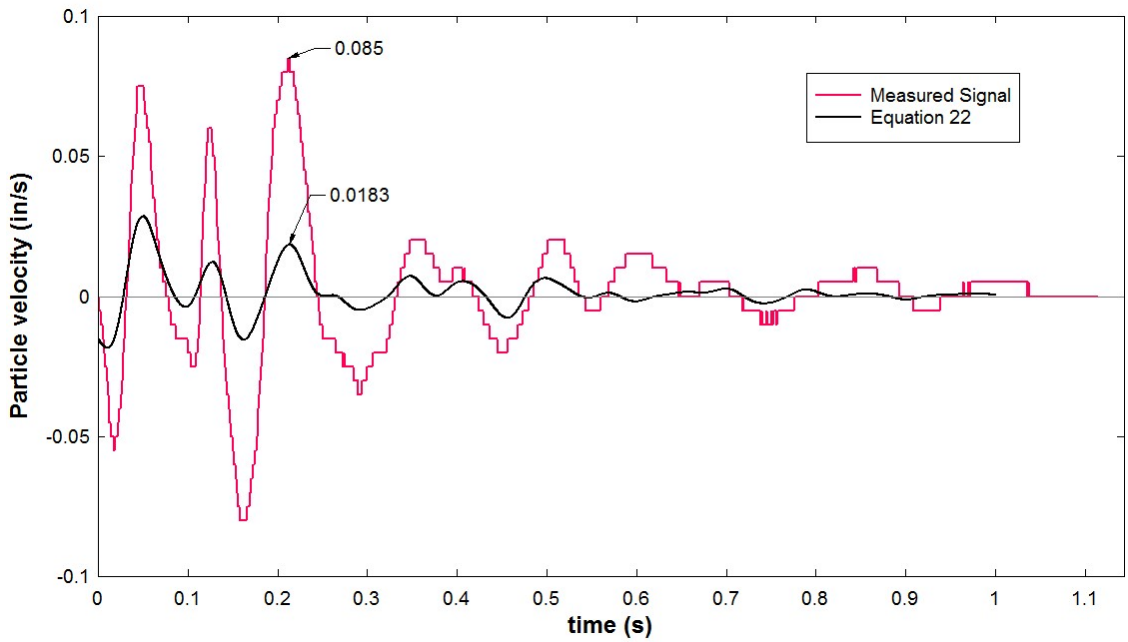

Figure 4.16 Measured signal Vs base equation including exponential decay factor

c. Amplitude factor calculation

Finally, matching the peak value of the measured signal and the amplitude of the curve given by Equation 4.44 at the time when the peak of the measured signal is reached, it is possible to calculate the amplitude scale factor given by:

$$ASF = \frac{0.085}{0.0183} = 4.64$$

[4.45]

Figure 4.17 show the adjusted equation after match the maximum amplitude.

$$\begin{aligned} f(t) = \mathbf{4.64} * (&0.002353 + 0.01625 * \sin(2\pi * 6.68 * t - 0.4495\pi) + 0.01140 \\ &* \sin(2\pi * 10.70 * \mathrm{t} - 0.27924\pi) + 0.01196 \\ &* \sin(2\pi * 13.74 * \mathrm{t} + 0.9513\pi) + 0.003033 \\ &* \sin(2\pi * 22.72 * \mathrm{t} + 0.5429\pi)) * \boldsymbol{e^{-3.35*t}} \end{aligned}$$

[4.46]

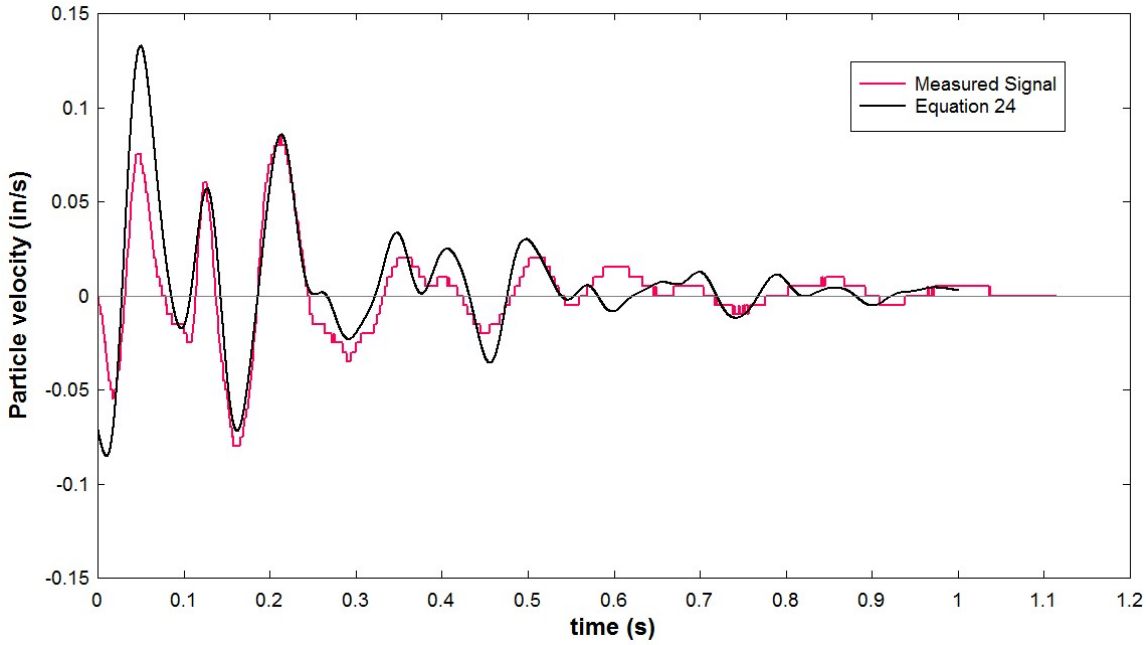

Figure 4.17 Measured signal Vs final approach

When measured signal and Equation 4.46 are deducted following the procedure previously described, a good correlation between both curves is clearly observable. When a cross correlation is used to measure the differences between the measured signature waveform and the approach or simulated waveform a coefficient of 0.85 is obtained (one is perfect correlation or exact waveform between two signals when they are compared). Next, it is necessary also to compare the signals in frequency domain.

Comparison in frequency domain

It is necessary to compare both signals, measured and approximated, in frequency domain in order to see if the approximation keeps the energy content of the measured signal. Figure 4.18 shows the frequency content comparison.

Figure 4.18 shows the similarity between both signals in frequency domain. The dominant frequencies in the approximated signal keep the peak values of the measured signal and they are between the zones previously defined (Zone 1 to Zone 4).

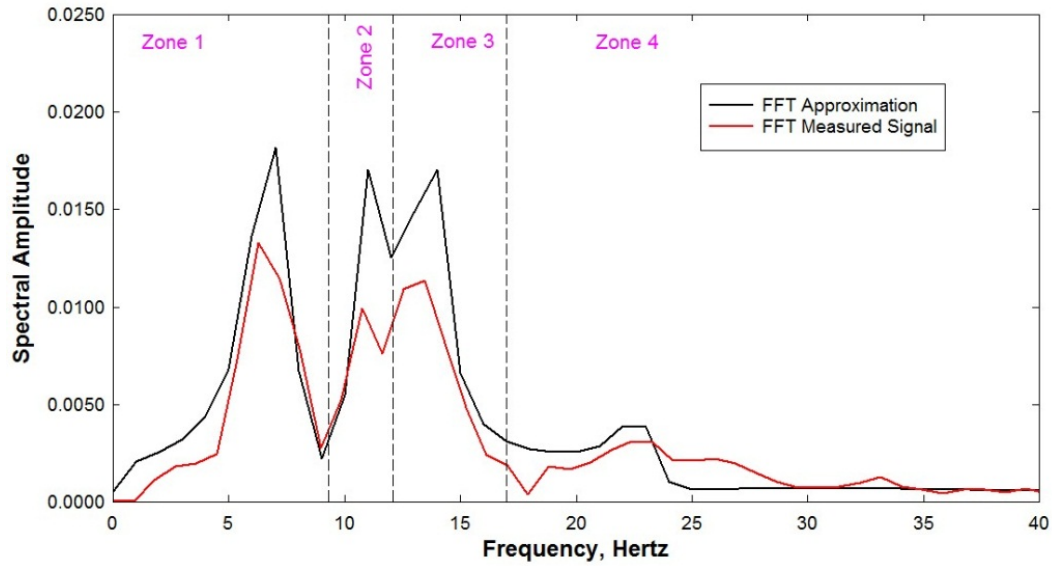

Figure 4.18 Frequency domain comparison

Bigger values in the peaks of the approximated signal means that the approximated signal carries more energy content than the measured signal this is evident when the signals are compared in the time domain.

In conclusion, in this research a basic equation base on Fourier series to approach the signature waveform is proposed. The equation (Silva-Lusk equation) has the general form:

$$f(t) \approx \left[c_o + \sum_{n=1}^{m} \boldsymbol{ASF_m} * \{A_m * sin(2\pi * \boldsymbol{frequency_m} * t + \emptyset_m)\}\right] * e^{-\boldsymbol{decay\ factor} * \boldsymbol{t}}$$

[4.47]

where:

ASF_m:	amplification scale factor for frequency m.
c_o:	first term in the Fourier series
m:	number of frequencies chose to approach the measured signature waveform.
A_m:	amplitude coefficient for frequency m in the Fourier series
$frequency_m$:	frequency value chose to approach the measured signature waveform.
t:	time
$\emptyset_m$:	phase for frequency m
$decay\ factor$:	factor related to the attenuation energy in that particular monitoring point.

To introduce the variability hole-to-hole in the signature waveform, there are three parameters where it was assumed to follow a random normal distribution behavior;

they are the amplification scale factor, frequency content of the signal and decay factor. The formulation is as follows:

$$ASF_m = \overline{ASF_m} + randn * Std(ASF_m)$$

$$frequency_m = \overline{frequency} + randn * Std(frequency)$$

$$Dec_{fact} = \overline{Dec_{fact}} + randn * Std(Dec_{fact})$$

[4.48]

Where:

$\overline{ASF}, \overline{frequency}, \overline{Dec_{fact}}$:	mean values for the parameters in Equation 4.47
$Std(ASF), Std(frequency), Std(Dec_{fact})$:	standard deviation for the parameters in Equation 4.47
$randn$:	pseudorandom values drawn from the standard normal distribution

Using Equation 4.47 and Equation 4.48, a random signature waveform is generated for each hole in the modeling process of the complete waveform from a specific production blast. In vibration modeling using the proposed approach, there are two scenarios; the first one where there is only one record for the signature waveform. In such case, it is necessary to assume all the statistical parameters in Equation 4.48.

If there are not statistical values for Equation 4.48, it is possible to assess at least one value for $ASF, frequency\ and\ DEC_{fact}$ from the signature signal. To proceed to use the current proposal, a standard deviation equals to one third of the estimated value for $ASF\ and\ DEC_{fact}$ is proposed. On the other hand, for the frequency, it is proposed to assume a standard deviation value equal to the lower boundary of the zone where the main frequency for that zone is present. This concept for the assumption of the frequency is explained in Figure 4.19.

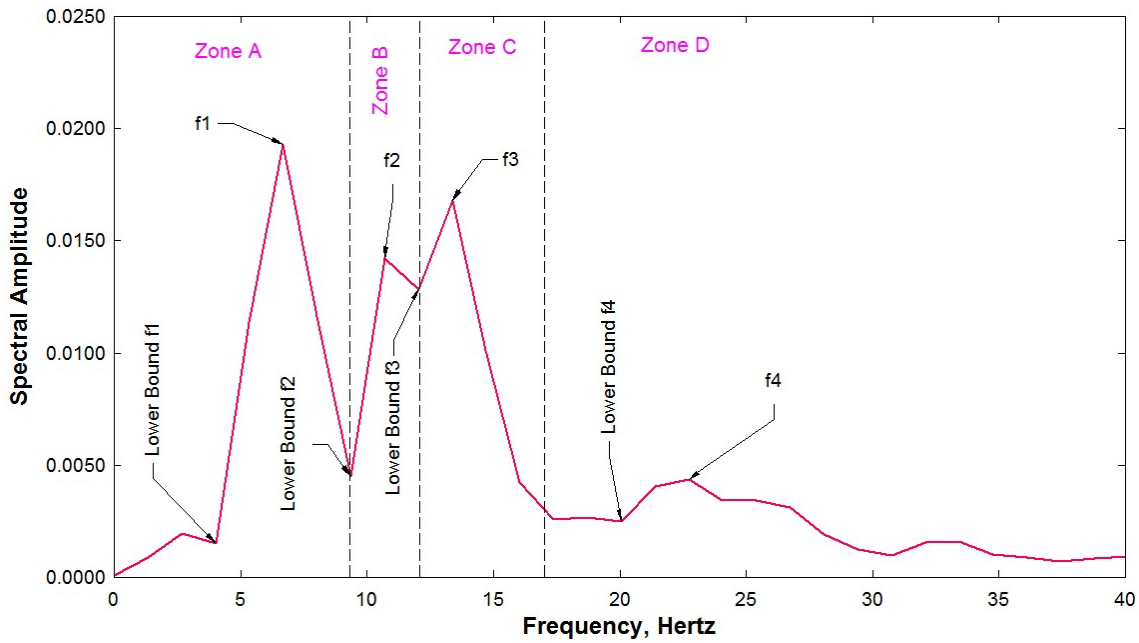

Figure 4.19 Frequency parameter for Equation 4.48

In Figure 4.19, there are four zones and four main frequencies. In this case, the statistical parameters for frequency parameter in Equation 4.48 are given by:

$$\begin{aligned} frequency_1 &= f_1 + randn * (f_1 - Lower\ Bound\ f_1) \\ frequency_2 &= f_2 + randn * (f_2 - Lower\ Bound\ f_2) \\ frequency_3 &= f_3 + randn * (f_3 - Lower\ Bound\ f_3) \\ frequency_4 &= f_4 + randn * (f_4 - Lower\ Bound\ f_4\ ) \end{aligned}$$

[4.49]

Regarding to the other parameters in Equation 4.48, in the case that only one signature is available, they are given by:

$$ASF = ASF + randn * (\frac{ASF}{3})$$

$$Dec_{fact} = Dec_{fact} + randn * (\frac{Dec_{fact}}{3})$$

[4.50]

When more than one signature is available, it will be possible to evaluate the parameters using common statistics to assess the values in Equation 4.48. Next an example using test 01 described previously, is included to illustrate the procedure and the results in both case scenarios.

4.3.1.4 Numerical example random signature waveform generation

In this example, assume that only signature one was measured for the point of interest (scenario one). As previously explained, the values for the parameters are:

- Number of Frequencies: 4
  Values: 6.68Hz, 10.70Hz, 13.74Hz and 22.72Hz
- Amplitude Scale Factor: 4.64
- Decay Factor: 3.35

The statistical parameters for the frequencies are assessed using Figure 4.20 are:

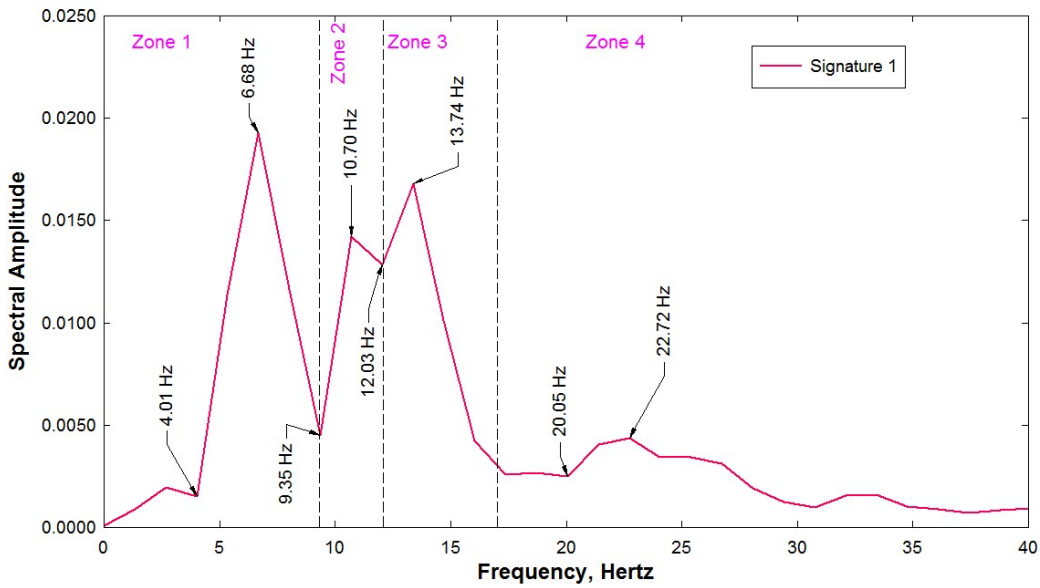

Figure 4.20 Numerical example frequencies signature 1 test 01

$$
\begin{gathered}
frequency_1 = 6.68 + randn * (2.67) \\
frequency_2 = 10.70 + randn * (1.35) \\
frequency_3 = 13.74 + randn * (1.71) \\
frequency_4 = 22.72 + randn * (2.67) \\
ASF = 4.64 + randn * (1.54) \\
Dec_{fact} = 3.35 + randn * (1.11)
\end{gathered}
\qquad [4.51]
$$

Using the values of Equation 4.51 in to Equation 4.47, it is possible to generate random signals for each hole in a production blast event (for example 11 holes in this test). Figure 4.21 show a comparison between the three signature signals measured in test 01 and eleven signatures generated using the current approach. Notice that the parameters of only one signal was used to generate the random signals; however a set of signatures that envelop the three measured signatures is generated

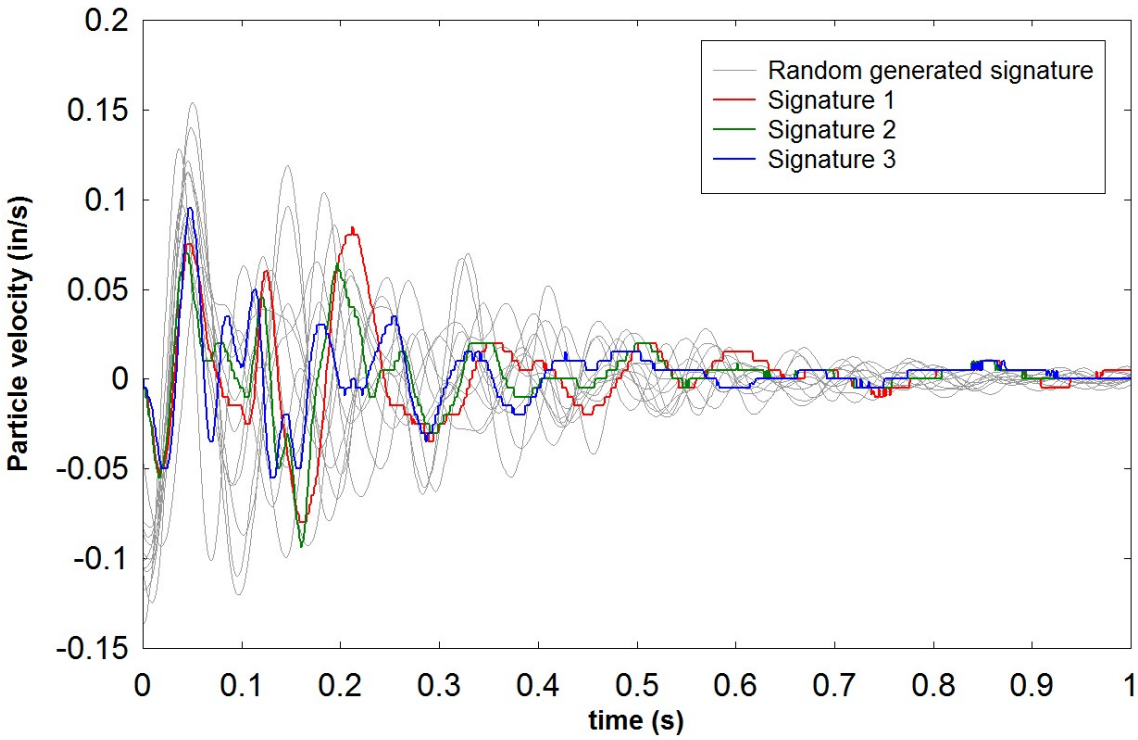

Figure 4.21 Random generated signatures using Silva-Lusk equation.

Two case scenarios were mentioned before. In the second case scenario, more than one signature is available to proceed with the modeling of signatures. Using the three signatures measured in test 01 and evaluating the statistical parameters (despite only three values for each parameter are available) we have in Table 4-1:

Table 4-1 Statistical parameters to modeling random signals

Signature	**Frequencies (Hz)**				**ASF**	**Decay**
1	6.68	10.70	13.74	22.72	4.46	3.35
2	7.01	-	13.05	22.09	5.81	3.10
3	6.71	10.74	13.42	30.20	4.50	3.19
Mean	***6.80***	***10.72***	***13.40***	***25.00***	***4.92***	***3.21***
Stdev					***0.77***	***0.13***

Regarding the standard deviations for the frequencies, to introduce more variability to the signals and cover a more reasonable assessment of possible outcomes, it is necessary to keep the low boundary value.

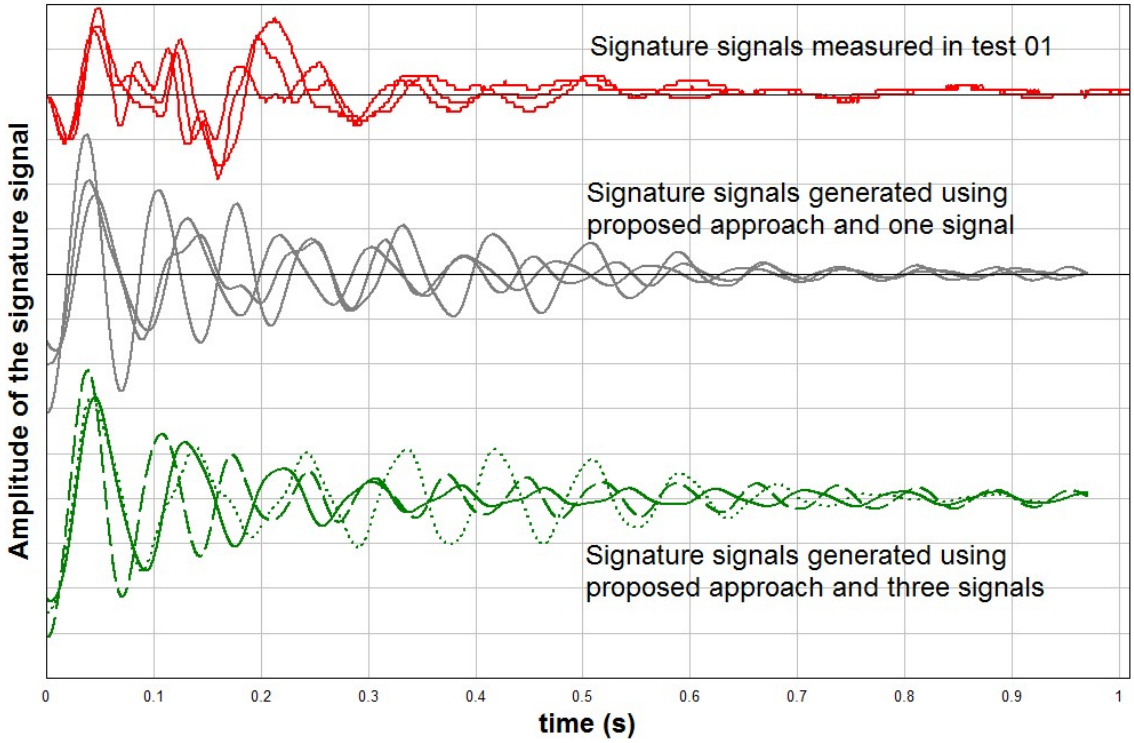

Figure 4.22 Signature signals measured vs Generated using one and three signals

In this case only three signals are used to estimate the statistical parameters for Equation 4.47 so the difference is not so evident. The benefits of using random signatures for each hole (random but with some boundaries) will be explained in chapter 5 and 6. An explanation about the introduction of the statistical parameters in the timing explosion sequence is included in the following section.

4.4 Wave arrival time distribution and time sequence

4.4.1 *Wave arrival time*

In Figure 4.23, if hole (i) is blasted, vibration waves take to travel from hole (i) to the monitoring point a time given by dt_{is}. It is usual in a production blast to use a delay time between holes. In Figure 4.23 delay time between holes is given by dt_{ji} and the vibration waves generated by hole (j) take to travel from hole (j) to the monitoring point a time given by dt_{js}. If the detonation of the hole (i) is the reference, the vibration from hole (j) is going to be recorded at the station at a time given by $dt_{ji} + dt_{js}$.

In this research, the traveling time of the waves from the source to the monitoring point are introduced in the model through the compressional or shear wave propagation velocity according to the vibration component that is going to be modeled. If the blast vibration component to model is the longitudinal component, the wave propagation velocity to use is the *p-wave velocity*. If any other component of the vibration is needed (vertical or transverse), *s-wave velocity* should be used.

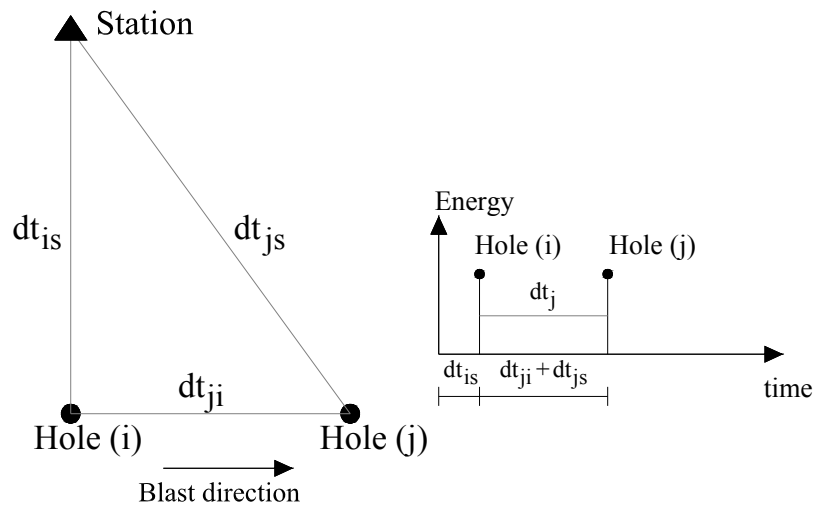

Figure 4.23 Delay times involved in the signature analysis

In the Figure 4.23 we have:

dt_{is} vibration travel time between hole *i* and station *S*.
dt_{ji} delay time between hole *j* and hole *i*.
dt_{js} vibration travel time between hole *j* and station *S*.
dt_j total delay time between holes in the sequence for the hole *j*

The best practice to assess the numerical value of the wave propagation velocity is through field tests similar to those used in earthquake engineering to measure the dynamic properties of the rock and soil. There are different methods between them:

- Seismic reflection
- Seismic refraction

Those methods are based on the general physics equation for velocity:

$$v = \frac{x}{t} \qquad [4.52]$$

Where:
x: distance source receiver
t: arrival time

Table 4-2 contains typical rock velocities for some of the rocks existing in Appalachian region.

Table 4-2 Typical rock velocities (from Bourbié, Coussy, and Zinszner, Acoustics of Porous Media)

Type of formation	P wave velocity (m/s)	S wave velocity (m/s)	Density (g/cm^3)
Scree, vegetal soil	300-700	100-300	1.7-2.4
Dry sands	400-1200	100-500	1.5-1.7
Wet sands	1500-2000	400-600	1.9-2.1
Saturated shales and clays	1100-2500	200-800	2.0-2.4
Marls	2000-3000	750-1500	2.1-2.6
Saturated shale and sand sections	1500-2200	500-750	2.1-2.4
Porous and saturated sandstones	2000-3500	800-1800	2.1-2.4
Limestones	3500-6000	2000-3300	2.4-2.7
Chalk	2300-2600	1100-1300	1.8-3.1
Salt	4500-5500	2500-3100	2.1-2.3
Anhydrite	4000-5500	2200-3100	2.9-3.0
Dolomite	3500-6500	1900-3600	2.5-2.9
Granite	4500-6000	2500-3300	2.5-2.7
Basalt	5000-6000	2800-3400	2.7-3.1
Gneiss	4400-5200	2700-3200	2.5-2.7
Coal	2200-2700	1000-1400	1.3-1.8
Water	1450-1500	-	1.0
Ice	3400-3800	1700-1900	0.9
Oil	1200-1250	-	0.6-0.9

In this research, assume a normal distribution for the wave velocity and 10% of the main value as standard deviation in order to calculate the traveling time between the hole and the station or monitoring point. The statistical parameter for the wave velocity is given by:

$$v = \bar{v} + randn\ (0.1 * \bar{v}) \tag{4.53}$$

In order to estimate the traveling time, using Equation 4.52 and Equation 4.53, it is obtained for the time:

$$dt_{ns} = \frac{x}{\bar{v} + randn\ (0.1 * \bar{v})} \tag{4.54}$$

Where:

dt_{ns}:	traveling time between hole n and station or measuring point s
x:	distance between hole hole n and station or measuring point s
$\bar{v}$:	wave velocity, assumed or measured
$randn$:	pseudorandom values drawn from the standard normal distribution

In the situation that field measurements for wave velocity are available, it is not necessary to assume any parameters and the measured statistical parameters can be used in Equation 4.53 and Equation 4.54.

4.4.2 *Blasting time sequence*

The blasting sequence depends on the initiation devices used to initiate the explosives. Two well known initiation system devices are commonly used; electronic and non-electric. To establish the statistical parameters to use in the current vibration prediction methodology using signature hole techniques and Monte Carlo schemes, the accuracy of the two initiation systems were tested. In total, 674 detonators were tested. Each system (electronic and non-electric) was tested over the viable ranges of delays available.

4.4.2.1 Experimental setup

To collect the information from the tests, a National Instruments PCI-6602 counter-timer card along with a custom software application developed in LabView was used. The selected PCI-6602 counter-timer card from National Instruments was an expansion card for use with personal computers. It included eight 32 bit counter channels and 32 configurable digital IO lines. With the onboard clock running at 80 megahertz, it was capable of measuring events down to 6.25nanoseconds (6.25e-006 ms) making it well suited for this testing. Six of the channels were configured for monitoring break wires. A seventh channel was used to monitor the control signals coming from the electronic initiator blasting machine.

To monitor the tested detonators, the break wire principle was used. The main idea about the break wire is that at the moment of detonation, the break wire is severed, causing a loss of continuity through the wire. The counter-timer card triggered on this event and reported a detonation time. It was also necessary to determine the zero reference time for the event, or the time at which the detonator was initiated. The difference between the measured detonation time and the zero reference time represented the realized delay achieved by the initiator.

The channels on the counter-timer card relied on two signals for measuring time. The first was the counter source, which was connected to a known internal timebase. It produced an 80 megahertz signal. The hardware counted every occurrence of a rising edge produced by the clock. The gate was the other important input used when performing period measurements. The gate signal determines when the hardware should report a count to the software application. This is demonstrated in Figure 4.24. The arm start trigger shown was used to determine when the counter started counting. It counts every edge received from the internal timebase. The gate was connected to the break

wire. Once continuity was lost and that signal went low, the gate was asserted and the appropriate output was captured.

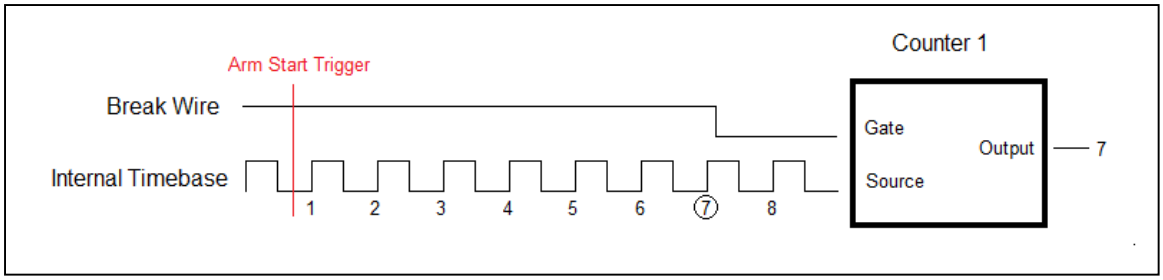

Figure 4.24 Illustration of Interaction between Break Wire and Counter

For the electronic detonator systems, the blasting machine communicated with the detonators using a low frequency AC signal. The necessary commands to program the detonator timing, arm them, and detonate them were sent via this signal. It was observed that communication is ceased prior to detonation, presumably because a fire signal has been transmitted to the detonators. This break in the signal was used to determine a zero reference time for the application to calculate the achieved delay timing. Figure 4.25 demonstrates this as realized in the counter time hardware. The arm start trigger, common across all counter channels, signaled the hardware to begin counting. It is important to note that all counters began counting at the same moment due to the arm start trigger, so they are effectively synchronized. Every falling edge on the signal generated from the blasting machine was captured at the gate. The corresponding count values were reported to the output for processing in the software application.

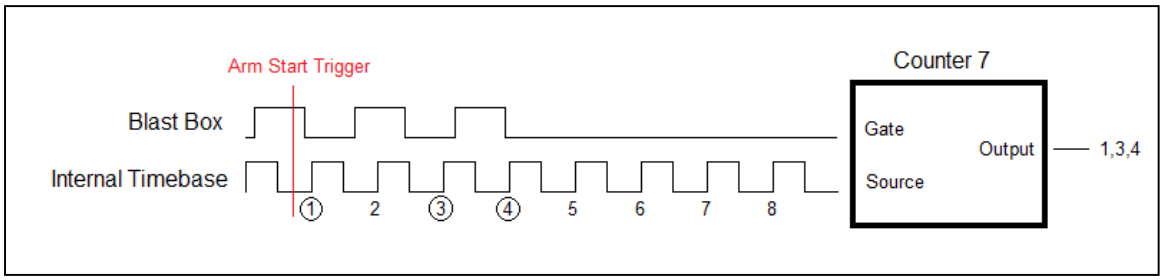

Figure 4.25: Blasting Machine Counter Interaction

For non-electric detonator systems, the zero reference time was determined in a similar fashion to the detonation time. The detonators being tested were connected via a bunch block. The bunch block ensured that the detonators under test shared a common start time. A break wire positioned within the bunch block captured this time which served as the zero reference time. This can be seen in Figure 4.26. The detonators being tested can be seen as the shock tube leading from the bunch block to the right of the figure (orange tubes). The detonator used to initiate them can be seen as the shock tube leading into the bunch block from the left of the figure (yellow tube). The small wires

(green wires) are the break wire which were positioned with and directly adjacent to the initiator.

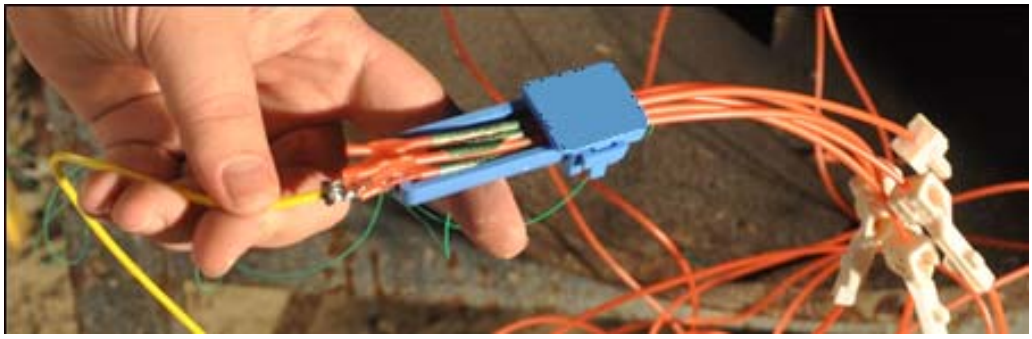

Figure 4.26: Bunch Block Configuration

Once the hardware captured the detonation and reported the corresponding counts, it would convert this value to time. Due to the synchronization, it is simply a matter of subtracting the two values and dividing the count by the frequency of the internal timebase. This was accomplished once the measured counts were transferred to the LabVIEW application.

The LabVIEW application was responsible for a number of activities. It provided a graphical user interface for the person conducting the test (Figure 4.27). Fields were included to record information pertinent to the testing. It also provided feedback to the user to ensure proper operation.

The application was also responsible for controlling the hardware. It configured the counter devices for the task. It controlled the various digital lines used to establish the levels in the break wires and manage the reset-set latches. Finally, it set the arm start trigger to synchronize the channels on the card. Another function was calculating the times from the measured counts and accumulating those values. When convenient for the user, it generated a report including the test times and summary statistics.

To validate the data collected by this system, a Blaster Ranger high speed camera was used to document several of the tests from each detonator system using an appropriate frame rate. This footage was manually reviewed and it was concluded that the system was accurately collecting the times of detonation.

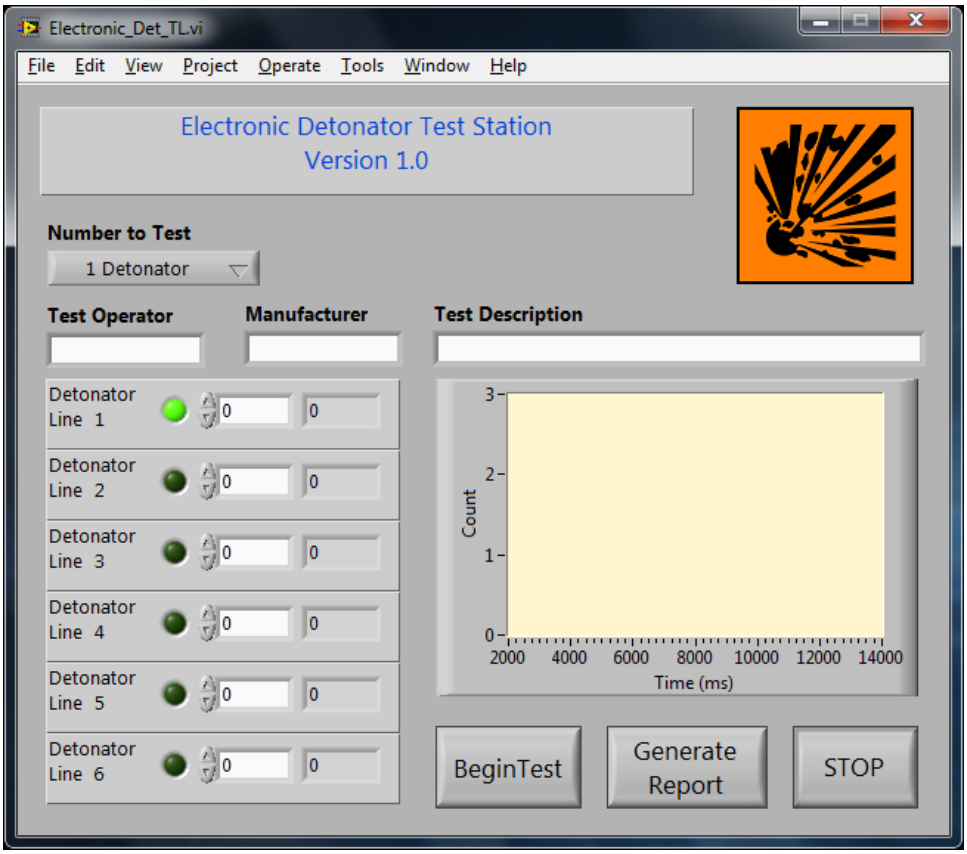

Figure 4.27: Graphical User Interface test setup

Validation of the system was performed using images captured and analyzed from high speed video data. For some tests, high speed video data was recorded, showing the detonation process of the initiation system. Viewing the video on a frame-by-frame basis allowed for the visual confirmation of when each detonator initiated relative to the others. For timing analysis using high speed video, the first detonator initiating in a test sample was considered time zero, with timing for each following detonator based on this reference point. This was done since the true time zero could not be obtained from the video data.

The use of high speed imaging was a relatively straight forward process. For each data set, the video was recorded at a specified frame rate, varying from 1,000 frames per second (fps) to as high as 16,000 fps. With the frame rate for each data set known, the time from one frame to the next could be calculated. For example, recording at 4,000 fps results in a time lapse of 0.25 millisecond (ms) from frame to frame. Therefore, if the first detonator initiating is time zero and the following detonator is shown to detonate 10 frames later, it can then be calculated that the difference between the two detonators initiating is 2.5 ms. This process was repeated for each subsequent detonator in the test sample.

As mentioned previously, the detonators selected for testing consisted of two electronic systems and two non-electric systems. When possible, different lots were procured to provide a more representative sample. In total 674 detonators were tested. Table 4-3 outlines the testing matrix.

Table 4-3 Detonator Matrix

Electronic Detonator Matrix						
Manufacture	**Electronic Detonator A**			**Electronic Detonator B**		
Delay (ms)	10	1000	8000	10	1000	8000
Lots	3	3	3	3	3	4
Total Detonators	53	43	50	51	52	47

Non-electric Detonator Matrix						
Manufacture	**Non-electric Detonator A**			**Non-electric Detonator B**		
Delay (ms)	9	1000	1400	25	100	700
Lots	1	1	1	2	2	2
Total Detonators	68	60	67	59	65	59

The idea about the different delays used, was to include a wide range including short and long timing to analyze the influence of the delay time in the accuracy of the initiation system for both non-electric and electronic.

With the high degree of automation built into the testing apparatus, the methodology proved to be fairly simple. The detonators to be tested were first loaded into the test cell consisting of short sections of steel pipe. The steel pipe served the purpose of deflecting the shrapnel away from adjacent test cells and directing it away from the break wire leads. A bar running the length of the test cells had small holes through which the detonators were placed (Figure 4.28).

Figure 4.28 Test Cells

The break wire used for all of the testing was Belden 30 AWG solid copper hook-up wire with polyvinyl chloride insulation. The break wire was held firmly against the tip of the detonator and secured with a piece of vinyl tape. Care was taken to ensure the break wire was placed running through the center of the tip. This technique is displayed in the next figure.

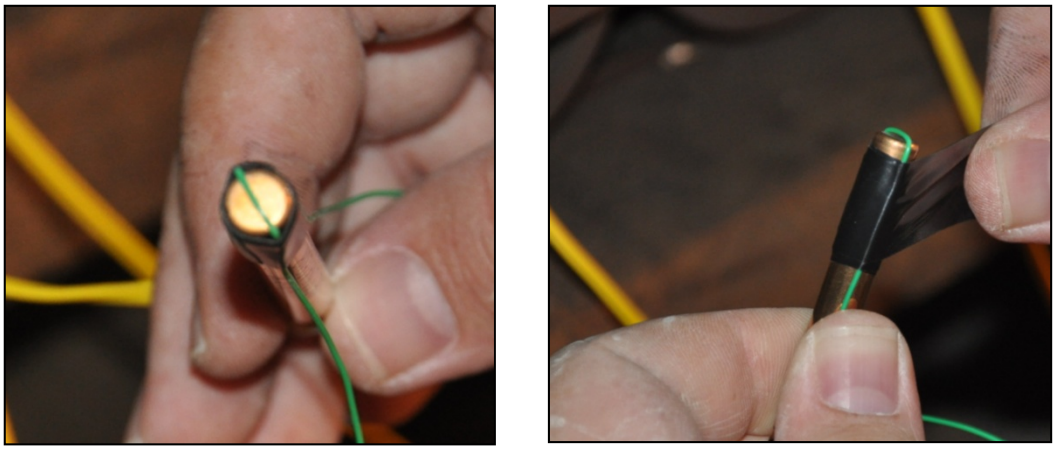

Figure 4.29 Break Wire Placement

Figure 4.30 shows detonators awaiting test in the test cells.

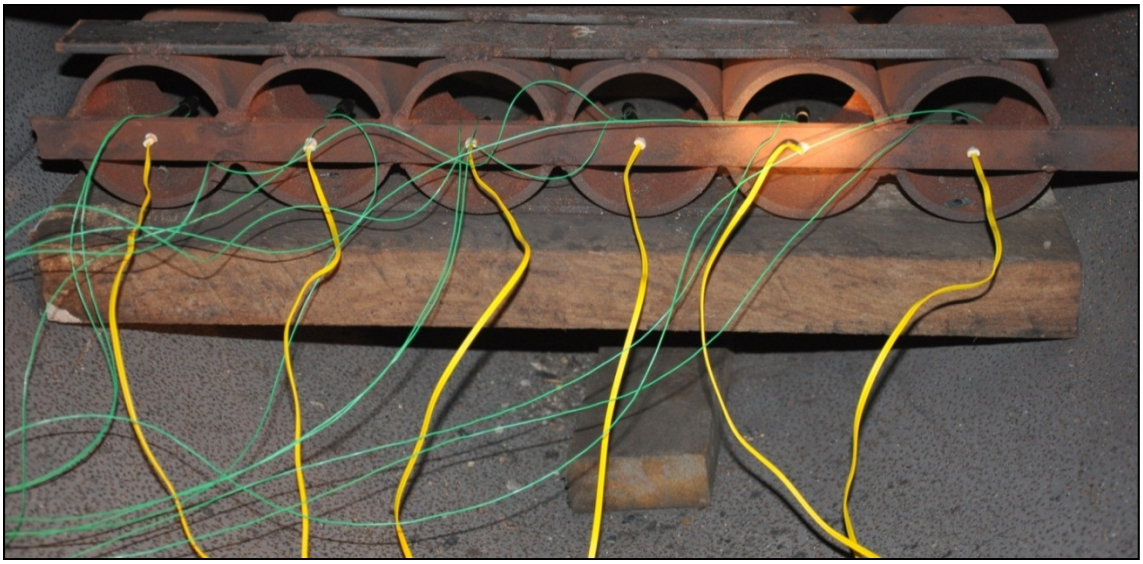

Figure 4.30 Detonators Awaiting Test

The following image shows the break out box, housing the interface electronics, with the break wires and blasting machine control wires attached (Figure 4.31).

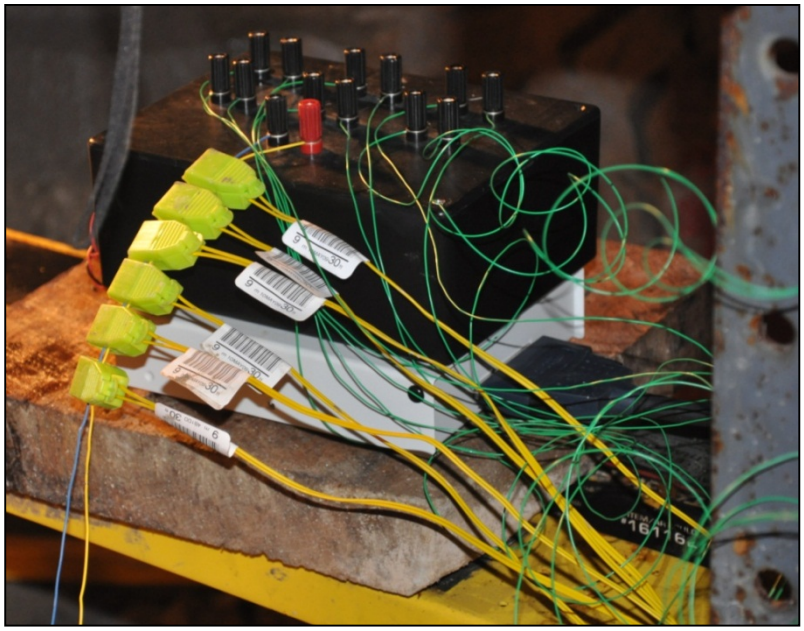

Figure 4.31: Electronics Break Out Box

The only difference to note with the methodology, as it pertains to the non-electric testing, consisted of where to place the detonator in the bunch block used to establish the zero reference time. During much of the testing it was placed under the test cell. After a number of misfires occurred the setup was changed. The bunch block was placed in a galvanized trash can filled with sand and buried. After this change in the experimental setup, no other misfires occurred.

4.4.2.2 Non-electric detonators results

The frame grabs shown in Figure 4.32 illustrate the detonation sequences for one test sample of non-electric detonators, in this case five detonators filmed at 4,000 fps. For this series, a detonation event is shown to occur at Frames 00, 08, 68, 105, and 121. The frame prior to each event is also shown for comparison purposes. Table 4-4 provides a summary of the frame number at which a detonation event occurred, the calculated time using the given frame rate, and the time recorded by the testing system.

Table 4-4 Summary of Results for Non-Electric Validation Example

Non-electric 4000 fps			
Order	**Number of Frames**	**Calculated time using high speed video (ms)**	**System recorded time (ms)**
5	121	30.25	30.57
3	68	17.00	16.82
1	0	0.00	0.00
4	105	26.25	26.13
2	8	2.00	1.76

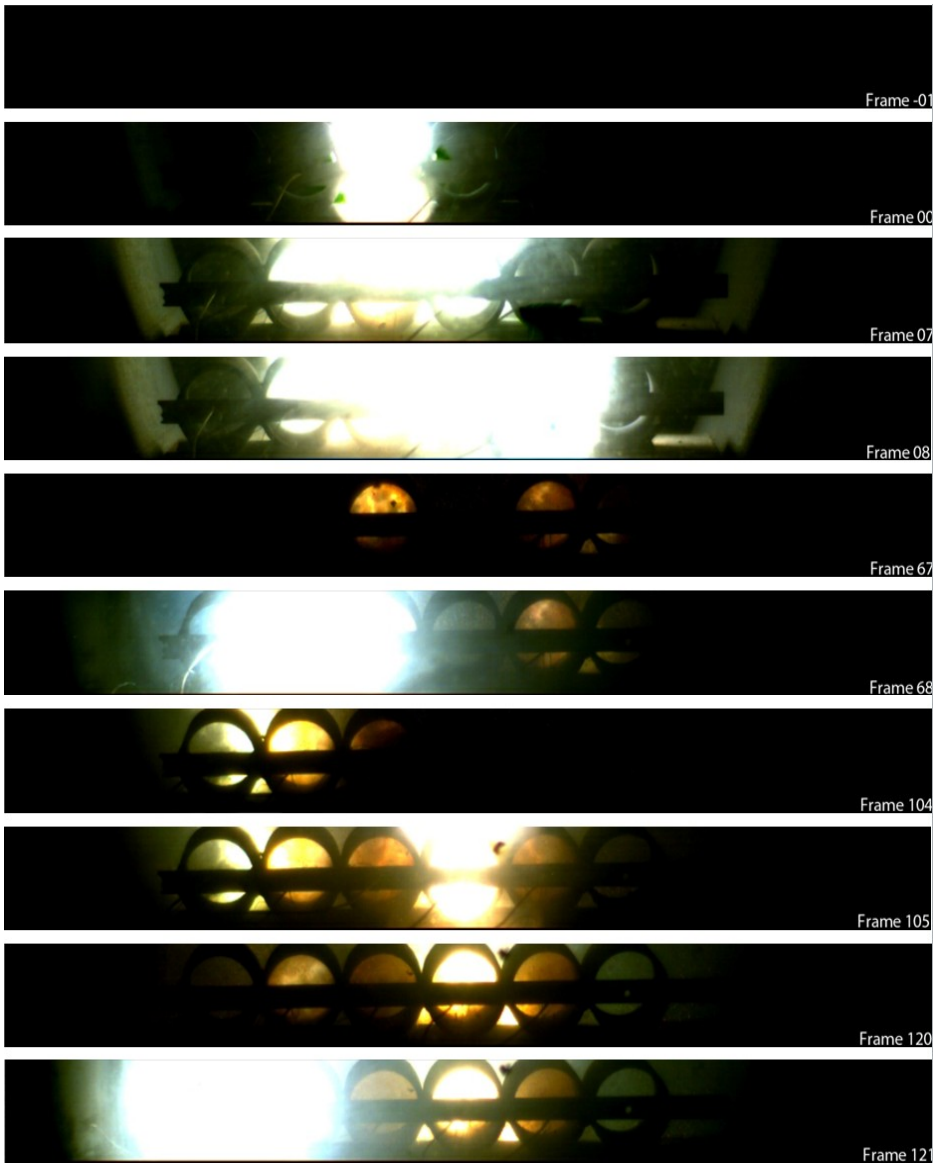

Figure 4.32 Frame grabs from non-electric sample showing detonation sequence

It is important to note two temporal considerations when reviewing the visual analysis. One is that each frame represents a window of time created by the shutter speed. This window for a video shot at 4,000 fps is 0.25 ms long. An event shown in a single frame could have occurred at any point in this window. The second consideration is that the detonation event is not an instantaneous one. There is a variable amount of time inherent with this process and how it is represented visually too is variable. This can be seen when comparing Frames 68 and 105 in Figure 4.32. The breakwire in immediate contact with the detonator would be a more accurate measure of this event.

The results of the testing from the non-electric detonator systems are summarized in Table 4-5 and graphically in Figure 4.33, Figure 4.34 and Figure 4.35.

Table 4-5 Summary non-electric detonator results

Non-electronic Detonator Results						
	Non-electronic Detonators A			Non-electronic Detonators B		
Nominal Delay (ms)	9	1000	1400	25	100	700
Number of detonators Tested	68	60	67	59	65	59
Delay Average (ms)	11.342	1125.501	1418.766	27.751	102.730	715.710
Standard Deviation	4.594	6.550	19.054	0.765	11.250	6.195
Maximum (ms)	15.756	1146.782	1462.381	29.304	123.193	730.575
Minimum (ms)	1.534	1114.704	1367.035	26.155	79.835	697.925
Percent Error	26.023%	12.550%	1.340%	11.005%	2.730%	2.244%

Normal distribution probability density function was chose to compare the results. All the non-electric detonators results are included in Figure 4.33. In this figure, it is clear, how the most precise delay time is presented at 25ms nominal delay, despite that the average value for this detonator show a difference of 2.751ms when compared to the nominal time delay (25ms), the precision of this delay is reflected in the lower value of the standard deviation. Figure 4.33, also shows how the least accurate delay time is the 1000ms detonator, the difference between the nominal delay time and the average tested is around 125.501ms.

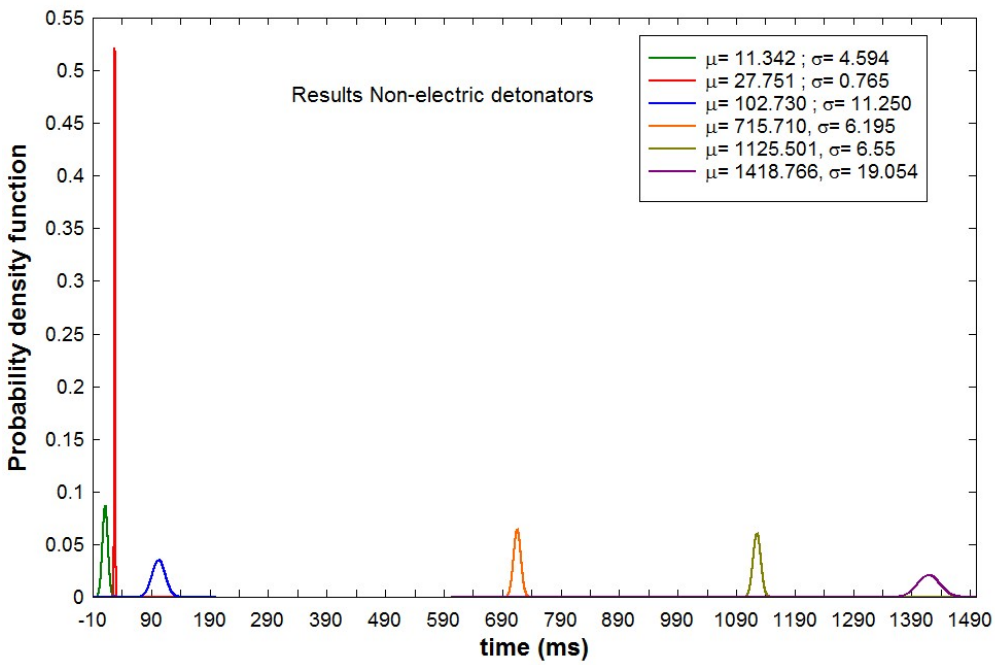

Figure 4.33 Normal distribution, density function, non-electric detonators tested.

Next figures show the graphical results for “short and long” delay times.

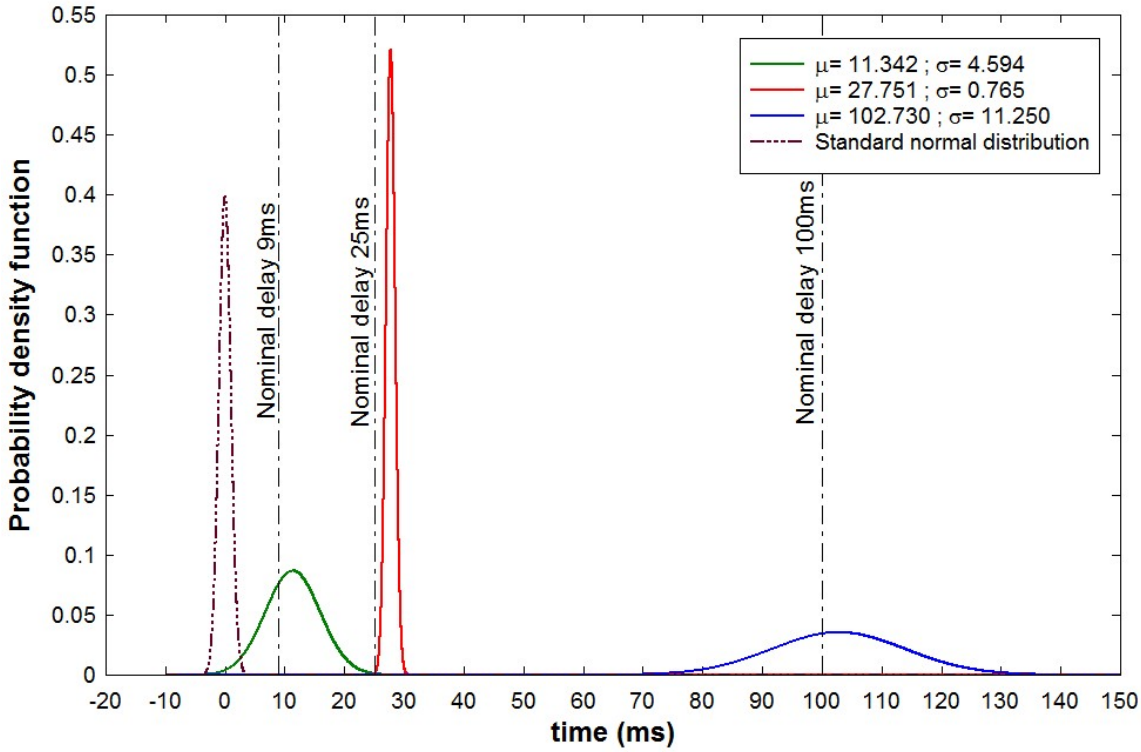

Figure 4.34 Normal distribution, density function, non-electric detonators at 9, 25 and 100 ms nominal delays.

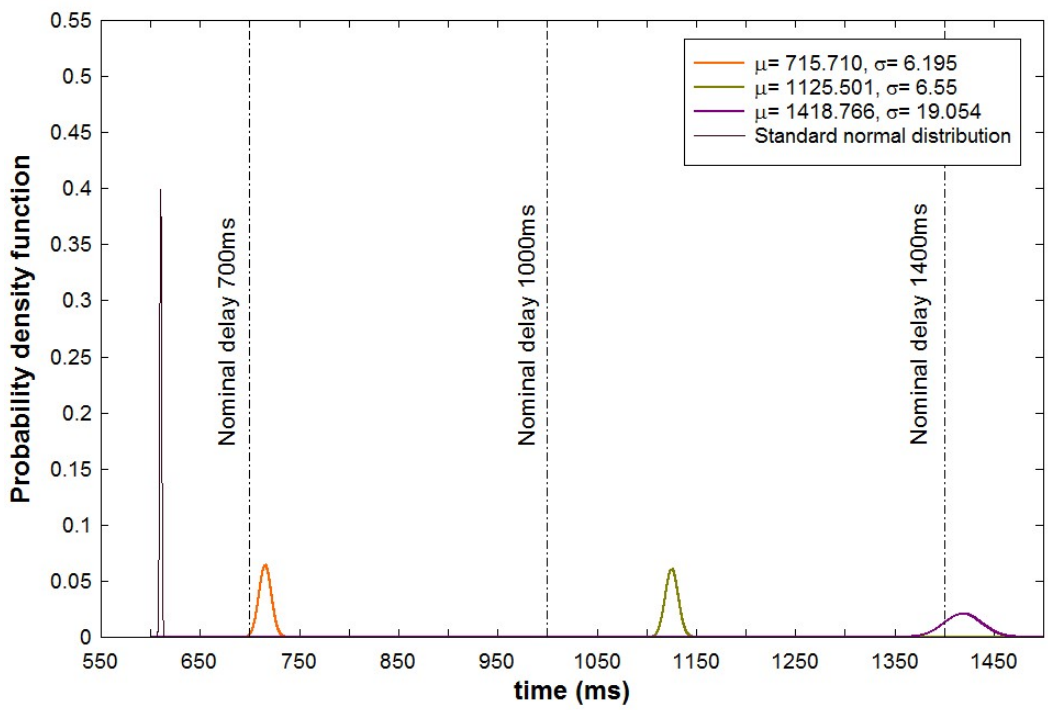

Figure 4.35 Normal distribution, density function for nominal delays, non-electric detonators at 700, 1000 and 1400 ms.

4.4.2.1 Electronic detonators results

The frame grabs shown in Figure 4.36 illustrate the detonation sequence for one test sample of electronic detonators, in this case five detonators filmed at 8,000 fps. For this series, a detonation event is shown to occur at Frames 00, 11, 18, 22, and 26. The frame prior to each event is also shown for comparison purposes.

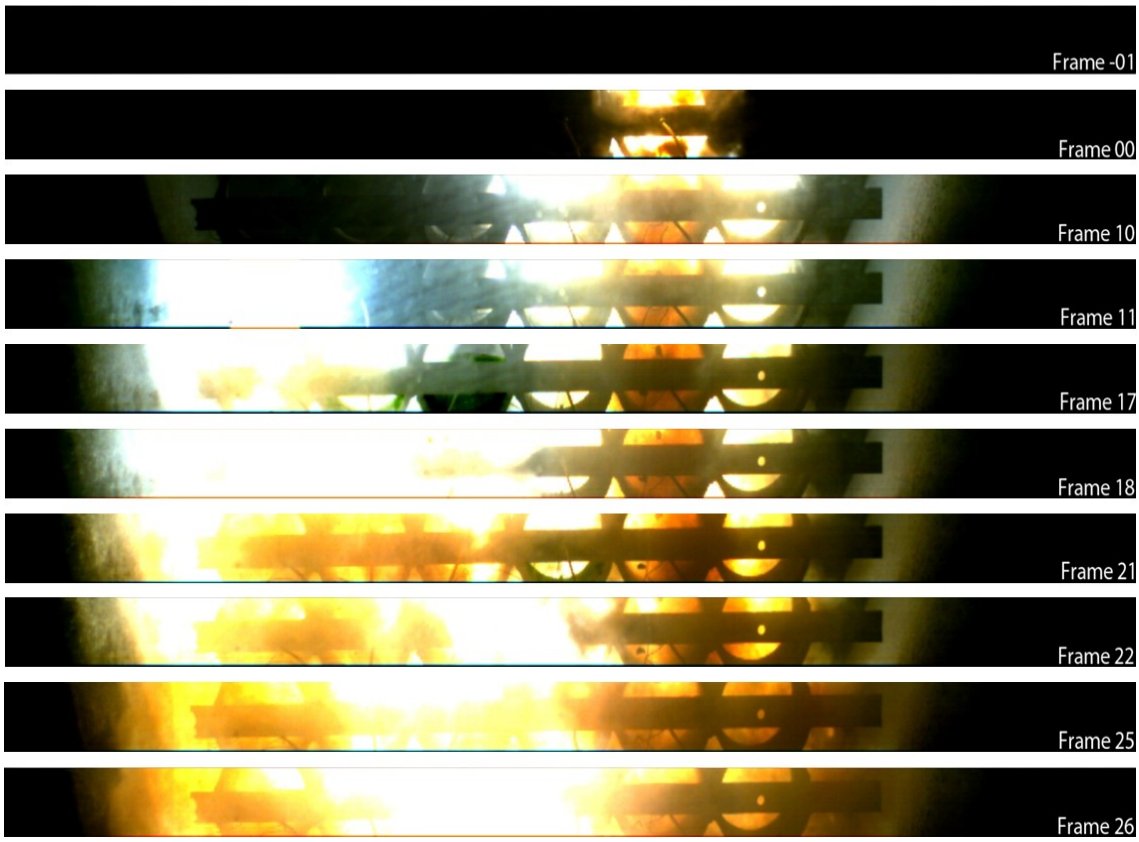

Figure 4.36: Frame grabs from electronic sample showing detonation sequence

Table 4-6 provides a summary of the frame number at which a detonation event occurred, the calculated time using the given frame rate, and the time recorded by the testing system.

Table 4-6 Summary of Results for Electronic Validation Example

Electronic 8000 fps			
Order	**Number of Frames**	**Calculated time using high speed video (ms)**	**System recorded time (ms)**
2	11	1.38	1.48
3	18	2.25	2.26
4	22	2.75	2.27
5	26	3.25	2.76
1	0	0.00	0.00

The results of the testing from the electronic detonator systems are summarized in Table 4-7 and graphically from Figure 4.37 to Figure 4.40.

Table 4-7 Summary statistics electronic system

Electronic Detonator Results						
	Electronic Detonators A			Electronic Detonators B		
Nominal Delay (ms)	10	1000	8000	10	1000	8000
Number of detonators Tested	53	43	50	51	52	47
Delay Average (ms)	9.950	1000.543	8003.375	9.987	999.804	7998.589
Standard Deviation	0.092	0.321	3.751	0.030	0.107	0.851
Maximum (ms)	10.201	1001.120	8015.625	10.052	999.954	7999.400
Minimum (ms)	9.816	999.960	7995.190	9.910	999.460	7995.800
Percent Error	-0.501%	0.054%	0.042%	-0.130%	-0.020%	-0.018%

Normal distribution probability density function was chose to compare the results. All the electronic detonators results are included in Figure 4.37. In this figure, it is clear, how detonators from maker A are less accurate and precise when compared to maker B. Also in this result, it is evident how the precision of electronic detonators decreases when the delay time increases. It is evident when standard normal distribution is used to compare results Figure 4.38 to Figure 4.40 (see how the shape of the standard normal distribution change in those figures).

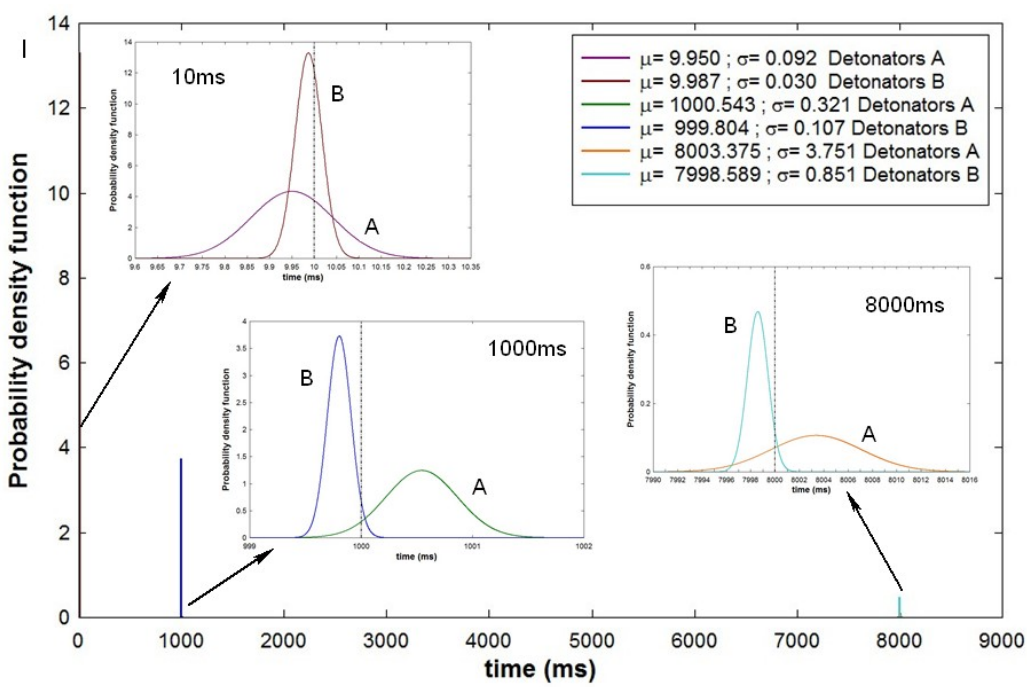

Figure 4.37 Normal distribution, density function, electronic detonators tested.

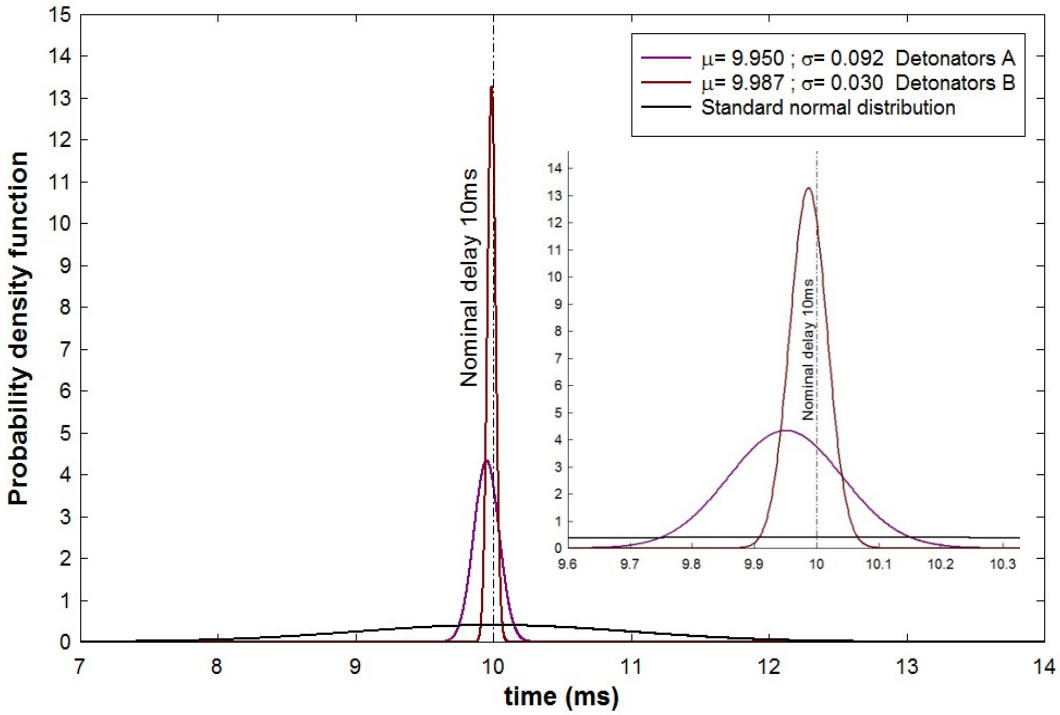

Figure 4.38 Normal distribution, density function, electronic detonators at 10ms nominal delays.

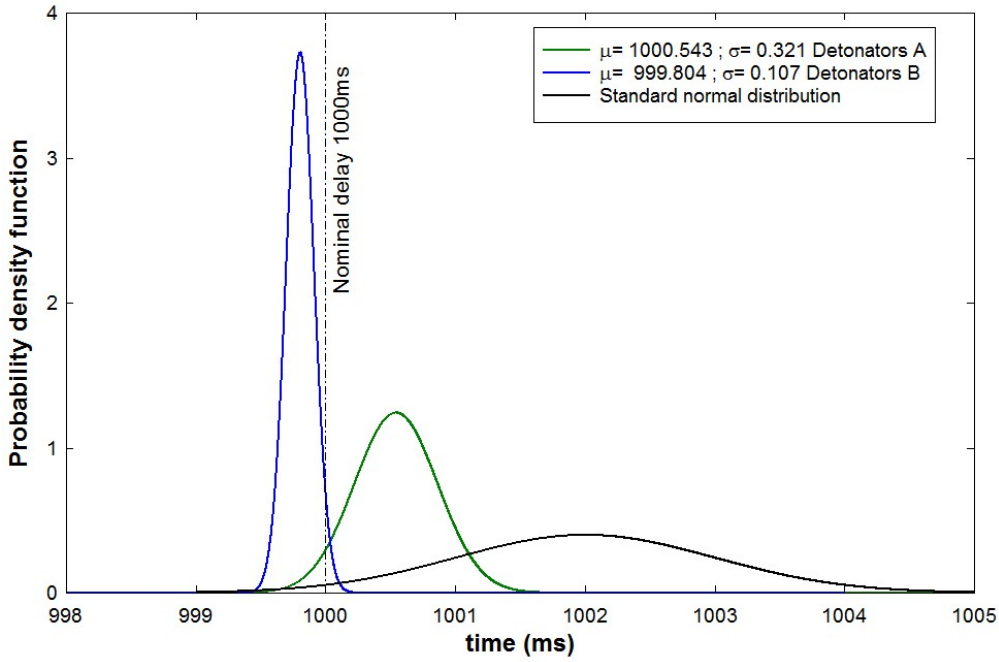

Figure 4.39 Normal distribution, density function, electronic detonators at 1000ms nominal delays.

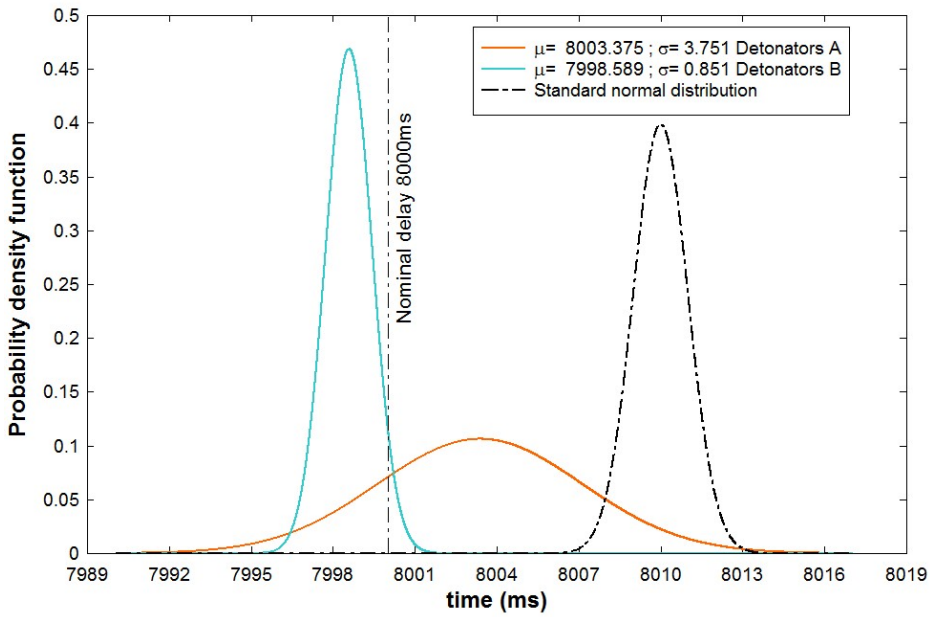

Figure 4.40 Normal distribution, density function, electronic detonators at 8000ms nominal delays.

Finally, when non-electric and electronic initiation systems are compared side by side, at nominal delay time of 9 and 10ms respectively, Figure 4.41 is obtained.

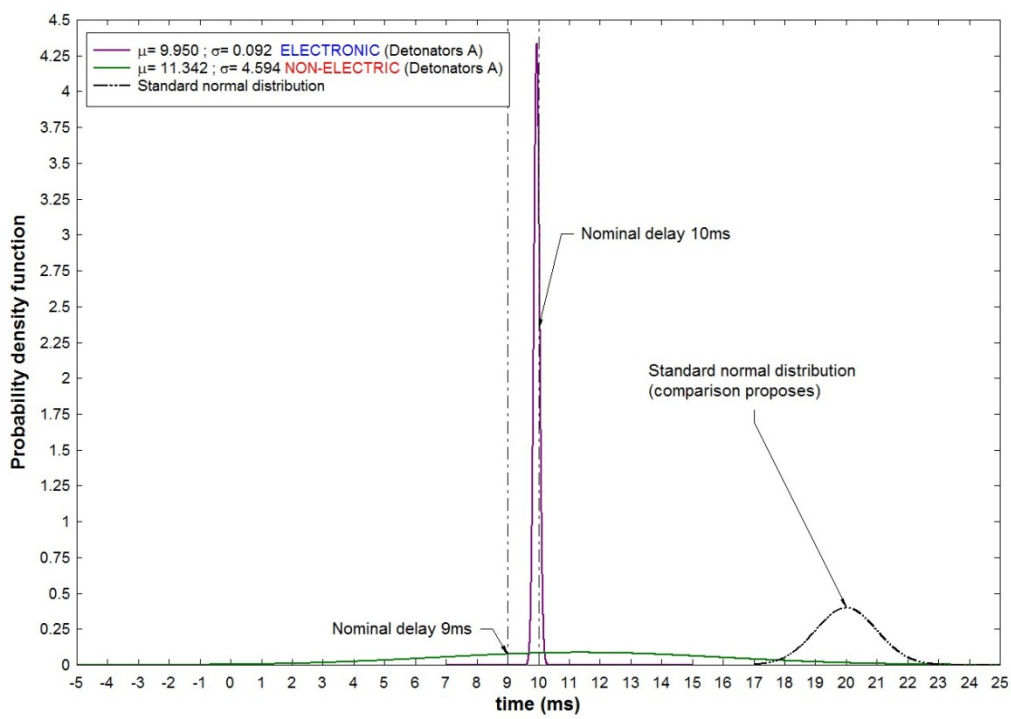

Figure 4.41 comparison 9ms and 10ms nominal delay (non-electric Vs electronic)

Figure 4.41 shows clearly the big difference between both initiation systems regarding precision and accuracy.

In this research, the statistics for the initiation systems were taken in to account assuming a random normal distribution, and using the founded parameters of mean and standard deviation for both initiation systems.

The general equation used in the Monte Carlo scheme to predict vibrations levels from mining blast and regarding to delay timing between holes is given by:

$$\Delta dt_{ji} = \overline{dt} + randn * (\sigma_t) \qquad [4.55]$$

Where:

Δdt_{ji}:	time interval between detonation hole (i) and hole (j).
$\overline{dt}$:	average delay timing, measured or assumed
σ_t:	standard deviation of the normal distribution of the average delay timing, assumed or measured
$randn$:	pseudorandom values drawn from the standard normal distribution

Finally, the time used to perform the linear superposition is given by the time of the arrival of the vibration wave plus the time interval between detonation holes. For example and using Figure 4.23, the time of hole (j), using hole (i) as time reference is giving by:

$$t_j = \Delta dt_{ji} + dt_{js} \qquad [4.56]$$

Where:

t_j:	time for hole (j) reference to hole (i)
Δdt_{ji}:	time interval between detonation hole (i) and hole (j). Equation 4.55
dt_{js}:	traveling time between hole (j) and station or measuring point (s). Equation 4.54

4.5 Linear superposition and discrete convolution

As stated in section 2.33, signature hole technique is based on signals and system theories. After several assumptions regarding the system to model, the response $y[n]$ (output) of one system can be calculated using the discrete convolution equation given by:

$$y[n] = \sum_{k=0}^{n} h[n-k]u[k] = \sum_{k=0}^{n} u[n-k]h[k] \qquad [4.57]$$

Where:

$y[n]$:	current output of the system (blast vibration prediction)
k, n:	integer values in one sequence

$h[n]$: impulse response (signature hole); impulse response is the response of the system under one input equal to one impulse sequence $\delta[n]$ or Dirac delta function. In blasting $\delta[n]$ is assumed like the detonation of one hole.

$u[n]$: arbitrary input sequence (delay pattern used in a production blast).

Discrete convolutions are algebraic equations and can be computed by direct substitution (Chi-Tsong Chen, 2004). To show the numerical convolution procedure, assume that a hole was blasted and one signature signal was recorded in a monitoring point as indicating in Figure 4.42. In this example, to simplify the numerical example, the signature signal was discretized using only the values indicated in red colors.

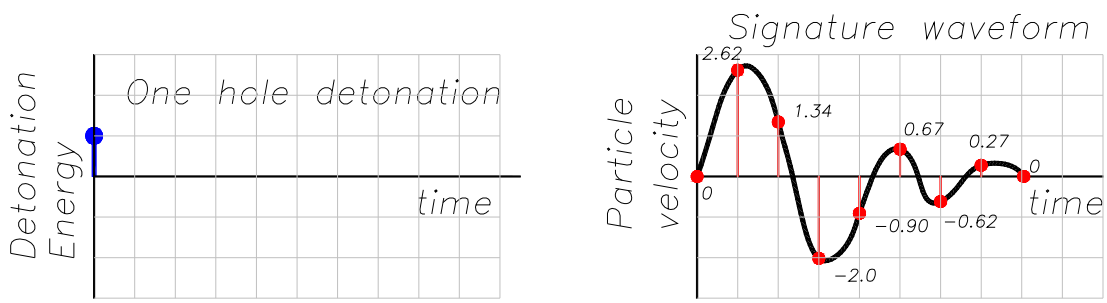

Figure 4.42 Pair impulse – signature waveform

Using the mathematical notation, we have in the case of Figure 4.42 that:

$$u[n] = \delta[n] = \{1\}$$
$$h[n] = \{0,2.62,1.34,-2.00,-0.90,0.67,-0.62,0.27,0.00\} \quad [4.58]$$

Now assume that we will blast three holes using one unit time of delay, the graphical representation is included in Figure 4.43

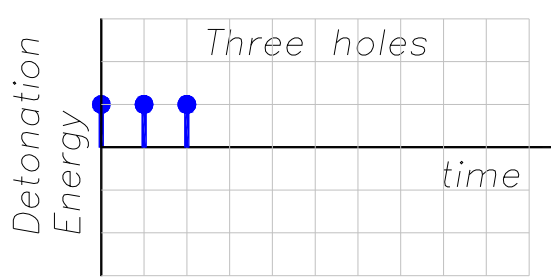

Figure 4.43 Three holes numerical example

The problem is to predict the vibration levels produced by three holes detonated as shown in the previous figure. In such case the "new" input is given by;

$u[n] = \{1,1,1\}$. Using Equation 4.57 and computing manually each value of $y[0], y[1], y[2], \ldots$ etc. we have:

$u[n] = \{1,1,1\}$
$h[n] = \{0,2.62,1.34,-2.00,-0.90,0.67,-0.62,0.27,0.00\}$

$\boldsymbol{n = 0}$
$y[0] = h[0]u[0] = 0 * 1 = 0$
$\boldsymbol{n = 1}$
$y[1] = h[1]u[0] + h[0]u[1] = 2.62 * 1 + 0 * 1 = 2.62$
$\boldsymbol{n = 2}$
$y[2] = h[2]u[0] + h[1]u[1] + h[0]u[2] = 1.34 * 1 + 2.62 * 1 + 0 * 1 = 3.96$
$\boldsymbol{n = 3}$
$y[3] = h[3]u[0] + h[2]u[1] + h[1]u[2] + h[0]u[3]$
$= -2 * 1 + 1.34 * 1 + 2.62 * 1 + 0 * 0 = 1.96$
$\boldsymbol{n = 4}$
$y[4] = h[4]u[0] + h[3]u[1] + h[2]u[2] + h[1]u[3] + h[0]u[4]$
$= -0.90 * 1 - 2 * 1 + 1.34 * 1 + 2.62 * 0 + 0 * 0 = -1.56$
Following this procedure we have:
$y[5] = -2.23$; $y[6] = -0.85$; $y[7] = 0.32$; $y[8] = -0.35$;$y[9] = 0.27$
$y[10] = 0$

So the result of three holes detonated at one delay time unit is:
$y[n] = \{0,2.62,3.96,1.96,-1.56,-2.23,-0.85,0.32,-0.35,0.27,0\}$

The graphical result is included in Figure 4.44.

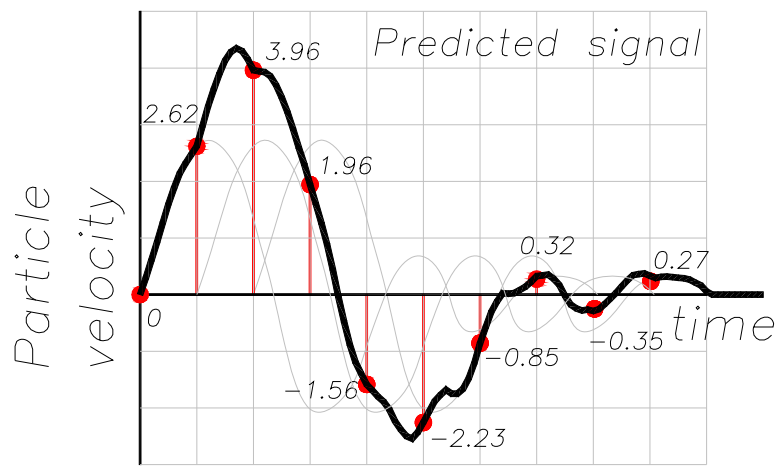

Figure 4.44 Result of three holes detonation mathematical convolution

The implementation of the convolution algorithm is quite simple. The basic code in MS Visual Basic® VB is following:

```
for i=0 to n-1
        for k=0 to i
                a= u(i-k)*h(k)
                aa=aa+a
        next k
        y(i)=aa
next i
```

Figure 4.45 Implementation of convolution in VB®

Also, Matlab® use a built in function called $conv$ function, the syntax is quite simple as follows:

```
u=[1,1,1]
h=[0,2.62,1.34,-2.00,-0.90,0.67,-0.62,0.27,0.00]
y=conv(u,h)
y =[0.00, 2.62, 3.96, 1.96, -1.56, -2.23, -0.85, 0.32, -0.35,
0.27, 0
```

Figure 4.46 Convolution in Matlab®

If a more fine discretization is made, for example half of the time interval unit is used, using matlab, the graphical results are included in Figure 4.47 and Figure 4.48.

```
u=[1,0,1,0,1]
h=[0.0000,1.6062,2.6096,2.5160,1.3422,-0.6509,-2.0284,-
1.9028,-0.9096,0.3524,0.6721,-0.1698,-0.6188,-
0.1544,0.2745,0.3161,0.0000]
y=conv(u,h)
y    =[0.00,1.61,2.61,4.12,3.95,3.47,1.92,-0.04,-1.60,-2.20,-
2.27,-1.72,-0.86,0.03,0.33,-0.01,-0.34,0.16,0.27,0.32,0.00]
```

Figure 4.47 Convolution using Matlab

In this case, notice vector u increases the number of elements to keep holes blasted at one time unit, (in this example the holes are blasted using a delay of one time unit in Figure 4.43).

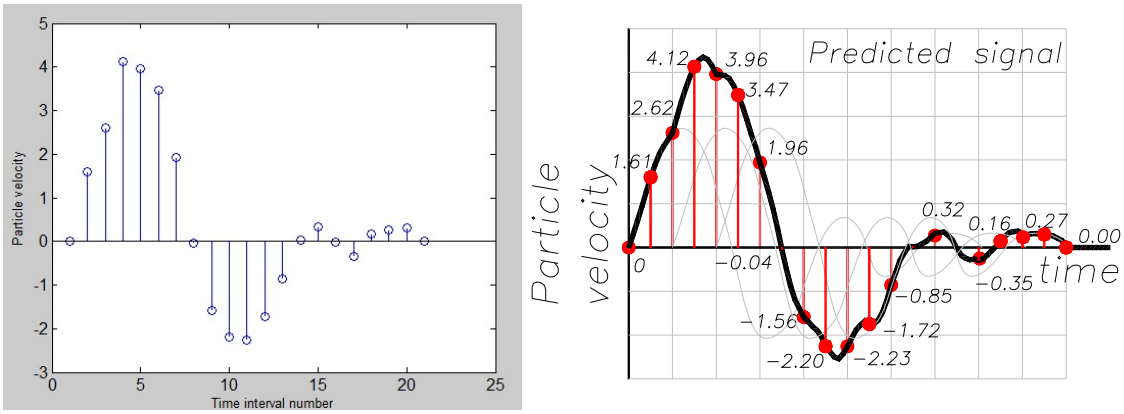

Figure 4.48 Convolution results using matlab and a more discretized signal.

Mathematically, the discrete convolution is an operation between two finite sequences $u[n]$ and $h[n]$. If there is no changes in the seed waveform, using the previous algorithms or functions in Matlab® it is possible to calculate the predicted vibration signal for a production blast. However, if the seed waveform changes hole to hole, it is necessary to use another approach to sum the different seeds waveform and them calculate the predicted vibration signal.

Due to the increase in the storage and computation capacity of modern computers, a simple graphical sum term by term is proposed to calculate the predicted signal. Using the previous example, the seed signals should be shifted in time according to the blasting pattern as indicated in Figure 4.49.

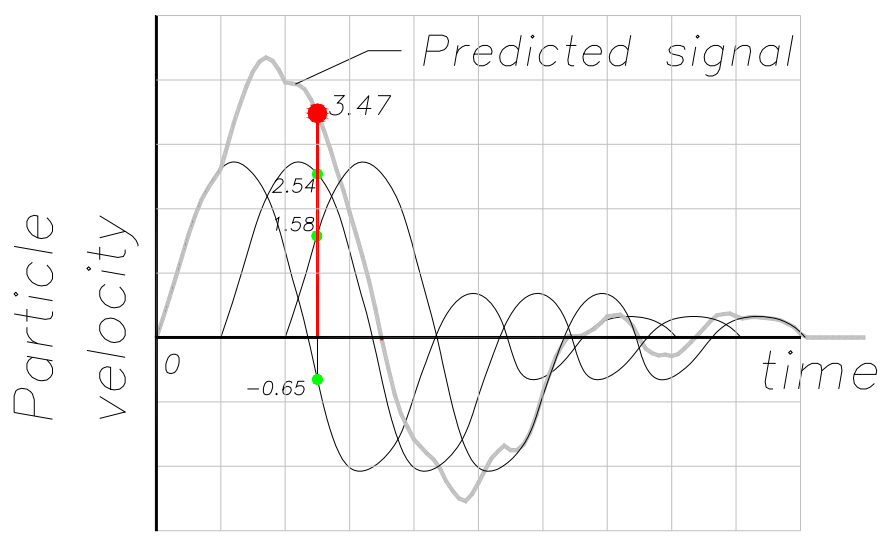

Figure 4.49 Shifted signals to perform the sum.

After shifting the signals, and performing the sum for a specific instant of time it is possible to calculate the vibration level for that instant of time. So the output for the n term is given by:

$$y[n] = \sum_{k=1}^{N} h_k[n]$$

[4.59]

Where:

N: total number of signals to sum (equal to the number of blast holes)

h_k: seed waveform finite sequence for hole k

Following the numerical example, in Figure 4.49 for 2.5 s, the vibration level is calculated as:

$$y[2.5] = -0.65 + 2.54 + 1.58 = 3.47$$

[4.60]

This is the same numerical value calculated using convolution. In this research, the graphical procedure was used to calculate the predicted signal.

4.5.1 *Practical example*

Next, using information collected in a blasting test, the results to calculate the vibration prediction using the convolution and the graphical methodology is compared. During the development of the current research, several tests were performed at Guyan mine in West Virginia. The mine is a typical surface coal mine using contour mining methods. One of the tests was performed using electronic detonators and measuring a signature waveform followed by the complete blasting. Table 4-8 shows the main parameters of the blast test.

Table 4-8 Blast test parameters

Parameter	Value
Total holes	69
Face height (ft)	44
Depth (ft)	44
Burden = spacing (ft)	20
Diameter (in)	9
Total explosive (lbs)	55,050.03

The timing delay used was 4 ms between holes detonated at the same time. A seismograph was setup at 900ft from the blast site. The records of three vibration components were recorded and they are included in Figure 4.50. The particular characteristic of this test is the use of four holes detonated at the same time (to record the signature or seed waveform and during the complete production blast).

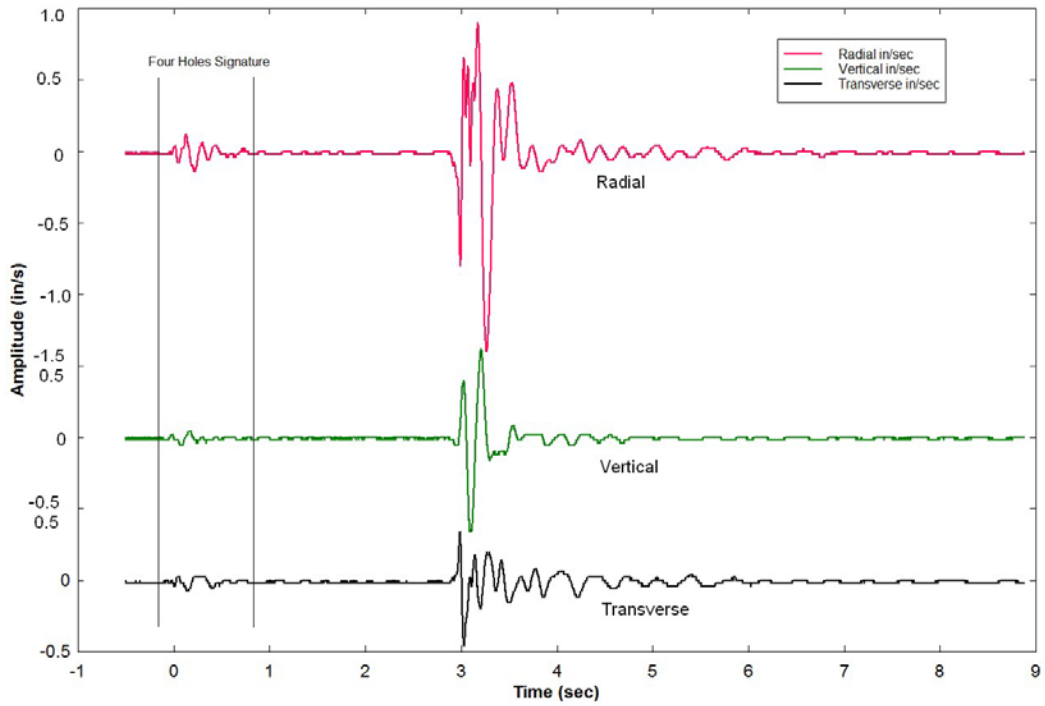

Figure 4.50 Vibration record for test blast 4 holes detonated at the same time

A plan view from the blast report is included in Figure 4.51.

Figure 4.51 Plan view from the blast report for the test

In total to perform the convolution, the finite sequence representing the blast pattern $u[n]$ vector will be composed by a vector with seventeen elements (17 ones) if a discretization of 4ms is made in time. Figure 4.52 shows the radial signature waveform isolated from the complete record included in Figure 4.50.

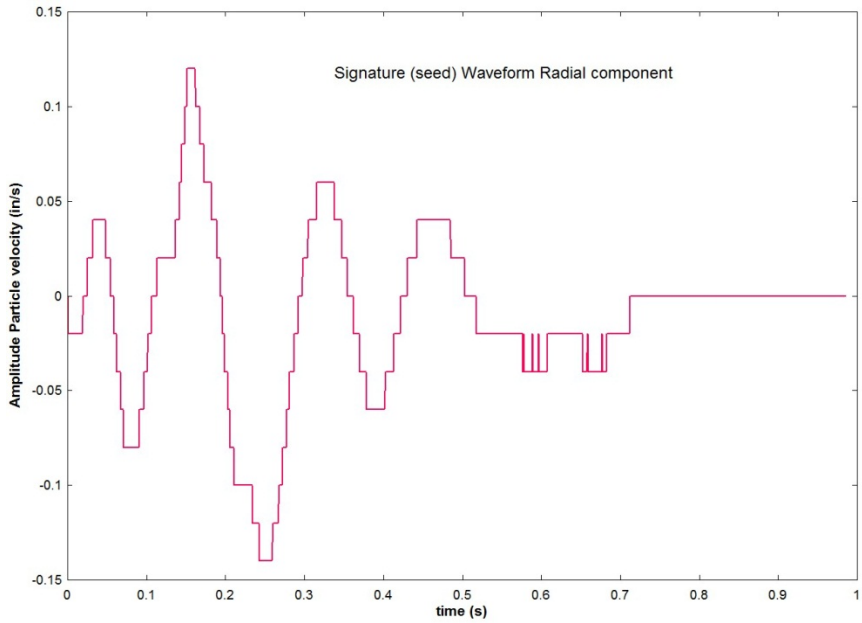

Figure 4.52. Radial signature (seed) waveform

Using a discretization of 1 ms, and generating two vectors of two columns (first column time, and second column values) containing the signature waveform (Signature.txt) and the timing sequence (timing.txt), the command to load such vectors in Matlab® is given in Figure 4.53. The first ten elements of vectors h, u and y are included in Figure 4.53

```
load Signature.txt;
t=Signature(:,1);
h=Signature(:,2);
load timing.txt;
u=timing(:,2);
```

Vector u	
time	Value
0	1
0.001	0
0.002	0
0.003	0
0.004	1
0.005	0
0.006	0
0.007	0
0.008	1
0.009	0

Vector h	
time	Value
0	0
0.001	-0.02
0.002	-0.02
0.003	-0.02
0.004	-0.02
0.005	-0.02
0.006	-0.02
0.007	-0.02
0.008	-0.02
0.009	-0.02

Vector y	
time	Value
0	0
0.001	-0.02
0.002	-0.02
0.003	-0.02
0.004	-0.02
0.005	-0.04
0.006	-0.04
0.007	-0.04
0.008	-0.04
0.009	-0.06

Figure 4.53 Matlab command to load signature and timing vectors

Now using the convolution built in command in Matlab® given by; $y = conv(u, h)$, the graphical result is included in Figure 4.54.

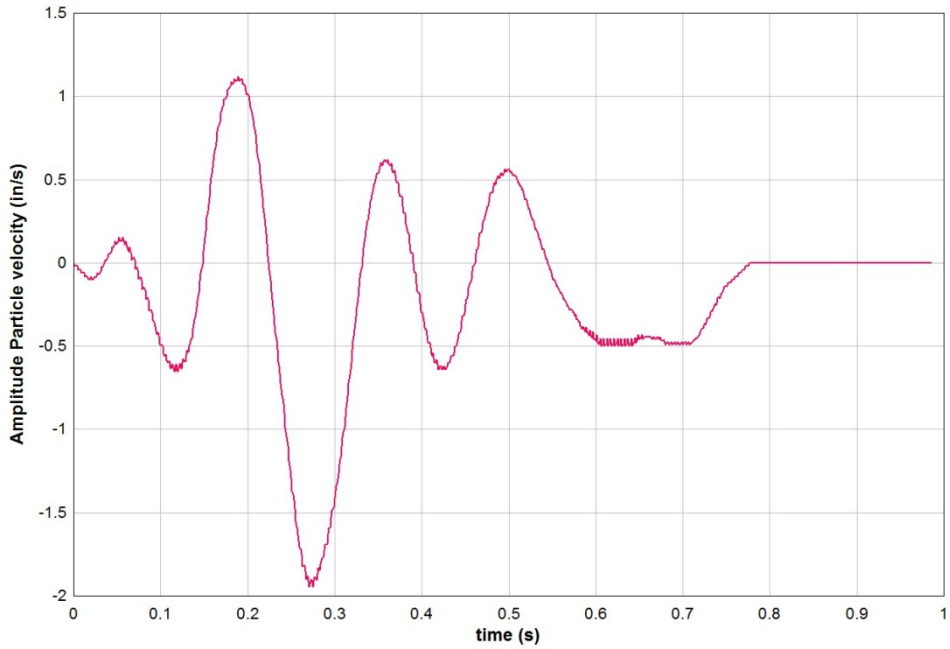

Figure 4.54 Convolution for radial component

The graphical procedure to calculate the predicted vibration waveform using the signature waveform is included in Figure 4.55 for the first three signals representing the blast of twelve initial holes and the last signal in this test.

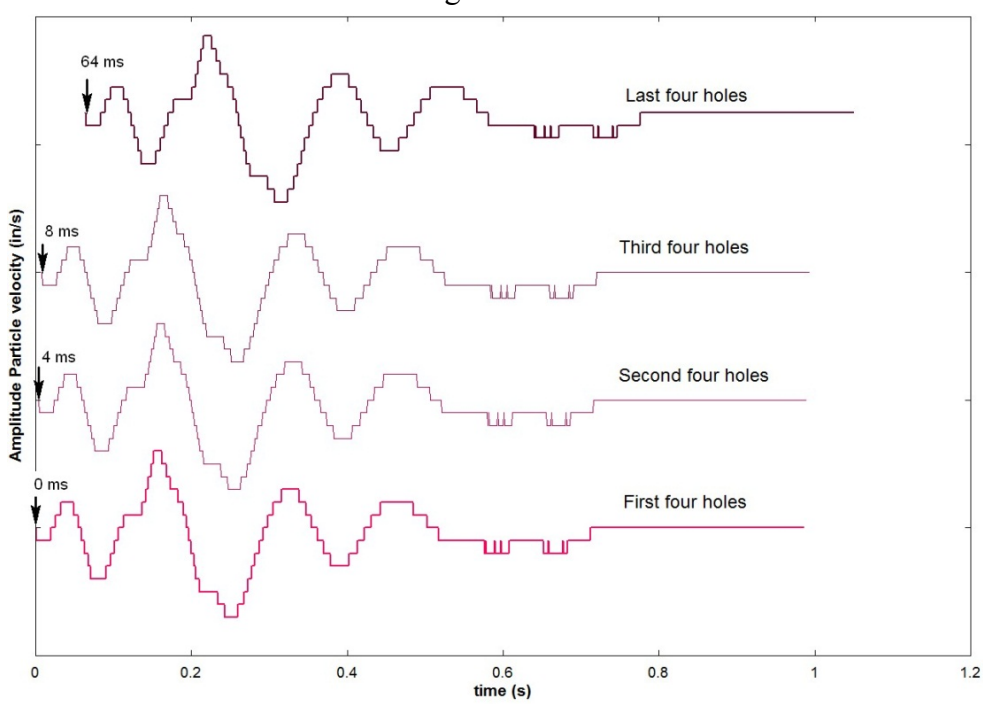

Figure 4.55 Graphical procedure to calculate vibration waveform in test

When all signals are added together, it is obtained the waveform included in Figure 4.56.

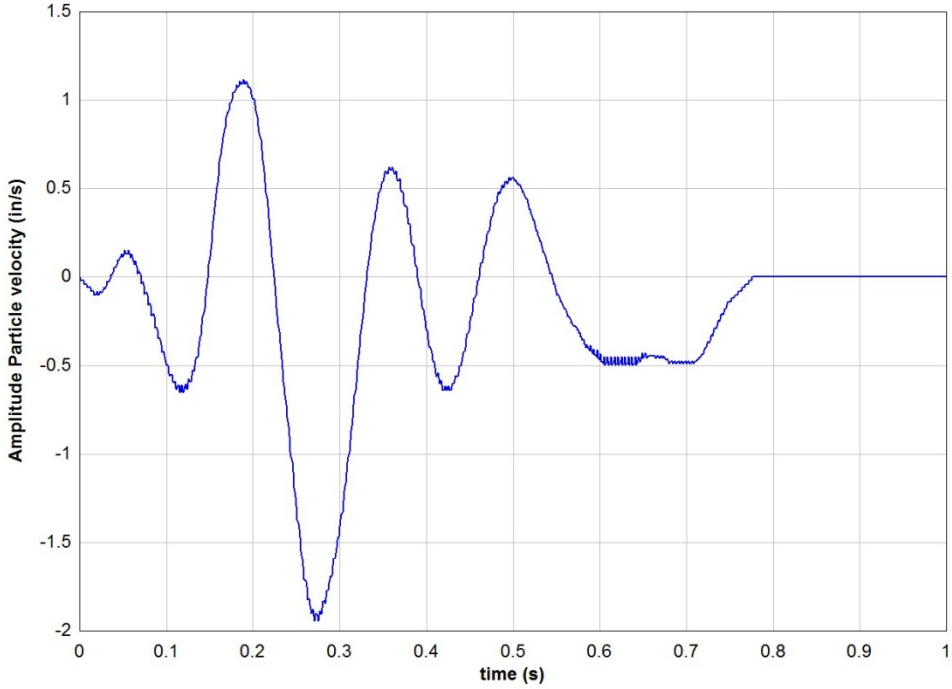

Figure 4.56 Final waveform after sum 17 signals using graphical procedure

Alpha-Blast software from White Industrial Seismology Inc. was used to calculate the complete waveform of the blasting test in order to compare previous results with the results of one commercial software already tested by the mining industry,. The simulated waveform is included in Figure 4.57.

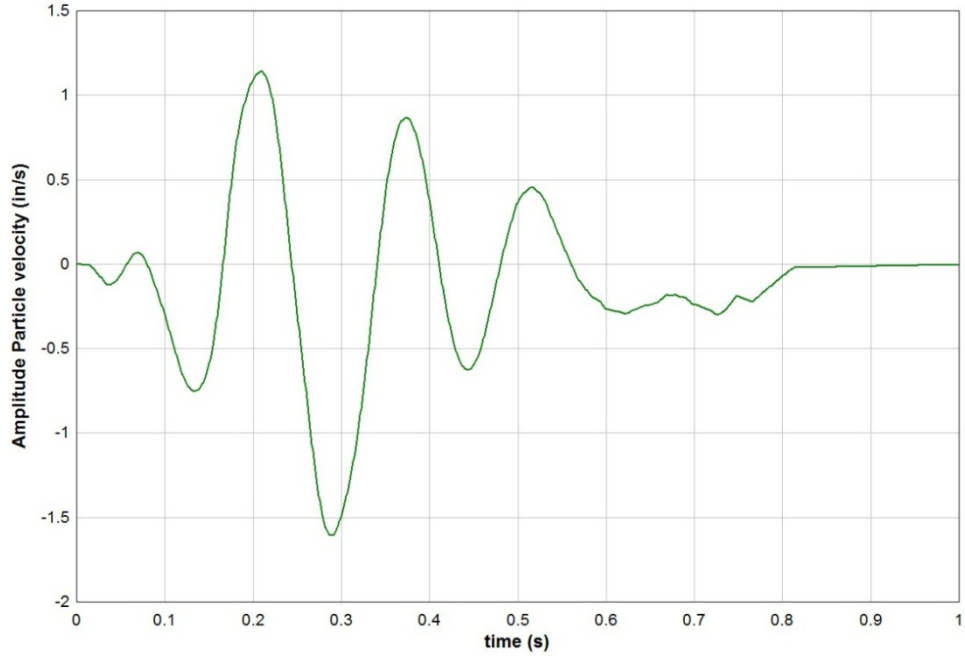

Figure 4.57 Final waveform simulation using commercial software Apha-Blast®

The measured waveform for this test and the different simulations are included in Figure 4.58.

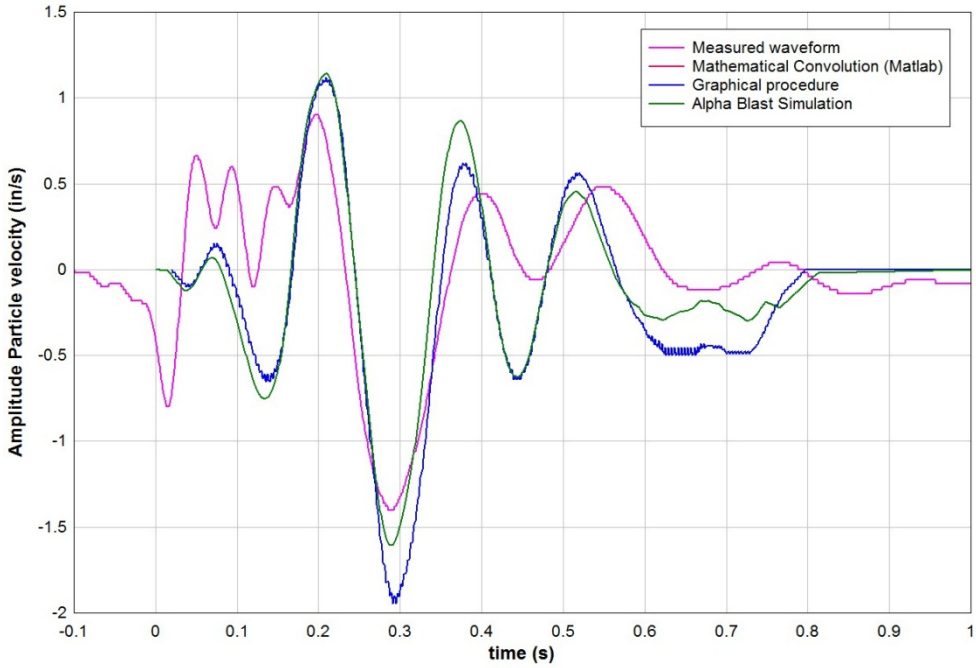

Figure 4.58 Complete waveform comparison using different methodologies.

Figure 4.58 shows that there is no difference between mathematical convolution and the graphical procedure. On the other hand, there is some small difference between graphical procedure and Alpha-Blast software. However, since Alpha-Blast is commercial software and there is no access to the code, it is not clear what methodology and filtering process is performed by the software in the background that can give a different result.

In the proposed Monte Carlo method, since for each hole a signature waveform is generated randomly for each hole, the summation of the signals is done using the graphical procedure explained previously. Notice that, if a standard convolution were used, there is no chance to combine different waveforms.

The field test performed at Guyan mine are described in the next sections. The results of the blast test are compared to simulations when the improved signature hole technique is introduced.

IMPROVED SIGNATURE HOLE TECHNIQUE VALIDATION

5.1 Introduction

To validate the proposed improved signature hole technique, several field tests were performed at a surface coal mine in West Virginia. Validation of the methodology was achieved through analysis of blast vibration signals recorded at the mine for different experimental setups. Description of the site, instrumentation setup, designed tests and recorded data are included next.

5.2 Field Experiments

5.2.1 *Instrumentation and data collection*

5.2.1.1 Site description

Guyan mine is located in southern West Virginia, in Logan County. The site was chosen according to the matching in-kind contribution for the project offered by OSM, Patriot Coal Corporation and the University of Kentucky. This operation is a typical surface coal mine. The mine utilizes blasting, truck and shovel/loader machines to perform the contour mining method at the site. The coal is sourced from the Freeport, Kittanning, Stockton and Coalburg seams, with a 15 to 1 average overburden coal ratio. (Source: Patriot Coal Corporation). Figure 5.1 shows the location of the site where the information was collected.

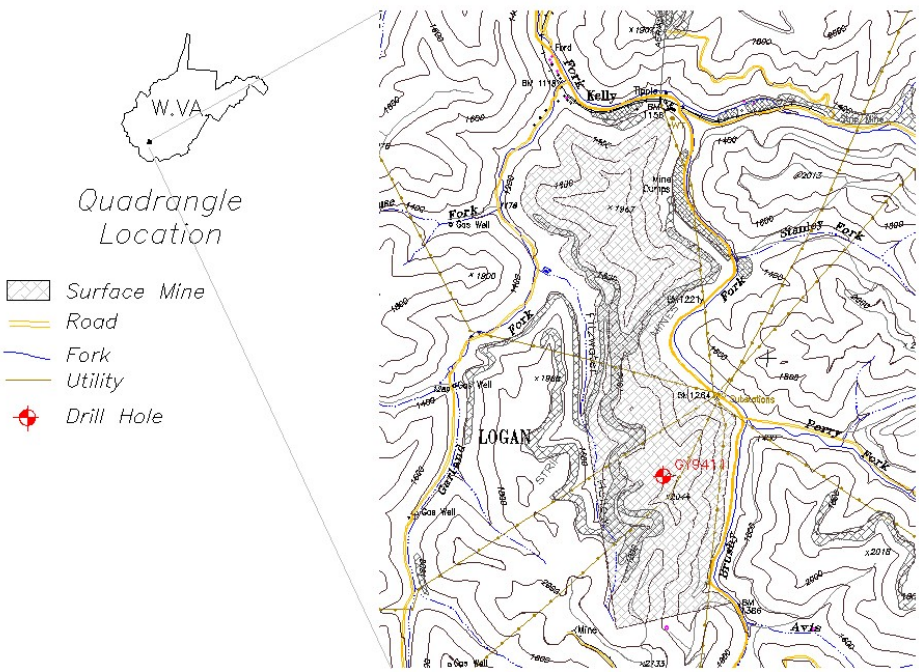

Figure 5.1 Location of the mine where the field experiments were conducted

Stratigraphic units present within the area include the Homewood Sandstone, multiple splits of the Stockton Coal seams, Upper Coalburg Sandstone and the Coalburg Coal seam. The overburden where the blasting activity took place mainly is the Coalburg Sandstone which is a massive Sandstone and ranges in thickness from about 70 to 100 feet. Figure 5.2 shows a simplified stratigraphic column in the area where the blasting activity took place during the collection of information.

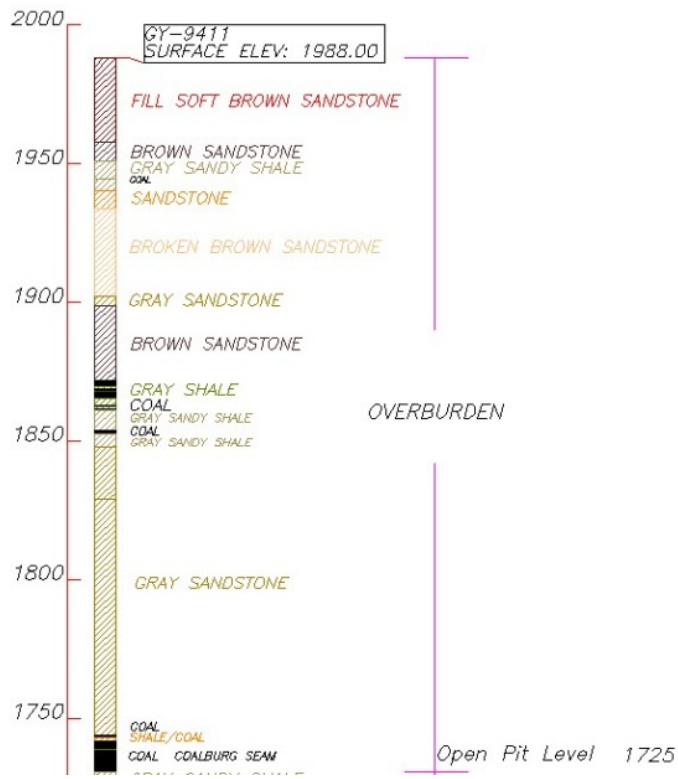

Figure 5.2 Drill Hole GY 9411, stratigraphic column

5.2.1.2 Instrumentation

The objective of the instrumentation was the measurement of the environmental effects of the production blast; specifically blast vibrations and air blast for several blast.

The instrumentation was performed in two different stages according to the frame of time where the information was collected. The first run of collection of information was between summer and fall 2010 and the second stage occurred in summer 2011. Next, the most important information regarding the instrumentation during each period of time is described.

Instrumentation for summer and fall 2010

For this period of time, in a first approach, seismograph locations were planned to follow a radial pattern having as center the Drill hole GY9411 (Figure 5.1). However

after three site visits to verify the site conditions for the seismographs, it was necessary to perform several modifications. The modifications were necessary either due to access difficulties to some places or because the seismograph location planned were located in areas outside of the property boundary of the mine. In order to protect the seismographs, it was necessary to adapt tool boxes to contain the seismographs. An external battery was used to extend the internal battery of the seismograph. Figure 5.3 shows the modified tool box to contain and protect the seismographs.

Figure 5.3 Case for the seismograph setup

In total, during this first run of collection of information, 12 seismographs were installed in the area under study. Table 5-1 includes the description of the seismographs and the coordinates in both systems NAD 83 and NAD27.

Three of the seismographs (2,3 and 4) were NOMIS® 5400 while the others nine were White Industrial MINI-SEIS series. Some of the seismographs were supplied by WVDEP, OSM, Dep Mines Minerals and Energy and UKY. All the devices were calibrated by the original provider of the seismographs, before the data collection activity.

The seismographs setup was designed to keep a radial pattern reference to the centroid of the exploitation area for the years 2010-2011. This centroid was located coinciding with the geological drill hole GY9411. Finally the arrangement of the seismographs was completed following three well defined lines. The lines were named according to the line's orientation as North, East and South. Figure 5.4 show the pattern followed to setup the seismographs. North line (seismographs 9,10,11 and 12), East line one (seismographs 2,3,4) at the bottom of the valley, East line two (seismographs 5 and 6) at the top of the valley over reclaimed area and South line (seismographs 7 and 8).

Table 5-1 Seismograph location and their characteristics

SEIS	DESCRIPTION	NAD 83		NAD 27		Owner
		E	W	X	Y	
1	MINI-SEIS II Inst# MS II 2D2G 1/4M S/N: 4763	37.827306	81.79722222	1769695.032	302194.887	UK
2	NS 5400 S/N: 2722	37.829722	81.7926667	1771018.239	303063.285	Saul's
3	NS 5400 S/N: 2242	37.829306	81.78955556	1771915.431	302904.128	Saul's
4	NS 5400 S/N: 2774	37.828472	81.78608333	1772915.656	302591.914	Saul's
5	MINI-SEIS II Inst# MS II 2D2G 1/4M S/N: 4762	37.827417	81.791	1771492.406	302219.877	UK
6	MINI-SEIS II Inst# MS II 2D2G 1/4M S/N: 3599	37.82575	81.78622222	1772867.112	301601.13	Ken - OSM
7	MINI-SEIS Inst# MS 2D2G S/N: 429	37.819056	81.79911111	1769123.556	299195.638	UK
8	MINI-SEIS Inst# MS 2D2G S/N: 2832	37.814444	81.79691667	1769742.925	297510.868	WVDEP
9	MINI-SEIS Inst# MS 2D2G S/N: 2467	37.834833	81.80225	1768266.722	304948.143	WVDEP
10	MINI-SEIS Inst# MS 2D2G S/N: 2468	37.8385	81.80044444	1768799.694	306278.84	WVDEP
11	MINI-SEIS Inst# MS 2D2G S/N: 180	37.841389	81.79933333	1769129.628	307327.998	UK
12	MINI-SEIS II Inst# MS II 2D2G 1/4M S/N: 1513	37.846167	81.79777778	1769593.786	309063.868	Dep Mines, Minerals and Energy. Big Stone GAP VA

Initially in the North line it was planned that all devices were at the same elevation (seismographs 9 to 12) but when it was implemented in field, many access problems arose. It was not practical to setup those devices at the same elevation.

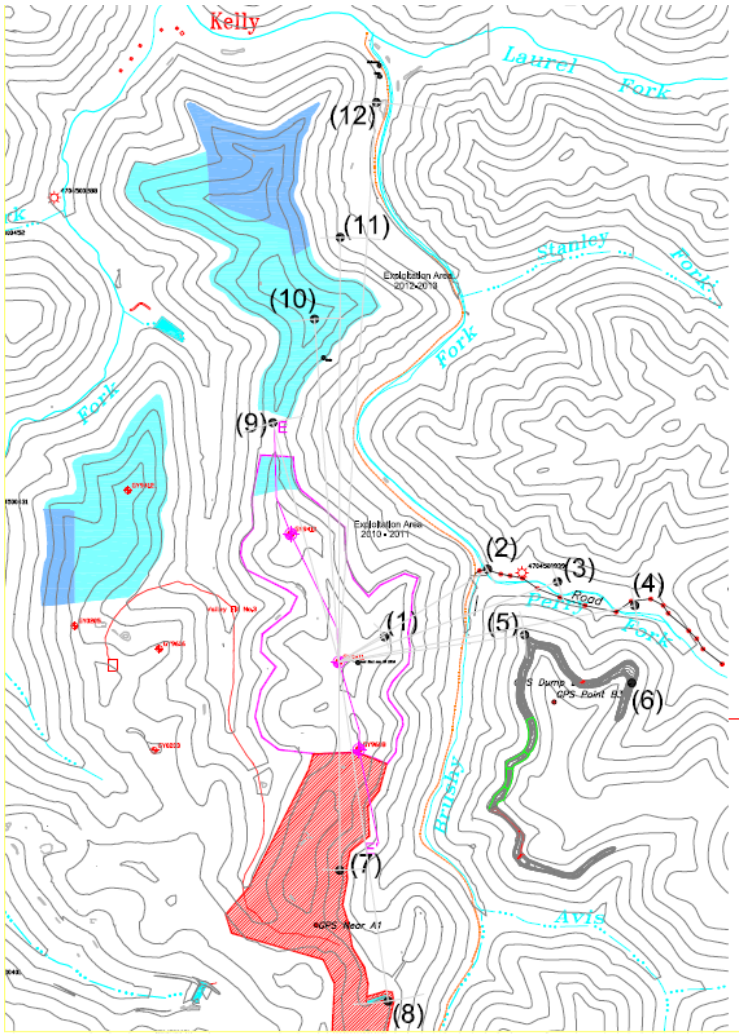

Figure 5.4 Seismographs location

The trigger levels of the seismographs were set after several tests to guarantee the collection of the information in all the points under study. In the adjustment of the trigger levels, the proximity of the seismographs to roadways to prevent false triggers, topographic conditions of the site, the distance from the source to recording point and others factors that affect the expected levels of airblast and vibrations were considered.

Table 5-2 includes the final arrangement for the seismographs trigger levels. The table includes the seismograph number, the distance from the drill hole GY9411, which was taken as the exploitation area centroid, the elevation and the trigger levels. It should be noticed that distances seismograph-blast changed while the blasting activity was developed through the collection of the information, so distances in Table 5-2 should be taken as one initial reference.

Table 5-2 Seismograph's triggering parameters

	Trigger parameters					
Seismograph	Distance (ft)	Elevation (ft)	Particle velocity (in/s)	Airblast (dB)	Duration (s)	Samples/second
1	667.0	1900	0.08	122	10	1024
2	2242.0	1300	0.05	118	10	1024
3	2286.8	1350	0.05	118	10	1024
4	3859.6	1355	0.05	118	10	1024
5	2404.8	1770	0.05	118	10	1024
6	3763.8	1797	0.05	118	10	1024
7	2675.4	1800	0.08	122	10	1024
8	40405.4	1900	0.08	122	10	1024
9	3191.3	1800	0.08	122	10	1024
10	4418.9	1910	0.03	120	10	1024
11	5457.1	1400	0.03	120	10	1024
12	7208.9	1200	0.03	120	10	1024

Initially it was planned to attach some of the seismographs to rock. Due to the geological conditions of the area, where the layer of soil is more than 3 feet thick, it was not possible to fix the geophones to the rock. All records collected were representative of vibration records in soils where the houses in the area are usually found. Finally, to setup the devices, all the field practices guidelines for blasting seismographs were reviewed and applied. (ISEE Field Practice Guidelines For Blasting Seismographs 2009 Edition).

Instrumentation parameters caused a reduction in the collected number of events for some of the seismographs. Continuous false triggers (based on low trigger levels and high ambient vibration) deactivated the capacity of the device and only allowed recording of peak values instead of the vibration trace. This was especially true for seismograph 1 and seismograph 5 and 6. Considerable quantities of false triggers in seismograph 1 were due to the proximity of this seismograph to the blasting area. Machinery activity provided additional seismic input close to this point. Seismograph 1 was also lost for a short period because a dozer buried the device.

Seismographs 5 and 6 were in an area where significant animal activity was occurring, perhaps close to a trail path for deer and bears. Frequently the boxes containing seismographs were founded lying down, and had teeth marks. Despite these problems, the data base contained enough information to analyze regarding vibrations when the delay system is non-electric or electronic.

Instrumentation for summer 2011

Following analysis of the information collected in 2010, it was decided to perform some specific blast tests in summer 2011. The second seismograph instrumentation setup took centroid the mining exploitation area for summer 2011 and was performed at the same ridge of the mine. The new centroid was located 5000 feet to the North measured from the point of reference for 2010 tests (drill hole GY9411). Since after the 2010 tests,

all the seismographs were removed (for maintenance), it was necessary to setup a new seismograph arrangement to collect the information for the second monitoring period of time (summer 2011). In this second round of tests, five (5) seismographs were used.

The locations of the seismographs for the second round of test are included in Figure 5.5. As reference in Figure 5.5, the drill hole GY 9411 is included as well as the location of some of the seismographs used during the 2010 tests (locations in grey).

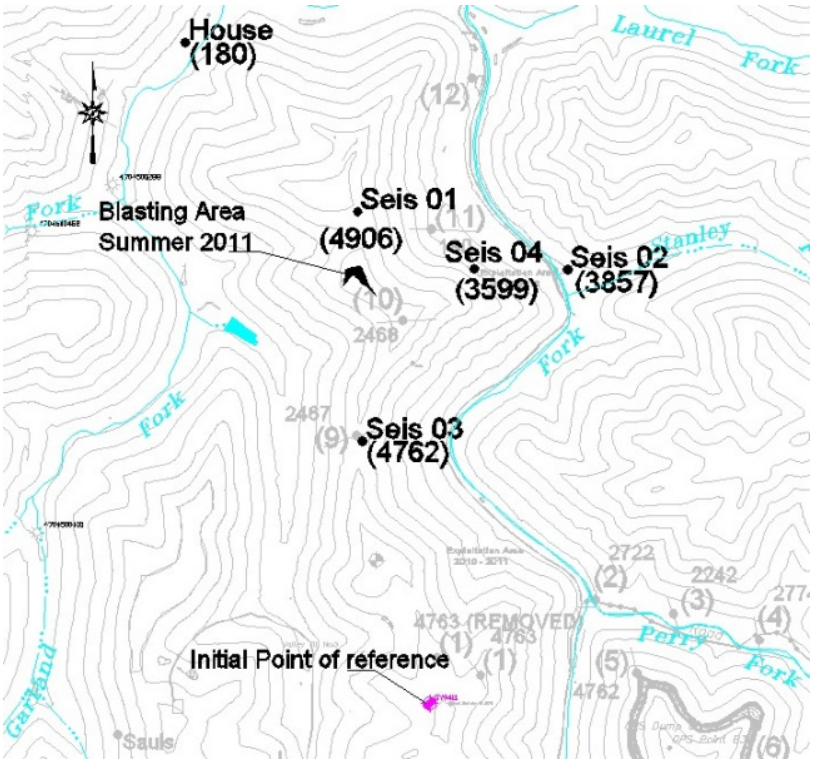

Figure 5.5 Seismographs location for second round of test. (Summer 2011)

Only two seismograph locations were kept similar during the two periods of collection of information, seismograph 9 (2010 test) and seismograph 3 (2011 test) and the seismograph installed in the backyard of the house that belongs to the mine (seismograph named as House). This last seismograph was located in that place by request of the blasting crew because some of the blasting tests used delay timing less than 8 milliseconds.

Figure 5.6 shows the NOMIS 5400 system used to collect vibration and airblast information in fall 2010.

Figure 5.6 NOMIS® 5400 System used to collect blast vibrations and airblast

Table 5-3 includes the characteristic of the triggering used to setup the seismographs in the second round of test.

Table 5-3 Triggering levels used in the second round of test

	Trigger parameters					
Seismograph	Distance (ft)	Elevation (ft)	Particle velocity (in/s)	Airblast (dB)	Duration (s)	Samples/second
4906 (1)	691.9	1850	0.01	148	12	1024
3857 (2)	2410.1	1200	0.01	142	12	1024
4762 (3)	1937.8	1800	0.03	148	12	1024
3599 (4)	1348.1	1500	0.01	142	12	1024
180 (House)	3278.3	1200	0.01	148	12	1024

5.3 Test's description

The complete data base of vibrations collected during this project is composed by 200 events. However, only those tests where at least one signature hole was recorded are described next. This is because for those events, it is possible to use the proposed methodology and compare the prediction versus the vibration waveform recorded for the complete blast event. Table 5-4 summarizes the tests including the main characteristics like number of holes, depth of the holes diameter etc.

Table 5-4 Tests including signature hole

Test	Date	Holes	Depth (ft)	B (ft)	S (ft)	Det	Total explosive	Main Delay	Signature
1	09/10/2010	25	30	18	18	Elect	10,450.21	8ms	NO
2	09/11/2010	29	95	9	9	Elect	2,125.57	1ms	Three hole@same time (Pre-split)
3	09/11/2010	66	30	18	18	Elect	21,160.37	80ms	
4	09/15/2010	194	90	20	20	Elect	342,763.93	4ms	One hole
5	09/16/2010	69	44	20	20	Elect	55,050.03	4ms	Four Holes@same time
6	09/17/2010	41	30	18	18	Elect	11,069.31	100/42 ms	One hole
7	09/18/2010	96	95	18	18	Elect	181,778.14	4ms	Two holes@same time
8	09/22/2010	67	75	20	20	Elect	86,719.03	4ms	Two holes@ same time
9	10/01/2010	176	95	20	20	Elect	298,139.26	17ms	One hole
10	06/22/2011	11	45	18	18	Elect	5,928.63	5ms	Three signatures
11	06/23/2011	26	30	18	18	Elect	22,090.28	100/5 ms	Two signatures
12	06/24/2011	29	45	18	18	Elect	24,271.73	5ms	Two signatures
13	06/29/2011	32	45	18	18	Elect	26,039.31	3ms	One hole signature
14	06/29/2011	35	45	18	18	Non-elect	30,106.45	42/100 ms	NO-Signature
15	06/29/2011	40	45	18	18	Elect	33,478.25	42/100 ms	NO-Signature

In total, 15 field tests were used to prove the proposed methodology in this research. Appendix A contains the blasting log report from the mine and the vibration and airblast signals for each test.

The location of the holes in the last six tests, (performed in 2011) were controlled using topographic survey of precision. The plan layout of those tests are included in appendix B.

Figure 5.7 shows the plan layout for the test 06/24/2011 (test No.12). Red indicates the hole number, in black the nominal delay used. In this test two signature holes were recorded at 2500 and 7000ms. In total, the duration of this blast was 9.172 seconds. This test accounts for 29 holes blasted. The order of the number of holes as

shown in Figure 5.8 is six (6) holes, one (1) signature, ten (10) holes, one (1) signature and finally eleven (11) holes. This figure shows the radial, vertical and transverse component of the vibration as it is recorded normally.

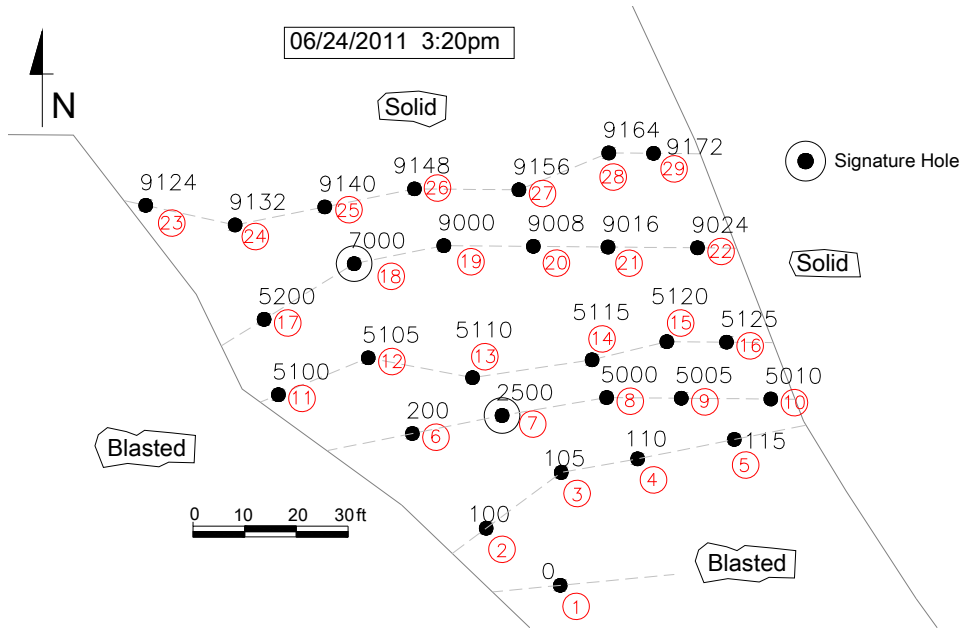

Figure 5.7 Plan layout test 06/24/2011

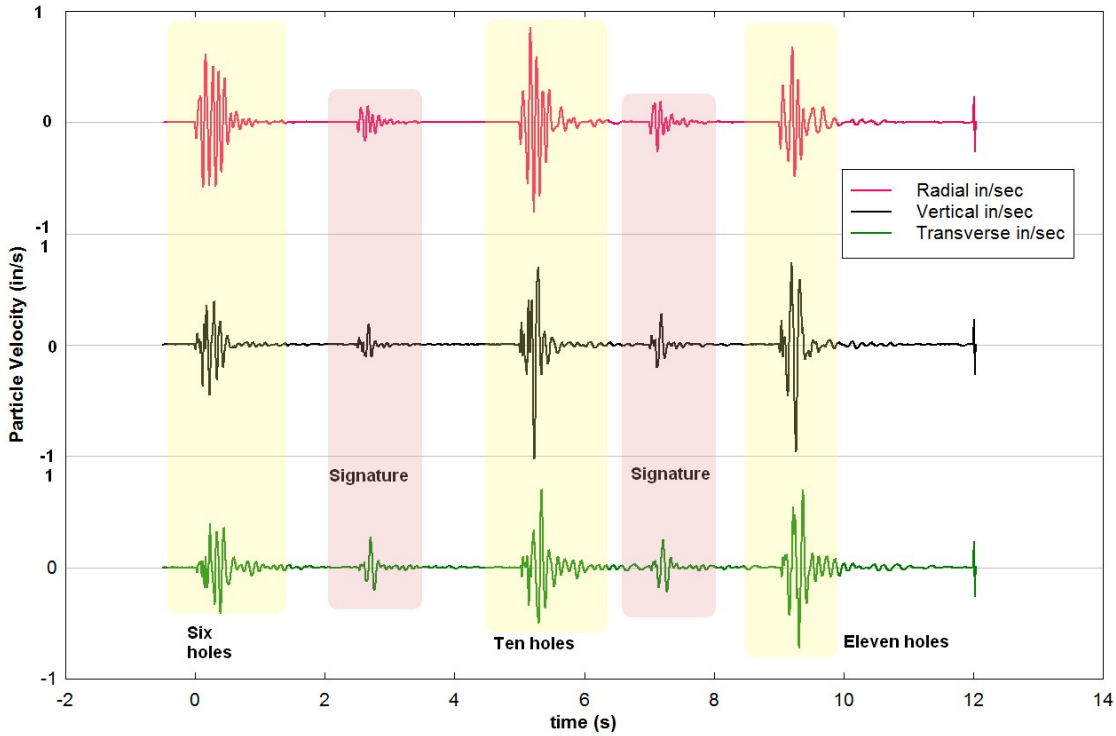

Figure 5.8 Vibration record for test No.12, seismograph 4906 (approx. 767ft from source)

Figure 5.9 is obtained when the other seismographs are included in the graph using only the radial component (just for convenience).

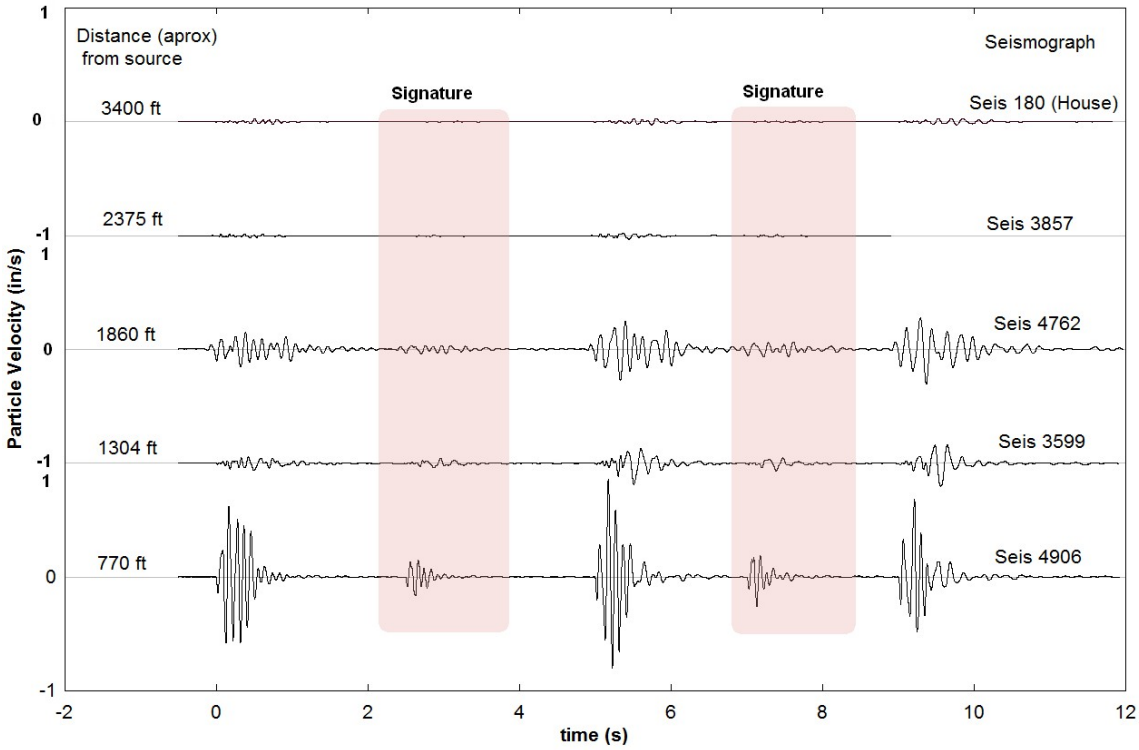

Figure 5.9 Radial vibration component for test No.12 and all the seismographs in summer 2011

In Figure 5.9 it is possible to see the attenuation of the vibration with distance. In this figure, despite seis 3599 being closer than seis 4762, vibration levels are higher for the seismograph further away (between 3599 and 4762). This situation may be the effect of topographic influence on blast vibrations and the change in elevation between the source and the monitoring point. Seismograph 4906, 4762 and the source are more or less at the same elevation (1825ft) when compared to seismograph 3599 that is approximately 300 ft below the source of the blast vibration (1500ft). When signature signals are isolated from the complete record (red areas in Figure 5.9), it can be seen that it is not possible to assess, in this case, a signature for the point located at 2375 and 3400ft away from the source point, this is because at such distances the vibrations had been completely attenuated. In those cases, it is not possible to use signature hole techniques, because no signature is available to calculate a prediction using this methodology. Appendix C includes the vibration records for the other fourteen events included in Table 5-4.

Results for airblast in test No.12 are included in Figure 5.10. This figure shows the problems regarding the sensitivity of the seismograph. The signals are stepwise and all signals include some level of noise (this is more evident in seismographs 4762 and 4906). This is an important factor to account when using signature hole technique to predict airblast and ground vibrations because the quality of the prediction is directly

related to the quality of the signature signal. By definition, a signal carries information that we are interested in. In the case of blast vibrations, the signal that is usually recorded contains particle velocity information of the monitoring point under the effects of the mining blast. Under that concept, noise is anything else in the signal. If a vibration records contains noise, it is necessary to perform several pre-process steps before convolution or superposition to avoid, filter or minimize the noise. If a noise signal is used to perform the superposition, due to the numerical nature of the superposition, the noise will propagate (like a propagating error).

When it is necessary to apply filters to the signal, some frequencies are eliminated from the original signal; for example in low pass filters high frequencies are eliminated, if high pass filter is applied to the signal the low frequencies are eliminated leaving the high frequencies. The risk from the prediction point of view when filters are applied is to eliminate information that we are interested in but it is eliminated when the signal is filtered.

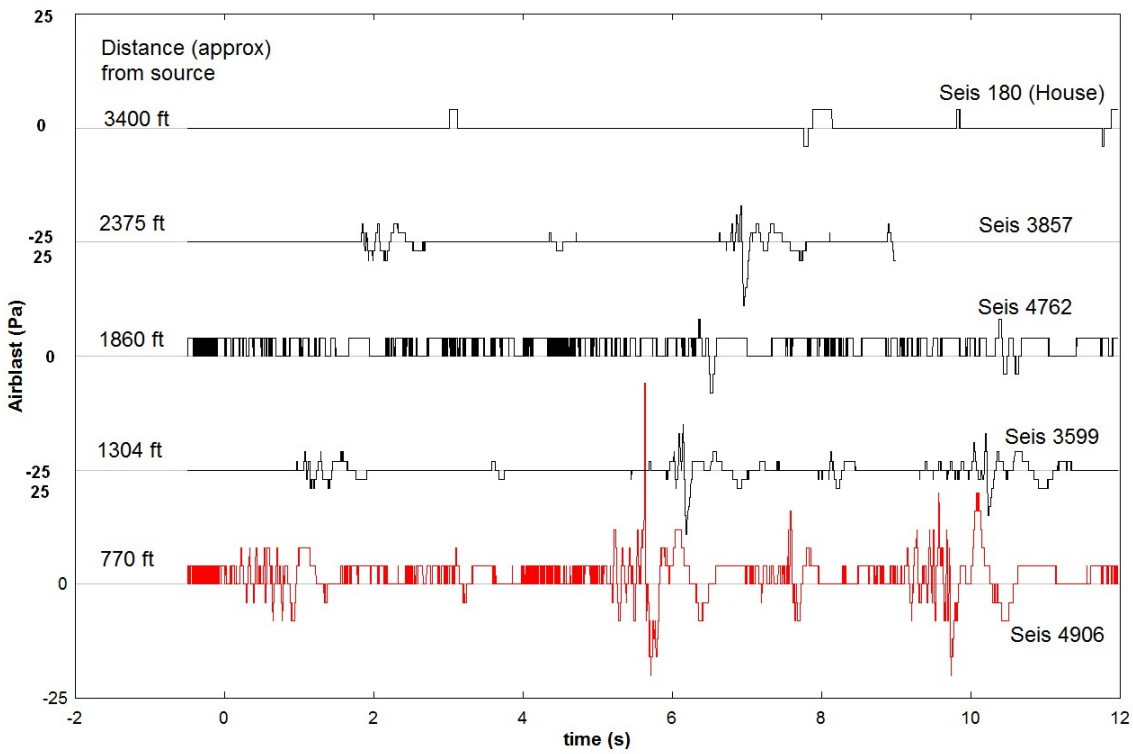

Figure 5.10 Airblast records for test No.12 and all the seismographs in summer 2011

A good signature signal for airblast, in order to perform a prediction using the signature hole technique, is included in Figure 5.11.

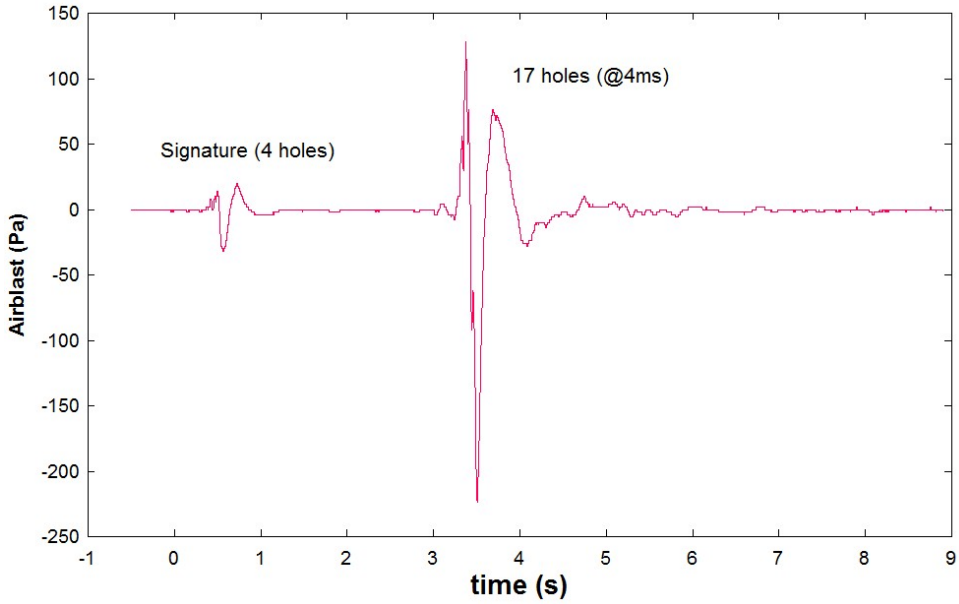

Figure 5.11 Airblast record for Test No.5 (Four holes signature)

Validation for the methodology is completed in detail using tests No.5, 10 12, 14 and 15.

Those tests were chosen for several reasons; test No.5 had a good signature signal for airblast. Tests 10 and 12 have similar geometry, depth, spacing, burden etc. In both cases six holes were detonated at different average delay time, so using these two tests it is possible compare the results when different delay timing is used. The two final tests (test No.14 and 15) have similar geometry, and similar delay time 42 and 100 ms. The difference between the final two tests was the initiation system used between non-electric and electronic.

5.4 Analysis and results of the models using improved signature hole technique

5.4.1 *Model 1. Airblast modeling (test No.5)*

Test No.5 was the same test used to show the practical example in Chapter 4 to calculate convolution using different methodologies. Next the main parameters of this test are included again.

Table 5-5 Blast test parameters test No.5

Parameter	Value
Total holes	69
Face height (ft)	44
Depth (ft)	44
Burden = spacing (ft)	20
Diameter (in)	9
Total explosive (lbs)	55,050.03

Figure 5.12 Plan view from the blast report for the test No.5

The signature waveform for air blast was included in Figure 5.11 (initial part of the signal). As mentioned before, in total 69 holes were detonated using four signatures at the same time and using electronic delay of 4ms. Next, the assumptions for modeling airblast using the improved signature hole technique are explained.

5.4.1.1 Signature test No.5

Figure 5.13 is obtained when the signature waveform is isolated from the complete record in Figure 5.11. In this figure, the value of the exponential decay factor is included. In this case, the value is 3.90, as indicated in Figure 5.13.

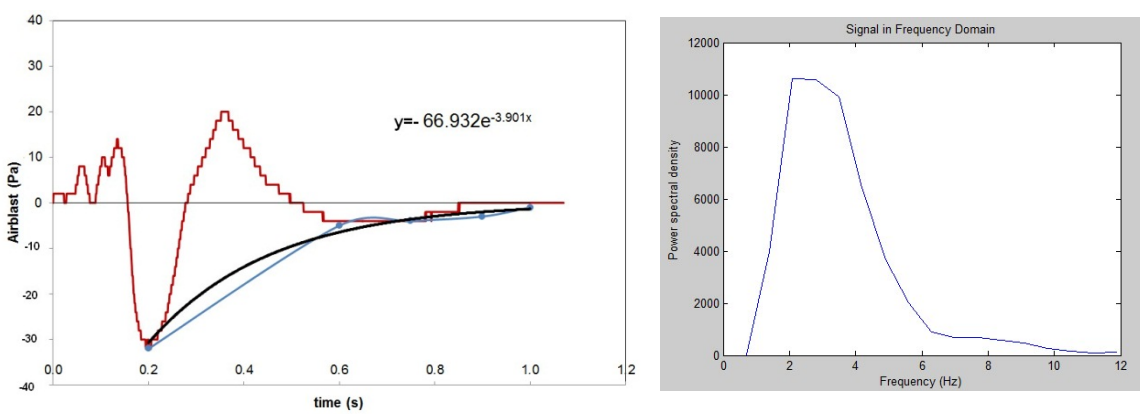

a) Waveform and decay factor b) Waveform in frequency domain

Figure 5.13. Airblast signature waveform test No.5

When the frequency content of the signal is reviewed, it is difficult to assess a specific value to generate the synthetic signals. As was explained in Chapter 4, using more coefficients in the Fourier series, result in more accurate simulation of the measured signal. In this case, the first five frequencies were chosen to simulate the signature waveform. Those frequencies are 1,2,3,4 and 5 Hz.

Using an amplification factor of 2.80, after running the software developed, the synthetic signature waveform for the airblast is calculated. The results are included in Figure 5.14.

In this model, in total 69 holes were detonated, however four holes were detonated at the same time using 4 millisecond delay between sets of four holes. As it was explained in chapter 4 and is included in Figure 5.12, it is possible to simplify complete blast to 17 detonations (four holes each). In order to model the complete airblast waveform, it is necessary to generate 17 different random signals using the results from Figure 5.14.

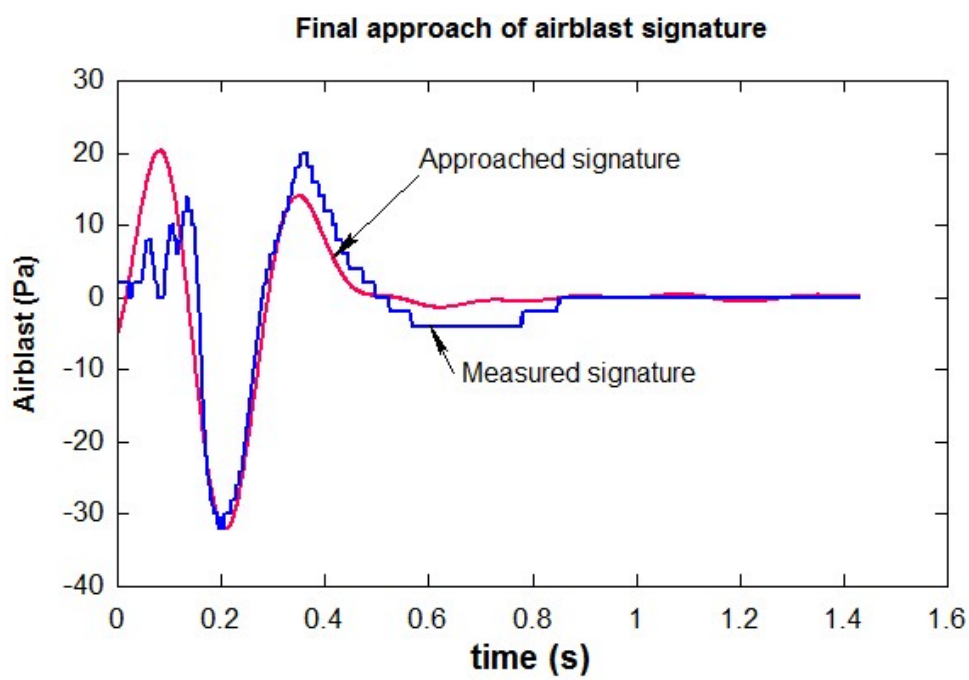

Figure 5.14 Airblast signature waveform and synthetic waveform (approach).

5.4.1.2 Synthetic signature signals

Using a lower and upper frequency interval of 0.50 Hz from the main frequencies, 17 signature airblast signals were generated. In the calculation, a scale factor average of 2.8, assuming a standard deviation of 0.50 was also used. Figure 5.15 shows the numerical values used to perform the calculations as entered into the software developed.

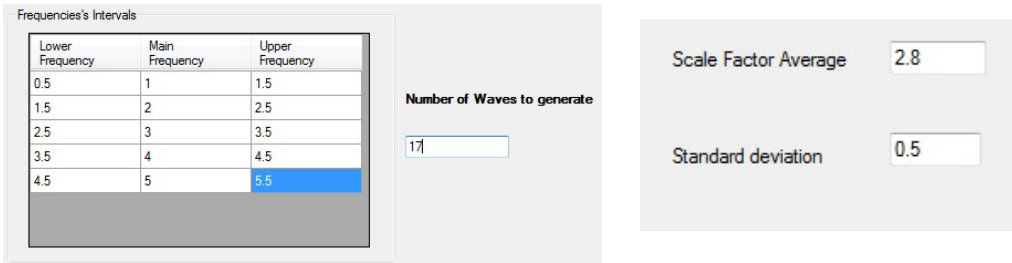

Figure 5.15 Frequency interval and scale factor for test No.5

The results when 17 random signature airblast waveform signals are generated are included in Figure 5.16. The random effects can include different quantity and quality, contamination of explosives in each of the four holes, changes in the temperature and air current effects between the source and the recording site that generate a change in the waveform between detonations.

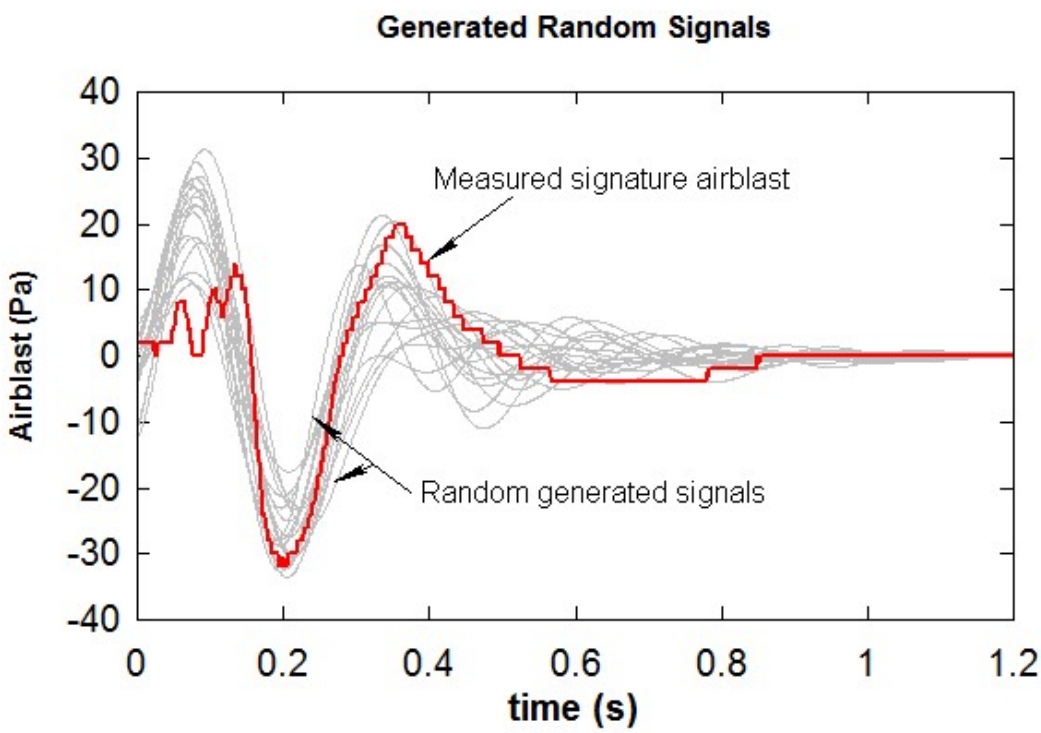

Figure 5.16 Random airblast signature waveform signals test No.5

5.4.1.3 Timing sequence

The delay between each four hole set in this test was uniform at 4ms. In the current validation example, there were observed no effects if timing due to distance

between the source and the monitoring point was included, so only timing due to detonator accuracy is calculated. The first calculation was done using zero standard deviation for detonators and the second one includes a standard deviation of 1ms as corresponds with the statistical calculations previously included in Chapter 4 (a linear variation for standard deviation with delay time was assumed to assess the standard deviation for 3000ms detonators).

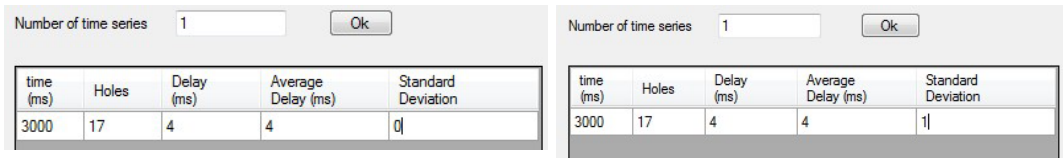

Figure 5.17 Delay time series for test No.5

The time function sequences for both scenarios are included in Figure 5.18. In this figure, it is possible to see how the sequence is affected when the scatter in the timing is included.

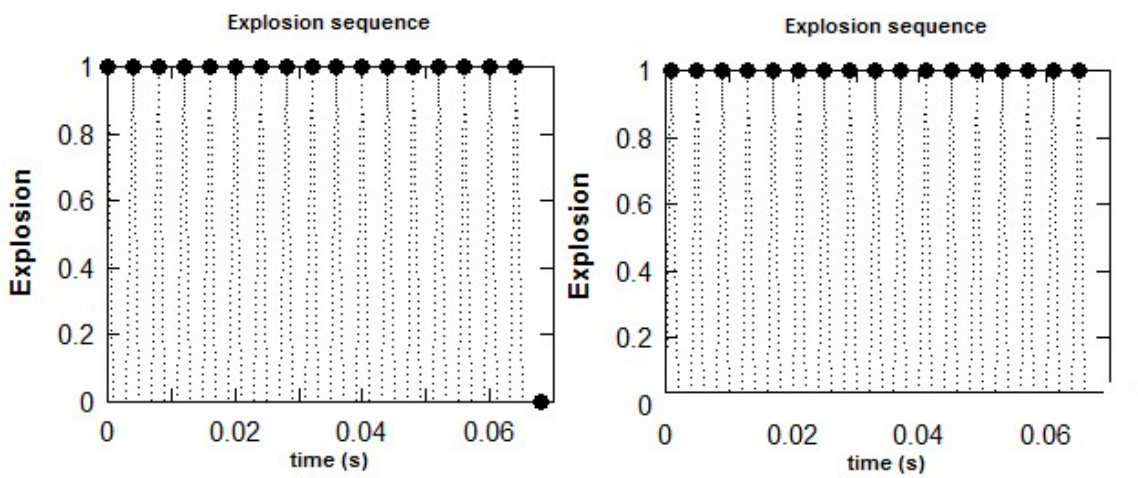

a) Zero standard deviation b) one millisecond standard deviation

Figure 5.18 Time function for test No.5. Zero and 1ms standard deviation in detonator

As mentioned before, no traveling time was included in the calculations.

5.4.1.4 Results Model 1

Zero standard deviation and one run

Figure 5.19 shows the result using one iteration (no-Monte Carlo analysis is performed) and zero standard deviation for delay timing.

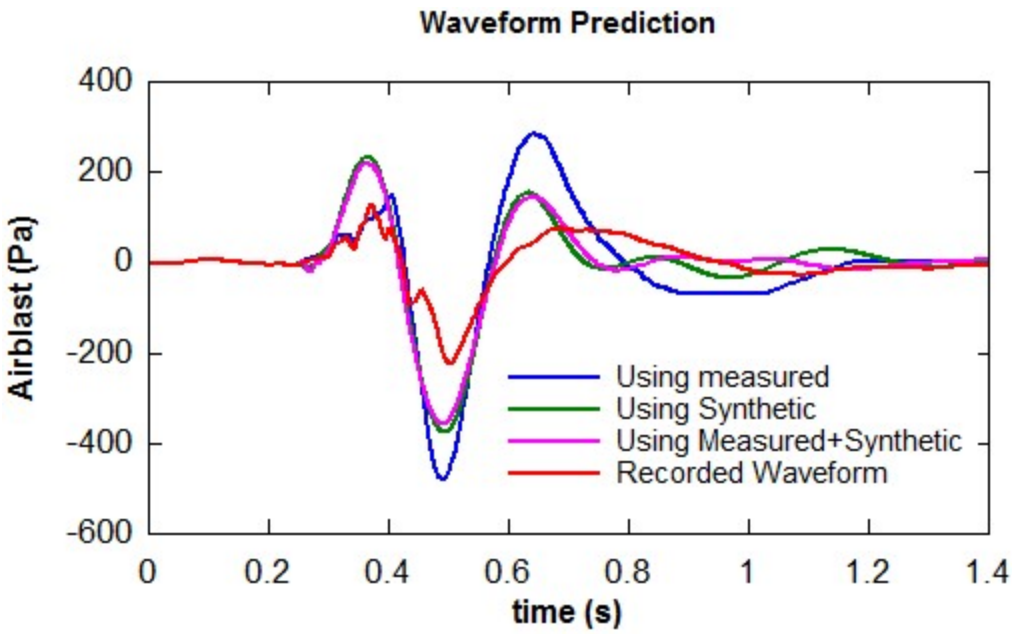

Figure 5.19 Results using one iteration and zero delay standard deviation

In this case, all the calculations overestimate the maximum measured value for airblast. This result is more evident in the case when only the measured signature airblast waveform is used to perform the calculations (current signature hole technique).

One millisecond standard deviation delay and Monte Carlo analysis (improved signature hole technique)

Using the improved methodology and the developed software, it is possible to analyze all the variables that are involved in the problem independently. Figure 5.20 shows the screen view for the current problem.

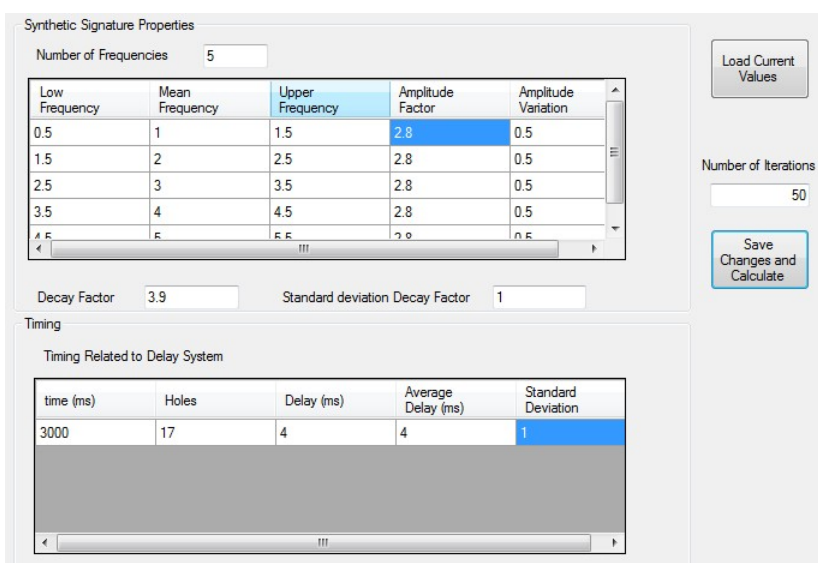

Figure 5.20 Variables involved in the prediction test No.5 using improved signature technique.

Using the parameters previously mentioned regarding frequency content, amplification factor, decay factor and delay time, Figure 5.21 is obtained for 50 iterations.

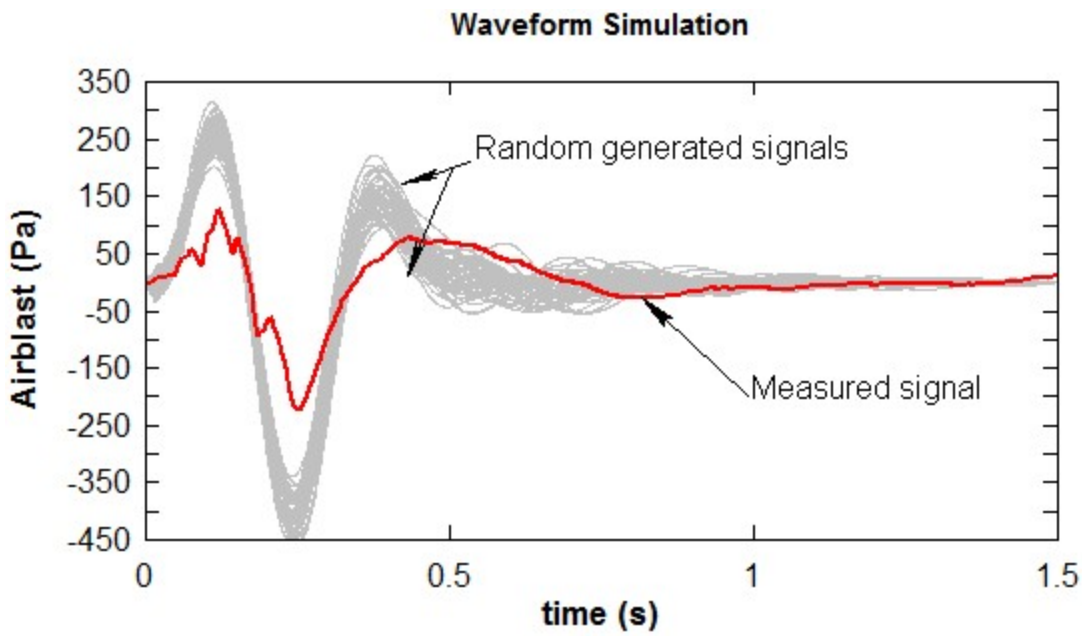

Figure 5.21 Monte Carlo result using initial parameters for test No.5

As shown in Figure 5.21, the peaks are overestimated for this case. This is because in the formulations, the same weight for the amplification factor has been assumed for frequencies between 1 and 5 Hz. If we analyze the frequency content of the signature airblast waveform (Figure 5.13b), only frequencies between 2 and 4 Hz contribute in an important way to the energy of the signal. Following this idea and assuming that the frequency of 3 Hz is the frequency that is more important for the amplitude of the signal and running the Monte Carlo analysis, we obtain the results in Figure 5.22.

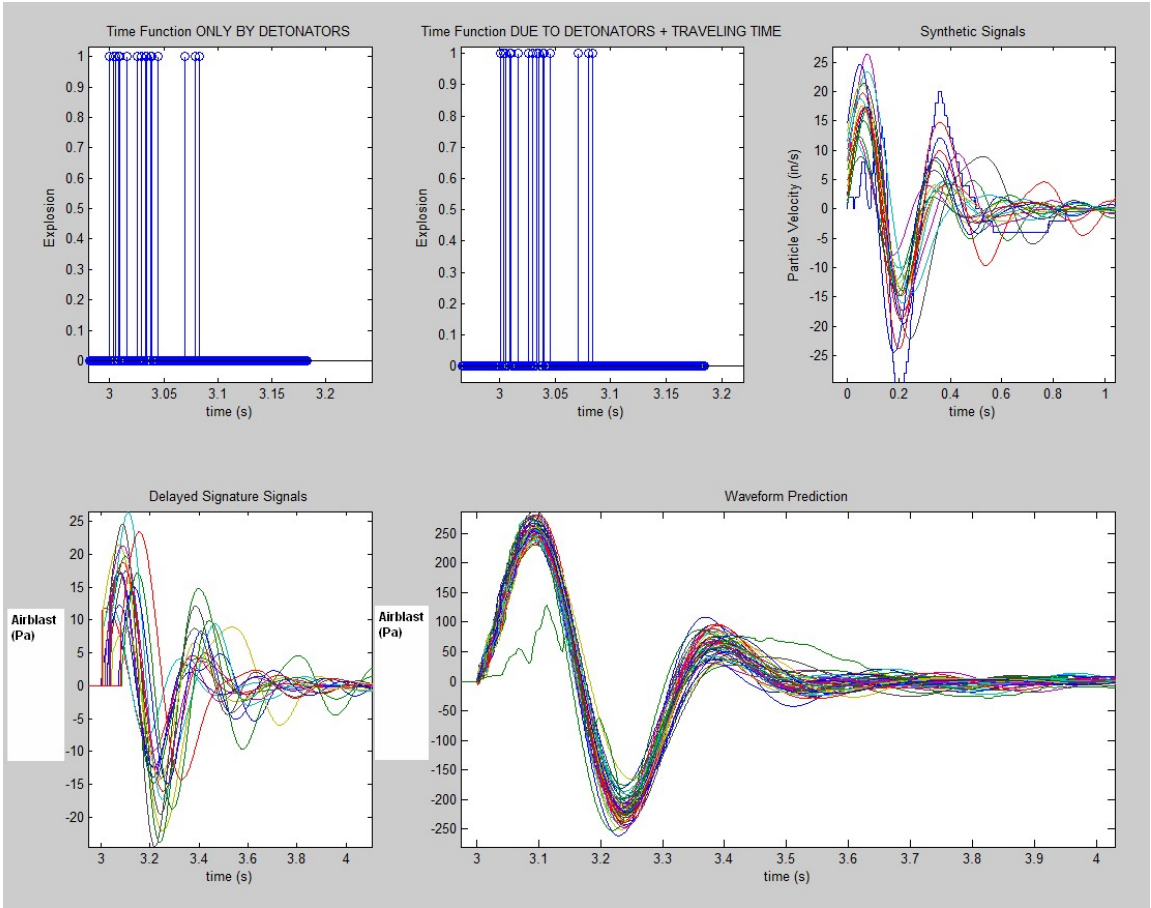

Figure 5.22 Monte Carlo results using 3Hz frequency as main frequency in test No.5

Amplitude factor for frequencies 1,2,4 and 5 Hz were assumed equal to one and amplitude factor for the main frequency of 3 Hz was assumed as previously mentioned of 2.80.

Using the maximum absolute values (the peaks), it is possible to create the histogram included in Figure 5.23. In this test, an average value of 258 Pa and a standard deviation of 18.42Pa were calculated using the improved signature hole technique. The airblast measured in this test was -224 Pa. So the absolute value of the measured peak is between two standard deviations from the mean calculated value.

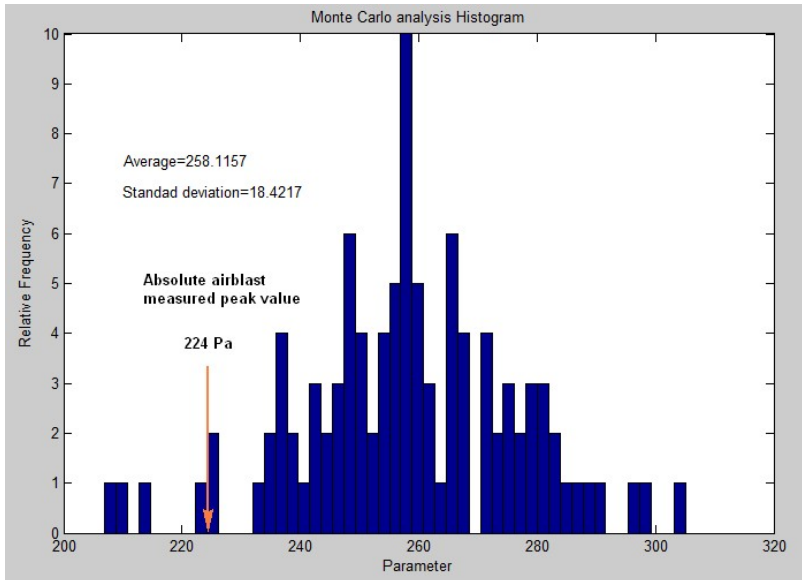

Figure 5.23 Histogram absolute maximum calculated values

In order to see the convergence of the improved signature hole methodology, the evolution of the parameter estimated, in this case the mean of the airblast against the number of samples or iterations, is included in Figure 5.24.

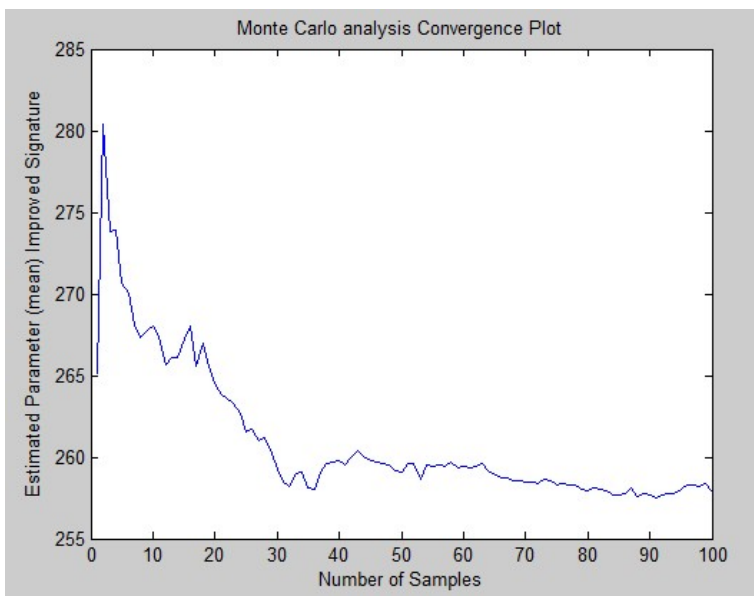

Figure 5.24 Convergence plot for test No.5

Figure 5.24 is a graphical representation of the central limit theorem and also is a measurement of the convergence of the mean of the peak particle velocity to certain value. This figure also shows the minimum number of iterations that are required to start to obtain a constant mean value for the peak particle velocity (in this particular case at least 30 to 40 iterations).

5.4.2 *Model 2. Particle Velocity (test No.10)*

Test No.10 was done in summer 2011. Next the main parameters of this test are included.

Table 5-6 Blast test parameters test No.10

Parameter	Value
Total holes	11
Face height (ft)	45
Depth (ft)	45
Burden = spacing (ft)	18
Diameter (in)	7.875
Total explosive (lbs)	5,928.63

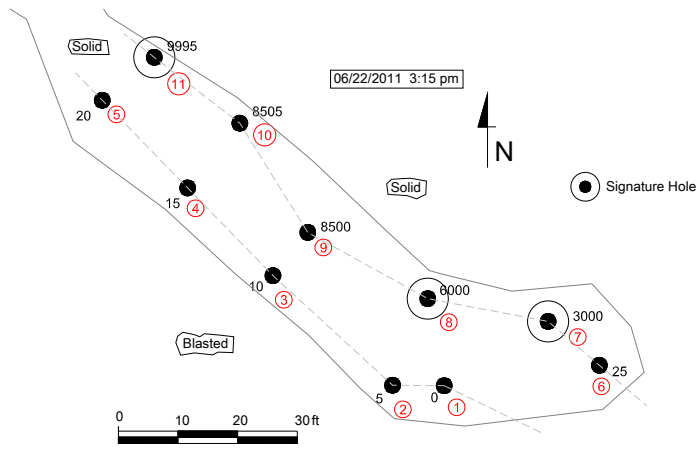

Figure 5.25 Test No.10, plan view from survey

In this test, there are three signature waveforms for the particle velocity.

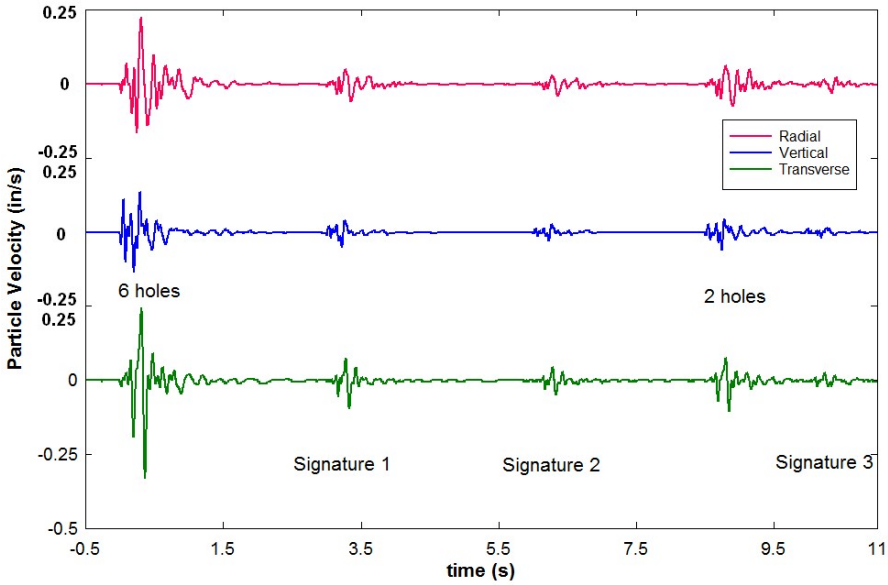

Figure 5.26 Vibration record seismograph 3599 test No.10

Seismograph 3599 was chosen to model the complete waveform for the six first holes in the test. It is possible to model any component; however for simplicity only the transverse component was used to compare the waveform prediction against the measured.

5.4.2.1 Signature test No.10

Figure 5.27 is obtained when a signature waveform for the traverse component is isolated from the complete record in Figure 5.26. In this test, there are three signature waveform signals, however only signature waveform two was used for modeling. In this figure, the value of the exponential decay factor is included. In this case, such value is 4.69, as indicated in Figure 5.27.

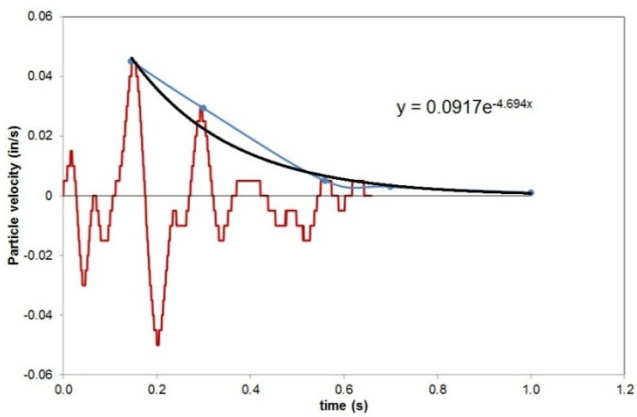

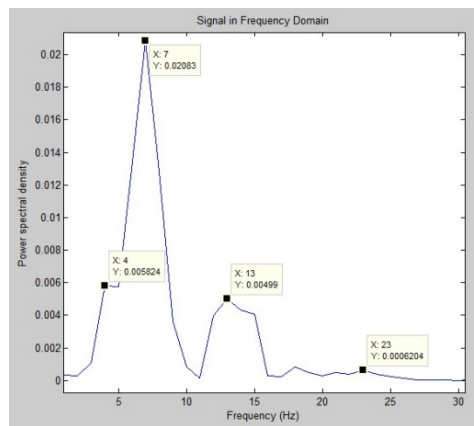

b) Waveform and decay factor b) Waveform in frequency domain

Figure 5.27. Ground vibration signature waveform test No.10

In this case, it is possible to use at least four frequencies to approach the signature waveform. Those frequencies are 4,7,13 and 23Hz.

Using an amplification factor of 5.25, after running the software developed, the synthetic signature waveform is calculated. The results are included in Figure 5.28.

In this model, 11 holes were detonated, using different timing configurations. The first six holes were detonated at 5 millisecond delay as indicated in Figure 5.25. In order to model the complete vibration waveform for the initial part of the record, it is necessary to generate 6 random signals.

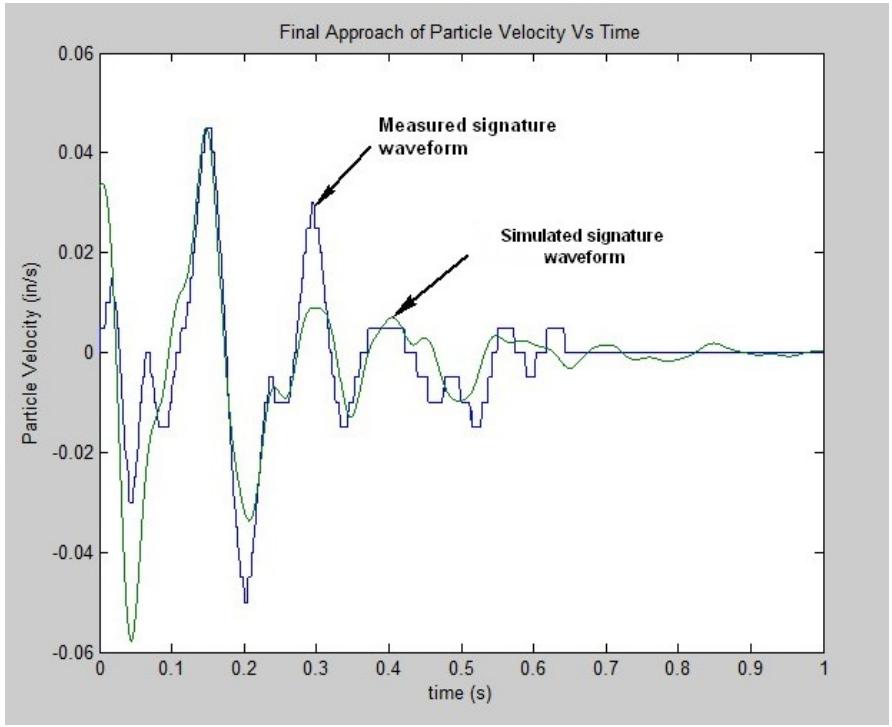

Figure 5.28 Signature waveform and synthetic waveform (approach) test No.10.

5.4.2.2 Synthetic signature signals

Using a lower and upper frequency interval as indicated in Figure 5.29, 6 signature ground vibration signals were generated. In the calculation, a scale factor average of 5.25, assuming a standard deviation of 1.0 was also used.

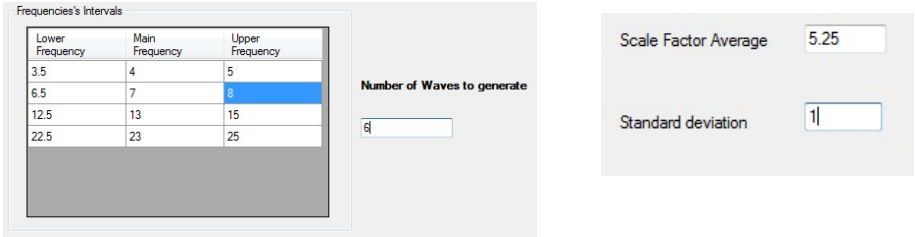

Figure 5.29 Frequency interval and scale factor for test No.10

The results when 6 random signatures waveform generated are included in Figure 5.30. In this case, the random effects can include different path, cracks, different quantity of explosives in each hole, etc.

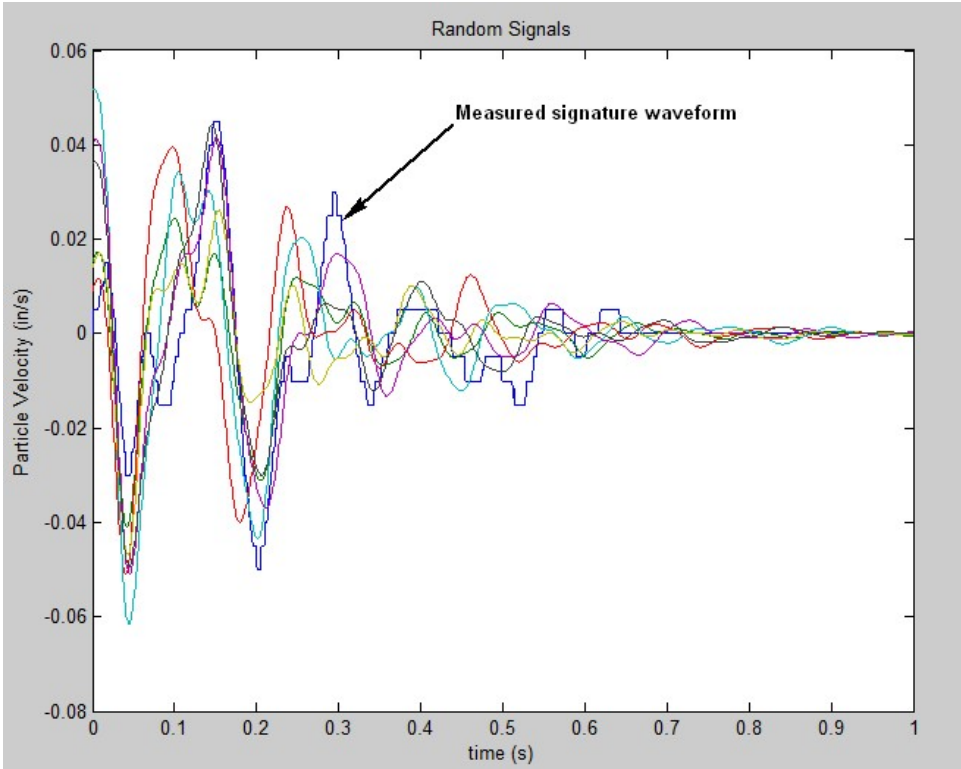

Figure 5.30 Random ground vibration signature waveform signals test No.10

5.4.2.3 Timing sequence

The delay between holes in this test was uniform at 5ms delay. In the current validation example, the effects in timing due to distance between the source and the monitoring point were included. This is because for this test the coordinates of each hole and the monitoring point was obtained through a survey of the area before blasting. As indicated in Chapter 4, the change in travel time for each hole depends on the seismic wave velocity, in this case an average of 16,000ft/s was assumed as mean value and a standard deviation of 4% of the mean value, in other words 640ft/s. Regarding the standard deviation for the detonators, despite no testing was performed for this nominal delay, 0.1ms was assumed because it is in the range of short times. Figure 5.31 shows the values used in this validation example.

Number of time series 1 Ok

time (ms)	Holes	Delay (ms)	Average Delay (ms)	Standard Deviation
0	6	5	5	0.1

a) Detonators

Average Wave Velocity 16000

Standard Deviation 640

Hole Id	Distance (ft)	Travel Time (s)
1	1154.85904	0.0722
2	1163.17757	0.0685
3	1177.75201	0.07595
4	1188.05172	0.07317
5	1198.61363	0.0756
6	1128.89726	0.06754

b) Traveling time

Figure 5.31 Time series for test No.10

The time function sequence including traveling time and hole delay time is included in Figure 5.32. In this figure, it is possible to see how the sequence is affected when the scatter in the timing is included.

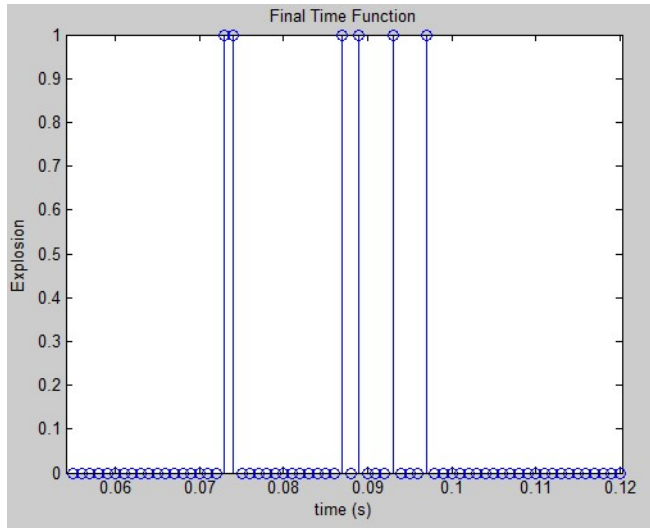

Figure 5.32 Time function for test No.10. Including both timing parameters

5.4.2.4 Results Model 2

Traditional signature methodology

Figure 5.19 shows the result using one iteration (no-Monte Carlo analysis is performed).

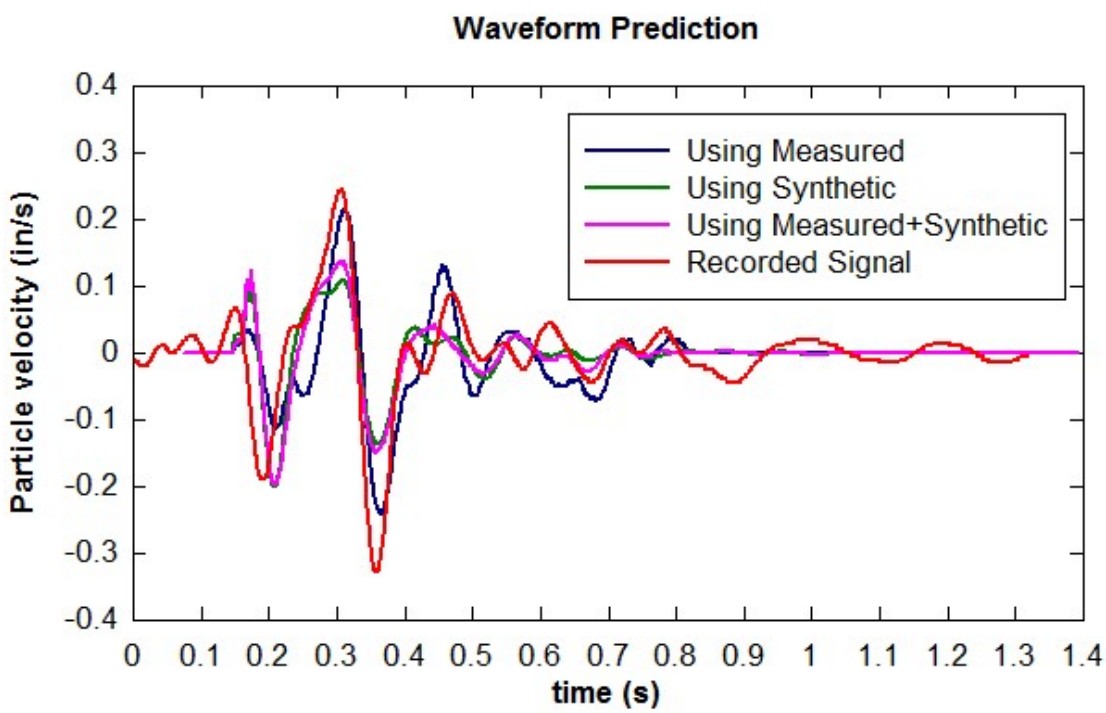

Figure 5.33 Results using one iteration for test No.10

In this case, all the calculations underestimate the maximum measured value for the vibration. The most close prediction value is reached using the measured signature waveform, (current signature hole technique).

Monte Carlo analysis (improved signature hole technique) test No.10

Using the improved methodology and the developed software, it is possible to analyze all the variables that are involved in the problem independently. Figure 5.34 shows the screen view for the current problem when all variables are included.

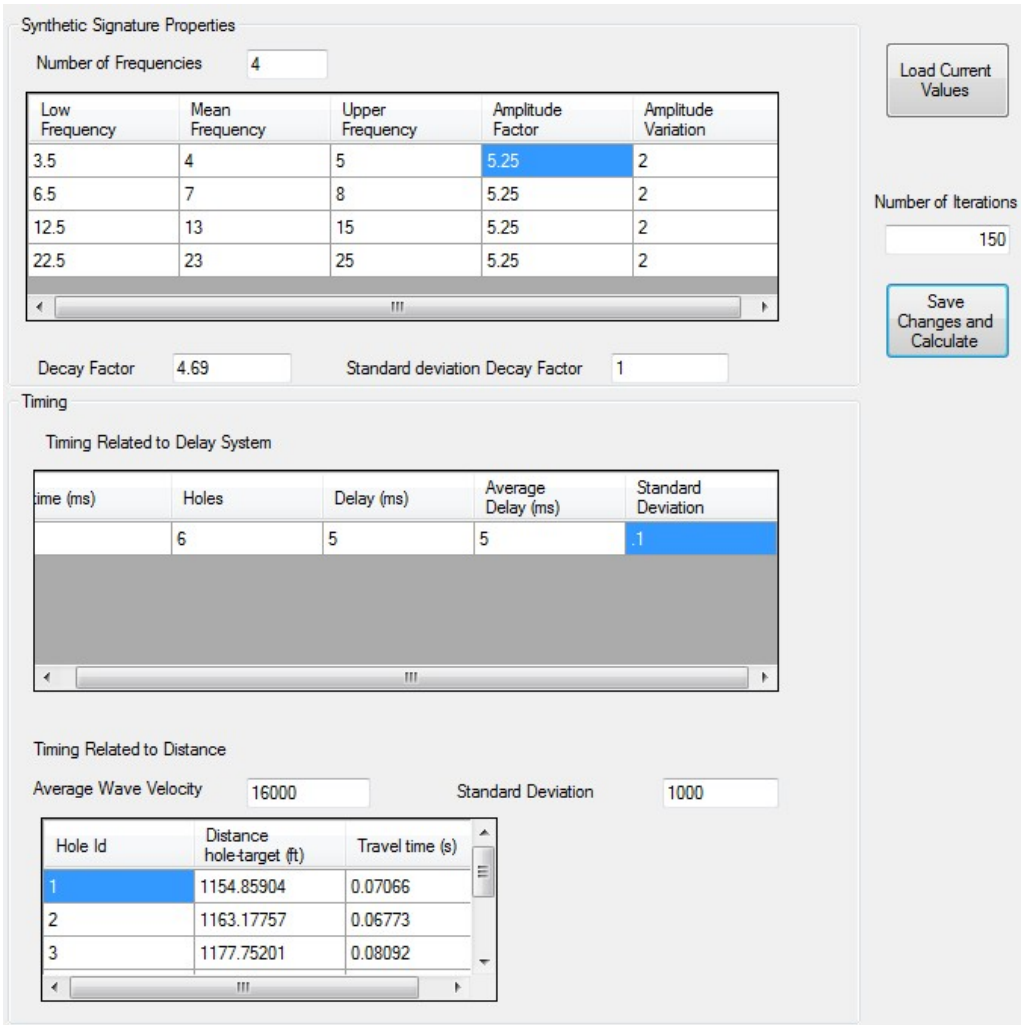

Figure 5.34 Variables involved in the prediction test No.10 using improved signature technique.

In this particular case, the complete record of six holes was available and it is possible to perform a back analysis to establish the parameters of the signature waveform. After a trial and error procedure, a standard deviation for the amplitude factor of 2 is used as well as a standard deviation of 1 for the decay factor and 1000 for the wave velocity. The results are included in Figure 5.35.

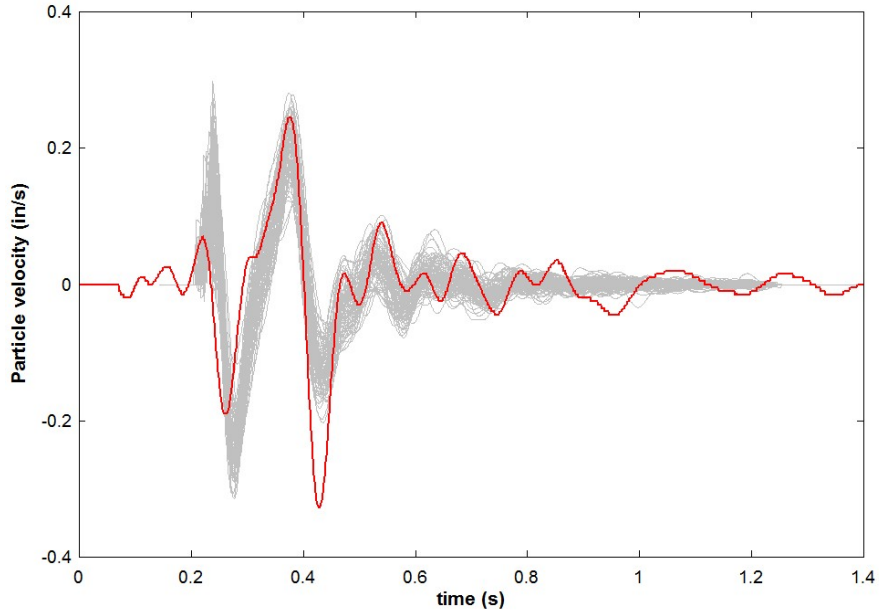

Figure 5.35 Monte Carlo result using fixed parameters for test No.10

In this case, as shown in Figure 5.35, some peaks in the complete waveform are overestimated.

Using the maximum absolute values (the peaks), the histogram included in Figure 5.36 is calculated. In this test, an average value of 0.242 in/s and a standard deviation of 0.035in/s were calculated using the improved signature hole technique. The peak velocity in this test was of -0.32in/s. So the absolute value of the measured peak is between 2.2 standard deviations from the mean calculated value.

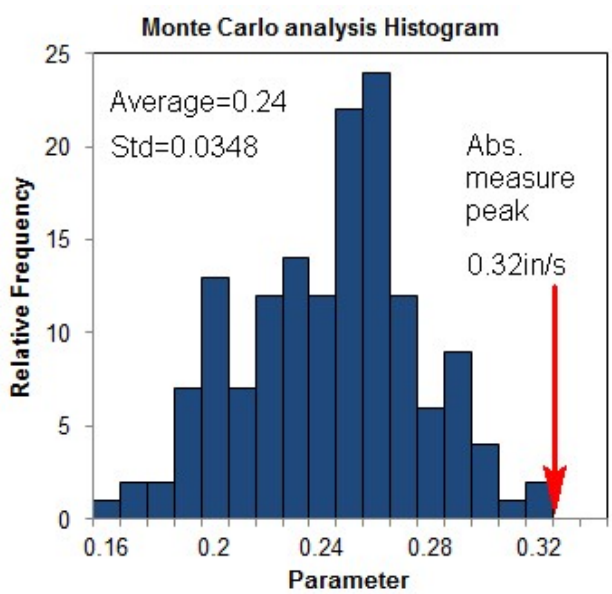

Figure 5.36 Histogram absolute maximum calculated values test No.10

In order to see the convergence of the improved signature hole methodology, the evolution of the parameter estimated, in this case the particle velocity against the number of samples or iterations is included in Figure 5.37.

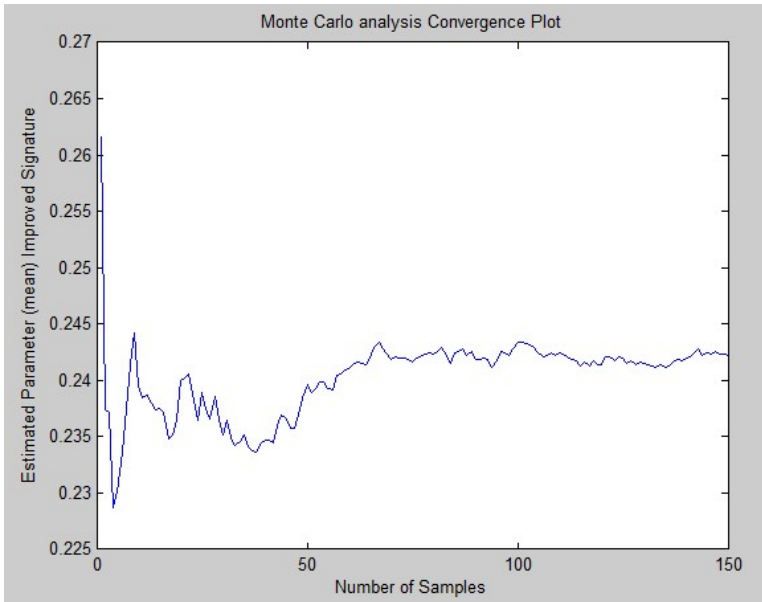

Figure 5.37 Convergence plot for test No.10

5.4.3 *Model 3. Particle Velocity (test No.12)*

Test No.12 also was done in summer 2011. Next the main parameters of this test are included.

Table 5-7 Blast test parameters test No.12

Parameter	Value
Total holes	29
Face height (ft)	45
Depth (ft)	45
Burden = spacing (ft)	18
Diameter (in)	7.875
Total explosive (lbs)	24,271.73

In this test in total 29 holes were detonated, this test had the same geometrical characteristics than test No.10. In other words, the same spacing, burden, hole diameter and explosives per hole. For modeling purposes only the first six holes are going to be included in the calculations.

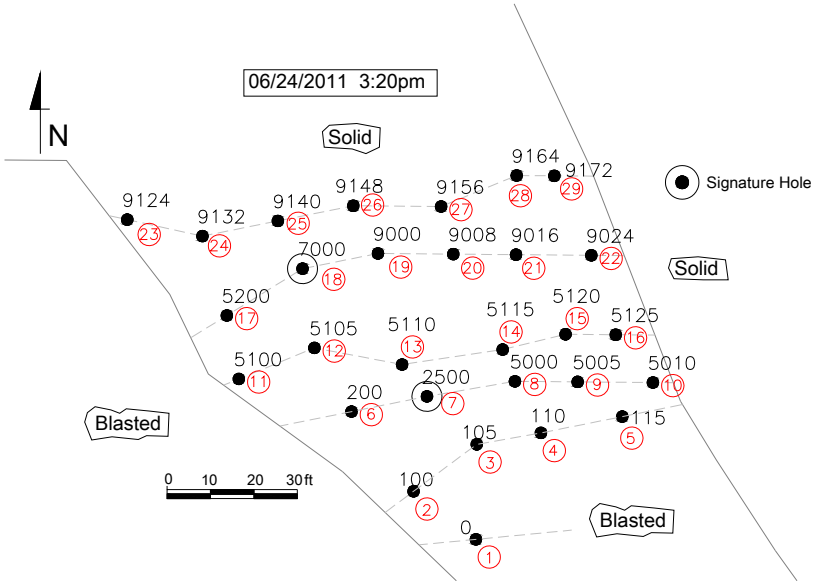

Figure 5.38 Test No.12, plan view from survey

In this test, there are two signature waveforms for the particle velocity.

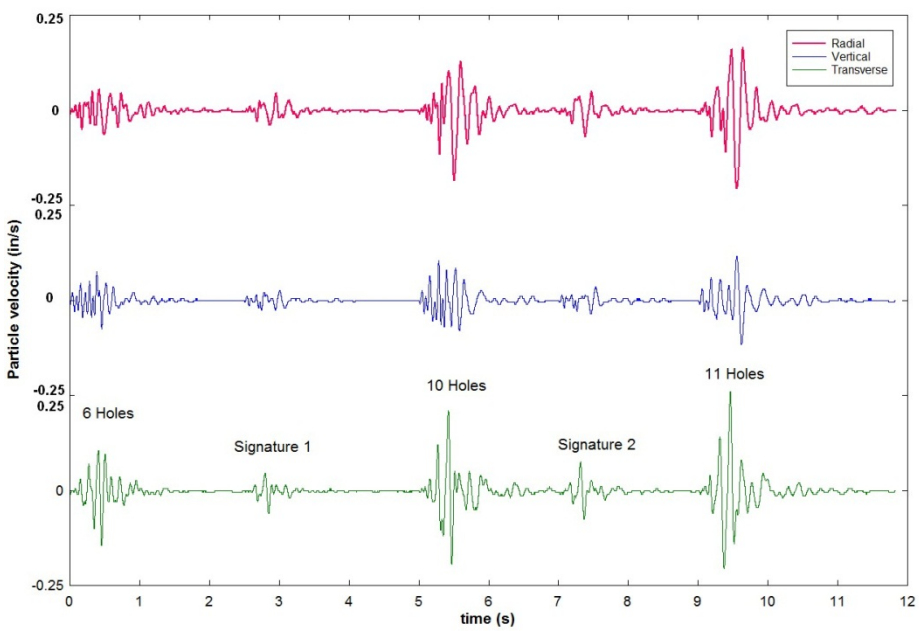

Figure 5.39 Vibration record seismograph 3599 test No.12

In order to compare two blast events where the geometry is the same and the distance and delay time change, seismograph 3599 was chosen to model the complete waveform for the six first holes in the test. The transverse component was used to compare the waveform prediction against the measured.

5.4.3.1 Signature test No.12

Figure 5.27 is obtained when the signature waveform for traverse component is isolated from the complete record in Figure 5.26. In this test, there are three signature waveform signals, however only signature waveform two was used for modeling. In this figure, the value of the exponential decay factor is included. In this case, the value is 4.69, as indicated in Figure 5.27.

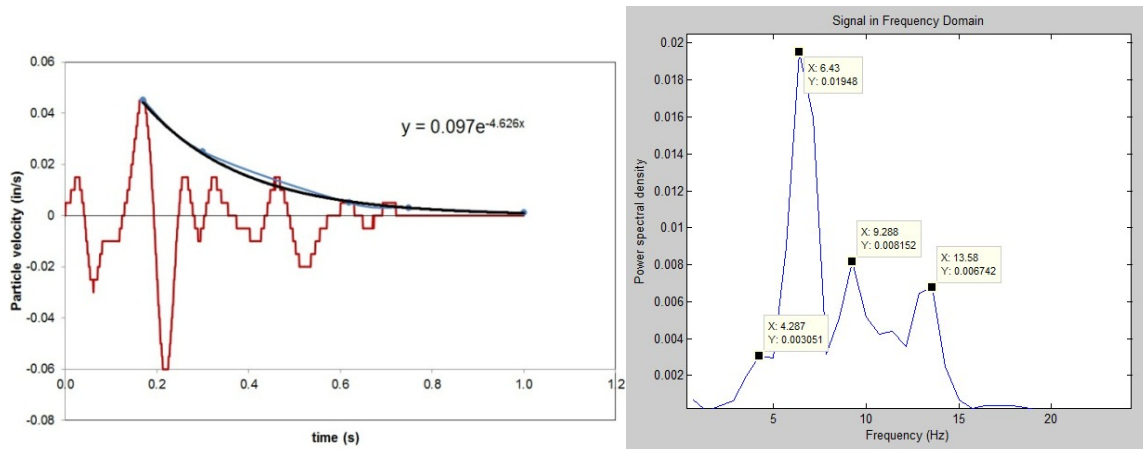

a) Waveform and decay factor b) Waveform in frequency domain

Figure 5.40. Ground vibration signature waveform test No.12

It is possible to use four frequencies to simulate the signature waveform. Those frequencies are 4.3, 6.43, 9.3 and 13.6Hz. As expected, these frequencies are similar to those for test No.10 (4, 7, 13 and 23Hz). Also the value of the decay factor is similar, this means that frequency content recorded at the monitoring point and decay factor are site specific parameters.

Using an amplification factor of 4.67, after runing the software developed, the synthetic signature waveform is calculated. The results are included in Figure 5.41.

In this model, in total 29 holes were detonated, using different timing configurations. Here we are modeling the first six holes detonated at 5 millisecond delay as indicated in Figure 5.38. In order to model the complete vibration waveform for the initial part of the record, it is necessary to generate 6 random signals.

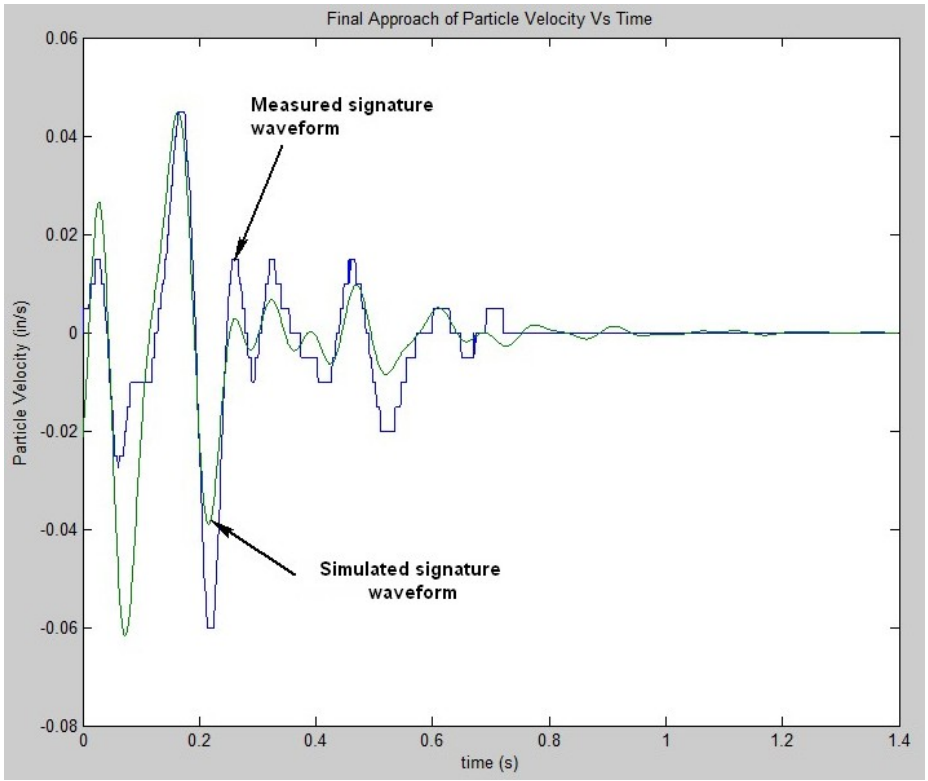

Figure 5.41 Signature waveform and synthetic waveform (approach) test No.12.

5.4.3.2 Synthetic signature signals

Using a lower and upper frequency interval as indicated in Figure 5.42, six (6) signature ground vibration signals were generated. In the calculation, a scale factor average of 4.67, assuming a standard deviation of 1.0 was also used.

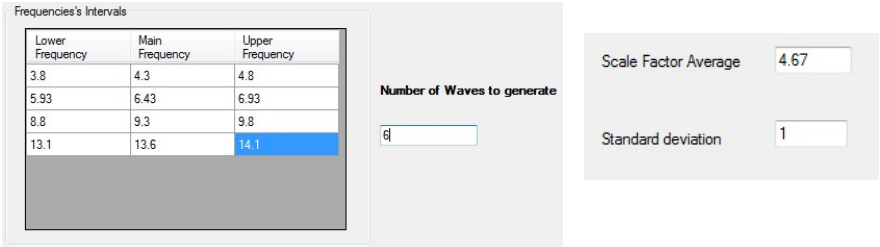

Figure 5.42 Frequency interval and scale factor for test No.12

The results when 6 random signatures waveform generated are included in Figure 5.43. In this case, the random effects can include different path, cracks, different quantity of explosives in each hole, etc.

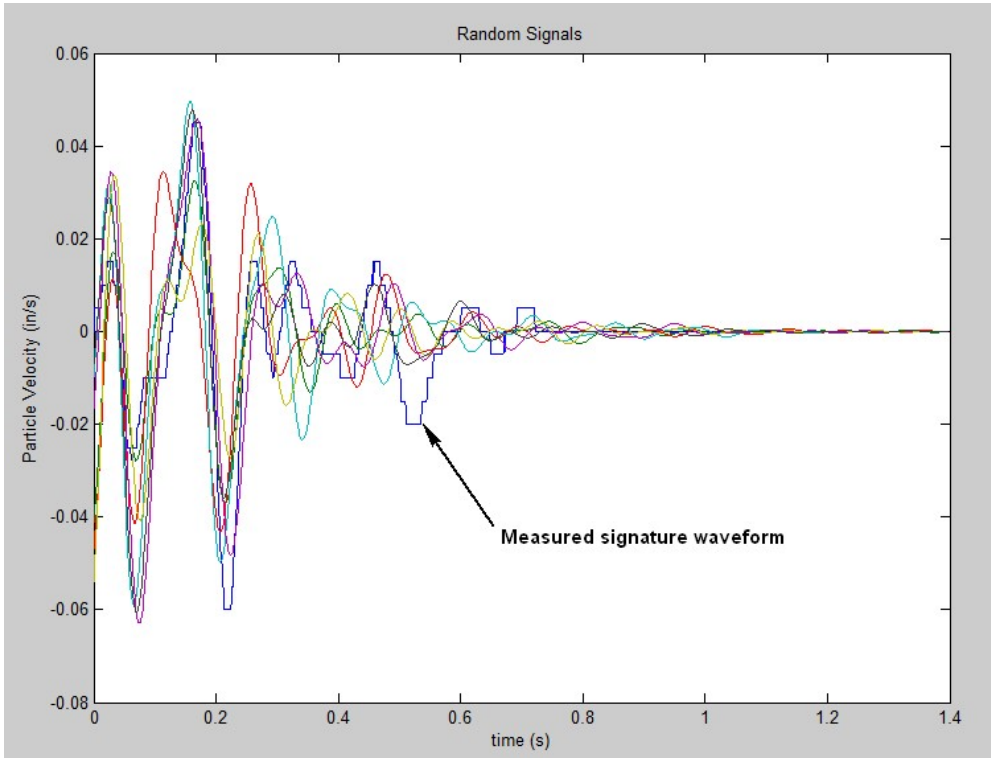

Figure 5.43 Random ground vibration signature waveform signals test No.12

5.4.3.3 Timing sequence

The delay between holes in this test was uniform at 5ms after 100ms. In the current validation example, the effects in timing due to distance between the source and the monitoring point were included using the coordinates for this specific test and the same values for wave velocity used in the previous model. Regarding the standard deviation for the detonators, a nominal delay, 0.1ms was assumed (shot time detonators). Figure 5.44 shows the values used in this validation example.

Number of time series 3 Ok

time (ms)	Holes	Delay (ms)	Average Delay (ms)	Standard Deviation
0	1	0	0	0
100	4	5	5	0.1
200	1	0	0	0.1

a) Detonators

Average Wave Velocity 16000

Standard Deviation 640

Hole Id	Distance (ft)	Travel Time (s)
1	1295.5351	0.0824
2	1308.50567	0.08068
3	1292.89798	0.07069
4	1277.92415	0.0719
5	1258.93045	0.08317
6	1320.81525	0.07361

b) Traveling time

Figure 5.44 Time series for test No.12

In Figure 5.45, it is possible to see how the sequence only for delay timing is affected when the traveling time is included.

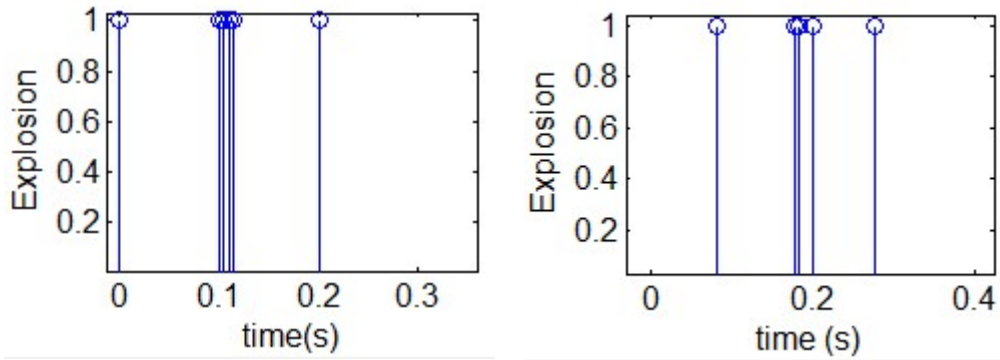

a) Time function detonator delay b) Time function detonator delay + traveling time

Figure 5.45 Time function for test No.12. Including both timing parameters

5.4.3.4 Results Model 3 (test No.12)

Traditional signature methodology

Figure 5.46 shows the result using one iteration (no-Monte Carlo analysis is performed).

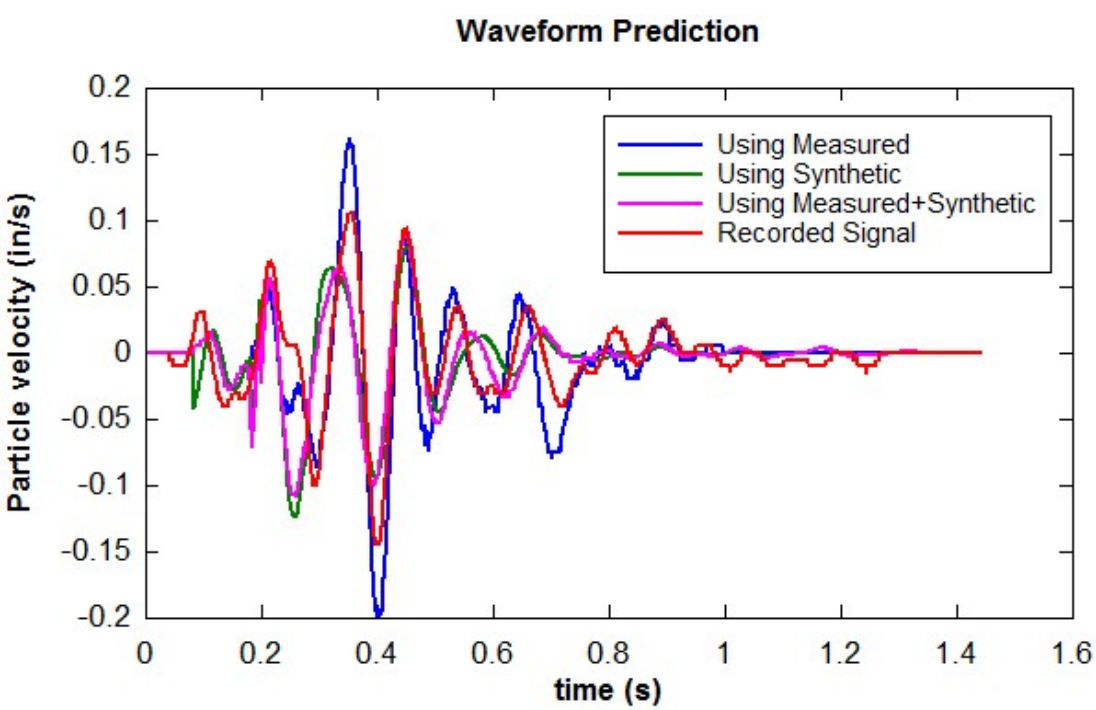

Figure 5.46 Results using one iteration for test No.12

In this case, the calculations using measured signature overestimate the maximum measured value for the vibration. Using the synthetic waves, the prediction is underestimated.

Monte Carlo analysis (improved signature hole technique) test No.12

Using the improved methodology and the developed software, it is possible to analyze all the variables that are involved in the problem independently. Figure 5.34 shows the screen view for the current problem when all variables are included.

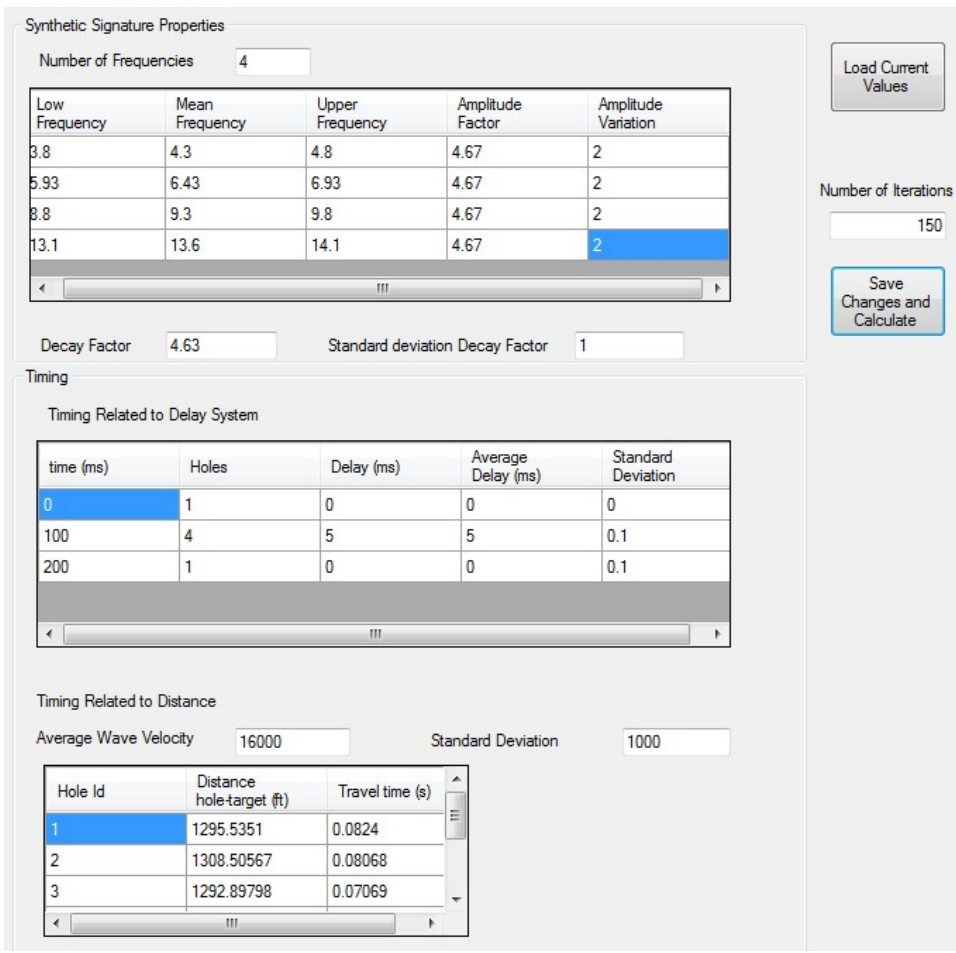

Figure 5.47 Variables involved in the prediction test No.12 using improved signature technique.

Similar to the previous case, the complete record of six holes was available and it is possible to perform a back analysis, to establish the parameters of the signature waveform that best reproduce the blast. After a trial and error procedure, a standard

deviation for the amplitude factor of 2 is used as well as a standard deviation of 1 for the decay factor and 1000 for the wave velocity. The results are included in Figure 5.48

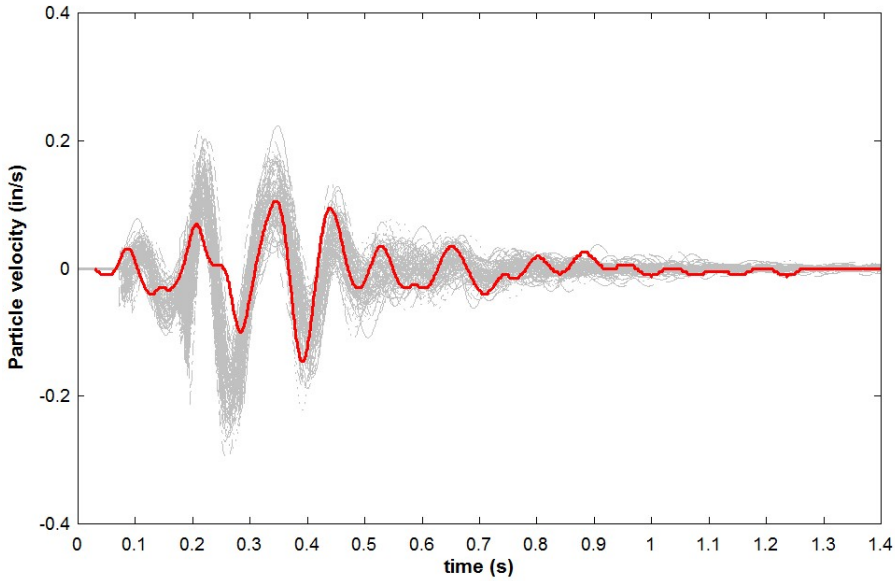

Figure 5.48 Monte Carlo result using fixed parameters for test No.12

In this case, as shown in Figure 5.35, some peaks in the complete waveform are overestimated.

Using the maximum absolute values (the peaks), the histogram included in Figure 5.36 is calculated. In this test, an average value of 0.203 in/s and a standard deviation of 0.042in/s were calculated using the improved signature hole technique. The peak velocity in this test was of -0.145in/s. So the absolute value of the measured peak is between 1.40 standard deviations from the mean calculated value.

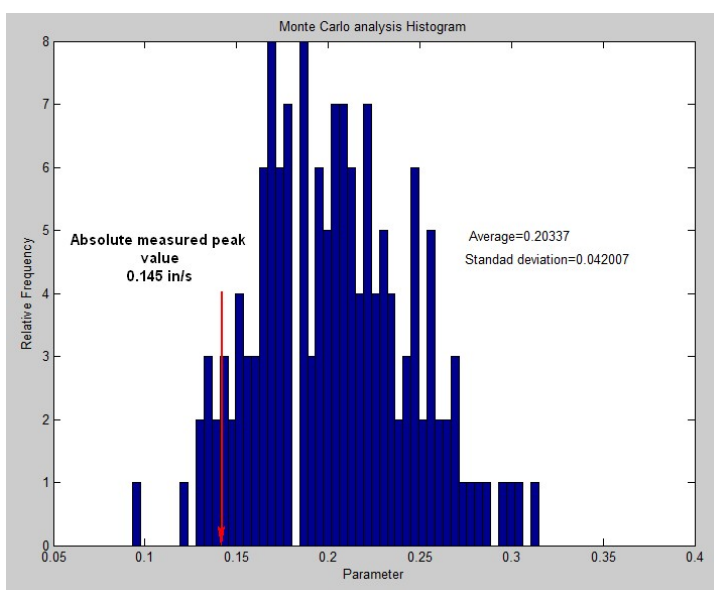

Figure 5.49 Histogram absolute maximum calculated values test No.12

In order to see the convergence of the improved signature hole methodology, the evolution of the parameter estimated, in this case the particle velocity against the number of samples or iterations is included in Figure 5.37

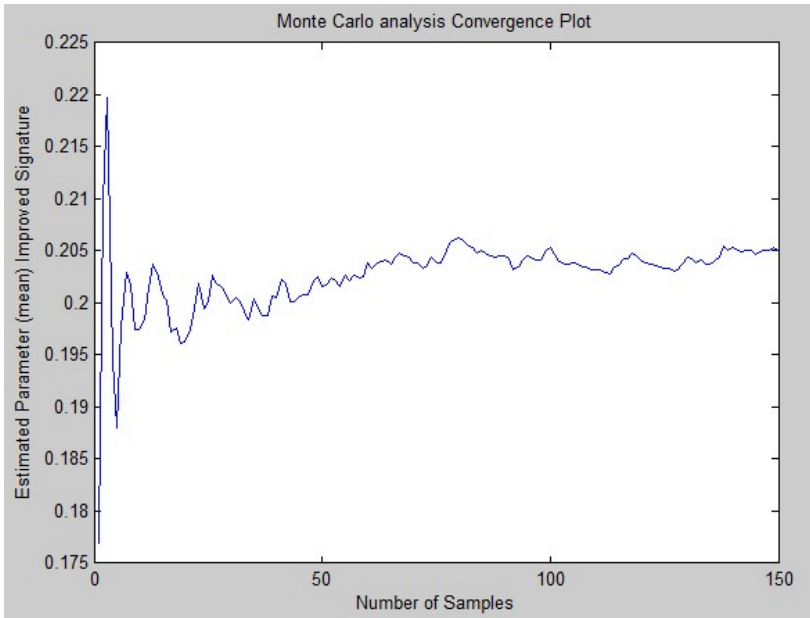

Figure 5.50 Convergence plot for test No.10

5.4.4 *Model 4 Pyrotechnic initiation (test No.14)*

This test used pyrotechnic initiation delay system so, it was not possible to get a signature waveform in the test as was obtained in previous tests. Next the main parameters of test No.14 are included.

Table 5-8 Blast test parameters test No.14

Parameter	Value
Total holes	34
Face height (ft)	45
Depth (ft)	45
Burden = spacing (ft)	18
Diameter (in)	7.875
Total explosive (lbs)	30,106.45

In this test, 34 holes were detonated. This test had the same geometrical characteristics as previous tests.

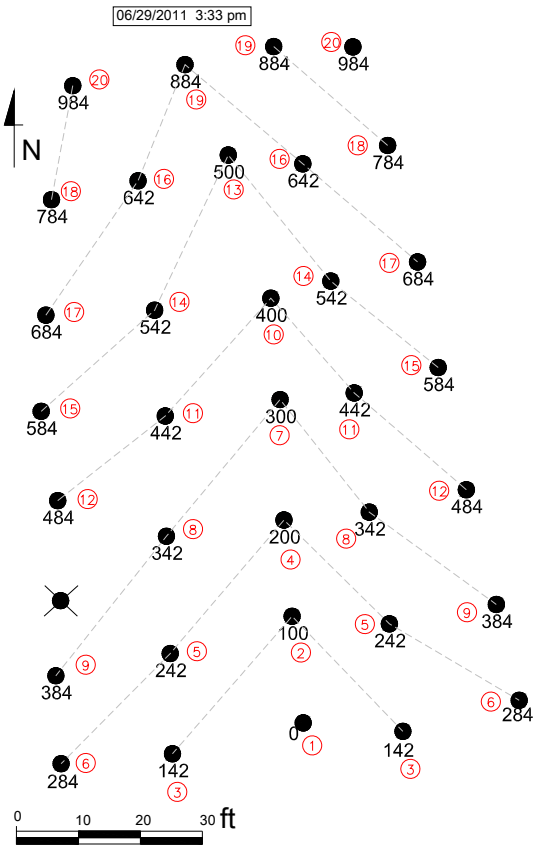

Figure 5.51 Test No.14, plan view from survey

In this test, there are no signature waveforms for the particle velocity.

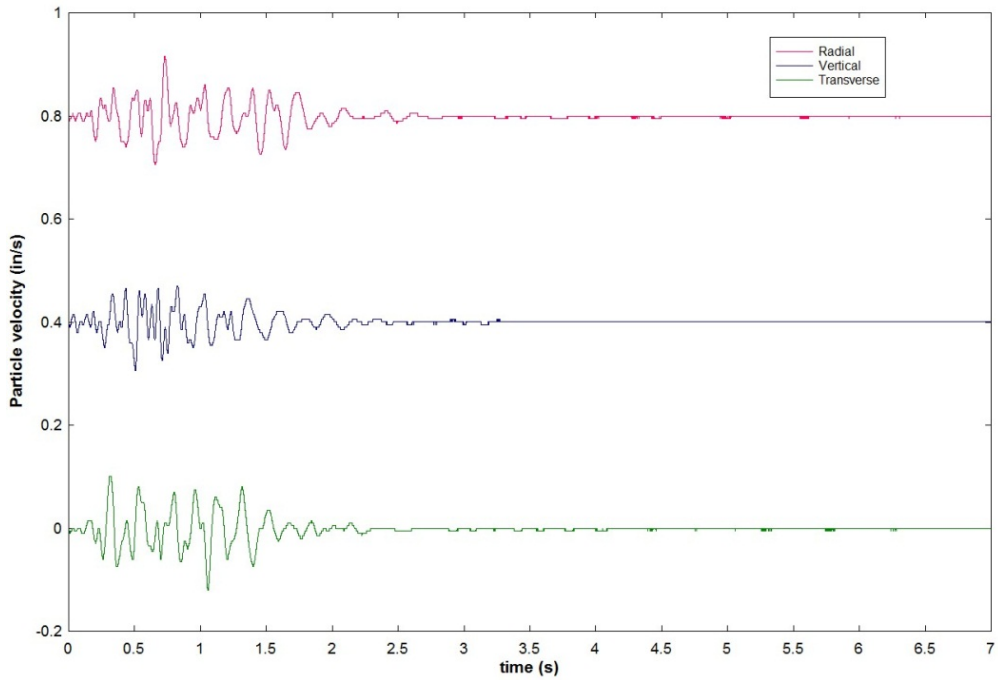

Figure 5.52 Vibration record seismograph 3599 test No.14

Despite the possibility to model any component, the transverse component was chosen.

5.4.4.1 Signature test No.14

In this case, the average between signature waveform for test No.12 and test No.10 was used as signature in this model.

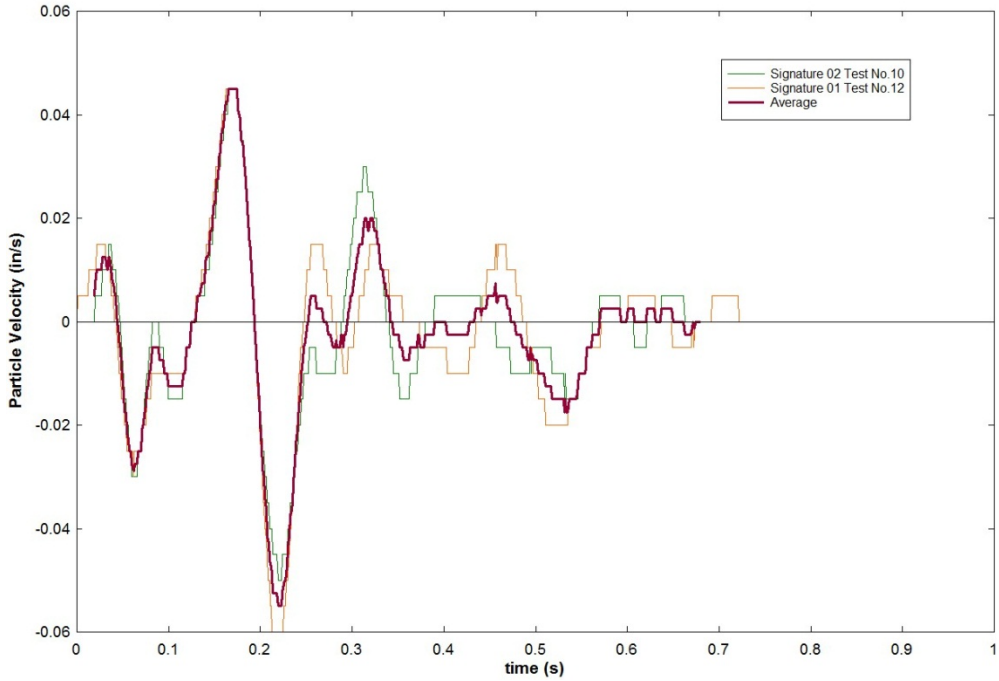

Figure 5.53 Signature waveform for test No.14

The decay factor and the main frequencies for the signature waveform are included in Figure 5.54.

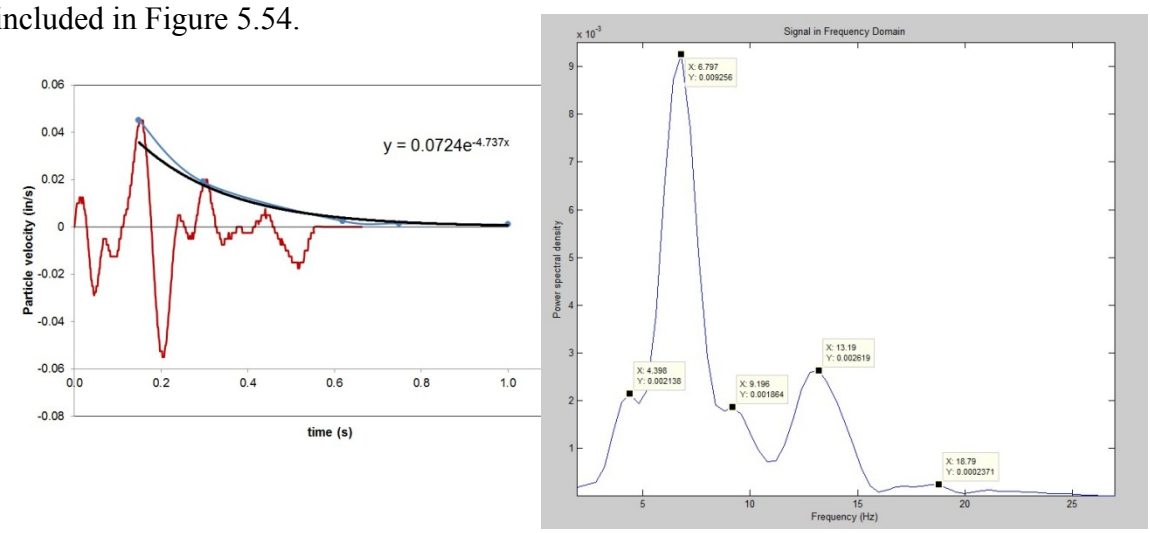

b) Waveform and decay factor b) Waveform in frequency domain

Figure 5.54. Ground vibration signature waveform test No.14

In this case, it is possible to use five frequencies to simulate the signature waveform. Those frequencies are 4.4, 6.8, 9.2, 13.19 and 18.79Hz. As expected, these frequencies are similar to those for test No.10 and No.12. Also the value of the decay factor is similar.

Using an amplification factor of 5.03, and after running the software developed, the synthetic signature waveform is calculated. The results are included in Figure 5.55.

In this model, 34 holes were detonated, using different timing configurations. In order to model the complete vibration waveform, it is necessary to generate 34 random signals.

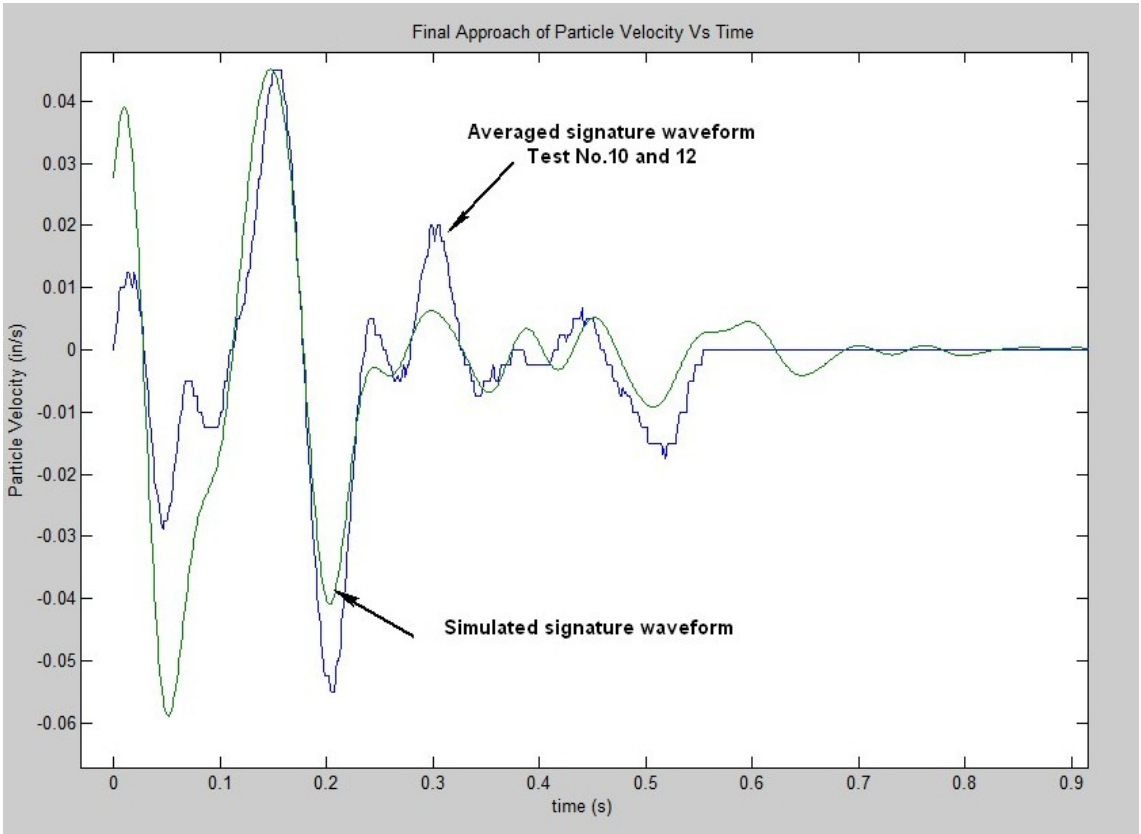

Figure 5.55 Signature waveform and synthetic waveform (approach) test No.14.

5.4.4.2 Synthetic signature signals

Using a lower and upper frequency interval as indicated in Figure 5.56, 34 signature ground vibration signals were generated. In the calculation, a scale factor average of 5.03, assuming a standard deviation of 1.0 was also used.

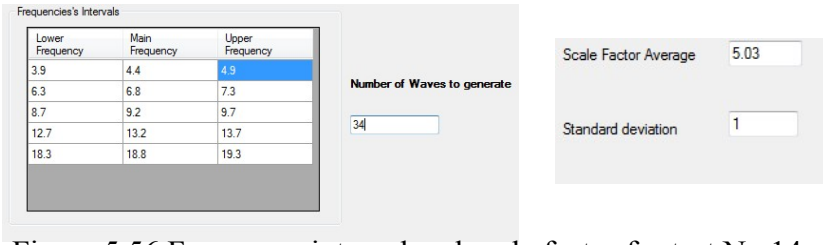

Figure 5.56 Frequency interval and scale factor for test No.14

The results when 34 random signatures waveform are generated, are included in Figure 5.57. In this case, the random effects can include different path, cracks, different quantity of explosives in each hole, etc.

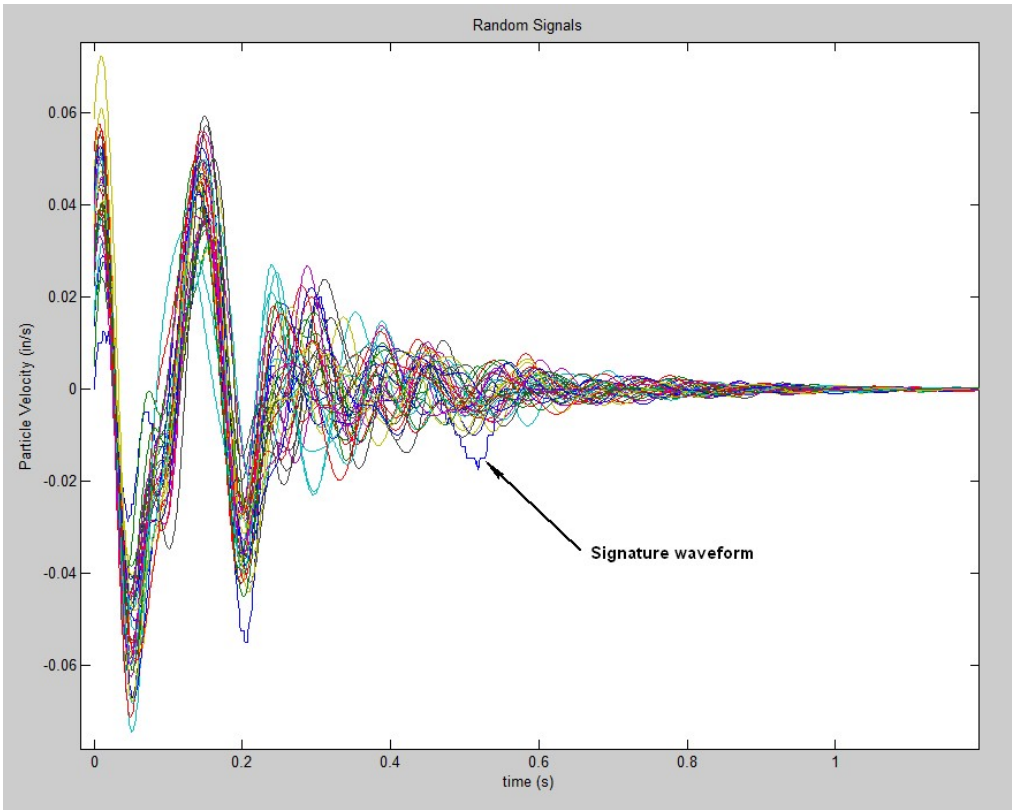

Figure 5.57 Random ground vibration signature waveform signals test No.14

5.4.4.3 Timing sequence

The delay between holes in this test was the typical delay used in this particular mine, 100 and 42ms. Regarding the standard deviation for the detonators, and using the information for pyrotechnic delay systems, 6ms was used. Figure 5.58 shows the values used in this validation example.

Number of time series 29 Ok

time (ms)	Holes	Delay (ms)	Average Delay (ms)	Standard Deviation
0	1	0	0	0
100	2	42	42	6
142	1	0	0	6
200	2	42	42	6
242	1	0	0	6
284	1	0	0	6

Average Wave Velocity 16000

Standard Deviation 642

Hole Id	Distance (ft)	Travel Time (s)
1	1485.48771	0.09088
2	1486.4977	0.08654
3	1469.49628	0.101
4	1506.82216	0.09103
5	1487.26263	0.09178
6	1470.85135	0.09702
7	1506.40087	0.09582
8	1450.49563	0.08943
9	1524.85135	0.08334
10	1487.43966	0.08367
11	1473.46019	0.09736
12	1506.30142	0.08392

b) Detonators b) Traveling time

Figure 5.58 Time series for test No.14

The time function sequence for delay timing and travelling time is included in Figure 5.59 In this figure, it is possible to see how the sequence only for delay timing is affected when the traveling time is included.

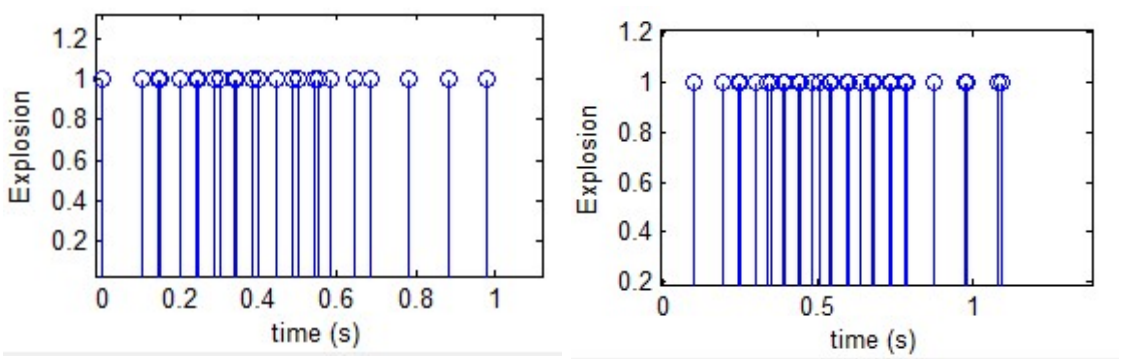

b) Time function detonator delay b) Time function detonator delay + traveling time

Figure 5.59 Time function for test No.14. Including both timing parameters

5.4.4.4 Results Model 4 (test No.14)

Traditional signature methodology

Figure 5.60 shows the result using one iteration (no-Monte Carlo analysis is performed).

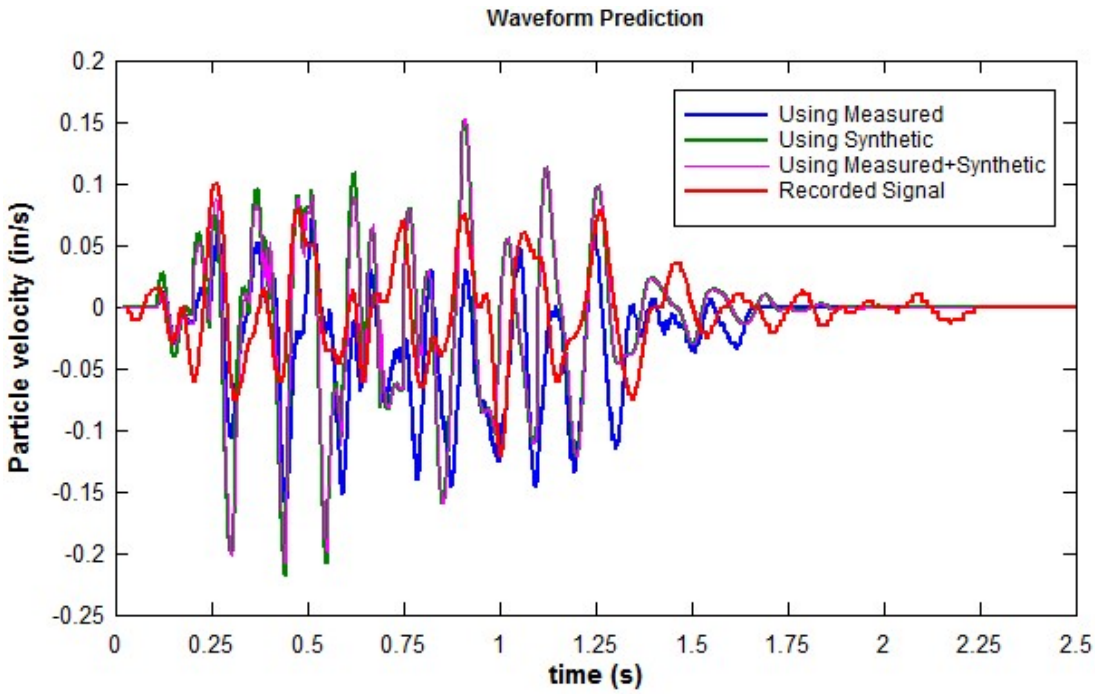

Figure 5.60 Results using one iteration for test No.14

In this case, the calculations using measured signature and synthetic waves overestimate the maximum measured value for the vibration.

Monte Carlo analysis (improved signature hole technique) test No.14

Using the improved methodology and the developed software, it is possible to analyze all the variables that are involved in the problem independently. Figure 5.61 shows the screen view for the current problem when all variables are included.

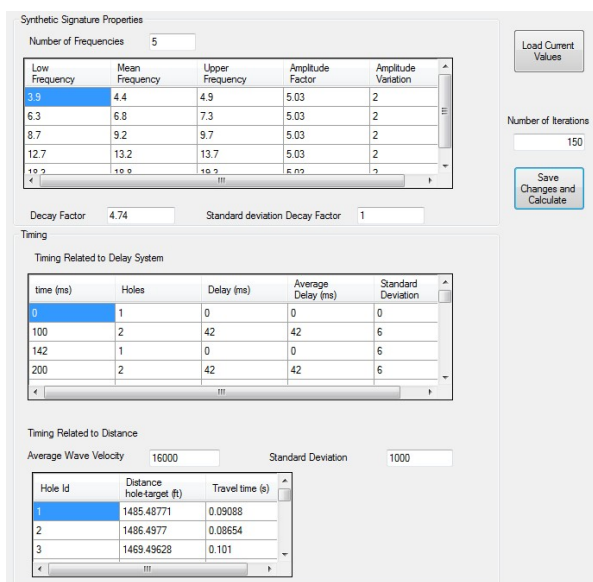

Figure 5.61 Variables involved in the prediction test No.14 using improved signature technique.

A standard deviation for the amplitude factor of 2 is used as well as a standard deviation of 1 for the decay factor and 1000 for the wave velocity. The results are included in Figure 5.62

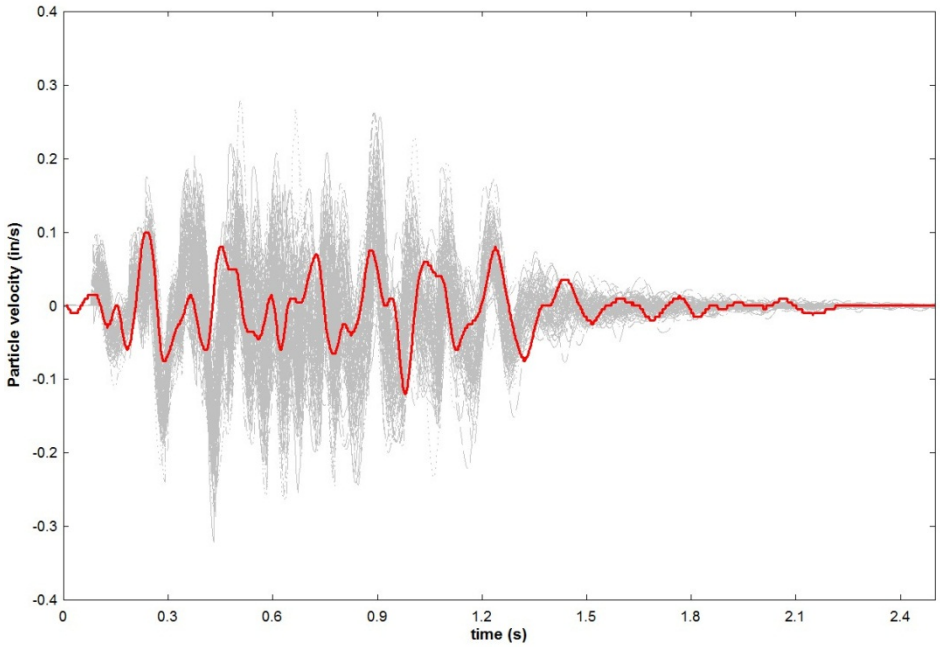

Figure 5.62 Monte Carlo result using fixed parameters for test No.14

Peak values histogram and convergence plot is included in Figure 5.63.

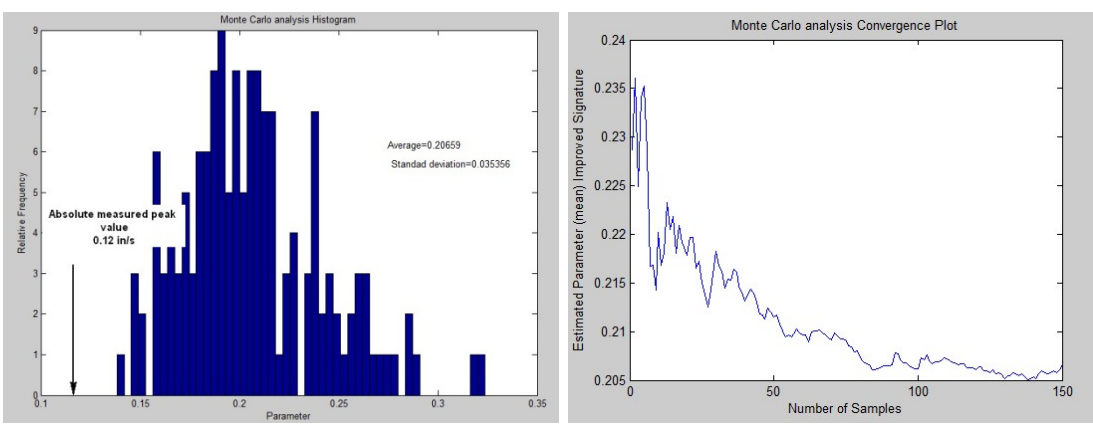

a) Histogram prediction test No.14 b) Convergence plot test No.14

Figure 5.63 Histogram and convergence plot of the prediction for test No.14

In the modeling process according to the convergence plot, more than 80 runs are needed to reach the convergence of the mean peak particle velocity. In this test, it is possible to see that measured value is between 2.44 standard deviations of the mean predicted value.

5.4.5 *Model 5 electronic initiation system (test No.15)*

This test had a similar geometry configuration that previous where pyrotechnic initiation delay system was used. The main idea of this test was to compare vibrations levels for similar shots (similar geometries) when different initiation systems are used (nonel vs electronic). Next the main parameters of test No.15 are included.

Table 5-9 Blast test parameters test No.15

Parameter	Value
Total holes	40
Face height (ft)	45
Depth (ft)	45
Burden = spacing (ft)	18
Diameter (in)	7.875
Total explosive (lbs)	33,478.25

In this test 40 holes were detonated.

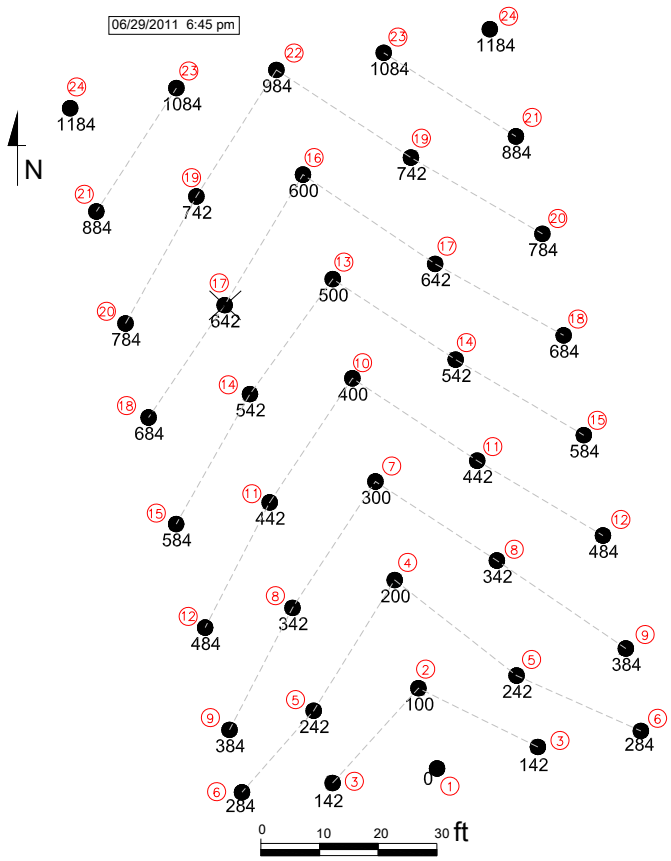

Figure 5.64 Test No.15, plan view from survey

In this test, there are no signature waveforms for the particle velocity.

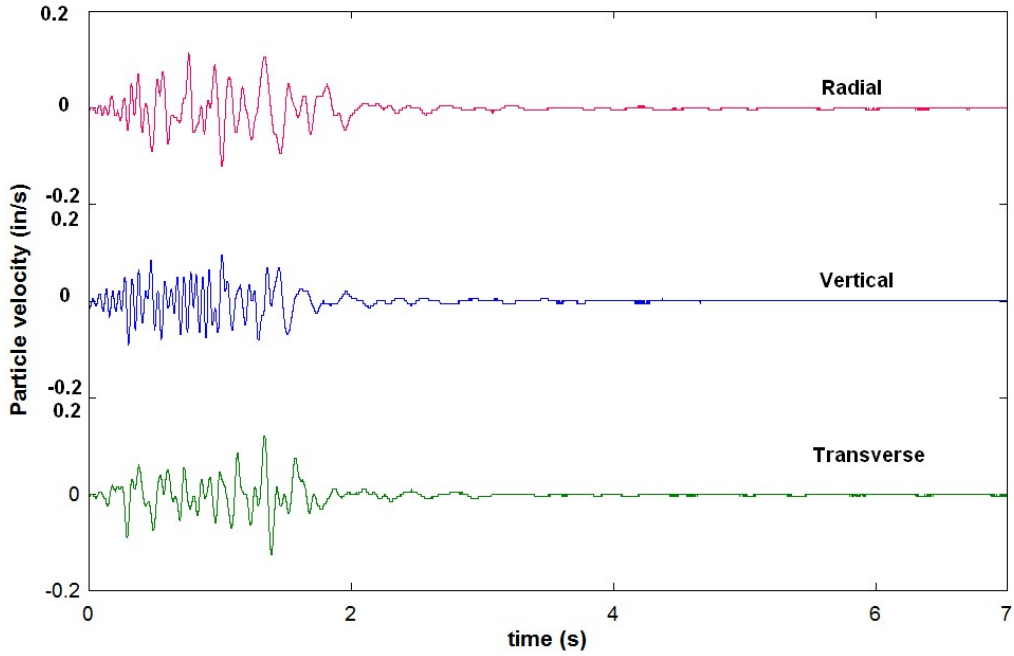

Figure 5.65 Vibration record seismograph 3599 test No.15

Despite the possibility to model any component, transverse component was chosen.

5.4.5.1 Signature test No.15

In this case, same signature average used in the previous model was chosen as signature waveform for this specific model.

5.4.5.2 Synthetic signature signals

Using the same frequency intervals for the previous test, 40 signature signals were generated. In the calculation, a scale factor average of 5.03, assuming a standard deviation of 2.0 was also used.

5.4.5.3 Timing sequence

The delay between holes in this test was the typical delay used in this particular mine 100 and 42ms. The difference with the previous model is that in this case the initiation system used was electronic. According to the information for this type of detonator, a standard deviation of 0.10ms was used.

5.4.5.4 Results Model 5 (test No.15)

Traditional signature methodology

Figure 5.66 shows the result using one iteration (no-Monte Carlo analysis is performed).

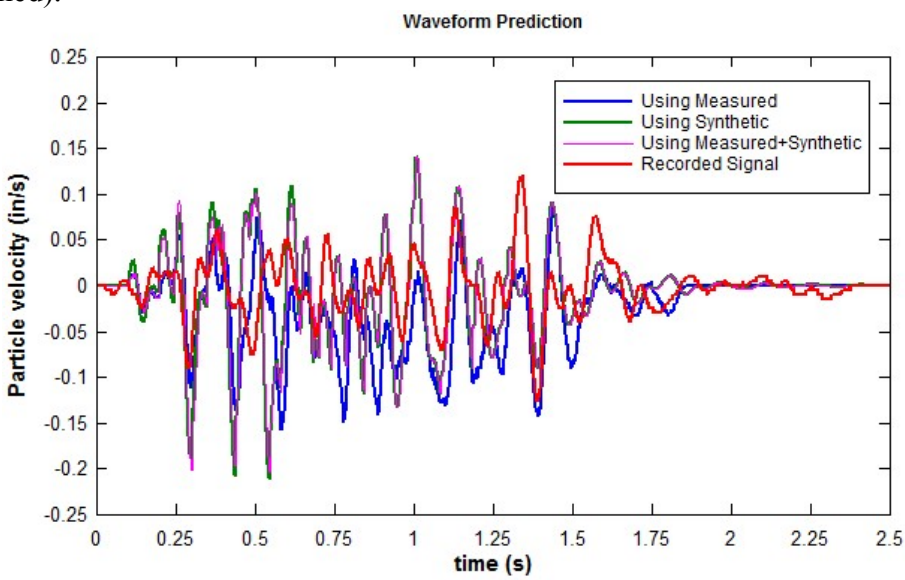

Figure 5.66 Results using one iteration for test No.15

In this case, the calculations using measured signature and synthetic waves overestimate the maximum measured value for the vibration.

Monte Carlo analysis (improved signature hole technique) test No.15

The results in this model are included in Figure 5.67.

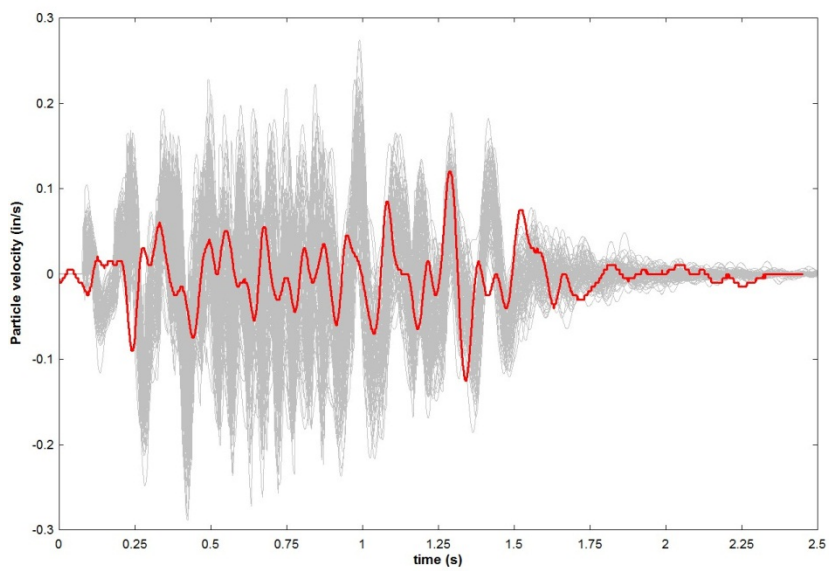

Figure 5.67 Monte Carlo result using fixed parameters for test No.15

Peak values histogram and convergence plot is included in Figure 5.68.

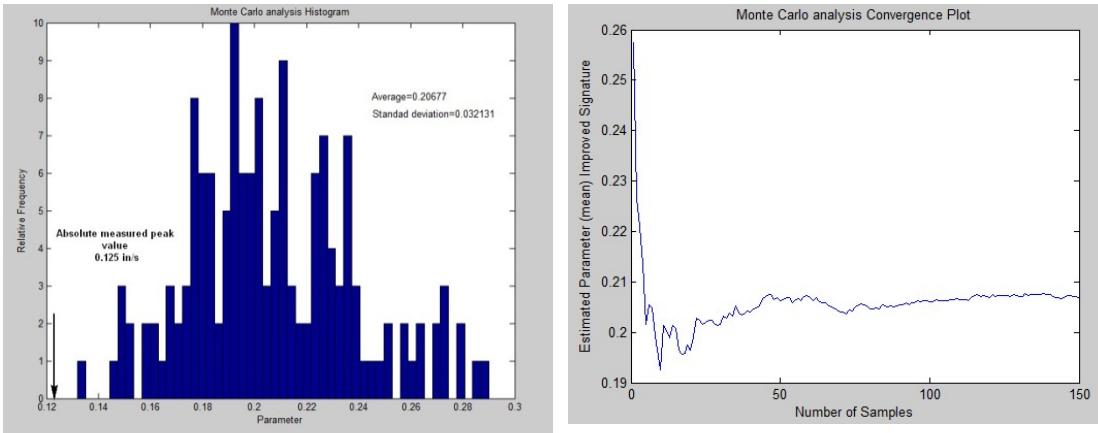

a) Histogram prediction test No.15 b) Convergence plot test No.15

Figure 5.68 Histogram and convergence plot of the prediction for test No.14

In this test, it is possible to see that measured value is between 2.54 standard deviations of the mean predicted value. Convergence plot in this case indicates that less than 50 runs are needed to approach a constant mean peak particle velocity value. If Figure 5.63b and Figure 5.68b are compared, when electronic initiation system is used, fewer number of iterations are required to approach a constant mean peak particle velocity value. This is basically due to the high scatter in timing delay in nonel initiation system compared to electronic. The likelihood that a previous run output have a similar value than the current run is higher when less scatter is used in the variables (in this case the initiation timing).

DISCUSSION OF RESULTS AND FUTURE WORK RECOMMENDATIONS

6.1 Discussion about the improved methodology and the validation results

Based on the results from the different models included in Chapter 5, a discussion about the main parameters of the improved signature hole technique is presented.

6.1.1 *Number of frequencies to model the signature signal*

The main concept behind the Fourier series to model the signature signal in the current research is to choose a finite number of frequencies (in this case the main frequencies) to approach a synthetic signal. There are two consequences when a finite number of frequencies are selected:

1. The shape of the synthetic waveform does not look like the original signature waveform, and;
2. A greater value is necessary for the amplification factor when less frequencies are used.

Those phenomenons are true for any signal (airblast or vibration signals).

For example, in the case of the signature signal for model 1 (test No. 5 airblast), the initial part of the synthetic signal does not match to the measured signal. In that case five frequencies were used to calculate the approach. Figure 6.1 shows the result when five frequencies are included.

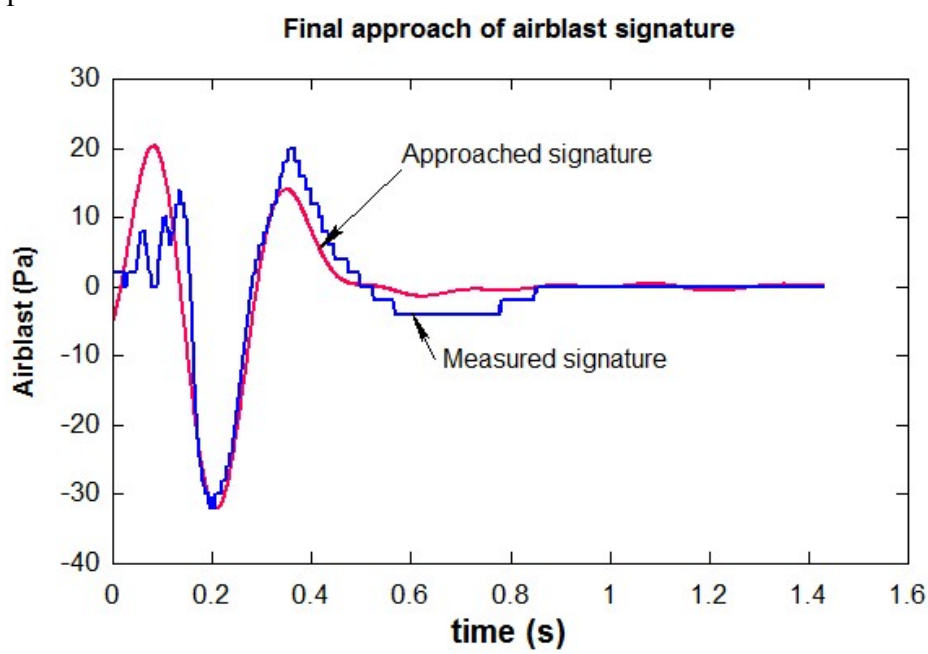

Figure 6.1 Signature signal test No.5 using five frequencies

In this case, the initial part of the synthetic signal represents a peak value higher than the positive peak value of the measured signal. As a consequence, the airblast

signature waveforms randomly generated (see Figure 5.16) will overestimate the airblast waveform in the initial part of the signal. Finally, when the prediction is calculated, the predicted value is going to be overestimated and it is necessary to adjust the scale factor to reduce the predicted value as explained in Chapter 5.

In this research, it has been concluded that when a more appropriate shape of the signature signal is needed, more frequencies are required to model the signature waveform. Figure 6.2 shows the random signature signals when 25 frequencies are used.

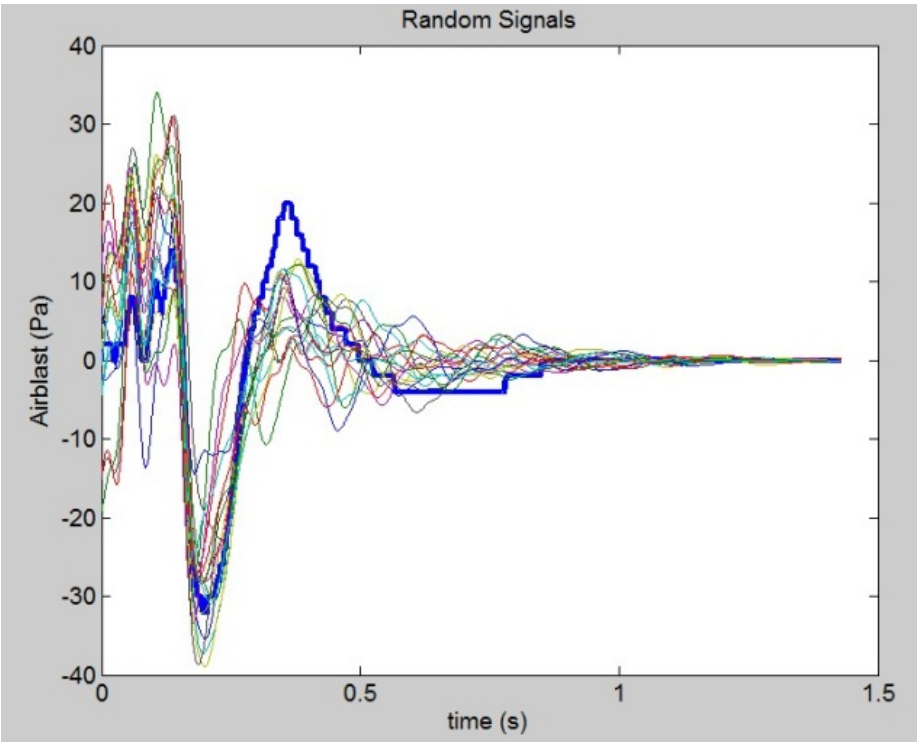

Figure 6.2 Random airblast signature waveform signals test No.5 using 25 frequencies.

In this case an amplification factor to match the maximum negative peak of the signal of 2.22 was used instead of 2.8 (see Chapter 5). When improved signature is used, including 25 frequencies, an average value of 227 Pa and a standard deviation of 30.20Pa is obtained. In this case, an amplification value of 2.22 was used for 3Hz and 1 for the other frequencies. The final waveform prediction for airblast is included in Figure 6.3.

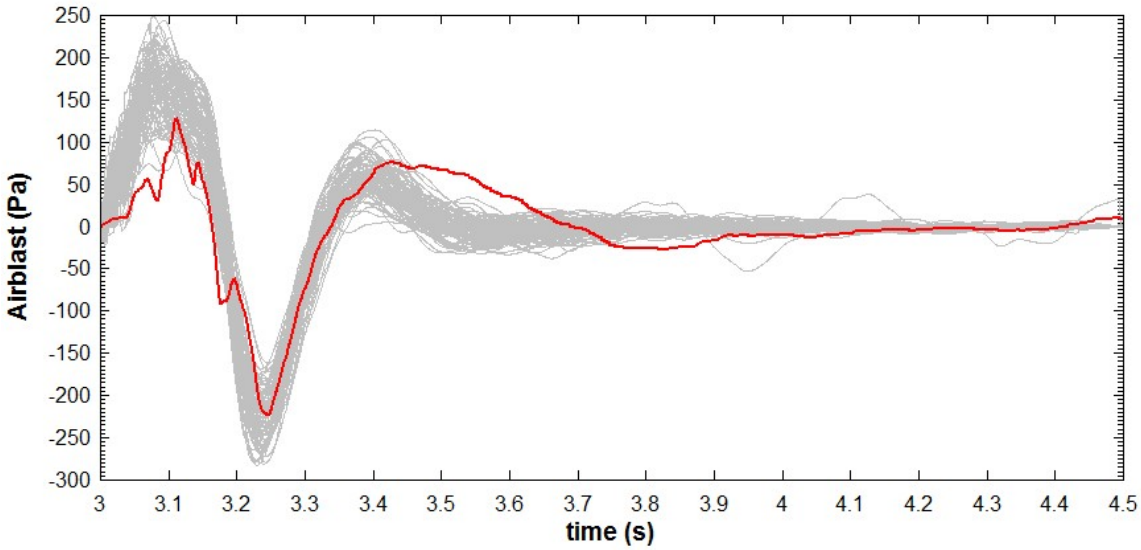

Figure 6.3 Final prediction for airblast using 25 frequencies and amplification factor of 2.2 for main frequency (3Hz).

Next table contains the results comparison and how the parameters change when more frequencies are used.

Table 6-1 Comparison results according to the number of frequencies used

Model (Test No.)	Peak particle velocity absolute value (measured)	Model using four frequencies			Model using 25 frequencies		
		Scale factor	Peak particle velocity mean	Standard deviation	Scale factor	Peak particle velocity mean	Standard deviation
02 (No.10)	0.32in/s	5.25	0.242in/s	0.035	2.77	0.29in/s	0.035
03 (No.12)	0.145in/s	4.67	0.203in/s	0.042	2.72	0.19in/s	0.031
04 (No.14)	0.12in/s	5.03	0.206in/s	0.035	2.75	0.22in/s	0.0325
05 (No.15)	0.125in/s	5.03	0.206in/s	0.032	2.75	0.22in/s	0.0304

Table 6-1 shows that increasing the number of frequencies used to simulate and generate the signature waveform reduces the scale factor. However the mean values and the standard deviation of the predictions are almost the same. To see the changes in the shape of the vibration envelop predicted, next figures show the final result when 25 frequencies are used for all the validation examples included in Chapter 5.

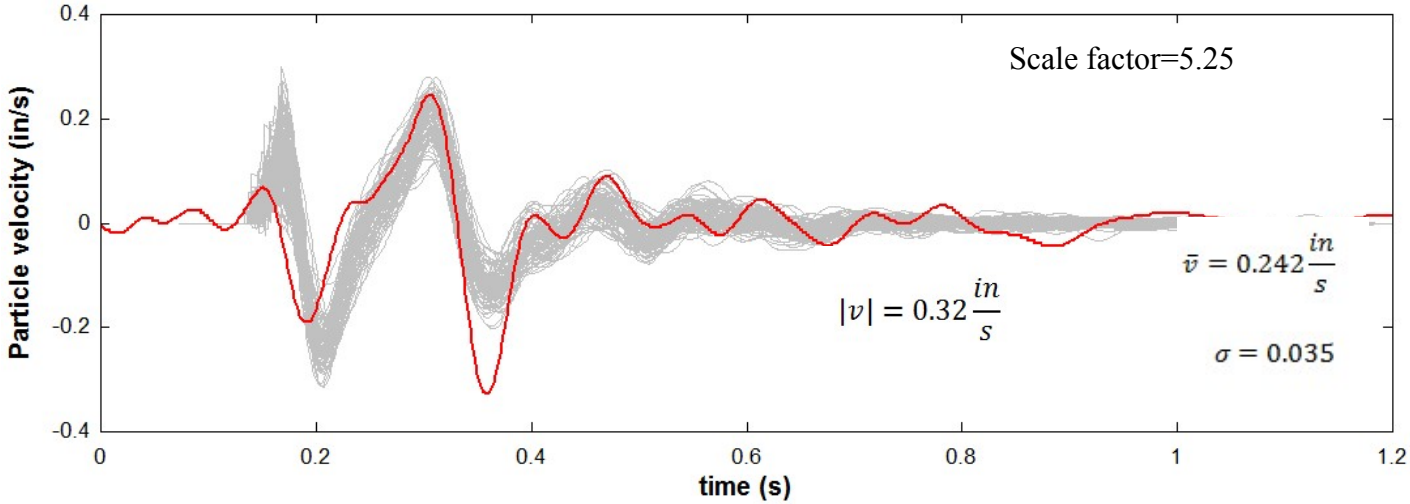

a) Enveloped using four frequencies test No.10

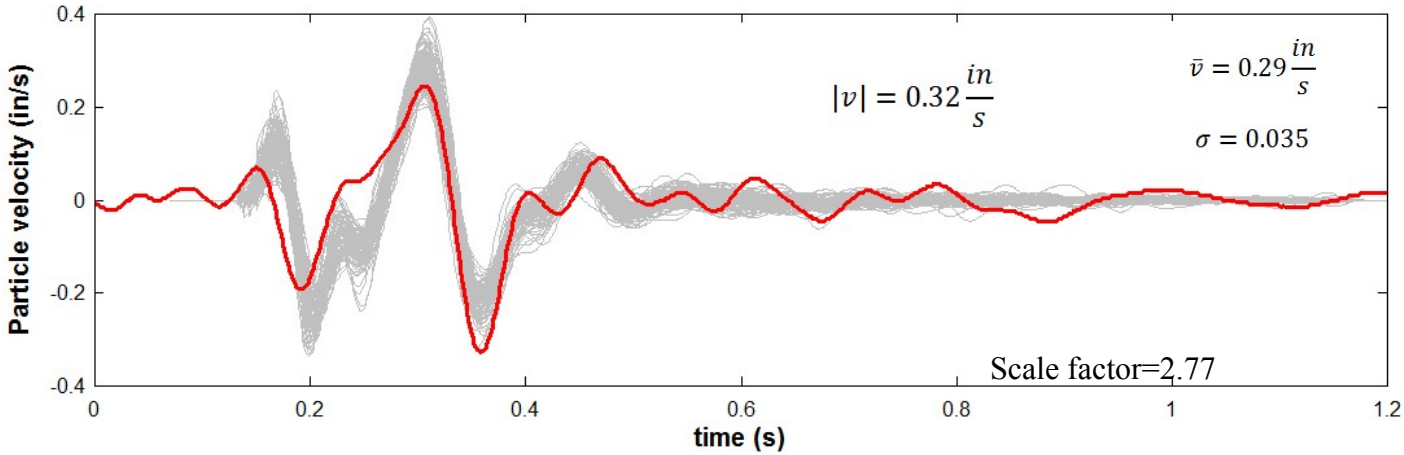

b) Enveloped using twenty five frequencies test No.10

Figure 6.4 Results comparison using four and twenty five frequencies for model 02, test No.10.

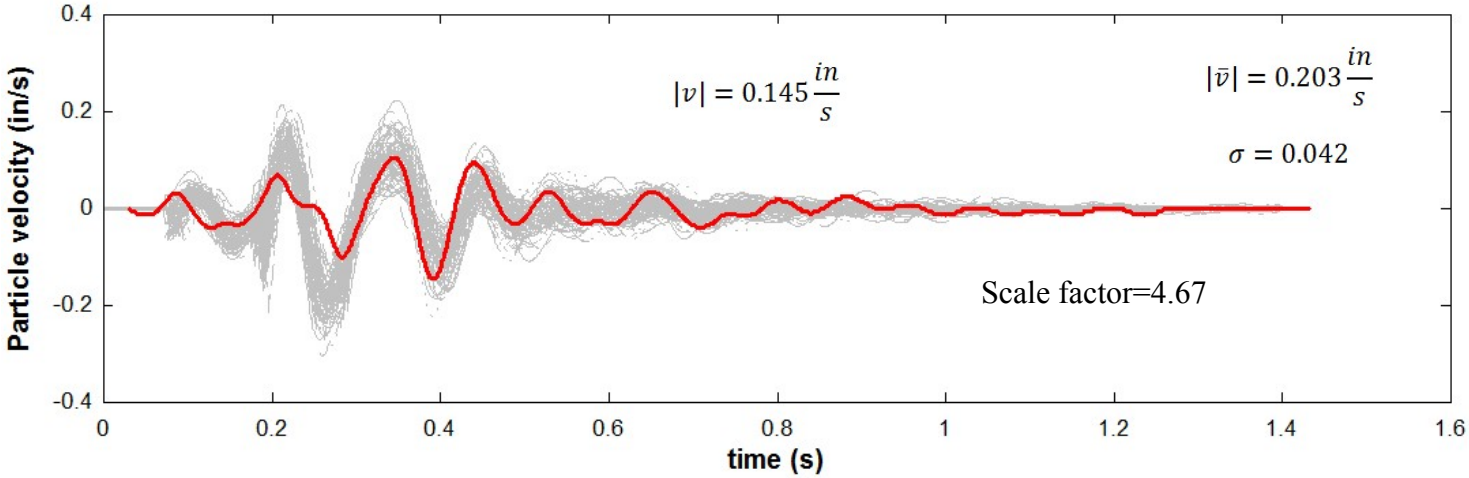

a) Enveloped using four frequencies test No.12

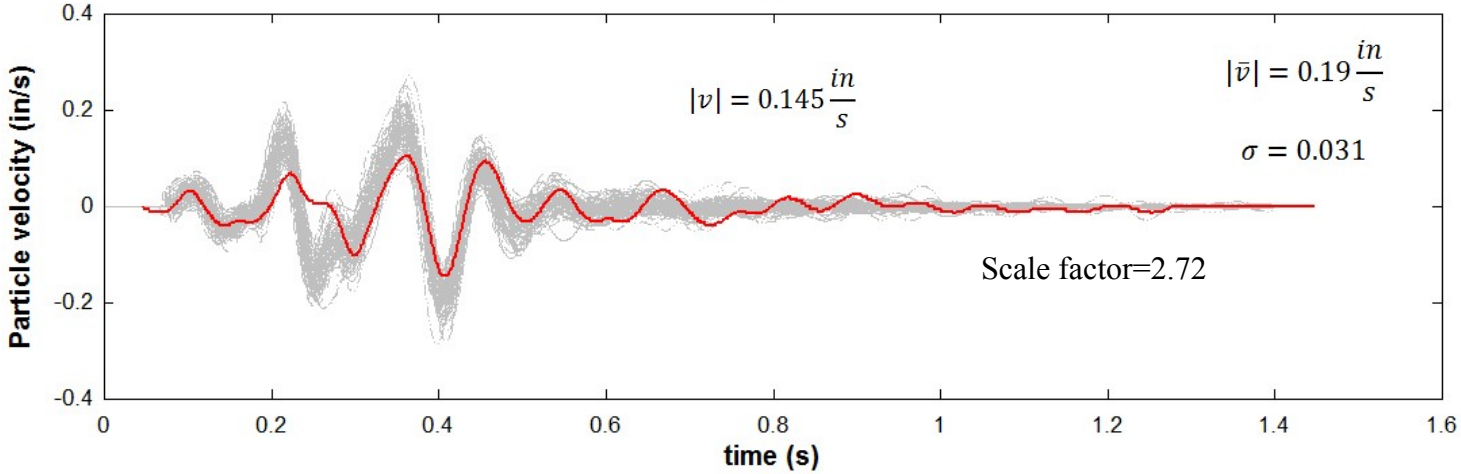

b) Enveloped using twenty five frequencies test No.12

Figure 6.5 Results comparison using four and twenty five frequencies for model 03, test No.12.

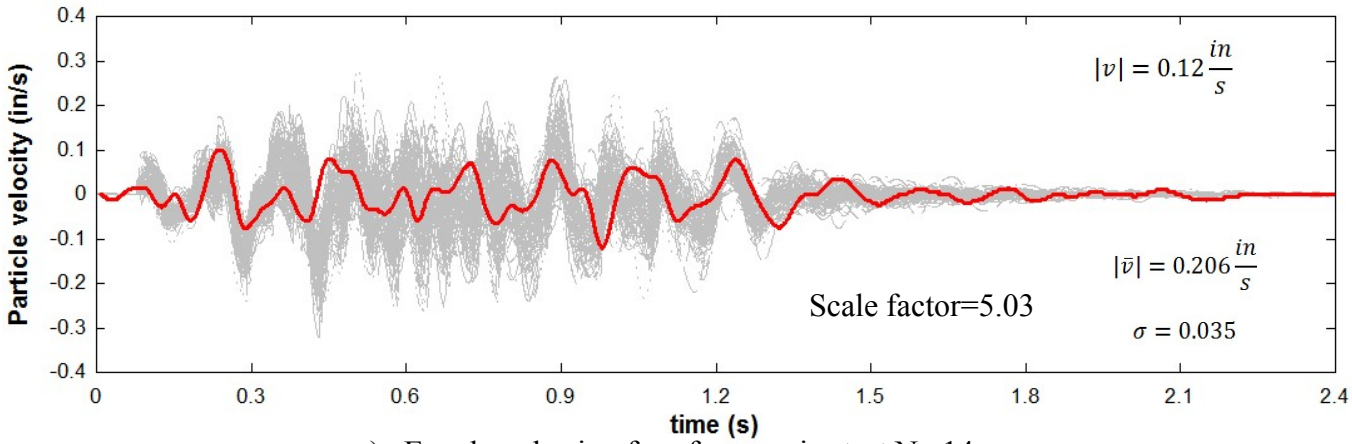

a) Enveloped using four frequencies test No.14

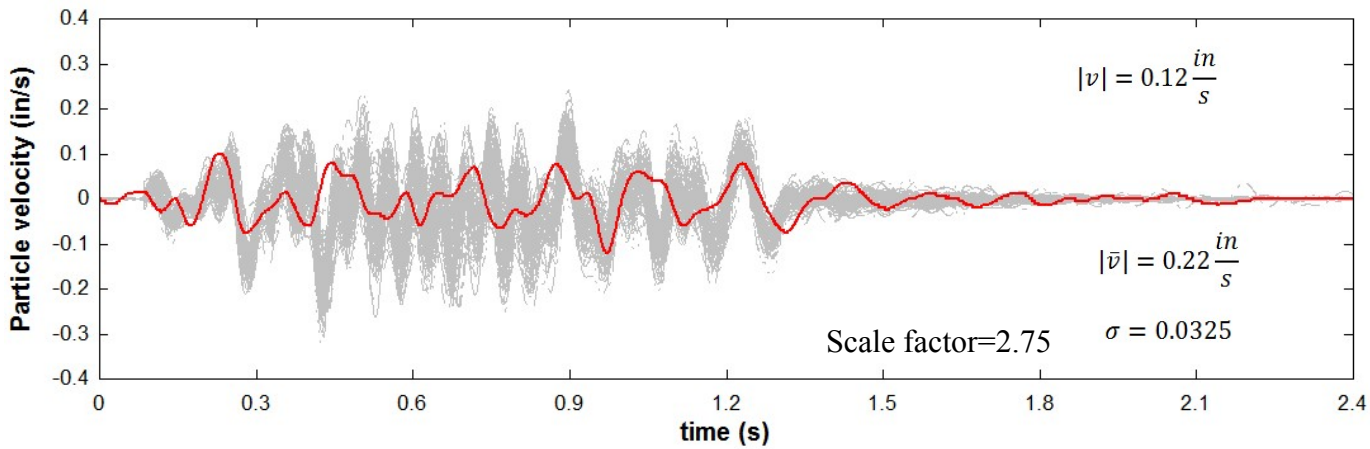

b) Enveloped using twenty five frequencies test No.14

Figure 6.6 Results comparison using four and twenty five frequencies for model 04, test No.14.

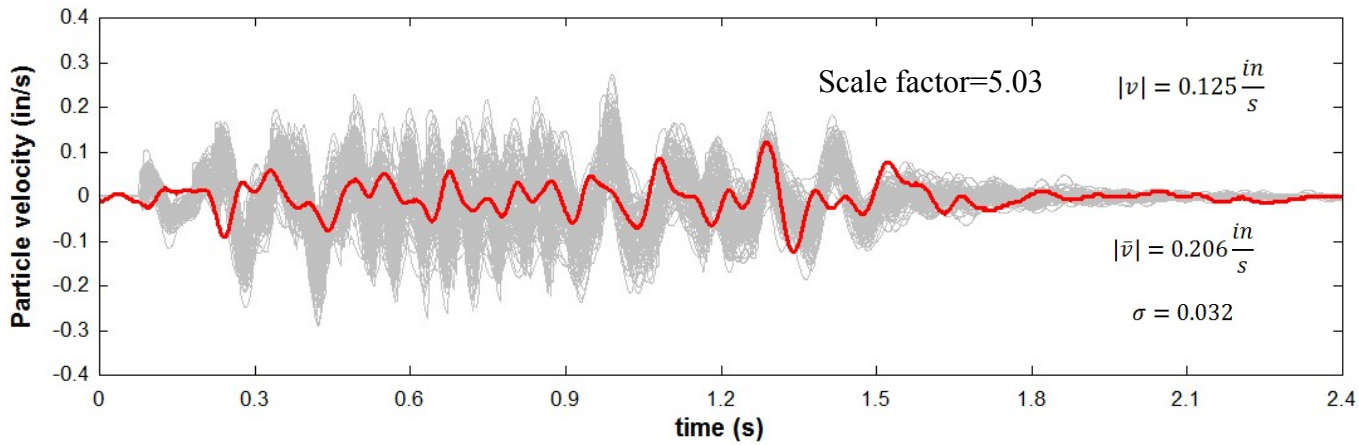

a) Enveloped using four frequencies test No.15

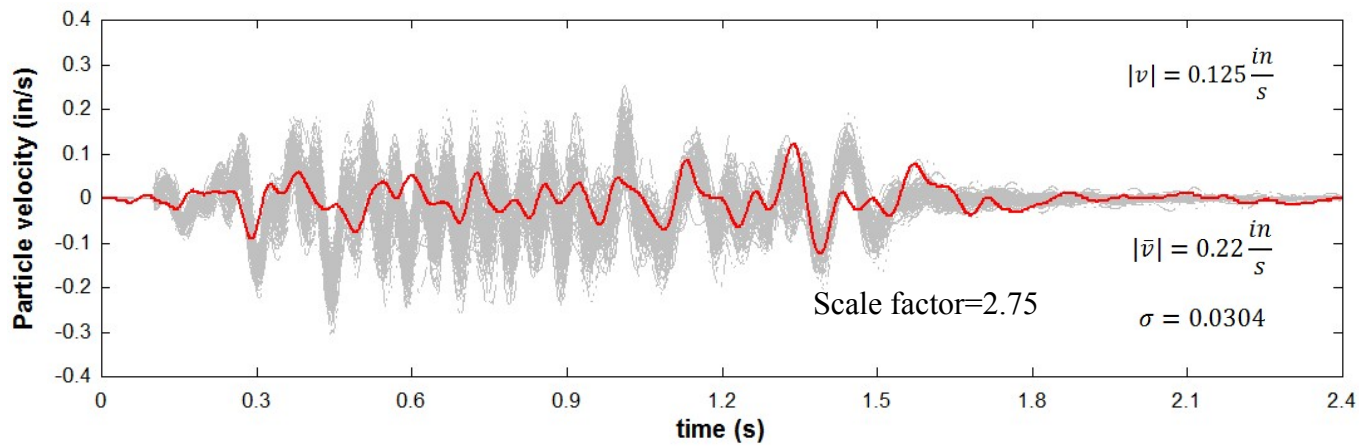

b) Enveloped using twenty five frequencies test No.15

Figure 6.7 Results comparison using four and twenty five frequencies for model 05, test No.15.

In conclusion regarding the number of frequencies involved in the prediction, increasing the number of frequencies involved in the prediction, shows an improvement in the shape of the complete waveform (the shape becomes close in shape to the measured). However, there is not a considerable improvement regarding the mean value and standard deviation calculated for the complete blast.

When more frequencies are used in the prediction, a lower value for the scale factor is needed. This is due to when more frequencies are used, the synthetic signal is more like the measured signal before the decay factor is applied. The decay factor is necessary to avoid the problem that the signal be repeated due to the character of the Fourier series. Figure 6.8 shows the synthetic signal for test No.14 when twenty five frequencies are used and before the decay factor is applied and before the scale factor is calculated.

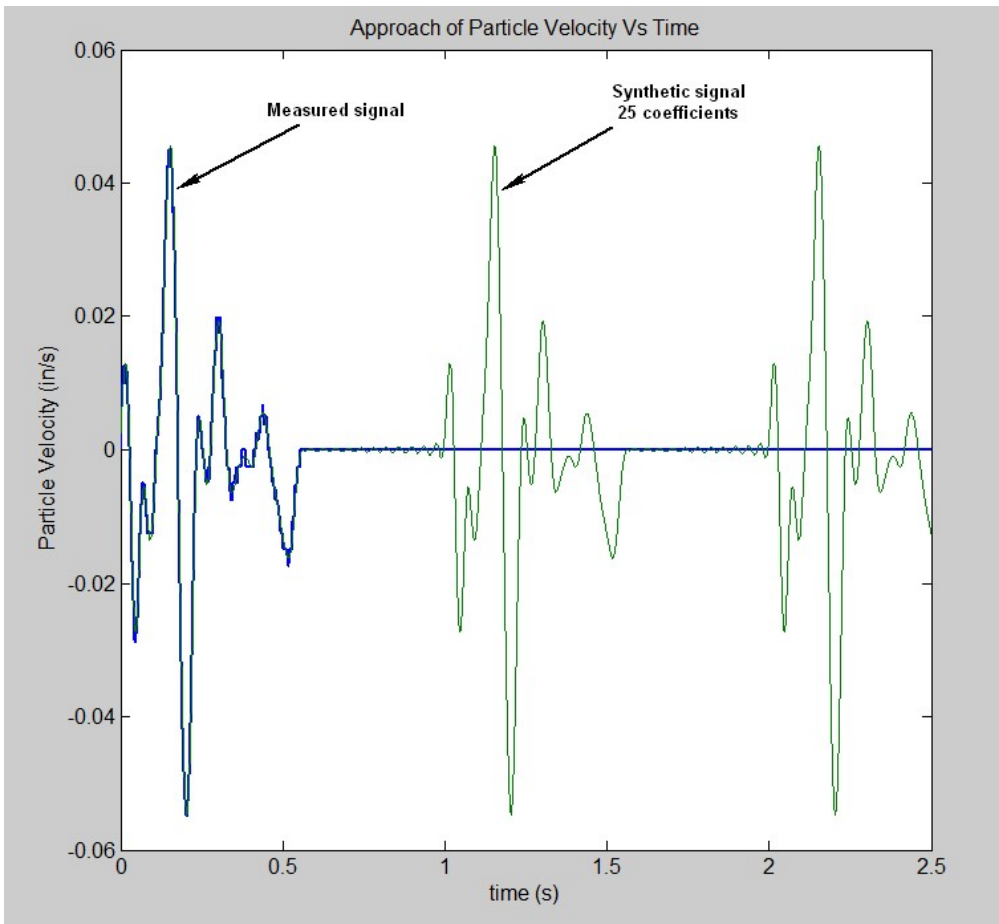

Figure 6.8 Synthetic signal for test No.14 before apply decay factor

In this case, the synthetic signal repeats itself after 1s. Using twenty five coefficients there is a perfect match between measured and synthetic within the first second. This fact will lead to a lower scale factor compared to a situation where only four frequencies are used.

6.1.2 *Decay factor*

Through the analysis of the signature waveforms for the specific chosen point, it was observed that the decay factor is a site and directional specific parameter. This parameter measures how the vibration energy is dissipated by the ground in the monitoring point. Table 6-1 shows the decay factor for some tests in this research. All values were calculated for the location of the seismograph 3599 and transverse direction.

Table 6-2 Decay factor signature waveforms at 3599 seismograph location

Test	Decay factor
10-S1	5.44
10-S2	4.70
11-S1	3.76
11-S2	4.49
12	4.63
13	4.50

The results of Table 6-2 show that having at least one signature hole, it is possible to assess the value of the decay factor for the site under consideration.

6.1.3 *Initiation system, timing and blast vibration*

As mentioned in Chapter 4, there is an appreciable difference in the accuracy and precision between electronic and non-electric initiation system. Such difference was included in Figure 4.41 and reproduced again in Figure 6.9.

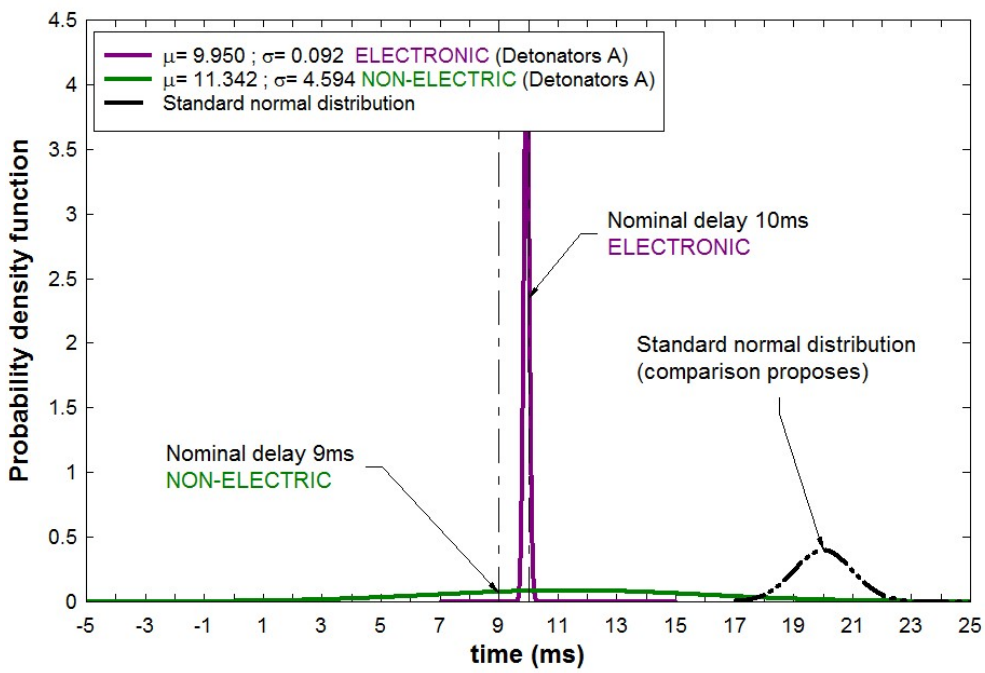

Figure 6.9 Accuracy and precision electronic vs non-electric system

As shown in the previous figure, the precision of non-electric detonators is very low when compared to electronic initiation systems.

In the case of tests No.14 and 15, they differ by four holes (34 holes test No.14 and 38 holes test No.15) and in both tests, the same nominal initiation sequence was used (delay timing was used based on 42 and 100ms delays). Assuming that the energy released by the four missing holes is not significant when compared to the entire blast, due to the timing used, the electronic initiations system should lead to higher particle velocity values. This is because through the blast, two holes are detonated at the same nominal time 142, 242, 342ms etc. and this should be more critical for electronics than for pyrotechnics because lower scatter in electronics increase the likelihood of two holes detonating at the same time. So more energy is released in the case of electronic detonators. However, it was observed that for seismograph 3599 which is in average 1440ft from the source, the complete vibration waveform, the peak particle velocity and the main frequency of the signals are almost the same for both test, as showed in Figures 6.10 and 6.11.

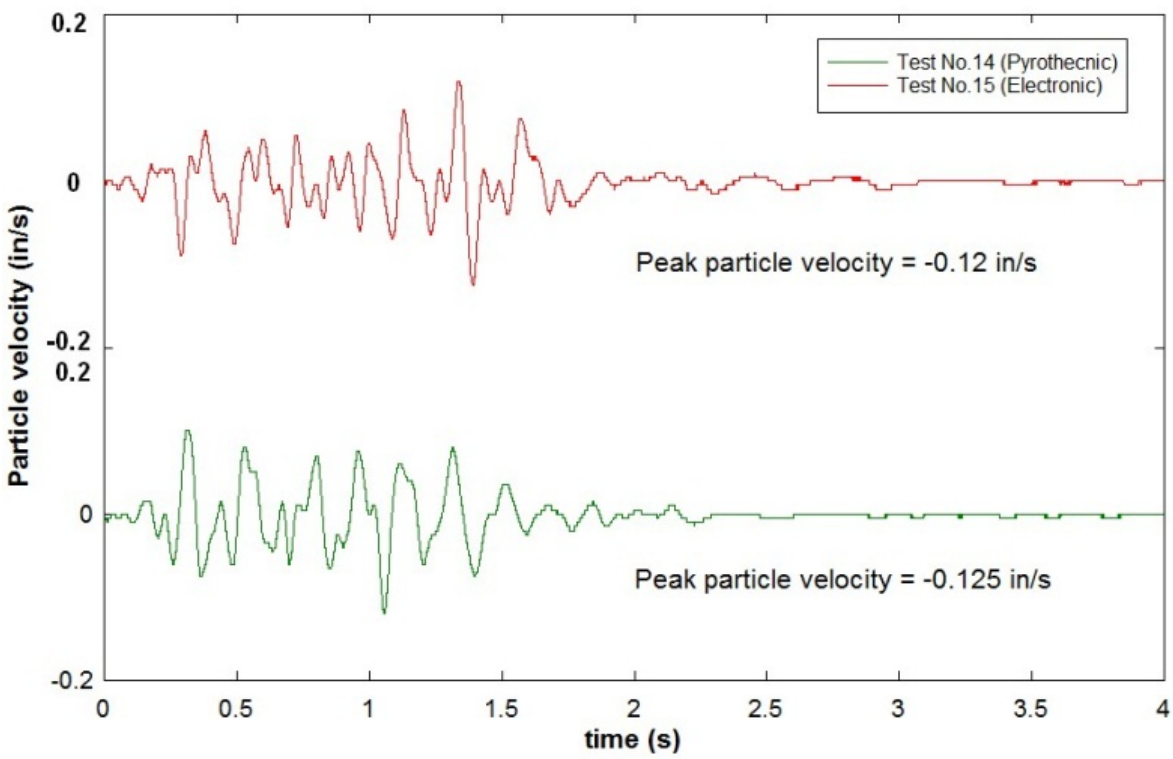

Figure 6.10 Waveform comparison test No.14 vs test No.15 transversal component (seismograph 3599)

In this case, the difference of the peak of the particle velocity is just about 0.05in/s between both tests.

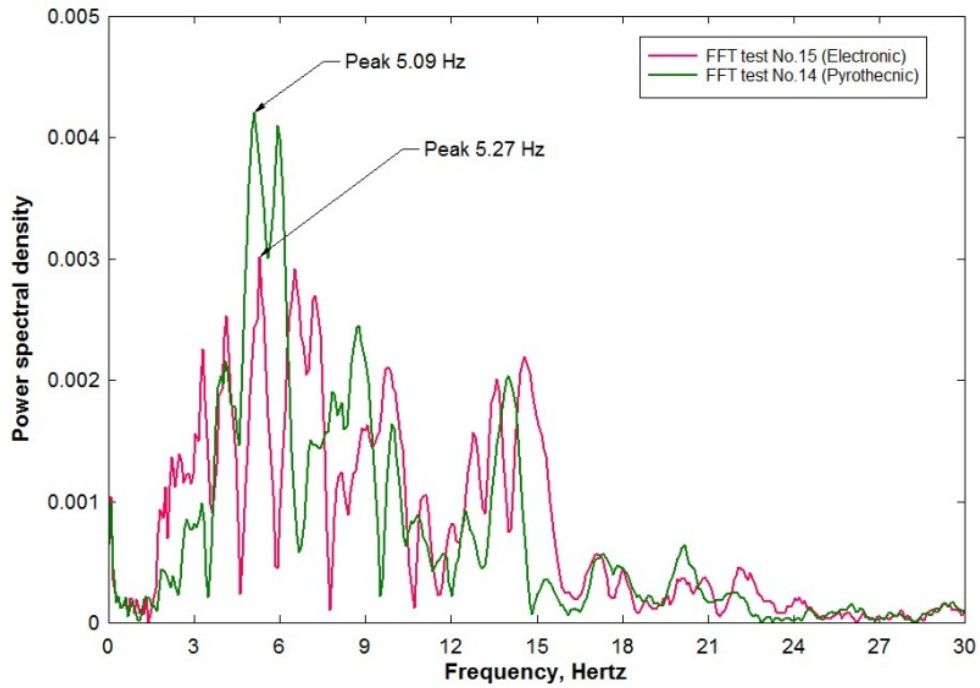

Figure 6.11 Frequency domain comparison test No14 vs test No.15 (seismograph 3599)

Similar trends were observed for the other seismographs, regardless its distance outside 1440ft. The actual readings of the peak values for all the seismographs in test No14 and 15 are included in Table 6-2.

Table 6-3 Results test 14 and 15 particle velocity peak values (actual readings)

Seismograph	Distance Average (ft)	Test 14: PPV (in/s) Rad.	Test 15: PPV (in/s) Rad.	Test 14: PPV (in/s) Vert.	Test 15: PPV (in/s) Vert.	Test 14: PPV (in/s) Trans.	Test 15: PPV (in/s) Trans.
4906	711	0.365	0.820	0.235	0.600	0.450	0.600
3599	1440	0.115	0.120	0.095	0.095	0.120	0.125
4762	1946	0.175	0.175	0.095	0.095	0.105	0.120
3857	2627	0.020	0.025	0.025	0.025	0.025	0.030
180	3160	0.020	0.035	0.020	0.020	0.015	0.025

Note: Test 14: Pyrotechnic delay system
Test 15: Electronic delay system

In conclusion, when using "traditional" nominal timing delay (in this case 100 and 42ms) in this particular mine, there is no difference between electronic and non-electric initiation system regarding the peak particle velocity for seismographs beyond 1440ft.

Similar results between the actual readings and the simulations were obtained using the improved signature hole methodology in the location of the seismograph 3599 (1440ft far from the blast). When modeling, for test No.14 (nonel), an obtained Transversal peak particle velocity of 0.206 in/s and standard deviation of 0.035, compared to 0.206 in/s and standard deviation of 0.032 for test No.15 (electronic) (see figures 6.6 and 6.7 (a)).

To analyze if this result is explained based on the scatter introduced by the travel time of waves or due to the initiation timing system, a model including only the scatter of both initiation systems was used. In other words, the traveling time due to the distance was not included in the calculations. Results are included in Figure 6.12.

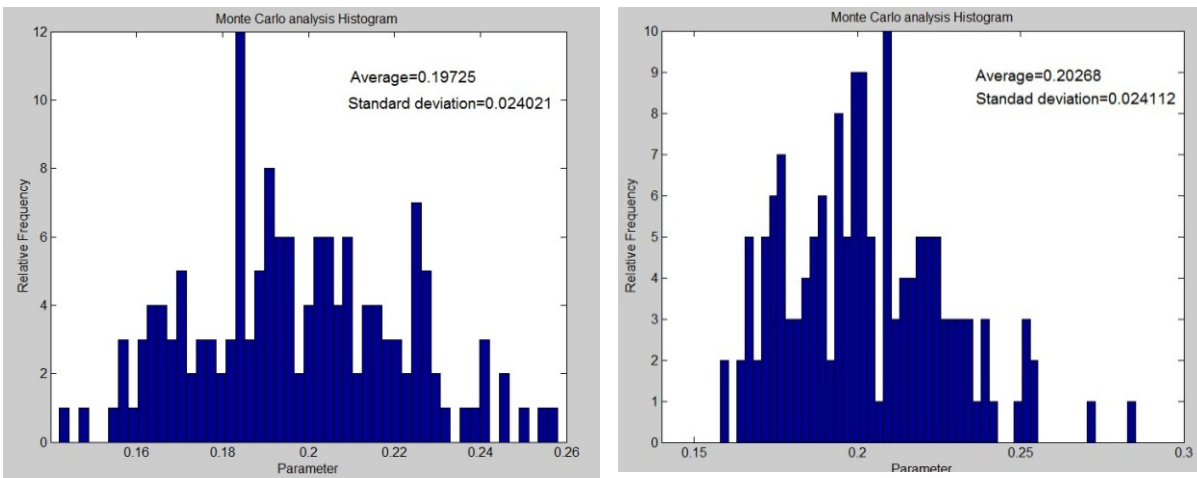

a) Pyrotechnic b) Electronic

Figure 6.12 Test No.15 simulating both initiation systems and including only time delay due to initiation sequence.

Figure 6.12 shows once again that in this case there is not a considerable difference for seismographs beyond 1440ft when pyrotechnic and electronic initiation systems are used. Other timing combinations for the location of the seismograph 3599 were analyzed in order to see any possible trend between nominal timing and the initiation system; the results are included in Table 6-3.

Table 6-4 Delay timing and initiation system simulation far seismographs (beyond 1440ft)

Timing	Electronic	Pyrotechnic
100/42ms	$\lvert\bar{v}\rvert = 0.20\,{}^{in}/_{s}$ $\sigma = 0.024$	$\lvert\bar{v}\rvert = 0.19\,{}^{in}/_{s}$ $\sigma = 0.024$
42/17ms	$\lvert\bar{v}\rvert = 0.20\,{}^{in}/_{s}$ $\sigma = 0.040$	$\lvert\bar{v}\rvert = 0.20\,{}^{in}/_{s}$ $\sigma = 0.040$
25/9ms	$\lvert\bar{v}\rvert = 0.25\,{}^{in}/_{s}$ $\sigma = 0.031$	$\lvert\bar{v}\rvert = 0.25\,{}^{in}/_{s}$ $\sigma = 0.034$
17/9ms	$\lvert\bar{v}\rvert = 0.38\,{}^{in}/_{s}$ $\sigma = 0.034$	$\lvert\bar{v}\rvert = 0.37\,{}^{in}/_{s}$ $\sigma = 0.040$
10/5ms	$\lvert\bar{v}\rvert = 0.60\,{}^{in}/_{s}$ $\sigma = 0.058$	$\lvert\bar{v}\rvert = 0.61\,{}^{in}/_{s}$ $\sigma = 0.055$

According to the results of Table 6-3, when using different nominal timing sequence there is no difference between electronic and pyrotechnic initiation system; however when the lower timing is used, an increment in the peak particle velocity is observed in the location of the seismograph 3599 (1440ft from blast).

In the bottom row timing of the Table 6-3 all holes basically are detonated 5ms apart with some holes detonated at the same time as explained. On the other hand, when a uniform sequence of 5ms is used, an average value of 0.32 in/s with a standard deviation of 0.045 was obtained; this result indicates the influence of the timing initiation sequence in the final peak particle velocity of the whole blast event.

Considerable differences in peak particle velocity between tests No.14 and 15 emerge when Table 6-2, is reviewed for seismograph 4906. The difference in peak particle velocity generated by the two initiation systems is around 1.5 and 2.5 times for all components. Due to this fact, the modeling for seismograph 4906 was performed and the results are presented next.

As previously mentioned, there is not a specific signature for tests No.14 and 15, so for modeling proposes, the average of the signatures between tests No.12 and 13 was used as the signature for modeling. Figure 6.13 shows the two signatures at the location of seismograph 4906 recorded and the average used for modeling.

Following the procedure for modeling explained previously, four frequencies; 2.4, 9.6, 10.8 and 16 Hz were chose to simulate the signature signal, additionally, a scale factor of 2.48 and a decay factor of 4.85 were used. It was assumed a standard deviation of 10ms for the pyrotechnic detonators.

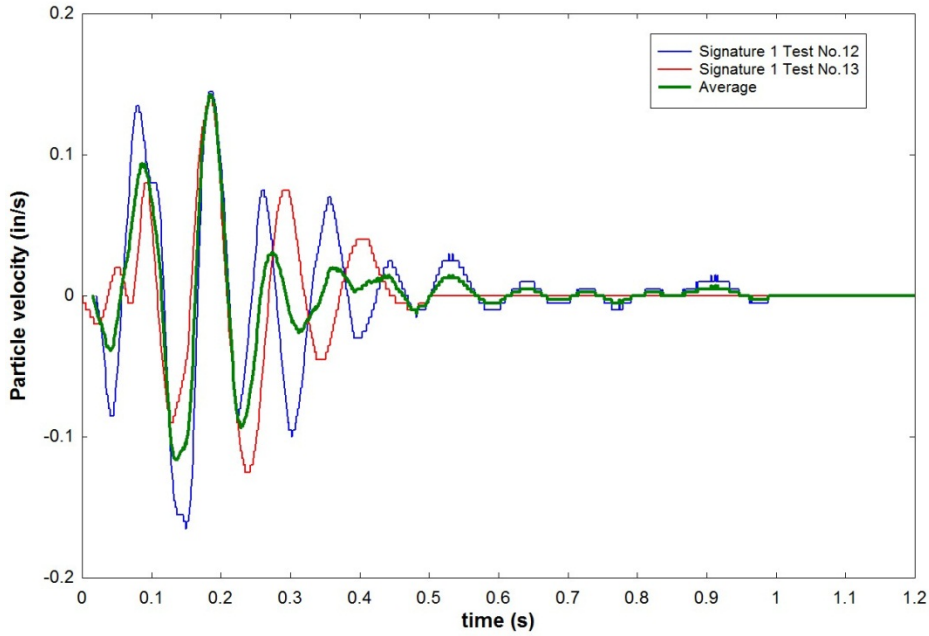

Figure 6.13 Signature used to model Tests No.14 and 15 (average) in seismograph 4906 location.

In the modeling of test No.15, a standard deviation of 0.1ms was assumed for electronic initiation system. In both cases, the traveling time was introduced in the model using a wave velocity of 16000ft/s and a standard deviation for wave velocity of 1000ft/s. Finally, the standard deviation of the amplitude and the decay factor was assumed as 1 in both cases. In modeling test No.15, it was necessary to adjust the amplitude factor to 4 and it was assumed a variation in amplitude of 2. This is needed because test No.15 is closer than test No.14, also it is necessary to take into account that here for modeling we are using signatures from test No.12 and 13 that are even further from test No.15.

The results for modeling Test No.14 and 15 are included in Table 6-5, Figure 6.14 and Figure 6.15 respectively.

Table 6-5 Modeling results for seismograph 4906 (Pyrotechnic vs electronic) Radial component

Test No.	Peak particle velocity absolute value (measured)	Modeling results	
		Peak particle velocity mean	Standard deviation
No.14 (Pyrotechnic)	0.365in/s	0.41in/s	0.062
No.15 (Electronic)	0.82in/s	0.65in/s	0.010

It is remarkable how the proposed methodology, using the same signature waveform to model pyrotechnic and electronic initiation systems show the same trend

than the actual readings for seismograph 4906. As previously stated, it is expected higher peak particle velocity values when electronic initiation system is used compared to pyrotechnic system. For this particular case the fact that two holes been detonated at the same delay time increase the peak particle velocity value.

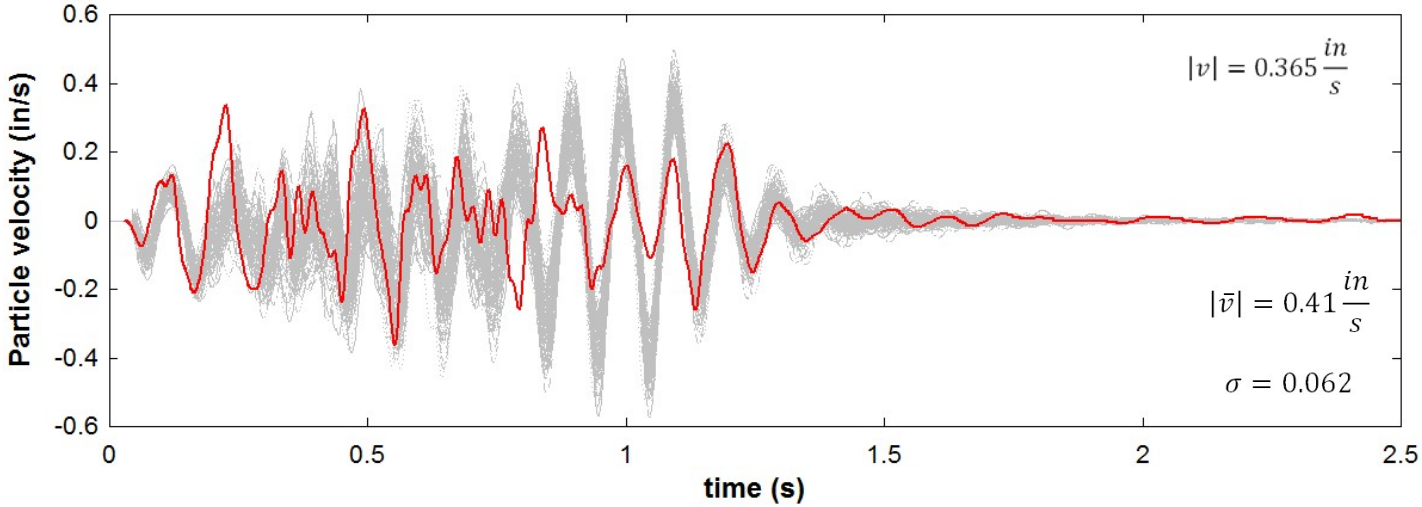

Figure 6.14 Modeling results test No.14 seismograph 4906 (Pyrotechnic)

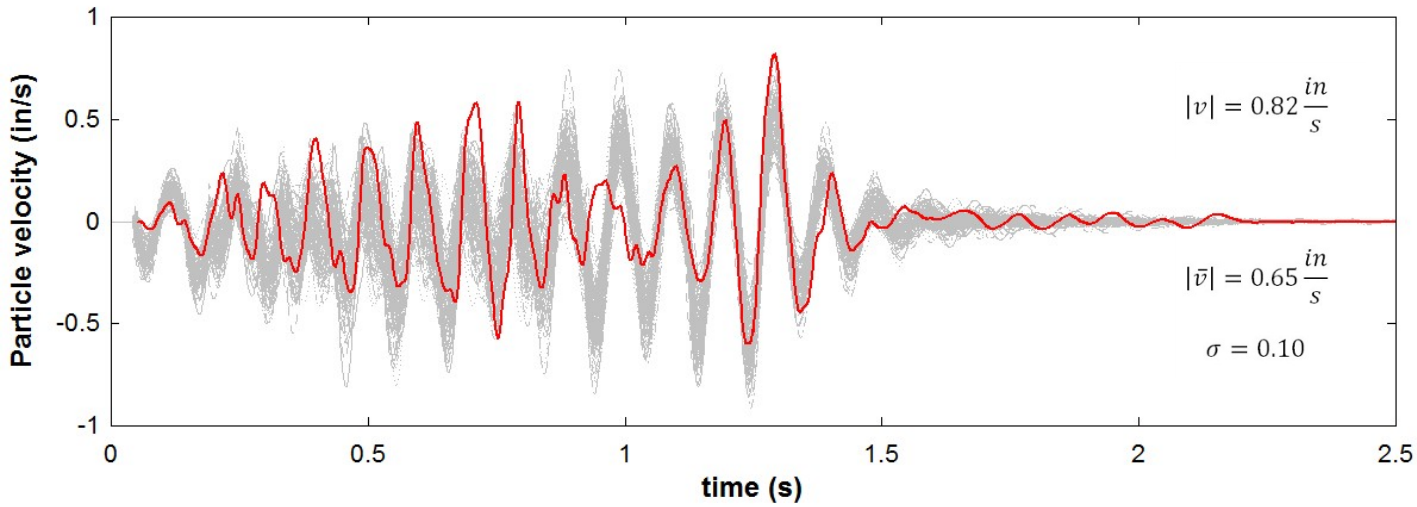

Figure 6.15 Modeling results test No.15 seismograph 4906 (Electronic)

Chapter 7

CONCLUSIONS AND FUTURE WORK

7.1.1 *Conclusions*

- Current methodologies to assess vibrations levels from blasting are low in accuracy and precision. This is an inevitable consequence of the high uncertainty of the variables involved in the problem. Specifically, in most of the cases, the high variability in the geological conditions made each mining blast a unique event, regardless of the consistency of the geometry, quantity and type of explosives, and nominal initiation sequence.

The most current methodology used to assess blast vibrations from blasting (scaled distance) presents important disadvantages and inaccuracies.

- A reliable and extensive database is required
- Weakness in the theoretical and physical support of the equations.
- There is no other parameter regarding delay time in a blast than the 8 milliseconds rule. No clue about how different initiations timing affect the vibration levels.

The first disadvantage is related to the requirement of a confident and extensive database to calculate the site specific geological constants in the scaled distance equation. This fact makes this methodology impossible to apply for some areas at the mine if no vibration information was collected near the site where vibration levels are needed to calculate. Another disadvantage is the weak theoretical and physical justification regarding to the square root of the weight of explosive used in the scaled distance calculations. This concept was developed by Blair (2000) and was included in this document in Chapter 4. Finally, through the validation of the current improved methodology, it was observed the high incidence of the nominal initiation timing sequence in the vibrations levels. Scaled distance methodologies do not take into account the initiation sequence timing when vibration levels are calculated.

- Current signature hole techniques assume the invariability of the signature waveform hole-to-hole (linear superposition). While the invariability of the signature waveform can be true under some exceptional conditions, like a rock mass containing few or no joint systems and a massive rock layer, in general the geological conditions change, even between holes affecting in some grade the signature waveform that each hole generate. In this research, the methodology proposed to improve current signature hole techniques is based in a probabilistic approach. The proposed methodology allows the change of the signatures hole to hole in a random fashion using Fourier series to generate different signatures for each hole. Through this mathematical tool variations in geology, geometry hole to hole, different explosives, contamination, change in the distance etc. are considered implicitly in the model.

- The equation (Silva-Lusk) base in Fourier Series to introduce random behavior in the signatures hole to hole is given by:

$$f(t) \approx \left[c_o + \sum_{n=1}^{m} \boldsymbol{ASF_m} * \{A_m * sin(2\pi * \boldsymbol{frequency_m} * t + \emptyset_m)\} \right] * e^{-\boldsymbol{decay\ factor}}$$

[7.1]

where:

ASF_m:	amplification scale factor for frequency m.
c_o:	first term in the Fourier series
m:	number of frequencies chose to approach the measured signature waveform.
A_m:	amplitude coefficient for frequency m in the Fourier series
$frequency_m$:	frequency value chose to approach the measured signature waveform.
t:	time
$\emptyset_m$:	phase for frequency m
$decay\ factor$:	factor related to the attenuation energy in that particular monitoring point.

- Based on the results from field tests conducted in this research, it can be concluded that the usage of electronic detonators against nonel has more impact in vibration levels closer to the site of the blast (this is included in the results of test No.14 and 15). In this particular case, the low scatter in electronic detonators increased the likelihood of two holes being detonated at the same time as initially designed. For the topographical and geological particular conditions where the test No.14 and 15 were developed. For distances further than 1440ft from the blast source, there is no difference in the vibration levels when electronic or pyrotechnic initiation system is used.

- The probabilistic methodology proposed in this research using a Monte Carlo scheme, allows the design of the initiation timing in mining blasts. According to the initiation sequence and timing selected for different scenarios, using the proposed methodology it is possible to predict or calculate vibration levels in a particular monitoring point base on the signature of one hole with the same geometrical characteristics than the production holes.

- The usage of signature holes recorded along with production holes is a practice that improves the quality of the results and confidence of the signature methodologies used in the assessment of vibration levels. This is because the signatures become more representative of the geological

conditions and the structural conditions of the rock mass where the explosions take place.

- It is possible to use signature techniques to assess the levels of airblast from a mining production blast.

7.1.2 *Novel contributions*

In the development of the current research several novel contributions where performed regarding blast vibration prediction:

- This research presents to the academia and the industry a clear and well supported methodology to assess blast vibration levels based on improved signature techniques. The methodology is based on one probabilistic approach using Monte Carlo scheme, thus, it allows to calculate vibration levels from a mining blast using confidence intervals according to the available information to perform the analysis.

- The randomization of the waveforms hole to hole allows to perform non-linear superposition when the complete waveform is calculated.

- The simulation of signature waves based on Fourier Series as part of signature hole techniques is a novel contribution to this methodology.

- The implementation of Monte Carlo scheme to signature hole technique is a novel contribution in the area of blast vibration prediction.

- The performance of signature holes along to the production blast is a novel contribution to signature hole techniques.

7.1.3 *Recommendations for Future Work*

The recommendations for future work in the area of blast vibration prediction include:

- In this research to randomize the variables involved in the problem, normal standard deviation distributions were used. It is necessary to perform more field test in different mines to verify or modify the probability distributions used for each variable.

- More field tests are required to verify, validate and adjust the proposed methodology. In this research, the methodology was used to match the recorded vibration from different production blasts. In a second stage of this research, it is necessary to predict the vibration levels before the production blast occurs using the appropriate information.

- Using the proposed methodology, it is possible to assess the vibration levels at the specific monitoring point where a previous signature had been recorded. It is necessary to implement a methodology to assess vibration levels where no signature information is available. This can be done through the use of transfer functions propagating the signature from the monitoring point to the point of interest and using the current proposed methodology.

- More research regarding the current monitoring devices used in mining industry is required. The limitations of the devices, the internal filtering processes of the recorded signals are not clear. How those parameters affect the assessment of vibration levels in blasts mining is not totally clear.

REFERENCES

Abuelma'Atti M.T., (2001). A New method for Fourier Analysis of discontinuous and peak periodic waveforms. Journal Computers and Mathematics with applications, 41, pp 1417-1423.

Aimone, C.T., (1992). Rock breakage: Explosives, blast design. Hartman, H.L. (ed.), SME Mining Engineering Handbook. Society of Mining Engineers, Littleton, pp 722-746.

Aldas, G.G.U., Ecevitoglu, B., (2008). Waveform analysis in mitigation of blast-induced vibrations. Journal of Applied Geophysics 66, pp 25-30.

Aldas, G.G.U., (2010). Investigation of blast design parameters from the point of seismic signals. International Journal of Mining, Reclamation and Environment. Vol. 24, No. 1, March 2010, 80–90

Aldas, G.G.U., (2010). Non-Linear Behavior of Blasting Noticed on Seismic Signals. Gazi University Journal of Science. 23(4):401-411 (2010)

Ambraseys, N. R. and Hendron, A. J., (1968), Dynamic Behavior of Rock Masses, Rock Mechanics in Engineering Practice, John Wiley & Sons, Inc., London.

Anderson, D. A. (2008). Signature Hole Blast Vibration Control- Twenty Years Hence and Beyond. The Journal od Explosives Engineers. September/Octuber., pp 6-14.

Anderson D. A., Winzer S. R., and P. Ritter A. (1982). Blast Design for Optimizing Fragmentation while Controlling Frequency of Ground Vibration. International Society of Explosives Engineers General Proceedings,. Pp 69-84.

Anderson, D.A., Winzer, S.R., and Reil, J.W., (1985). A method for Site-Specific Prediction and Control of Ground Vibration from Blasting. Proc. 11th Anual Conf. Expl. And Blast Tech.

Anderson D. A., (1989). The 8 Millisecond "Criterion": Have We Delayed Too Long in Questioning It?. International Society of Explosives Engineers General Proceedings, pp 381-395.

Ash, R.L., (1963). The mechanics of rock breakage, standards for blasting design. Pit and Quarry.

Bajpayee., T.S., Mainiero, R.J. (1990). Firing accuracy of electric detonators. International Society of Explosives Engineers, General proccedings., pp 89-98.

Barkley R.C. and Daemen J.J.K. (1986). Computer Simulation Predictor of Ground Vibration Indiced by Blasting. Report to U.S. Bureau of Mines, OFR 105(3)-81.

Batzle, M. L., Simmons, G., Sigfried, R. W. (1980). Microcrack Closure in Rocks Under Stress: Direct Observation. J. Geophysical Research, 85(B12), 7072–7090.

Blair, D.P. (2004). Charge weight Scaling Laws and the Superposition of Blast Vibrations Waves. Fragblast Vol.8. No.4, pp. 221-239.

Blair, S.C., Cook, N.G.W., (1998) Analysis of compressive fracture in rock usign statistical techniques. Int. J. Rock Mech. Min. Sci. 35 (7).

Blake, F. C. (1982) Spherical wave propagation in solid media. J. Acoustical 80c. Am., 24(2): 211-215.

Bobet, A., Fakhimi, A., Johnson S., Morris J., Tonon F., and M. Ronald Yeung., (2009). Numerical models in discontinuous media: Review of advances for rock mechanics applications. Journal of Geotechnical and Geoenvironmental Engineering, Nov 2009., pp 1547-1561.

Bollinger, G. A. (1980). Blast vibration analysis. Carbondale: Southern Illinois University Press, [1971].

Bourbie, T., Coussy, O., Zinszner, B., (1987), Acoustics of Porous Media, Gulf Pub. Co.

Buckingham, E. (1915). The principle of similitude. Nature 96.

Chiappetta, R.F., S.L. Burchell, J. W. Reil, and Anderson, D.A. (1986). Effects of accurate ms delays on productivity, energy consumption at ther primary crusher, oversize, ground vibrations and airblast. Proceedings of the 12th Annual Conference on Explosives and Blasting Techniques, Atlanta, GA, pp 213-234.

Chi-Tsong Chen (2004). Signals and Systems 3th edition. Oxford University Press

Christopherson, K., and Papillon B., (2008). Vibration reduction through production-signature hole blasting. The Jornal of Explosives Engineers, September/October, pp 16-20.

Cook, M.A., (1958) The Science of High Explosives, ASC Monograph No. 139, Reinhold.

Cundall, P. A., Detournay, C., (2008) Modeling Shock and Detonation Waves with FLAC. Continuum and Distinct Element Numerical Modeling in Geo-Engineering

(Proceedings, 1st International FLAC/DEM Symposium, Minneapolis, August 2008), Paper No.10-06. R. Hart et al., Eds. Minneapolis: Itasca Consulting Group, Inc., 2008.

Crenwelge Jr., O.E. and Peterson T. A., (1986). Overburden blasting vibrations: Analysis, prediction, and control. International Society of Explosives Engineers, General proccedings., pp 269-281.

Crenwelge Jr., O.E. (1988). Method for Determining Amplitude-frequency Components of Blast Induced Ground Vibrations. Research proceedings of the Fourth Mini-Symposium on explosives and Blasting Research. Society of Explosives Engineers. Houston, TX.. pp73-88.

Crenwelge Jr., O.E. (1988). Use of Single Charge Vibration Data to Interpret Explosive Excitation and Ground Transmission Characteristics. International Society of Explosives Engineers, General Proceedings., pp151-160.

Drake, J.L., Little, C.D., (1983). Ground Shock from Penetrating Conventional Weapons. Proceedings Symposium of the Interaction of Non-Nuclear Munitions with Structures, U.S. Air Force Academy, Colorado Springs, CO.

Dowding, C.H. (1985). Blast Vibration Monitoring and Control. Library of Congress. p6.

Duvall, W. I. Fogelson, D. E. (1961). Review of criteria for estimating damage to residences from blasting vibrations, Report of Investigation 5968, Bureau of Mines.

Edwards, A. T. Northwood, T. D. (1960). Experimental studies of the effects of blasting on structures, The Engineer Sept. 30.

Enescu D., Anca Georgescu, and Vasile Mârza (1973). Simulations of the underground explosions generating longitudinal and transverse waves. Bulletin of the Seismological Society of America. June 1973 63:753-760

Frantti G. E. (1963). Spectral energy density for quarry explosions. Bulletin of the Seismological Society of America. Vol.53. No.5, pp 989-996.

Frantti, G.E. (1977). Near-Field Elastic Ground Response Spectra for Multi-Hole Surface Explosions. General Proceedings., pp 149-164.

Furtney, J. K., Cundall, P. A., Chitombo, G. P. Developments in Numerical Modeling of Blast Induced Rock Fragmentation: Updates from the HSBM Project. Rock Fragmentation by Blasting (FRAGBLAST 9, Granada, Spain, September 2009), pp. 335-342.

Greenhalgh S. A. (1980). Effects of delay shooting on the nature of P-Wave seismograms. Bulletin of the Seismological Society of America. Vol.70. No.6, pp 2037-2050.

Harries, C., Gribble, D.P. (1993). The development of low shock energy explosive ANRUB, Proc. 4th Int. Symp. Rock Fragmentation By Blasting, Vienna. pp. 379-386.

Nicholls, H.R., Charles, F.J., Duvall, W.I. (1971). Blasting vibrations and their effects on structures. Bureau of Mines. U.S. Bulletin 656.

Hinzen, K.G., and R. Ludeling., (1987). A New Approach to predict and reduce blast vibration by modeling of seismograms and using a new electronic initiation system., Proceedings of the 13th Annual Conf. on Exp. And Blasting Techniques, New Orleans, LA.

Hossaini, S.M.F., Sen, G.C. (2004). Effect of explosive type on particle velocity criteria in ground vibration, The Journal of Explosive Engineering, July/August, pp. 34-39.

Hunter, C., Fedak, K. and Todoeschuck, J.P. (1993). Development of low density explosives with wall control applications, Proc.19th Annual Conf. Explosives and Blasting Techniques, Jan, 31-Feb. 4, San Diego, California, USA, ISEE, pp. 549-555.

International Society for Rock Mechanics. (1992). Suggested Methods for Blast Vibration Monitoring. ISRM., pp 145-156.

Kavetsky, A, Chitombo, G P F, McKenzie, CK and Yang, RL, (1990). A Model of Acoustic Propagation and its Application to Determine Q for a Rock Mass, Int J Rock Mech Min Sci Geomech Abstr, 27(1):33-41.

Khandelwal M., Singh T.N., (2006). Prediction of blast induced ground vibrations and frequency in opencast mine: A neural network approach. Journal of Sound and Vibration 289, pp 711-725.

Kjartansson, E. (1979). Constant Q wave propagation and attenuation. J. Geophys. Res. 84: 4737–4748.

Kramer, S.L., (1996). Geotechnical Earthquake Engineering. Prentice Hall.

Kranz, R.L. (1983) Microcracks in rocks: a review. Tectonophysics 100: pp 449-480.

Kreyszig, E., (2005) Advanced Engineering Mathematics. John Wile & Sons, pp 478.

Langefors, U., Kihlstrom, B., (1963). The modern technique of rock blasting. John Wiley & Sons, p 263.

Langefors, U., Kihlstrom, B., Westerberg, H. (1958). Ground vibration in blasting.Water Power, Sept-Nov.

Larsson B., Holmberg R., Westberg J., (1988) Super accurate detonators - a rockblaster's dream. International Society of Explosives Engineers General Proceedings.

Linehan, P. ; Wiss, J. F. (1983). Vibration and Air Blast Noise From Surface Coal Mine Blasting. AIME Transactions V. 272, 1982.

Lusk, B., Worsey, P., Oakes, K., Chambers, J., Crabtree, S., Brasier, T., and Wheeler R., (2006). Destructive Wave Interference in Underground Blasting Utilizing Precise Timing. International Society of Explosives Engineers General Proceedings,. Vol. 1.

Lusk, B., Hoffman, J., Silva C., Wedding W., Morris, E., Calnan J. (2012) Evaluation of Emergent Electronic Detonators and Modern Non-Electric Shocktube Detonaros Accuracy. Blasting and fragmentation. Vol.6. No.1. pp 1-17.

Lusk, B., Silva, C., Eltschlager, K., Hoffman, J. (2010) Acoustic Response of Structures to Blasting Analyzed Against Comfort Levels of Residents Near Surface Coal Operations. Office of Surface Mining. Final Report OSM cooperative Agreement S07AP12481.

Matsumoto, M., Nishimura, T. (1998) Mersenne Twister: A 623-dimensionally equidistributed uniform pseudorandom number generator. ACM Trans. on Modeling and Computer Simulation Vol. 8, No. 1, January pp.3-30

Miller, D., Drew, M. (2007). A review of the benefits being delivered using electronic delay detonators in the quarry industry. The Institute of Quarry Australia 50th National Conference, Hobart, Tasmania, October, pp 1615-1645.

Mortazavi, A. Katsabanis, P.D. (2001). Modelling burden size and strata dip effects on the surface blasting process. International Journal of Rock Mechanics and Mining Sciences, Vol 38, pp 481-498.

Olsson, M., Nie, S., Bergqvist, I., Ouchterlony, F. (2001). What causes cracks in rock blasting?. Proc. EXPLO2001. Hunter valley, NSW, Australia, pp 191-196.

Pollack, R.N (1963). Effect of delay time and number of delays on the spectra of ripple-fire shots. Earthquake Notes, 34, pp 1-12.

Randall, M. W., (1991). An Analysis of Firing Time Scatter Effects on Vibration Simulations from Waveforms with Low and High Frequency Components. International Society of Explosives Engineers, Research proccedings., pp 135-142.

Reisz, D.W., McClure, R., and Bartley, D. (2006). Why the 8MS rule Doesn`t Work. International Society of Explosives Engineers, Vol2. General proccedings.

Rholl S.A., Stagg M.S. (1988). A Computer Program to Predict the Probability of Overlap or Crowding of Adjacent-Period Millisecond-Delayed Initiators. Research proceedings of the Fourth Mini-Symposium on explosives and Blasting Research. Society of Explosives Engineers. Houston, TX.. pp91-104.

Rossmanith, H.P. (2003). The Mechanics and Physics of Electronic Blasting. General Proceedings Vol.1.

Sakamoto, M., M. Yamamoto, K. Aikou, E. Suzuki, H. Fukui, and K. Ichikawa (1989). A study on high accuracy delay detonator. Procceding of the 15th Annual Conf. Exp. And Blasting Techniques, New Orleans, LA., pp 185-195.

Sally,S. A., Daemen, J.J.K (1983). Ground and Air Vibrations Caused By Surface Blasting. Volume 2 Ground Vibration Monitoring And Assessment Of Conventional Predictors. Report to U.S. Bureau of Mines OFR 105(2)-84. p11

Saharan, M.R., Mitri, H.S. and Jethwa, J.L. (2006) Rock fracturing by explosive energy: review of state-of-the-art. Fragblast, 10: 12,61-81.

Saharan, M.R., Mitri, H.S. (2008) Numerical procedure for dynamic simulation of discrete fractures due to blasting. Rock Mechanics and Rock Engineering, 41 (5), pp 641-670.

Sanchidrián J.A., P. Segarr., L.M López. (2007). Energy components in rock blasting. International Journal of Rock Mechanics & Mining Sciences V.44, pp 130-147.

Silva Castro J, Sebastian L. B., Gamber, N., Lusk, B (2011). Numerical modeling of subsurface blasts. Pan-Am CGS Geotechnical Conference. October 2-6, Toronto, Canada.

Siskind, D.E,. Stagg, M.S., Kopp, J.W., and Dowding, C.H. (1980b). Structure response and damage produced by ground vibration from surface mine blasting. U.S. Bureau of Mines RI 8507.

Siskind, D.E,. (2005). Vibrations From Blasting. International Society of Explosives Engineers.

Sobol, I.M., (1960). The Monte Carlo Method. Popular lectures in mathematics. U.S Department of Health Education and Welfare National Institute of Education. The University of Chicago Press.

Spathis, A.T., 2010, A brief review of measurement, modeling and management of vibrations produced by blasting. Vibrations from blasting: Proceedings and Monographs in Engineering, Water and Earth Sciences, Taylor & Francis Group.

Stachura, V. J., D. E. Siskind, et al. (1981). Airblast instrumentation and measurement techniques for surface mine blasting. [Washington, D.C.], U.S. Dept. of the Interior, Bureau of Mines.

Villano, E.J., Charlie, W.A. (1993). Stress wave propagation in unsaturated sands-Vol II Field explosive tests. Colorado State University, Final report ESL-TR-92-73.

Wang, Z.L., and Konietzky, H. (2009) Modelling of blast-induced fractures in jointed rock masses. Engineering Fracture Mechanics 76 (2009) pp. 1945-1955.

Watson, J. T., (2002)

Willis, D.E. (1963). Comparison of seismic waves generated by different types of source. Bulletin of the Seismological Society of America. Vol.53. No.5, pp 965-978.

Willis, D.E. (1963). A note on the effect of ripple firing on the spectra of quarry shots. Bulletin of the Seismological Society of America. Vol.53. No.1, pp 79-85.

Worsey P. N., Tyler L. J. (1983). The Development Concept of The Integrated Electronic Detonator. International Society of Explosives Engineers General Proceedings,. Pp 489-496.

Yang, R., Scovira, D., 2010, A Model for Near and Far Field Blast Vibration Based on Multiple Seed Waveform and Transfer Functions. Blasting and Fragmentation Vol.4, No.2, 2010, pp91-116.

Young, R.P., and Hill, J.J. (1982). Statistical Analysis of Seismic Spectral Signatures for Rock Quality Assessment. Geoexploration, 20, pp 75-91.

Yu YaLun and He Jun. (1997) A New Method for Blasting Seismic Signals Processing. International Society of Explosives Engineers General Proceedings,. pp 349-353.

VITA

Jhon Silva-Castro was born on August 9, 1972 in Zipaquirá, Colombia, South America to Pedro Silva and Trinidad Castro. He attended the Universidad Nacional de Colombia in Bogotá, Colombia, and was awarded a Bachelor of Sciences Degree in Civil Engineering. Upon graduation, he was working for two years as field engineering in road and tunneling construction. Later he attended to the Universidad Nacional de Colombia in Bogotá, Colombia, and was awarded a Master of Scienciae in Geotechnical engineering. After five years working in mining related jobs, he moved to Lexington, Kentucky to attend the University of Kentucky to study Mining Engineering. He worked as both a research and teaching assistant to Dr. Braden Lusk. He expects to graduate in December 2012 with a Philosophy Doctorate in Mining Engineering. While in graduate school, he was awarded the Most Outstanding Graduate Student in the Mining Engineering Department in April, 2011 and had been a member of both SME and ISEE since 2008. He currently has three refereed journal publications and has several more under review. He also has numerous local and international conference papers in which he presented the findings of the papers. The three refereed journal publication citations can be found below.

- B.T. Lusk, J.M. Hoffman, J. Silva Castro, W.C. Wedding, E.G. Morris & J. Calnan "Evaluation of Emergent Electronic Detonators and Modern Non-Electric Shocktube Detonators Accuracy". 2012 Blasting and Fragmentation. Vol 6. No.1, June 2012.

- Lusk, B.T., J. Silva Castro, J. Hoffman, "Case Study of Blast Vibration Induced Sounds Recorded Inside a House Near a West Virginia Coal Mine." Transactions of Mining Engineering (Accepted for Publication, May, 2010).

- Lusk, B., J. Silva Castro, "A Public Relations Plan Based on Structure Generated Sounds and Public Input." The Journal of Explosives Engineering (Accepted for Publication).

APPENDIX A
Blasting log reports from the mine

Apogee Coal Company
Logan WV

BLASTING LOG

3739

APOGEE COAL

GENERAL INFORMATION

Blast Number S64 **Ticket Number** S64

Permittee Apogee Coal, LLC. **Date / Time** 6/22/2011 3:17 PM

Customer / Operator Apogee Coal, LLC. **Permit No.** S-5006-05

Location of Blast Ridge 1& 2 **Lat** ° ' 'N 306625 - X

Blasting Company APOGEE COAL LLC **Long** ° ' 'W 1768593 - Y

Nearest Protected Structure #5 Bill Joann Lambert **Method** Handheld GPS - NAD83

Distance and Direction 3,645 ft NW , ?° **SD to nearest protected** 111

Nearest Other Structure Consol Well 10844

Distance and Direction 8,027 ft SE , ?°

Weather Conditions Sunny 90°F, **Wind out of the** SW @ 0-5 **mph**

Type of Material Blasted Sandstone **Blast Type** BREAKDOWN

Matts or Protection Used None used **Total Tons** 0 **Total YD³** 5,940

Powder Factor: **tons/lb** 0.00 **lbs/yd³** 1.00

BLAST INFORMATION

Total Weight and Type(s) of Explosives used: **see attachment**

	ANFO	Emulsion	Packaged	11 Primers	Total Weight
	5,923.13 lbs.	0.00 lbs.	0.00 lbs.	5.50 lbs.	5,928.63 lbs.

Total Holes 11 **Angle** °

Face Height (ft) **Burden (ft)** 18 **Backfill (ft)**

Depth (ft) 45 **Spacing (ft)** 18 **Stemming (ft)** 15

Sub Drill (ft) **Diameter (in)** 7.875 **Stemming Material** Cuttings

Maximum Weight of Explosives Allowed per 8ms Period (lbs) :4392 **as determined by SD of :** 55

Maximum Weight of Explosives detonated per 8ms (lbs) :1078 **in** 2.0 **Holes**

INITIATION PRODUCT INFORMATION

Mfr	Delay Type	Qty	Mfr	Delay Type	Qty	Mfr	Delay Type	Qty
Orica	50 ft unitronics	11						
Orica	1 Roll - Lead in Line	2						

Method of Firing : Electric **Timer (ms) :** NA **Circuit Type :** Row by Row

Initiated by : Electronic **Blasting Unit :** E B M **No. of Circuits :**

COMMENTS

Signature Hole's UK

Operation	Apogee Coal, LLC.	Blast Number	S64	Date	6/22/2011
Permit Number	S-5006-05	Blast Type	BREAKDOWN	Time	3:17 PM

Hole Cross Section

Depth (ft) 45 Angle (deg)
B X S (ft) 18 X 18 Bench Ht.
Hole dia. (in) 7.875 Stem (ft) 15
PF: 1.00 lbs/YD³ Tons/Lb.

PRIMER TYPE (S)	UNIT WT.	QTY.
1/2 LB CAST BOOSTER	0.5	1.0

Holes loaded the same: 11

Timing Pattern

See Attached

Nearest Protected Structure: #5 Bill Joann Lambert

Distance and Direction: 3,645 ft NW , ? °

SEISMOGRAPH INFORMATION

Date and Time of Recording(s) 6/22/2011 3:17 PM

Seis SN	Location	Dist (ft)	Dir.	SD	T PPV	T Hz	V PPV	V Hz	L PPV	L Hz	Air dB	Air Hz

Reading(s) taken by : SAULS **Analyzed by :** SAULS

BLASTER INFORMATION

Name of Surface Blaster and Certification Number: **Crew:**

Brad Gregory - 3-299-88 Brad Gregory

Apogee Coal, LLC. | Blast Type BREAKDOWN | Date 6/22/2011

S-5006-05 | Blast / Ticket Number S64 / S64 | Time 3:17 PM

Hole Number	Bench Height	Sub Drill	Design Depth	Loaded Depth	Mfr.	Explosive Name	g/cc	Pounds	Mfr.	Primer Name	Qty
1-11			45	45	1 NEBCO	Bulk ANFO	0.85	538.47	1 Orica	1/2 LB Cast	1
Burden (FT)	Spacing (FT)		Stemming (FT)	Angle (Deg)	2				2		
18	18		15		3					Total Primer QTY / Hole	1
					4					Total Primer LBS / Hole	.5
					5						
					6						
					7						
					8						
						TotalExpl lbs. / hole		538.47		Expl-Primer LBS / Hole	538.97
Similar Holes -	11		11 Primers		5.50 LBS	Total Expl lbs. / Blast		5923.13		Similar Hole LBS	5929.00

Total Holes Loaded this blast

11

Grand Total Explosives Weight

5928.63

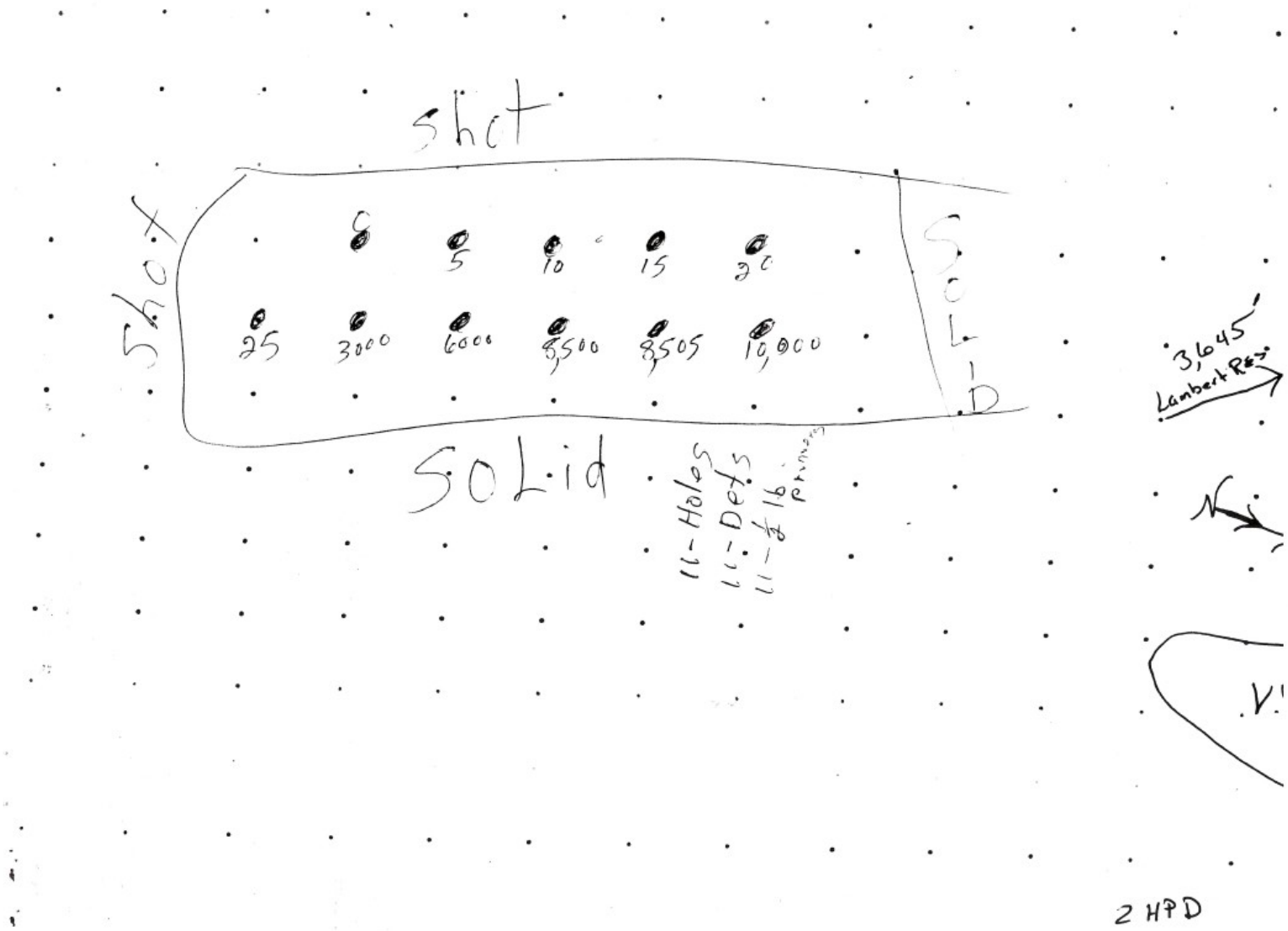
shot
shot
SOLID
SOLid
0
5
10
15
20
25
3000
6000
8,500
8,505
10,000
11-Holes
11-Dets
11-½ lb
3,645'
Lambert Rd
N
V!
2 HPD

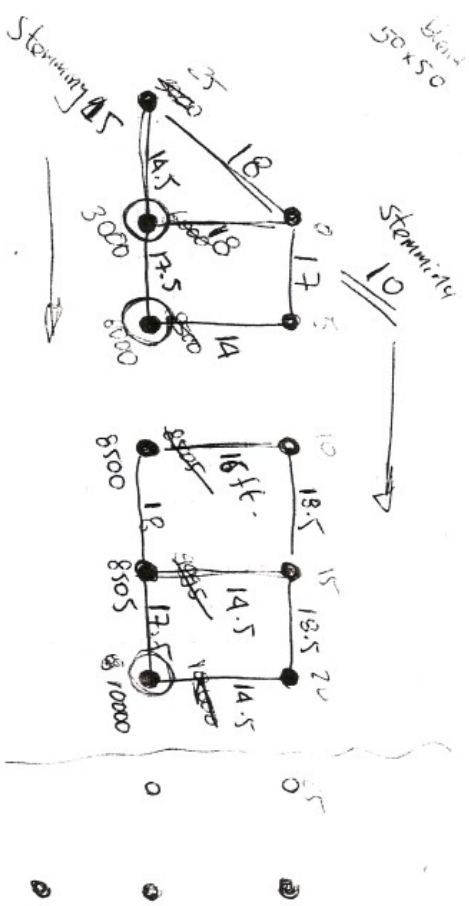

8 – 489 → 3

– 503 → 4

– 506 → Isolate Line
3 holes

8 – 550 → 10~11 holes

– 537

537
478
– 59

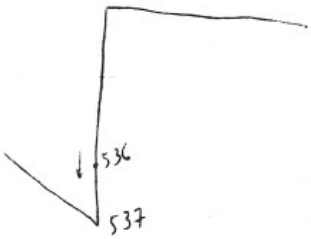

Apogee Coal Company
Logan WV

BLASTING LOG

GENERAL INFORMATION

Blast Number S69 **Ticket Number** S69

APOGEE COAL

Permittee Apogee Coal, LLC. **Date / Time** 6/23/2011 3:27 PM
Customer / Operator Apogee Coal, LLC. **Permit No.** S-5006-05
Location of Blast Ridge 1& 2 **Lat** ° ' 'N 306665 - X
Blasting Company APOGEE COAL LLC **Long** ° ' 'W 1768509 - Y
Nearest Protected Structure #5 Bill Joann Lambert **Method** Handheld GPS - NAD83
Distance and Direction 3,561 ft NW , ?° **SD to nearest protected** 86
Nearest Other Structure Consol Well 10844
Distance and Direction 8,116 ft SE , ?°
Weather Conditions Sunny 84°F, **Wind out of the** W @ 0-5 **mph**
Type of Material Blasted Sandstone **Blast Type** BREAKDOWN
Matts or Protection Used None used **Total Tons** 0 **Total YD³** 9,360
Powder Factor: **tons/lb** 0.00 **lbs/yd³** 2.36

BLAST INFORMATION

Total Weight and Type(s) of Explosives used: **see attachment**

	ANFO	Emulsion	Packaged	26 Primers	Total Weight
	13,242.47 lbs.	8,828.31 lbs.	0.00 lbs.	19.50 lbs.	22,090.28 lbs.

Total Holes 26 **Angle** °
Face Height (ft) 30 **Burden (ft)** 18 **Backfill (ft)**
Depth (ft) 30 **Spacing (ft)** 18 **Stemming (ft)** 10
Sub Drill (ft) **Diameter (in)** 7.875 **Stemming Material** Cuttings
Maximum Weight of Explosives Allowed per 8ms Period (lbs) :4193 **as determined by SD of :** 55
Maximum Weight of Explosives detonated per 8ms (lbs) :1699 **in** 2.0 **Holes**

INITIATION PRODUCT INFORMATION

Mfr	Delay Type	Qty	Mfr	Delay Type	Qty	Mfr	Delay Type	Qty
Orica	50 ft unitronics	26						
Orica	1 Roll - Lead in Line	1						

Firing : Electric **Timer (ms) :** NA **Circuit Type :** Row by Row
: Electronic **Blasting Unit :** E B M **No. of Circuits :**

COMMENTS

Shot

Operation	Apogee Coal, LLC.	Blast Number	S69	Date	6/23/2011
Permit Number	S-5006-05	Blast Type	BREAKDOWN	Time	3:27 PM

Hole Cross Section

Depth (ft) 30 Angle (deg)
B X S (ft) 18 X 18 Bench Ht. 30
Hole dia. (in) 7.875 Stem (ft) 10
PF: 2.36 lbs/YD³ Tons/Lb.

PRIMER TYPE (S)	UNIT WT.	QTY.
3/4 LB CAST PRIMER	0.8	1.0

Holes loaded the same: 26

Timing Pattern

See Attached

Nearest Protected Structure: #5 Bill Joann Lambert

Distance and Direction: 3,561 **ft** NW , ? °

SEISMOGRAPH INFORMATION

Date and Time of Recording(s) 6/23/2011 3:27 PM

Seis SN	Location	Dist (ft)	Dir.	SD	T PPV	T Hz	V PPV	V Hz	L PPV	L Hz	Air dB	Air Hz

Reading(s) taken by : SAULS **Analyzed by :** SAULS

BLASTER INFORMATION

Name of Surface Blaster and Certification Number: **Crew:**

Brad Gregory - 3-299-88 Brad Gregory

Apogee Coal, LLC. | Blast Type BREAKDOWN | Date 6/23/2011

S-5006-05 | Blast / Ticket Number S69 / S69 | Time 3:27 PM

Hole Number	Bench Height	Sub Drill	Design Depth	Loaded Depth	Mfr.	Explosive Name	g/cc	Pounds	Mfr.	Primer Name	Qty
1-26	30		30	30	1 Nelson	60/40	1.34	848.88	1	3/4 LB Cast	1
Burden (FT)	Spacing (FT)		Stemming (FT)	Angle (Deg)	2				2		
18	18		10		3					Total Primer QTY / Hole	1
					4					Total Primer LBS / Hole	.75
					5						
					6						
					7						
					8						
						TotalExpl lbs. / hole		848.88		Expl-Primer LBS / Hole	849.63
Similar Holes -	26		26 Primers		19.50 LBS	Total Expl lbs. / Blast		22070.78		Similar Hole LBS	22091.00

Total Holes Loaded this blast

26

Grand Total Explosives Weight

22090.28

Nelson Brothe

UNI Tronics

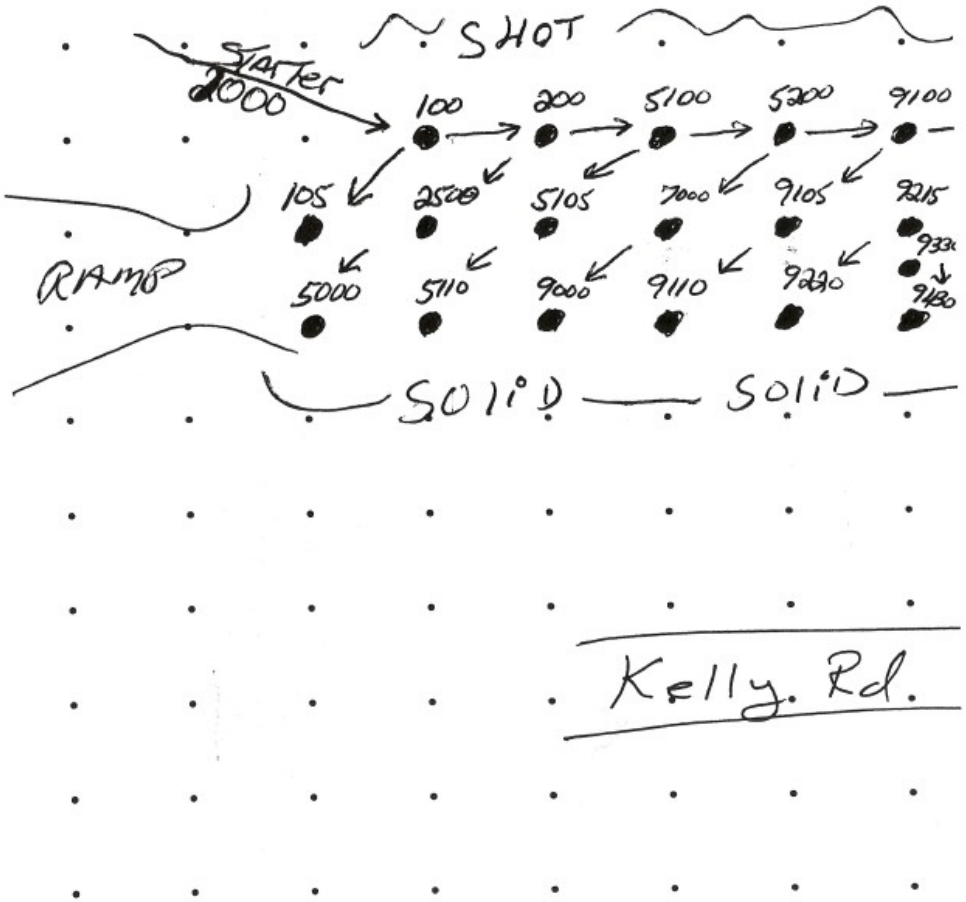

Booster
Spartan
350
Crack
Dip
Depth
Deep

Apogee Coal Company
Logan WV

BLASTING LOG

GENERAL INFORMATION

Blast Number S71 **Ticket Number** S71

APOGEE COAL

Permittee Apogee Coal, LLC. **Date / Time** 6/24/2011 3:20 PM
Customer / Operator Apogee Coal, LLC. **Permit No.** S-5006-05
Location of Blast Ridge 1& 2 **Lat** ° ' ' N 306889 - X
Blasting Company APOGEE COAL LLC **Long** ° ' ' W 1768347 - Y
Nearest Protected Structure #5 Bill Joann Lambert **Method** Handheld GPS - NAD83
Distance and Direction 3,285 ft NW , ?° **SD to nearest protected** 114
Nearest Other Structure Consol Well 10844
Distance and Direction 8,386 ft SE , ?°
Weather Conditions Sunny 85°F, **Wind** ~~out of the~~ E @ 0-5 **mph**
Type of Material Blasted Sandstone **Blast Type** Production
Matts or Protection Used None used **Total Tons** 0 **Total YD³** 15,660
Powder Factor: **tons/lb** 0.00 **lbs/yd³** 1.55

BLAST INFORMATION

Total Weight and Type(s) of Explosives used: **see attachment**

	ANFO	Emulsion	Packaged	29 Primers	Total Weight
	19,399.99 lbs.	4,850.00 lbs.	0.00 lbs.	21.75 lbs.	24,271.73 lbs.

Total Holes 29 **Angle** 0 °
Face Height (ft) 45 **Burden (ft)** 18 **Backfill (ft)**
Depth (ft) 45 **Spacing (ft)** 18 **Stemming (ft)** 9
Sub Drill (ft) **Diameter (in)** 7.875 **Stemming Material** Cuttings
Maximum Weight of Explosives Allowed per 8ms Period (lbs) : 3568 **as determined by SD of :** 55
Maximum Weight of Explosives detonated per 8ms (lbs) : 837 **in** 1.0 **Holes**

INITIATION PRODUCT INFORMATION

Mfr	Delay Type	Qty	Mfr	Delay Type	Qty	Mfr	Delay Type	Qty
Orica	50 ft unitronics	29						

Method of Firing : Digital **Timer (ms) :** NA **Circuit Type :** Row by Row
Initiated by : Electronic **Blasting Unit :** E B M **No. of Circuits :** 1

COMMENTS

Signature shot for UK

Operation	Apogee Coal, LLC.	Blast Number	S71	Date	6/24/2011
Permit Number	S-5006-05	Blast Type	Production	Time	3:20 PM

Hole Cross Section

Depth (ft) 45 Angle (deg) 0
B X S (ft) 18 X 18 Bench Ht. 45
Hole dia. (in) 7.875 Stem (ft) 9
PF: 1.55 **lbs/YD³** **Tons/Lb.**

PRIMER TYPE (S)	UNIT WT.	QTY.
3/4 LB CAST PRIMER	0.8	1.0

Holes loaded the same: 29

Timing Pattern

See Attachment

Nearest Protected Structure: #5 Bill Joann Lambert

Distance and Direction: 3,285 **ft** NW , ? °

SEISMOGRAPH INFORMATION

Date and Time of Recording(s) 6/24/2011 3:20 PM

Seis SN	Location	Dist (ft)	Dir.	SD	T PPV	T Hz	V PPV	V Hz	L PPV	L Hz	Air dB	Air Hz

Reading(s) taken by : SAULS **Analyzed by :** SAULS

BLASTER INFORMATION

Name of Surface Blaster and Certification Number:
Richard Cope - 5 506 08

Crew:

Apogee Coal, LLC.

S-5006-05

Blast Type Production

Blast / Ticket Number S71 / S71

Date 6/24/2011

Time 3:20 PM

Hole Number	Bench Height	Sub Drill	Design Depth	Loaded Depth
1-29	45		45	45
Burden (FT)	**Spacing (FT)**	**Stemming (FT)**		**Angle (Deg)**
18	18	9		0

	Mfr.	Explosive Name	g/cc	Pounds
1	Nelson	80/20	1.10	836.21
2				
3				
4				
5				
6				
7				
8				

	Mfr.	Primer Name	Qty
1		3/4 LB Cast	1
2			

Total Primer QTY / Hole 1

Total Primer LBS / Hole .75

TotalExpl lbs. / hole 836.21

Expl-Primer LBS / Hole 836.96

Similar Holes - 29 29 **Primers** 21.75 **LBS**

Total Expl lbs. / Blast 24249.98

Similar Hole LBS **24272.00**

Total Holes Loaded this blast

29

Grand Total Explosives Weight

24271.73

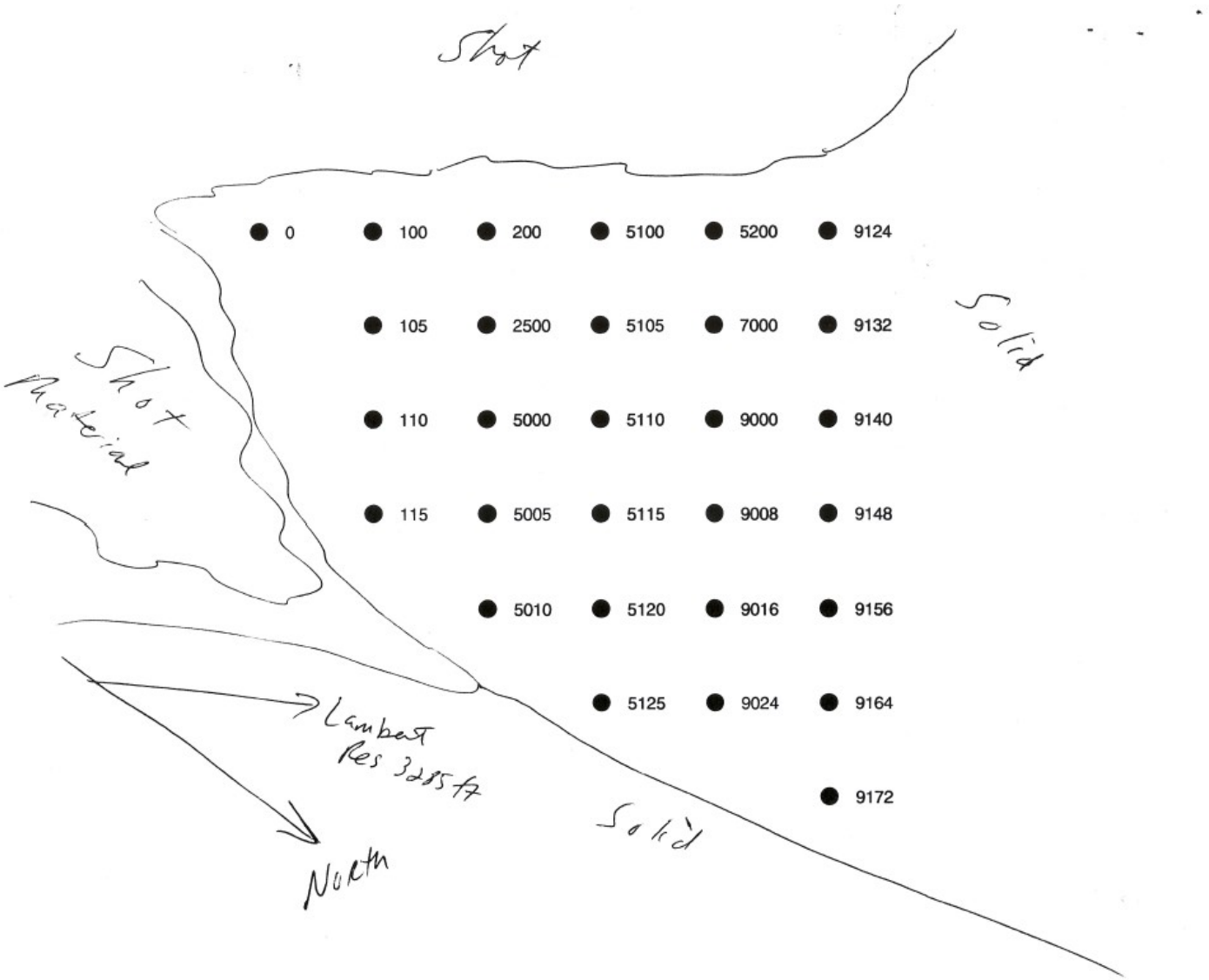
Shot
Solid
Shot material
Solid
Lambert
Res 3285 ft
North
0
100
200
5100
5200
9124
105
2500
5105
7000
9132
110
5000
5110
9000
9140
115
5005
5115
9008
9148
5010
5120
9016
9156
5125
9024
9164
9172

10/24/01
40%
N

Sig
40 ft
Top
Brinh
3ms
Brinh
3ms

Apogee Coal Company
Logan WV

BLASTING LOG

GENERAL INFORMATION

APOGEE COAL

Blast Number S81 **Ticket Number** S81

Permittee Apogee Coal, LLC.
Customer / Operator Apogee Coal, LLC.
Location of Blast Ridge 1& 2
Blasting Company APOGEE COAL LLC
Nearest Protected Structure #5 Bill Joann Lambert
Distance and Direction 3,311 ft NW , ?°
Nearest Other Structure Consol Well 10844
Distance and Direction 8,403 ft SE , ?°
Weather Conditions Sunny 90°F,
Type of Material Blasted Sandstone
Matts or Protection Used

Date / Time 6/29/2011 11:16 AM
Permit No. S-5006-05
Lat ° ' ' N 306749 - X
Long ° ' ' W 1768201 - Y
Method Handheld GPS - NAD83
SD to nearest protected 116
Wind out of the W @ 0-2 mph
Blast Type BREAKDOWN
Total Tons 0 **Total YD³** 17,280
Powder Factor: **tons/lb** 0.00 **lbs/yd³** 1.51

BLAST INFORMATION

Total Weight and Type(s) of Explosives used: see attachment

	ANFO	Emulsion	Packaged	32 Primers	Total Weight
	20,812.25 lbs.	5,203.06 lbs.	0.00 lbs.	24.00 lbs.	26,039.31 lbs.

Total Holes 32 **Angle** °
Face Height (ft) 95 **Burden (ft)** 18 **Backfill (ft)**
Depth (ft) 45 **Spacing (ft)** 18 **Stemming (ft)** 10
Sub Drill (ft) **Diameter (in)** 7.875 **Stemming Material** Cuttings
Maximum Weight of Explosives Allowed per 8ms Period (lbs) :3625 **as determined by SD of :** 55
Maximum Weight of Explosives detonated per 8ms (lbs) : 814 **in** 1.0 **Holes**

INITIATION PRODUCT INFORMATION

Mfr	Delay Type	Qty	Mfr	Delay Type	Qty	Mfr	Delay Type	Qty
Orica	50 ft unitronics	32						

Method of Firing : Electric **Timer (ms) :** NA **Circuit Type :**
Initiated by : Electronic **Blasting Unit :** E B M **No. of Circuits :**

COMMENTS

~~Signature~~ UK Shot Signture Hole

Operation	Apogee Coal, LLC.	**Blast Number**	S81	**Date**	6/29/2011
Permit Number	S-5006-05	**Blast Type**	BREAKDOWN	**Time**	11:16 AM

Hole Cross Section

Depth (ft) 45 Angle (deg)
B X S (ft) 18 X 18 Bench Ht. 95
Hole dia. (in) 7.875 Stem (ft) 10
PF: 1.51 **lbs/YD³** **Tons/Lb.**

PRIMER TYPE (S)	UNIT WT.	QTY.
3/4 LB CAST PRIMER	0.8	1.0

Holes loaded the same: 32

Timing Pattern

See Attached

Nearest Protected Structure: #5 Bill Joann Lambert

Distance and Direction: 3,311 **ft** NW , ? °

SEISMOGRAPH INFORMATION

Date and Time of Recording(s) 6/29/2011 11:16 AM

Seis SN	Location	Dist (ft)	Dir.	SD	T PPV	T Hz	V PPV	V Hz	L PPV	L Hz	Air dB	Air Hz

Reading(s) taken by : SAULS **Analyzed by :** SAULS

BLASTER INFORMATION

Name of Surface Blaster and Certification Number: **Crew:**

Todd Keffer - 5-645-05

Todd Keffer

Apogee Coal, LLC.

S-5006-05

Blast Type BREAKDOWN

Blast / Ticket Number S81 / S81

Date 6/29/2011

Time 11:16 AM

Hole Number	Bench Height	Sub Drill	Design Depth	Loaded Depth
1-32	95		45	45

Burden (FT)	Spacing (FT)	Stemming (FT)	Angle (Deg)
18	18	10	

	Mfr.	Explosive Name	g/cc	Pounds
1	Nelson	80/20	1.10	812.98
2				
3				
4				
5				
6				
7				
8				

	Mfr.	Primer Name	Qty
1		3/4 LB Cast	1
2			

Total Primer QTY / Hole 1

Total Primer LBS / Hole .75

TotalExpl lbs. / hole 812.98

Expl-Primer LBS / Hole 813.73

Similar Holes - 32 **32 Primers** 24.00 **LBS**

Total Expl lbs. / Blast 26015.31

Similar Hole LBS **26040.00**

Total Holes Loaded this blast

32

Grand Total Explosives Weight

26039.31

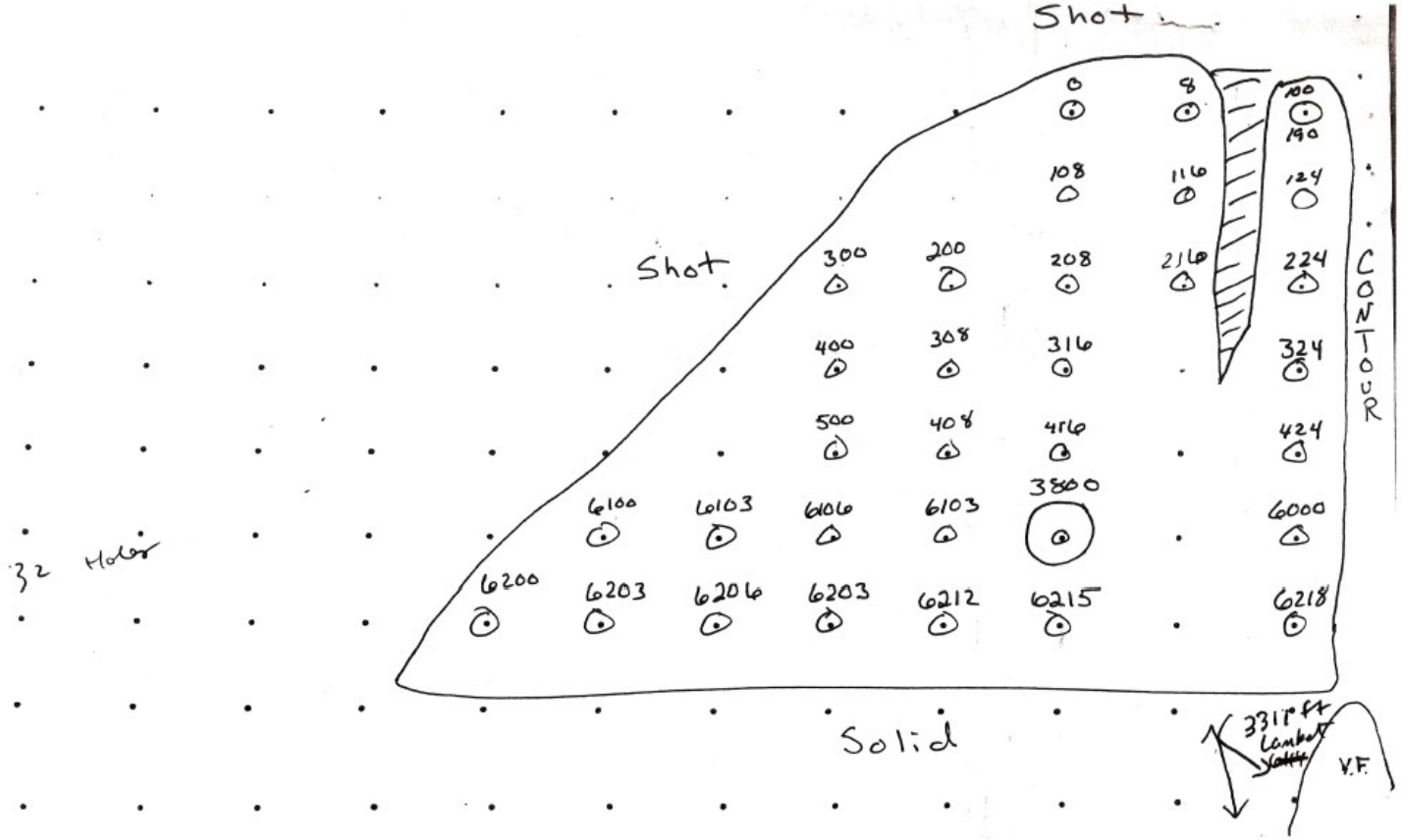
Shot
Shot
Solid
CONTOUR
V.F.
32 Holes
0
8
100
190
108
116
124
300
200
208
216
224
400
308
316
324
500
408
416
424
3800
6100
6103
6106
6103
6000
6200
6203
6206
6203
6212
6215
6218

Apogee Coal Company
Logan WV

BLASTING LOG

GENERAL INFORMATION

Blast Number S82 **Ticket Number** S82

APOGEE COAL

Permittee Apogee Coal, LLC. **Date / Time** 6/29/2011 3:33 PM

Customer / Operator Apogee Coal, LLC. **Permit No.** S-5006-05

Location of Blast Ridge 1& 2 **Lat** ° ' 'N 306912 - X

Blasting Company APOGEE COAL LLC **Long** ° ' 'W 1768217 - Y

Nearest Protected Structure #5 Bill Joann Lambert **Method** Handheld GPS - NAD83

Distance and Direction 3,188 **ft** NW , ?° **SD to nearest protected** 77

Nearest Other Structure Consol Well 10844

Distance and Direction 8,499 **ft** SE , ?°

Weather Conditions Sunny 90°F, **Wind out of the** SE @ 0-5 **mph**

Type of Material Blasted Sandstone **Blast Type** BREAKDOWN

Matts or Protection Used None used **Total Tons** 0 **Total YD³** 18,900

Powder Factor: **tons/lb** 0.00 **lbs/yd³** 1.59

BLAST INFORMATION

Total Weight and Type(s) of Explosives used: **see attachment**

	ANFO	Emulsion	Packaged	35 Primers	Total Weight
	24,064.16 lbs.	6,016.04 lbs.	0.00 lbs.	26.25 lbs.	30,106.45 lbs.

Total Holes 35 **Angle** 0 °

Face Height (ft) 45 **Burden (ft)** 18 **Backfill (ft)**

Depth (ft) 45 **Spacing (ft)** 18 **Stemming (ft)** 8

Sub Drill (ft) **Diameter (in)** 7.875 **Stemming Material** Cuttings

Maximum Weight of Explosives Allowed per 8ms Period (lbs) :3360 **as determined by SD of :** 55

Maximum Weight of Explosives detonated per 8ms (lbs) :1720 **in** 2.0 **Holes**

INITIATION PRODUCT INFORMATION

Mfr	Delay Type	Qty	Mfr	Delay Type	Qty	Mfr	Delay Type	Qty
Orica	1 Roll - Lead in Line	1						
Orica	EXCEL 80 FT - 20	35						
Orica	S. EXCEL 40 FT- 42	5						
Orica	S. EXCEL 40 FT-100	30						

Method of Firing : Non Electric **Timer (ms) :** NA **Circuit Type :** Row by Row

Initiated by : Non-Electric **Blasting Unit :** Handi Blaster **No. of Circuits :** 0

COMMENTS

Signature

Operation	Apogee Coal, LLC.	Blast Number	S82	Date	6/29/2011
Permit Number	S-5006-05	Blast Type	BREAKDOWN	Time	3:33 PM

Hole Cross Section

Depth (ft) 45 Angle (deg) 0
B X S (ft) 18 X 18 Bench Ht. 45
Hole dia. (in) 7.875 Stem (ft) 8
PF: 1.59 lbs/YD³ Tons/Lb.

PRIMER TYPE (S)	UNIT WT.	QTY.
3/4 LB CAST PRIMER	0.8	1.0

Holes loaded the same: 35

Timing Pattern

See Attached

Nearest Protected Structure: #5 Bill Joann Lambert

Distance and Direction: 3,188 ft NW , ? °

SEISMOGRAPH INFORMATION

Date and Time of Recording(s) 6/29/2011 3:33 PM

Seis SN	Location	Dist (ft)	Dir.	SD	T PPV	T Hz	V PPV	V Hz	L PPV	L Hz	Air dB	Air Hz

Reading(s) taken by : SAULS **Analyzed by :** SAULS

BLASTER INFORMATION

Name of Surface Blaster and Certification Number: **Crew:**

Todd Keffer - 5-645-05

Todd Keffer

Apogee Coal, LLC. | Blast Type BREAKDOWN | Date 6/29/2011

S-5006-05 | Blast / Ticket Number S82 / S82 | Time 3:33 PM

Hole Number	Bench Height	Sub Drill	Design Depth	Loaded Depth
1-35	45		45	45
Burden (FT)	**Spacing (FT)**		**Stemming (FT)**	**Angle (Deg)**
18	18		8	0

	Mfr.	Explosive Name	g/cc	Pounds
1	Nelson	80/20	1.10	859.43
2				
3				
4				
5				
6				
7				
8				

	Mfr.	Primer Name	Qty
1		3/4 LB Cast	1
2			
		Total Primer QTY / Hole	1
		Total Primer LBS / Hole	.75

TotalExpl lbs. / hole 859.43 | **Expl-Primer LBS / Hole** 860.18

Similar Holes - 35 | 35 **Primers** 26.25 **LBS** | **Total Expl lbs. / Blast** 30080.20 | **Similar Hole LBS** **30107.00**

Total Holes Loaded this blast

35

Grand Total Explosives Weight

30106.45

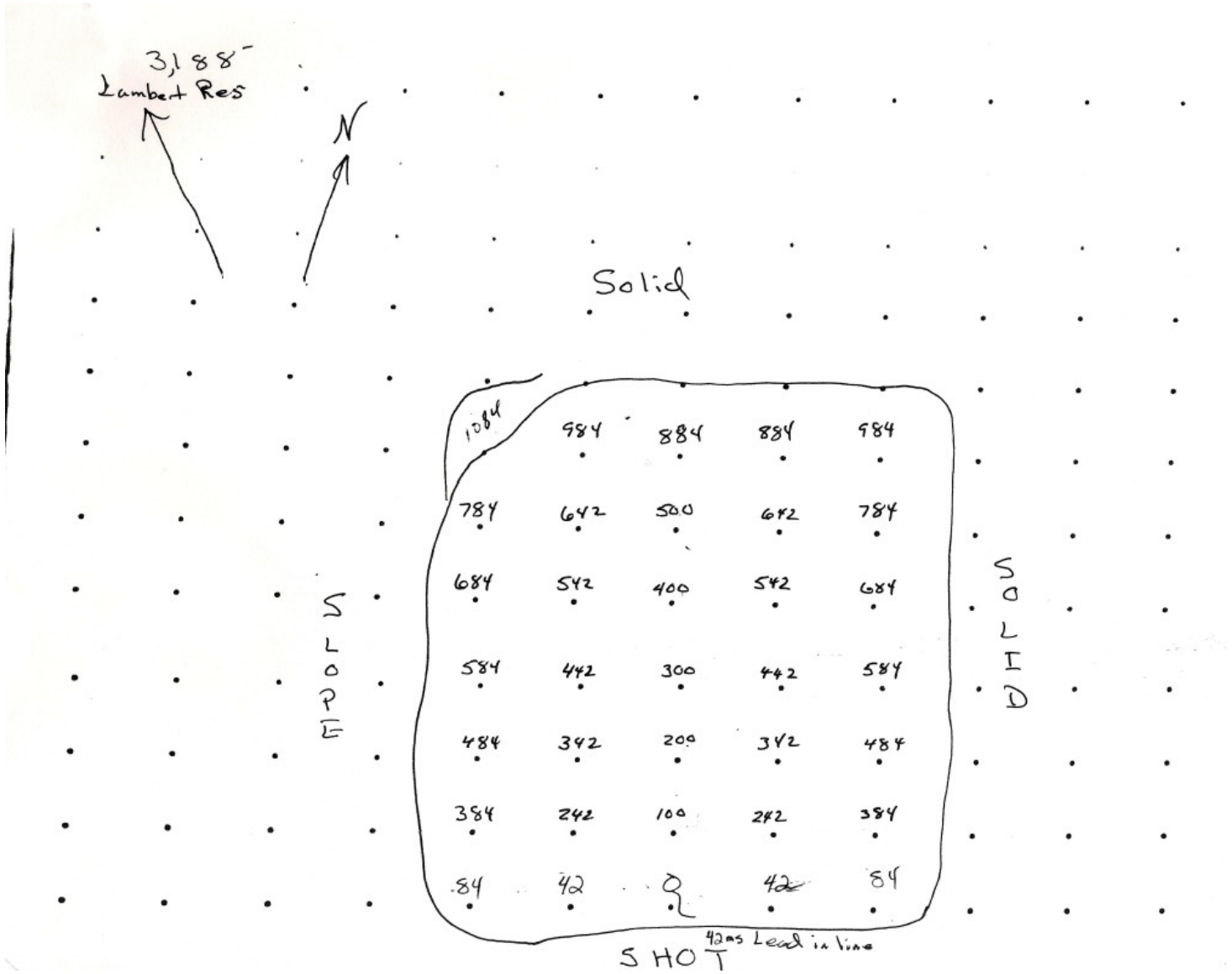
3,188'
Lambert Res
N
Solid
1084
984
884
884
984
784
642
500
642
784
684
542
400
542
684
584
442
300
442
584
484
342
200
342
484
384
242
100
242
384
84
42
0
42
84
SLOPE
SOLID
SHOT
42ms Lead in line

Apogee Coal Company
Logan WV

BLASTING LOG

GENERAL INFORMATION

Blast Number S85 **Ticket Number** S85

APOGEE COAL

Permittee Apogee Coal, LLC. **Date / Time** 6/29/2011 6:45 PM
Customer / Operator Apogee Coal, LLC. **Permit No.** S-5006-05
Location of Blast Ridge 1& 2 **Lat** ° ' 'N 306998 - X
Blasting Company APOGEE COAL LLC **Long** ° ' 'W 1768313 - Y
Nearest Protected Structure #5 Bill Joann Lambert **Method** Handheld GPS - NAD83
Distance and Direction 3,179 **ft** NW , ?° **SD to nearest protected** 78
Nearest Other Structure Consol Well 10844
Distance and Direction 8,485 **ft** SE , ?°
Weather Conditions Sunny 92 °F, **Wind out of the** SE @ 0-5 **mph**
Type of Material Blasted Sandstone **Blast Type** BREAKDOWN
Matts or Protection Used None used **Total Tons** 0 **Total YD³** 21,600
Powder Factor: **tons/lb** 0.00 **lbs/yd³** 1.55

BLAST INFORMATION

Total Weight and Type(s) of Explosives used: **see attachment**

	ANFO	Emulsion	Packaged	40 Primers	Total Weight
	26,758.60 lbs.	6,689.65 lbs.	0.00 lbs.	30.00 lbs.	33,478.25 lbs.

Total Holes 40 **Angle** 0 °
Face Height (ft) 45 **Burden (ft)** 18 **Backfill (ft)**
Depth (ft) 45 **Spacing (ft)** 18 **Stemming (ft)** 9
Sub Drill (ft) **Diameter (in)** 7.875 **Stemming Material** Cuttings
Maximum Weight of Explosives Allowed per 8ms Period (lbs) : 3340 **as determined by SD of :** 55
Maximum Weight of Explosives detonated per 8ms (lbs) : 1674 **in** 2.0 **Holes**

INITIATION PRODUCT INFORMATION

Mfr	Delay Type	Qty	Mfr	Delay Type	Qty	Mfr	Delay Type	Qty
Orica	50 ft unitronics	40						

Method of Firing : Digital **Timer (ms) :** NA **Circuit Type :** Row by Row
Initiated by : Electronic **Blasting Unit :** E B M **No. of Circuits :** 1

COMMENTS

VK Shot

Operation	Apogee Coal, LLC.	**Blast Number**	S85	**Date**	6/29/2011
Permit Number	S-5006-05	**Blast Type**	BREAKDOWN	**Time**	6:45 PM

Hole Cross Section

Depth (ft) 45 Angle (deg) 0
B X S (ft) 18 X 18 Bench Ht. 45
Hole dia. (in) 7.875 Stem (ft) 9
PF: 1.55 lbs/YD³ **Tons/Lb.**

PRIMER TYPE (S)	UNIT WT.	QTY.
3/4 LB CAST PRIMER	0.8	1.0

Holes loaded the same: 40

Timing Pattern

See Attached

Nearest Protected Structure: #5 Bill Joann Lambert

Distance and Direction: 3,179 ft NW , ? °

SEISMOGRAPH INFORMATION

Date and Time of Recording(s) 6/29/2011 6:45 PM

Seis SN	Location	Dist (ft)	Dir.	SD	T PPV	T Hz	V PPV	V Hz	L PPV	L Hz	Air dB	Air Hz

Reading(s) taken by : SAULS **Analyzed by :** SAULS

BLASTER INFORMATION

Name of Surface Blaster and Certification Number: **Crew:**

Todd Keffer - 5-645-05

Todd Keffer

Apogee Coal, LLC. | Blast Type BREAKDOWN | Date 6/29/2011

S-5006-05 | Blast / Ticket Number S85 / S85 | Time 6:45 PM

Hole Number	Bench Height	Sub Drill	Design Depth	Loaded Depth	Mfr.	Explosive Name	g/cc	Pounds	Mfr.	Primer Name	Qty
1-40	45		45	45	1 Nelson	80/20	1.10	836.21	1	3/4 LB Cast	1
Burden (FT)	Spacing (FT)		Stemming (FT)	Angle (Deg)	2				2		
18	18		9	0	3					Total Primer QTY / Hole	1
					4					Total Primer LBS / Hole	.75
					5						
					6						
					7						
					8						
						TotalExpl lbs. / hole		836.21		Expl-Primer LBS / Hole	836.96
Similar Holes -	40		40 Primers		30.00 LBS	Total Expl lbs. / Blast		33448.25		Similar Hole LBS	33479.00

Total Holes Loaded this blast

40

Grand Total Explosives Weight

33478.25

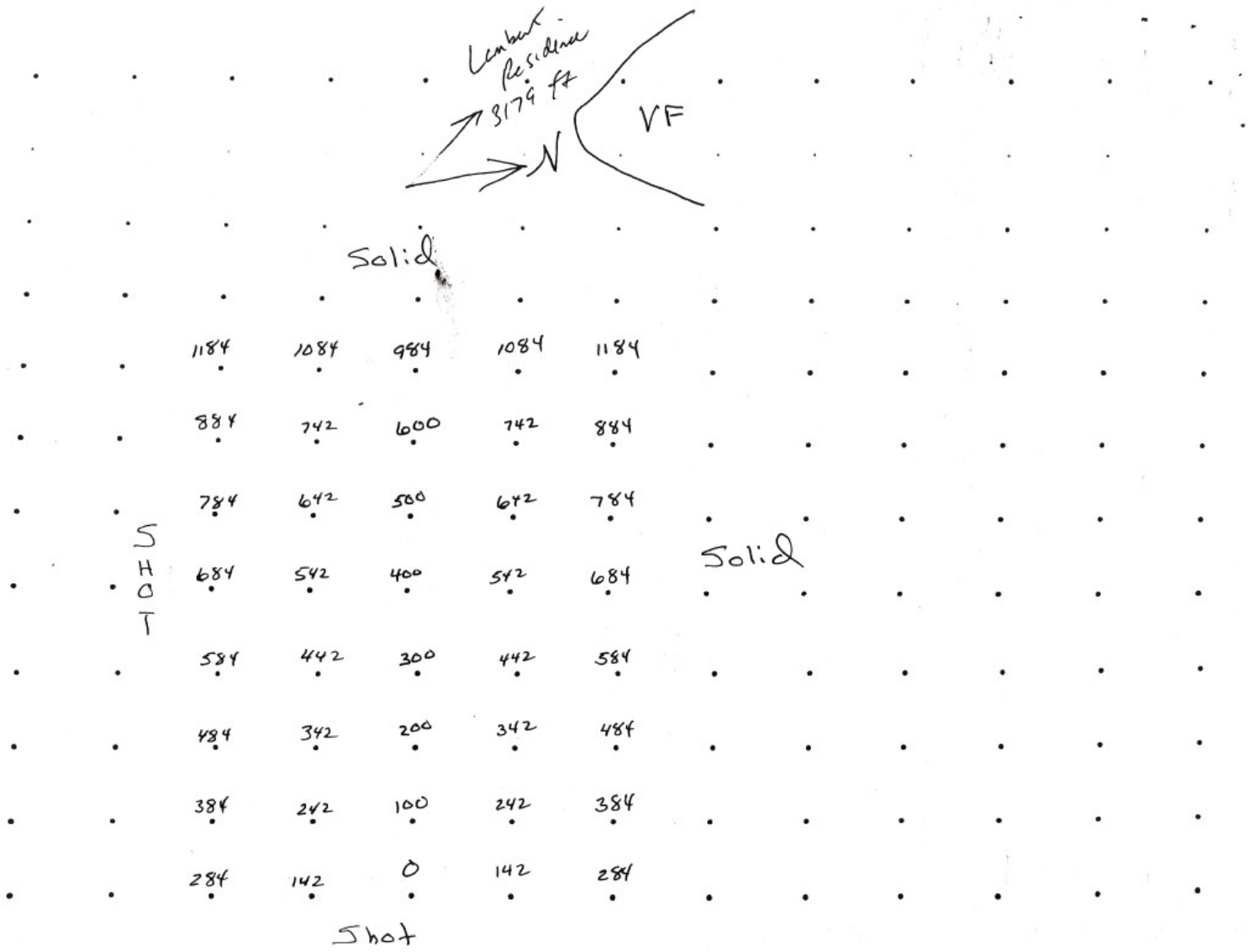
Lambert Residline
3179 ft
N
VF
Solid
1184 1084 984 1084 1184
884 742 600 742 884
784 642 500 642 784
684 542 400 542 684
584 442 300 442 584
484 342 200 342 484
384 242 100 242 384
284 142 0 142 284
SHOT
Solid
Shot

APPENDIX B
Plan Layout of tests performed in 2011

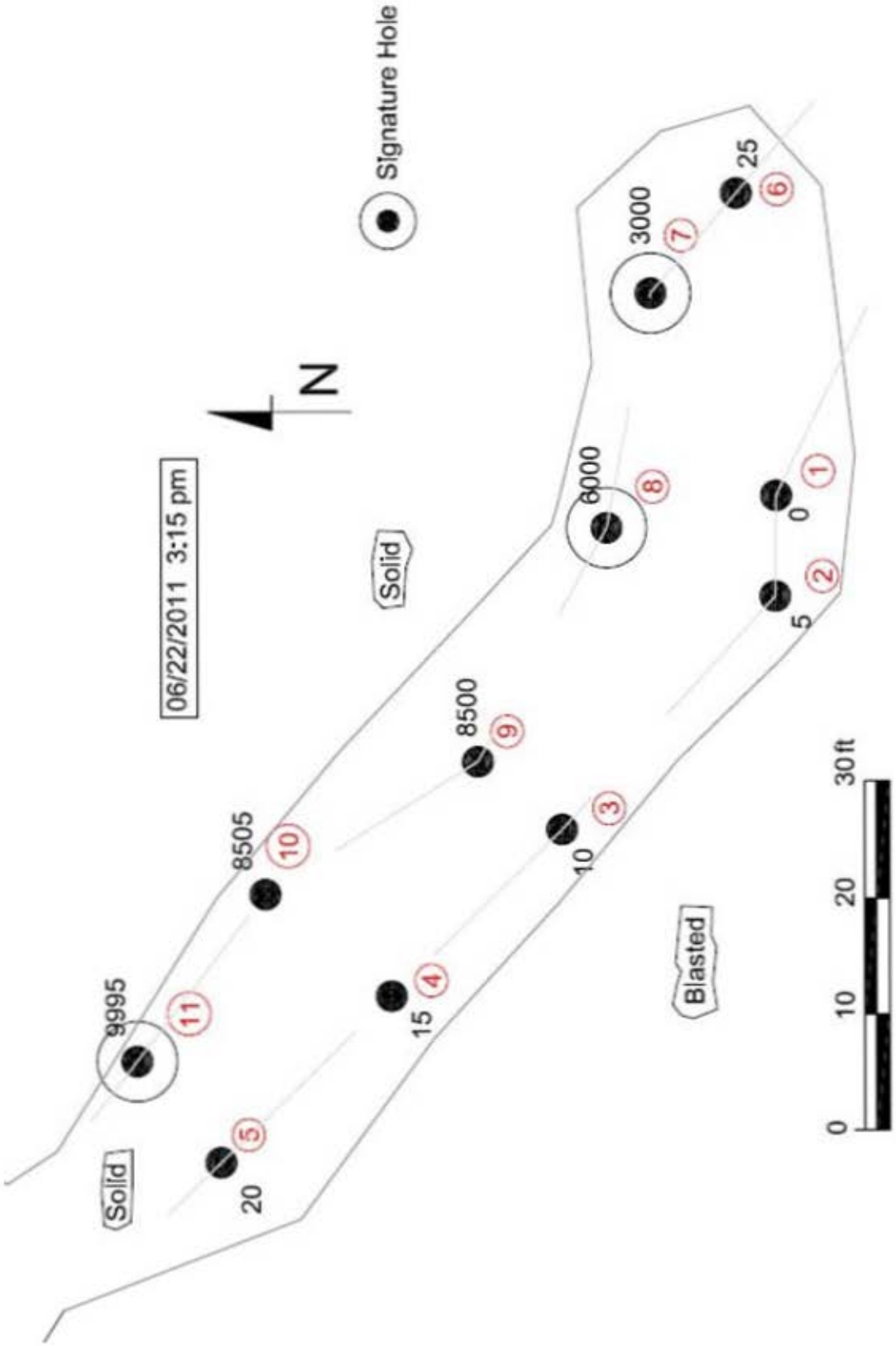
Signature Hole
N
06/22/2011 3:15 pm
Solid
Solid
Blasted
9995
8505
8500
6000
3000
25
20
15
10
5
0
1
2
3
4
5
6
7
8
9
10
11
0
10
20
30 ft

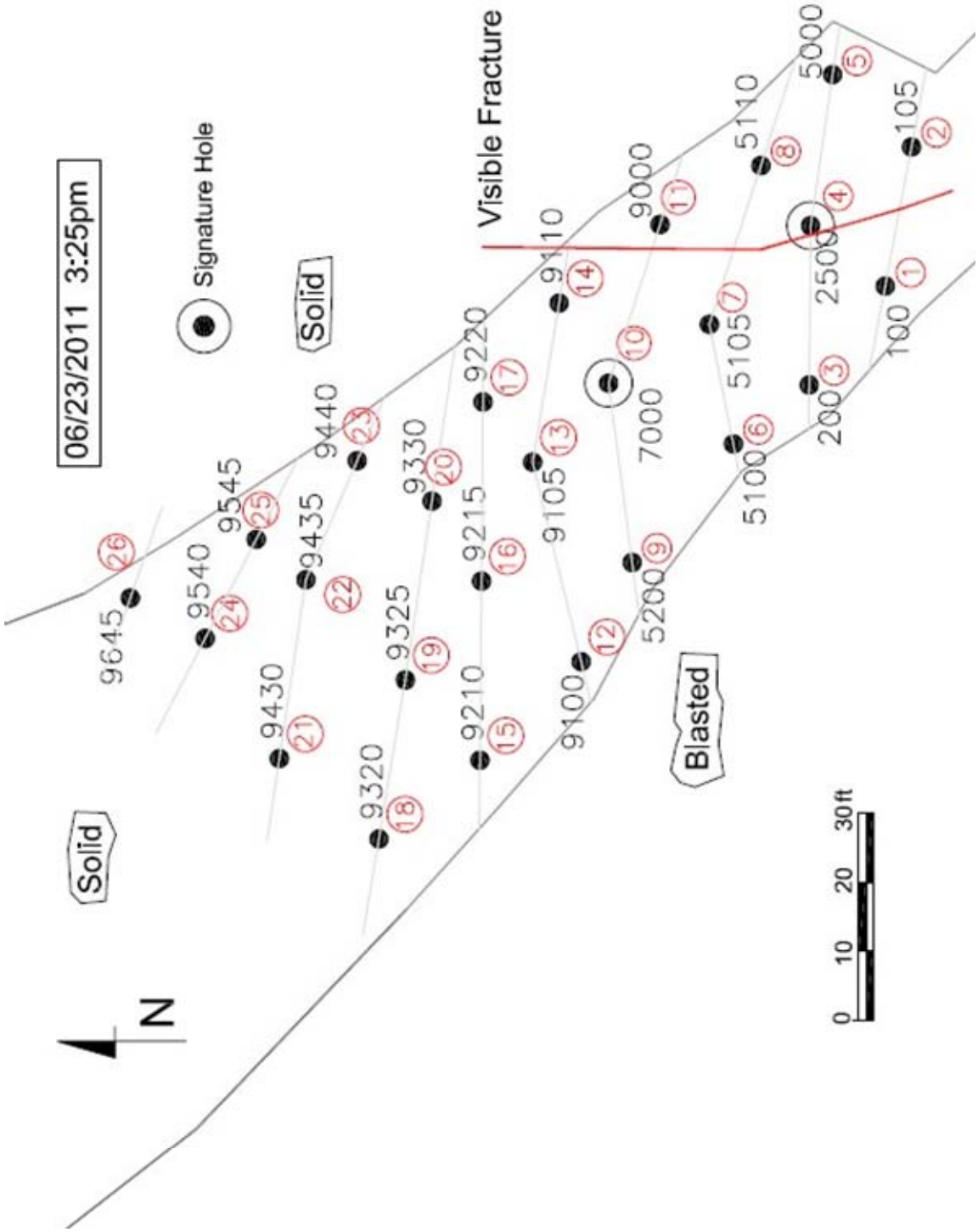
06/23/2011 3:25pm
Signature Hole
Solid
Visible Fracture
Solid
Blasted
N
0 10 20 30 ft
9645
9540
9545
9430
9435
9440
9320
9325
9330
9210
9215
9220
9100
9105
9110
5200
7000
9000
5100
5105
5110
200
2500
5000
100
105
1
2
3
4
5
6
7
8
9
10
11
12
13
14
15
16
17
18
19
20
21
22
23
24
25
26

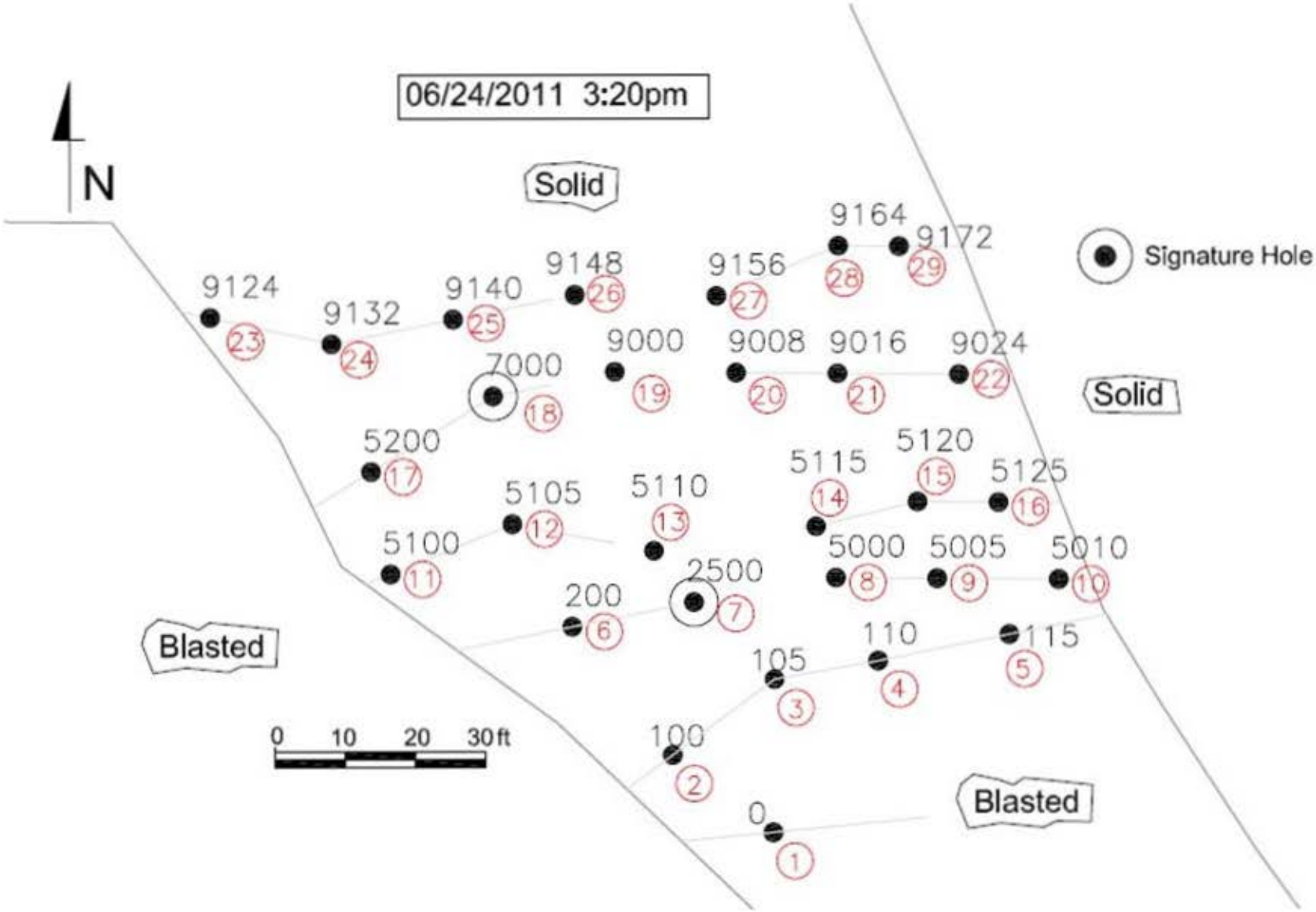
06/24/2011 3:20pm
N
Solid
Solid
Blasted
Blasted
Signature Hole
0 10 20 30 ft
9124
9132
9140
9148
9156
9164
9172
9000
9008
9016
9024
7000
5200
5105
5110
5115
5120
5125
5100
5000
5005
5010
2500
200
110
115
105
100
0
23
24
25
26
27
28
29
19
20
21
22
18
17
12
13
14
15
16
11
8
9
10
7
6
5
4
3
2
1

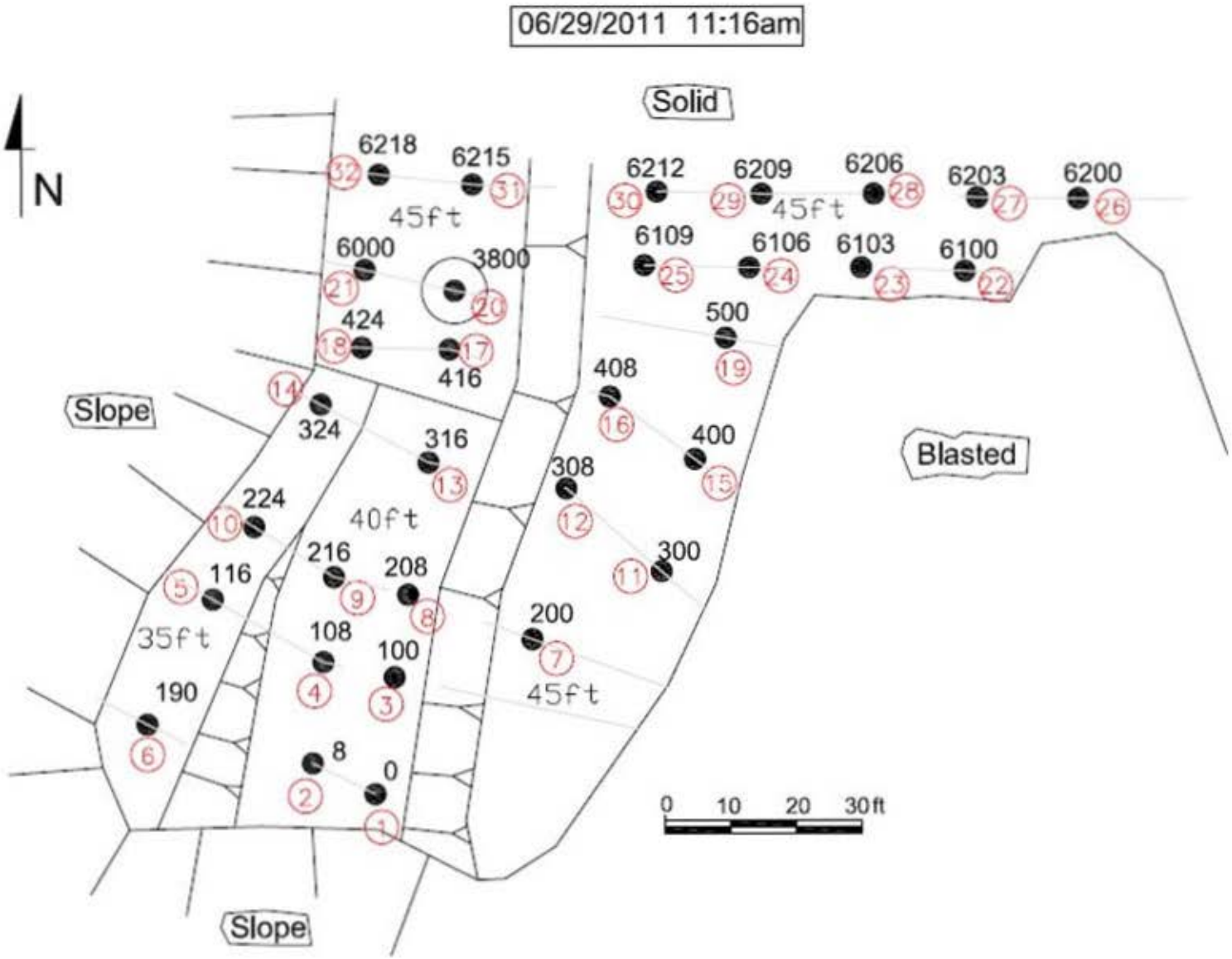
06/29/2011 11:16am
N
Solid
Slope
Blasted
Slope
6218
6215
6212
6209
6206
6203
6200
45ft
45ft
6000
3800
6109
6106
6103
6100
500
424
416
408
324
316
400
308
224
40ft
216
208
300
116
200
35ft
108
100
45ft
190
8
0
0 10 20 30ft

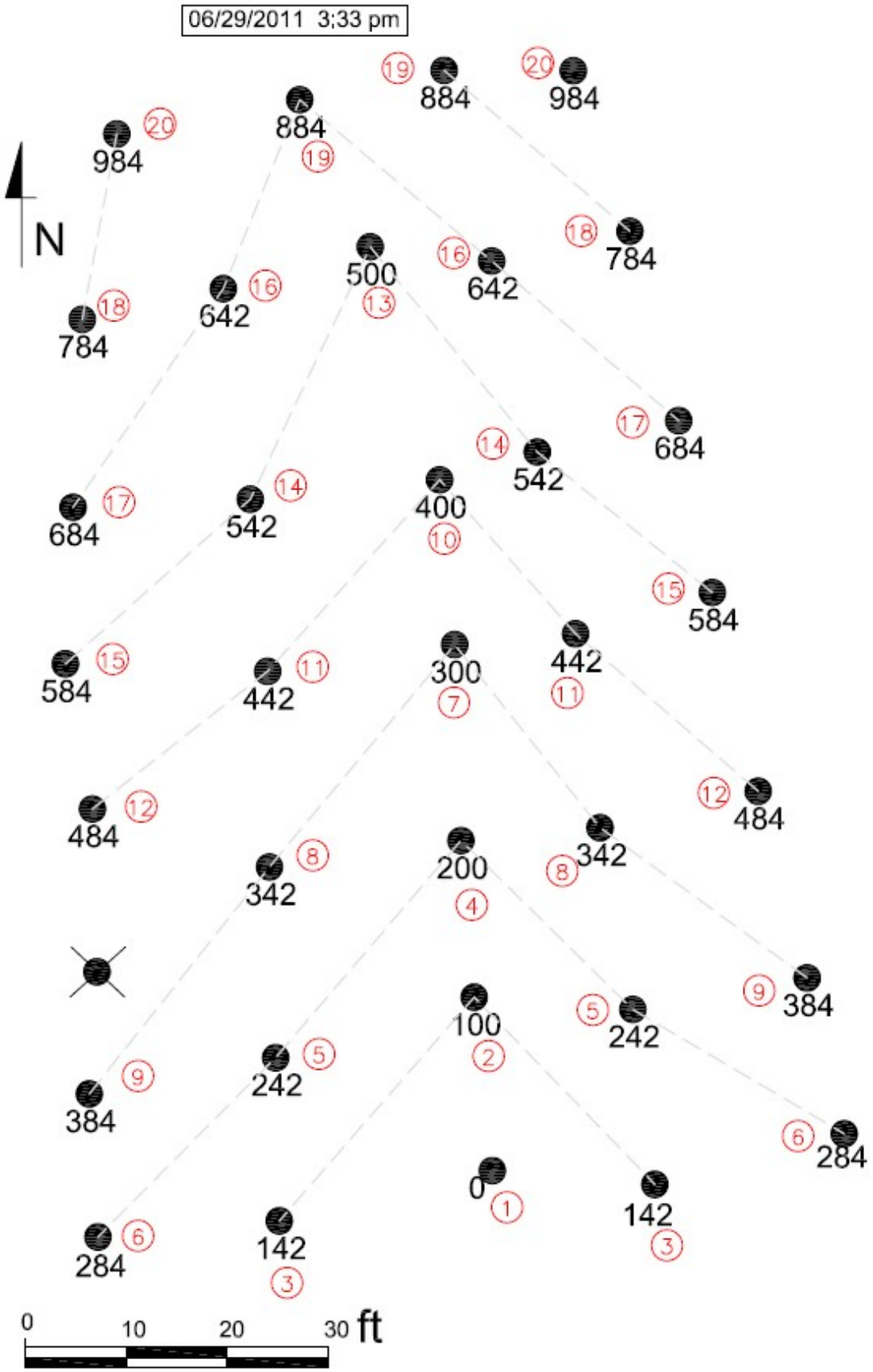
06/29/2011 3:33 pm
N
0
10
20
30
ft
0
100
200
300
400
500
142
242
342
442
542
642
784
884
984
284
384
484
584
684

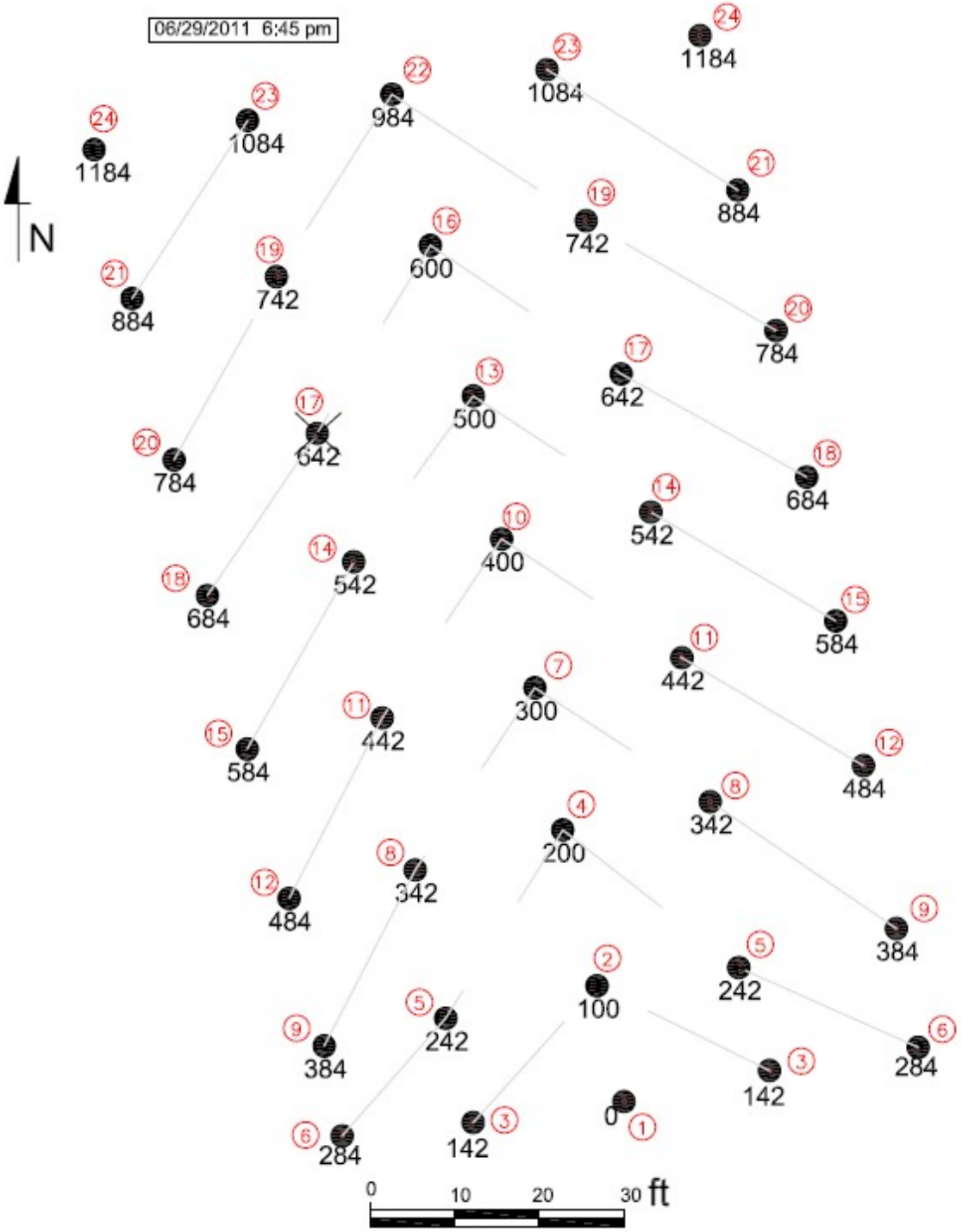
06/29/2011 6:45 pm
N
24 1184
23 1084
22 984
23 1084
24 1184
21 884
19 742
16 600
21 884
19 742
20 784
17 642
13 500
17 642
20 784
18 684
14 542
10 400
14 542
18 684
15 584
11 442
7 300
11 442
15 584
12 484
8 342
4 200
8 342
12 484
9 384
5 242
2 100
5 242
9 384
6 284
3 142
0 1
6 284
3 142
0 10 20 30 ft

APPENDIX C
Vibration records for events recorded in 2011

File: 4906201106231527002.dtb
Number: 002
Date: 6/23/2011
Time: 15:27
SN: 4906
Seis. Trigger: 0.010 in/sec
Air Trigger: 148
Sample Rate: 1024
Duration: 12.0 Seconds
Pre-Trigger: 0.50 Seconds
Gain: 2.0x
Voltage: 7.0

Peaks and Frequencies	Graph Information
PPV Maximum: 0.680 in/sec (9.2559 sec)	Duration: -0.500 s To: 12.000 s
Acoustic: 123 dBL 0.28 Mb 0.0041 psi 28 Pa @ 14.6 Hz (9.6494 sec)	Acoustic Scale: 40 Pa (10.0 Pa/Div)
Radial: 0.660 in/sec @ 10.2Hz (9.2314 sec)	Seismic Scale: 0.80 in/sec (0.200 in/sec/div)
Vertical: 0.680 in/sec @ 15.0Hz (9.2559 sec)	Time Intervals: 1.00 sec
Transverse: 0.640 in/sec @ 7.8Hz (9.4531 sec)	
Last Calibration Date: 12/13/2010	

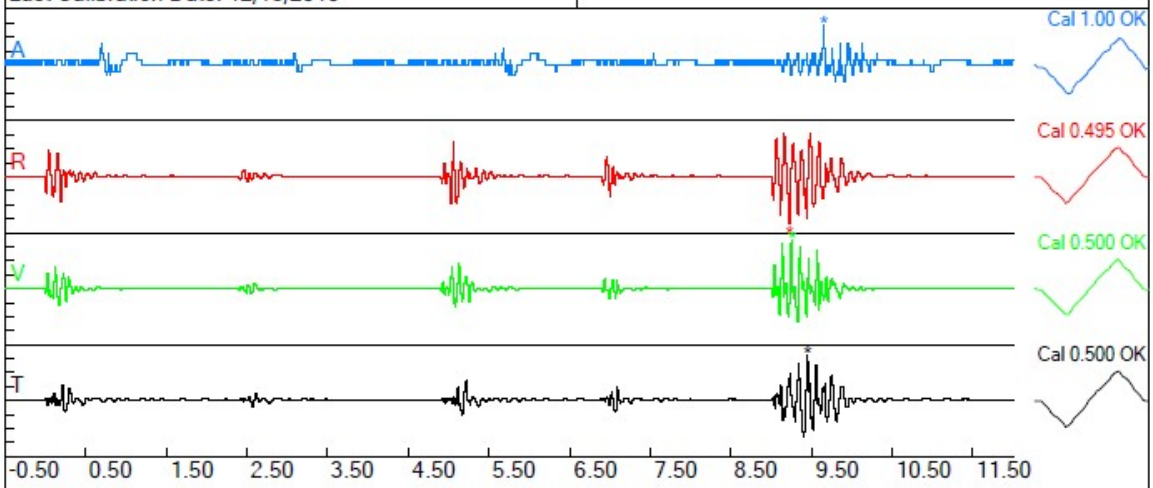

Fast Fourier Transform - Amplitude Spectrum

FFT Peak Frequencies	FFT Graph Information
Acoustic: 1.56 Hz (Amp = 53.17)	Range: 1 to 500 Hz
Radial: 10.19 Hz (Amp = 205.73)	Acoustic Scale: 53.17
Vertical: 9.19 Hz (Amp = 115.62)	Seismic Scale: 205.73
Transverse: 9.94 Hz (Amp = 131.35)	

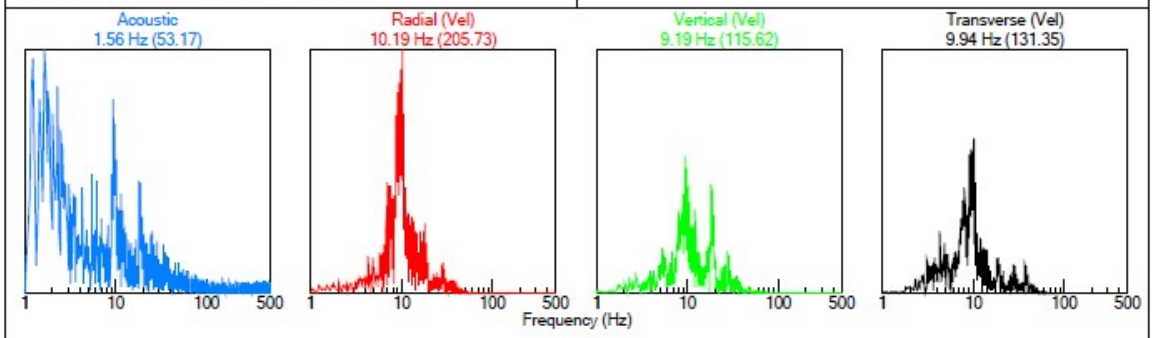

File: 3599201106231527003.dtb
Number: 003
Date: 6/23/2011
Time: 15:27
SN: 3599
Seis. Trigger: 0.010 in/sec
Air Trigger: 142
Sample Rate: 1024
Duration: 12.0 Seconds
Pre-Trigger: 0.50 Seconds
Gain: 2.0x
Voltage: 6.8

Peaks and Frequencies	Graph Information
PPV Maximum: 0.185 in/sec (9.3496 sec)	Duration: -0.500 s To: 12.000 s
Acoustic: 112 dBL 0.08 Mb 0.0012 psi 8 Pa @ 12.8 Hz (0.1788 sec)	Acoustic Scale: 40 Pa (10.0 Pa/Div)
Radial: 0.135 in/sec @ 8.8Hz (9.9307 sec)	Seismic Scale: 0.20 in/sec (0.050 in/sec/div)
Vertical: 0.135 in/sec @ 13.5Hz (9.3877 sec)	Time Intervals: 1.00 sec
Transverse: 0.185 in/sec @ 10.0Hz (9.3496 sec)	
Last Calibration Date: 6/10/2011	

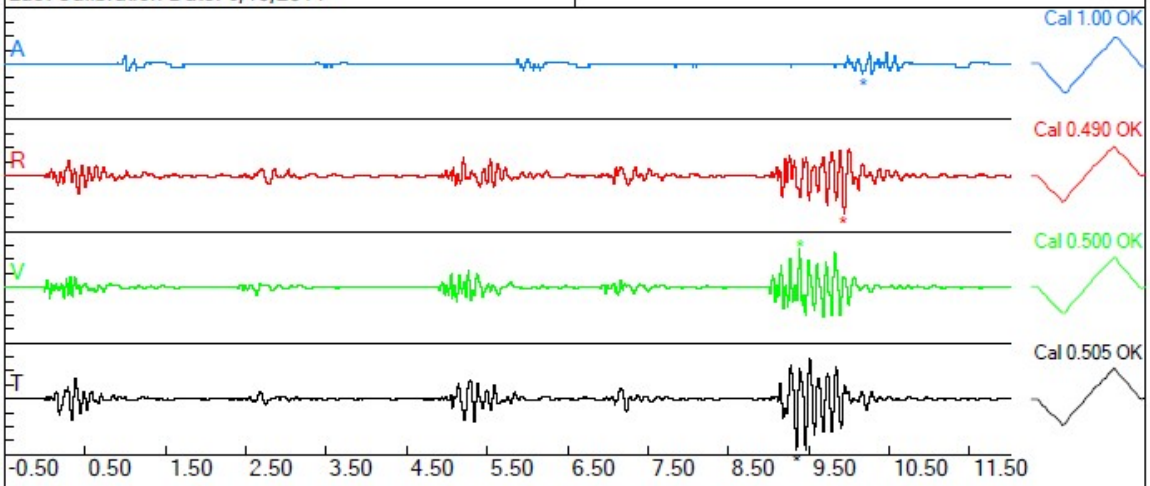

Fast Fourier Transform - Amplitude Spectrum

FFT Peak Frequencies	FFT Graph Information
Acoustic: 8.75 Hz (Amp = 20.15)	Range: 1 to 500 Hz
Radial: 9.63 Hz (Amp = 31.18)	Acoustic Scale: 20.15
Vertical: 9.00 Hz (Amp = 35.89)	Seismic Scale: 63.98
Transverse: 9.00 Hz (Amp = 63.98)	

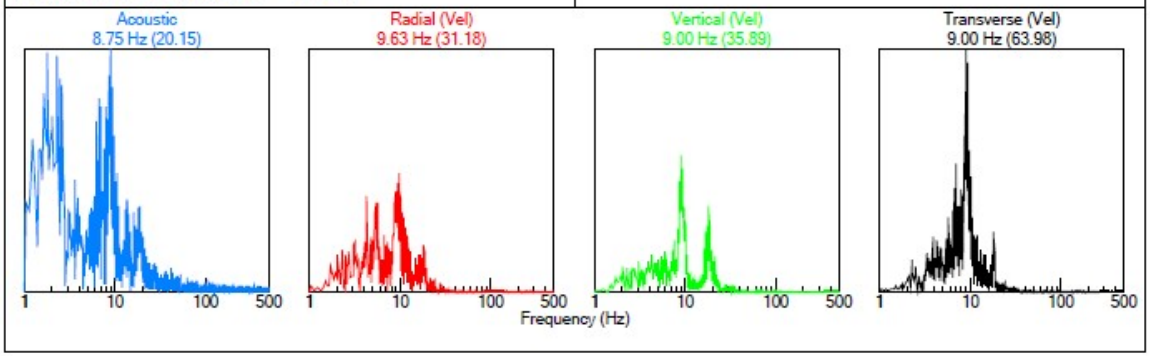

File: 3599201106241519002.dtb
Number: 002
Date: 6/24/2011
Time: 15:19
SN: 3599
Seis. Trigger: 0.010 in/sec
Air Trigger: 142
Sample Rate: 1024
Duration: 12.0 Seconds
Pre-Trigger: 0.50 Seconds
Gain: 2.0x
Voltage: 6.9

Peaks and Frequencies	Graph Information
PPV Maximum: 0.260 in/sec (9.4590 sec)	Duration: -0.500 s To: 12.000 s
Acoustic: 117 dBL 0.14 Mb 0.0020 psi 14 Pa @ 5.1 Hz (9.1787 sec)	Acoustic Scale: 40 Pa (10.0 Pa/Div)
Radial: 0.205 in/sec @ 5.2Hz (9.5518 sec)	Seismic Scale: 0.40 in/sec (0.100 in/sec/div)
Vertical: 0.115 in/sec @ 7.0Hz (9.5479 sec)	Time Intervals: 1.00 sec
Transverse: 0.260 in/sec @ 7.1Hz (9.4590 sec)	
Last Calibration Date: 6/10/2011	

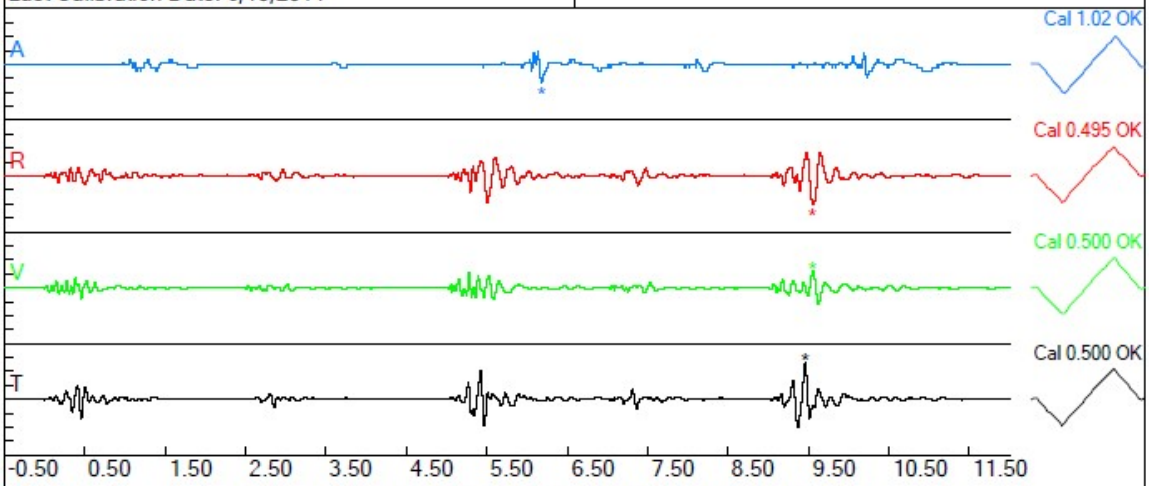

Fast Fourier Transform - Amplitude Spectrum

FFT Peak Frequencies	FFT Graph Information
Acoustic: 1.44 Hz (Amp = 35.13)	Range: 1 to 500 Hz
Radial: 5.19 Hz (Amp = 79.74)	Acoustic Scale: 35.13
Vertical: 8.38 Hz (Amp = 36.74)	Seismic Scale: 79.74
Transverse: 6.44 Hz (Amp = 68.53)	

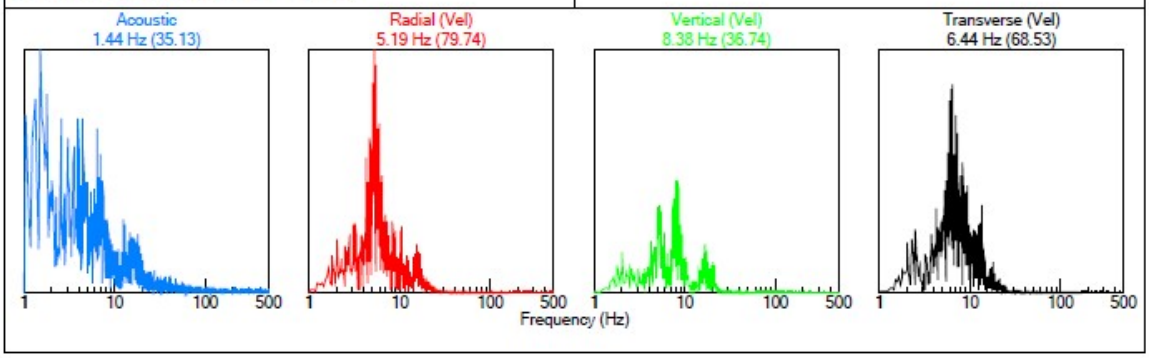

File: 4906201106241520002.dtb
Number: 002
Date: 6/24/2011
Time: 15:20
SN: 4906
Seis. Trigger: 0.020 in/sec
Air Trigger: 148
Sample Rate: 1024
Duration: 12.0 Seconds
Pre-Trigger: 0.50 Seconds
Gain: 2.0x
Voltage: 7.0

Peaks and Frequencies	Graph Information
PPV Maximum: 1.020 in/sec (5.2295 sec)	Duration: -0.500 s To: 12.000 s
Acoustic: 127 dBL 0.44 Mb 0.0064 psi 44 Pa @ 8.2 Hz (4.6999 sec)	Acoustic Scale: 80 Pa (20.0 Pa/Div)
Radial: 0.860 in/sec @ 9.5Hz (5.1689 sec)	Seismic Scale: 1.20 in/sec (0.300 in/sec/div)
Vertical: 1.020 in/sec @ 10.0Hz (5.2295 sec)	Time Intervals: 1.00 sec
Transverse: 0.720 in/sec @ 7.0Hz (9.3125 sec)	
Last Calibration Date: 12/13/2010	

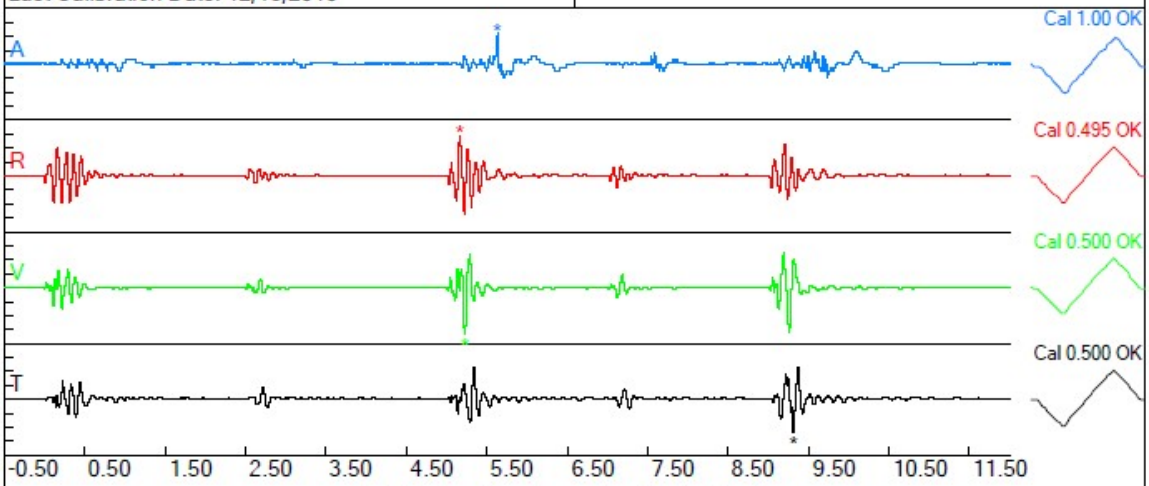

Fast Fourier Transform - Amplitude Spectrum

FFT Peak Frequencies	FFT Graph Information
Acoustic: 1.25 Hz (Amp = 106.89)	Range: 1 to 500 Hz
Radial: 10.19 Hz (Amp = 265.30)	Acoustic Scale: 106.89
Vertical: 8.44 Hz (Amp = 194.84)	Seismic Scale: 265.30
Transverse: 7.94 Hz (Amp = 231.03)	

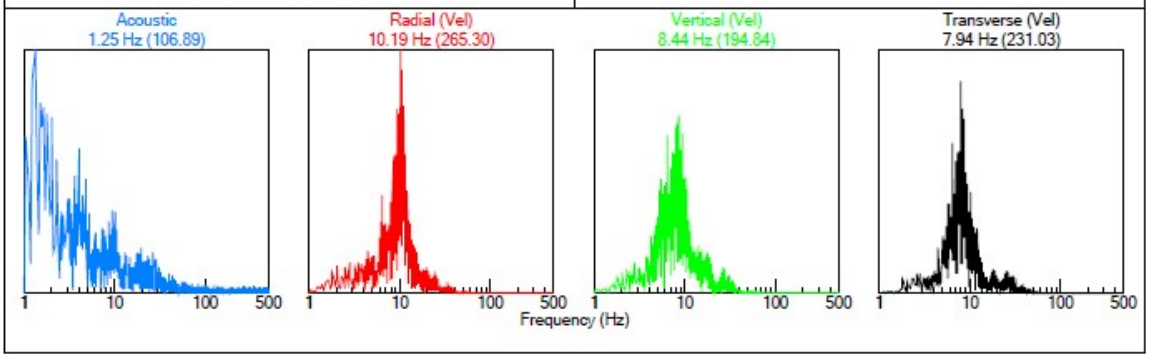

File: 4762201106241520002.dtb
Number: 002
Date: 6/24/2011
Time: 15:20
SN: 4762
Seis. Trigger: 0.100 in/sec
Air Trigger: 148
Sample Rate: 1024
Duration: 12.0 Seconds
Pre-Trigger: 0.50 Seconds
Gain: 2.0x
Voltage: 7.0

Peaks and Frequencies	Graph Information
PPV Maximum: 0.305 in/sec (9.3643 sec)	Duration: -0.500 s To: 12.000 s
Acoustic: 112 dBL 0.08 Mb 0.0012 psi 8 Pa @ 0.0 Hz (6.2447 sec)	Acoustic Scale: 40 Pa (10.0 Pa/Div)
Radial: 0.305 in/sec @ 6.4Hz (9.3643 sec)	Seismic Scale: 0.40 in/sec (0.100 in/sec/div)
Vertical: 0.155 in/sec @ 6.4Hz (5.4629 sec)	Time Intervals: 1.00 sec
Transverse: 0.170 in/sec @ 8.1Hz (5.4531 sec)	
Last Calibration Date: 6/8/2010	

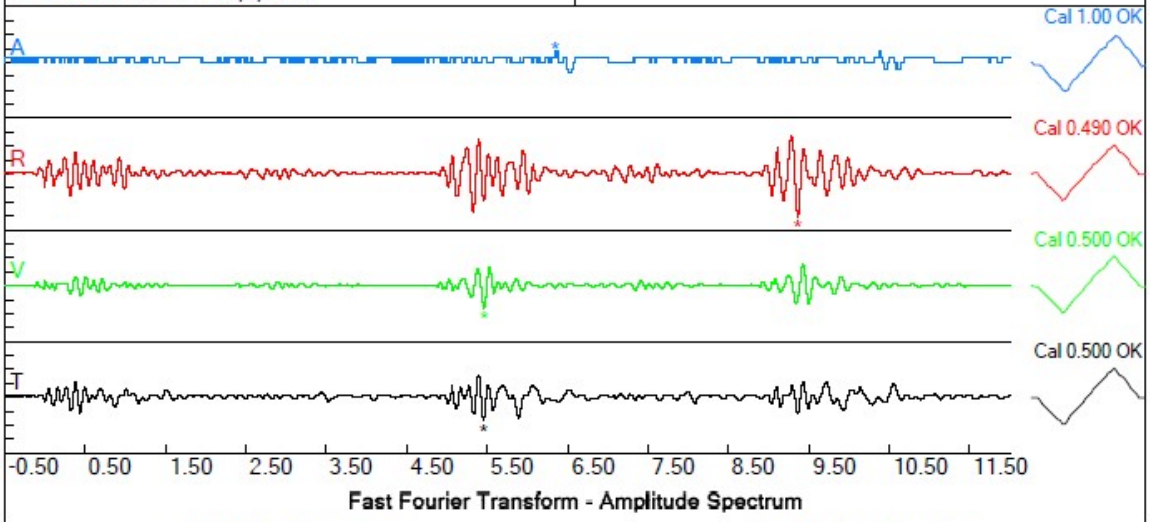

Fast Fourier Transform - Amplitude Spectrum

FFT Peak Frequencies	FFT Graph Information
Acoustic: 1.50 Hz (Amp = 39.68)	Range: 1 to 500 Hz
Radial: 5.94 Hz (Amp = 150.07)	Acoustic Scale: 39.68
Vertical: 5.94 Hz (Amp = 65.07)	Seismic Scale: 150.07
Transverse: 2.19 Hz (Amp = 76.36)	

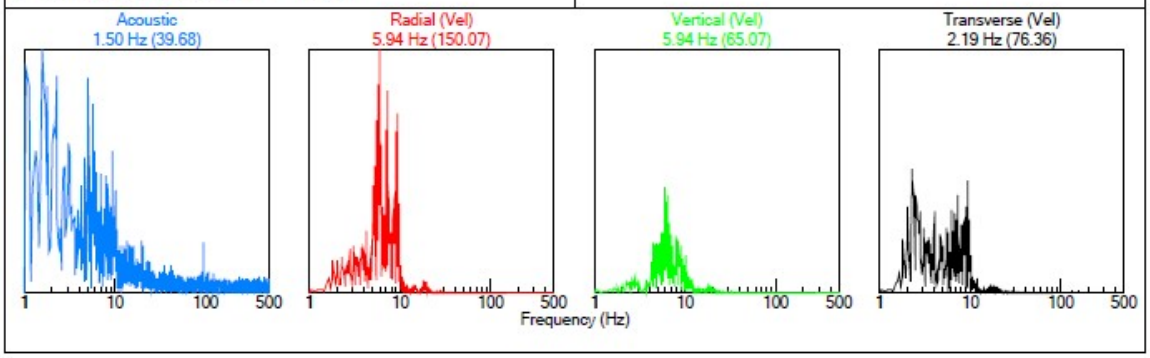

File: 3599201106291115006.dtb
Number: 006
Date: 6/29/2011
Time: 11:15
SN: 3599
Seis. Trigger: 0.010 in/sec
Air Trigger: 142
Sample Rate: 1024
Duration: 12.0 Seconds
Pre-Trigger: 0.50 Seconds
Gain: 2.0x
Voltage: 6.9

Peaks and Frequencies	Graph Information
PPV Maximum: 0.160 in/sec (6.4600 sec)	Duration: -0.500 s To: 12.000 s
Acoustic: 100 dBL 0.02 Mb 0.0003 psi 2 Pa @ 0.0 Hz (1.4764 sec)	Acoustic Scale: 40 Pa (10.0 Pa/Div)
Radial: 0.130 in/sec @ 10.2Hz (0.6016 sec)	Seismic Scale: 0.20 in/sec (0.050 in/sec/div)
Vertical: 0.050 in/sec @ 9.3Hz (6.5205 sec)	Time Intervals: 1.00 sec
Transverse: 0.160 in/sec @ 8.5Hz (6.4600 sec)	
Last Calibration Date: 6/10/2011	

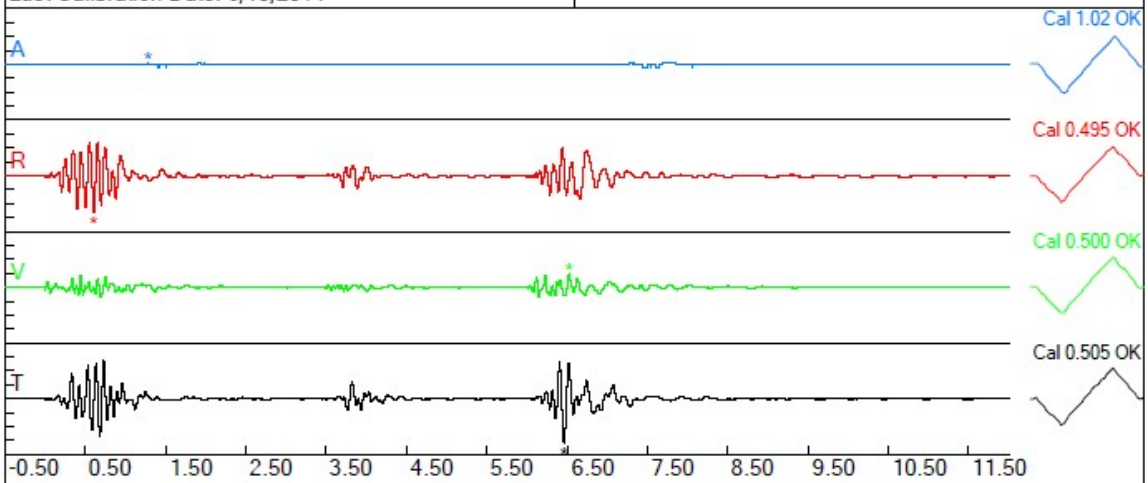

Fast Fourier Transform - Amplitude Spectrum

FFT Peak Frequencies	FFT Graph Information
Acoustic: 1.69 Hz (Amp = 6.01)	Range: 1 to 500 Hz
Radial: 10.38 Hz (Amp = 44.73)	Acoustic Scale: 6.01
Vertical: 10.00 Hz (Amp = 12.59)	Seismic Scale: 44.73
Transverse: 10.69 Hz (Amp = 39.05)	

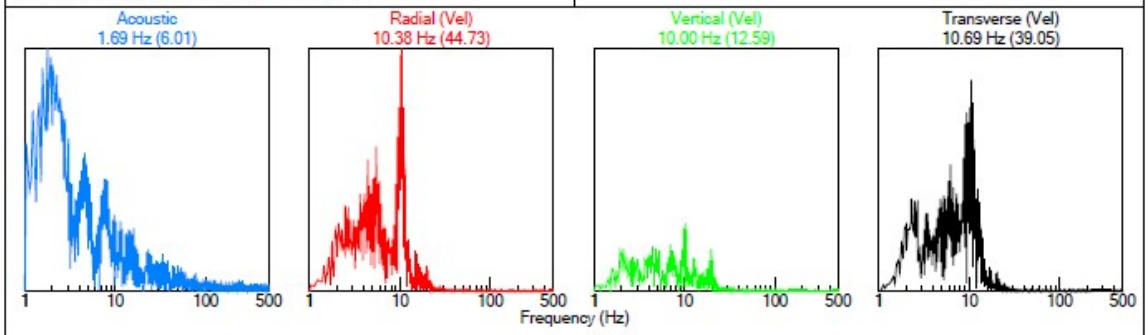

File: 4906201106291116005.dtb
Number: 005
Date: 6/29/2011
Time: 11:16
SN: 4906
Seis. Trigger: 0.050 in/sec
Air Trigger: 148
Sample Rate: 1024
Duration: 12.0 Seconds
Pre-Trigger: 0.50 Seconds
Gain: 2.0x
Voltage: 7.0

Peaks and Frequencies	Graph Information
PPV Maximum: 0.680 in/sec (6.1709 sec)	Duration: -0.500 s To: 12.000 s
Acoustic: 120 dBL 0.20 Mb 0.0029 psi 20 Pa @ 11.6 Hz (0.6572 sec)	Acoustic Scale: 40 Pa (10.0 Pa/Div)
Radial: 0.680 in/sec @ 8.6Hz (6.1709 sec)	Seismic Scale: 0.80 in/sec (0.200 in/sec/div)
Vertical: 0.350 in/sec @ 8.9Hz (6.2520 sec)	Time Intervals: 1.00 sec
Transverse: 0.380 in/sec @ 8.0Hz (6.1748 sec)	
Last Calibration Date: 12/13/2010	

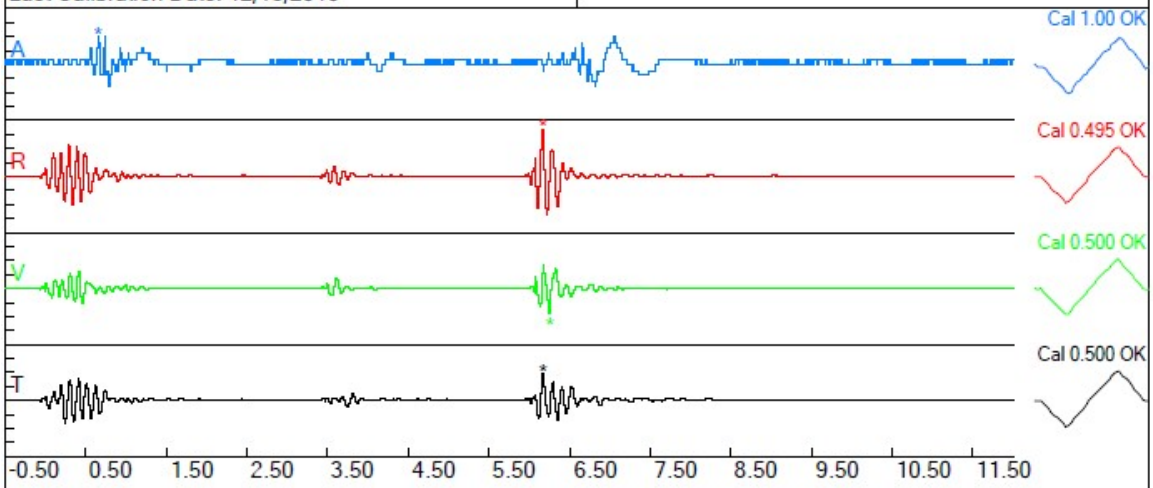

Fast Fourier Transform - Amplitude Spectrum

FFT Peak Frequencies	FFT Graph Information
Acoustic: 1.19 Hz (Amp = 94.57)	Range: 1 to 500 Hz
Radial: 9.69 Hz (Amp = 151.09)	Acoustic Scale: 94.57
Vertical: 7.44 Hz (Amp = 71.95)	Seismic Scale: 151.09
Transverse: 9.69 Hz (Amp = 132.47)	

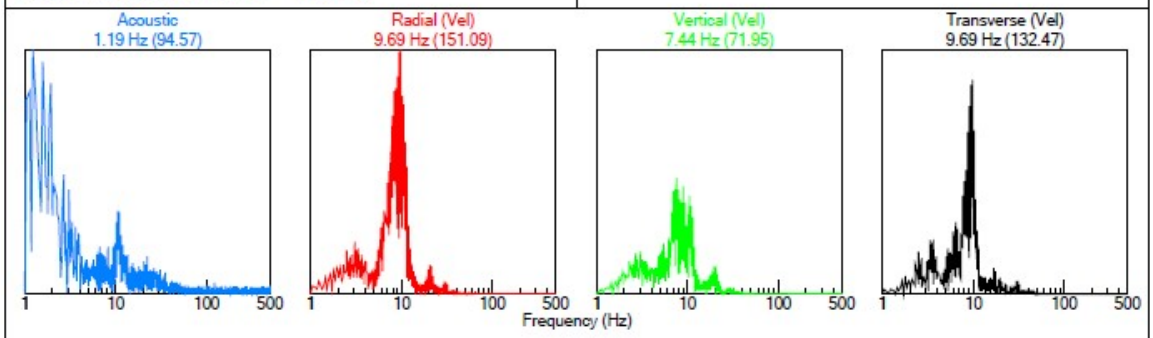

File: 4762201106291116005.dtb
Number: 005
Date: 6/29/2011
Time: 11:16
SN: 4762
Seis. Trigger: 0.100 in/sec
Air Trigger: 148
Sample Rate: 1024
Duration: 12.0 Seconds
Pre-Trigger: 0.50 Seconds
Gain: 2.0x
Voltage: 6.9

Peaks and Frequencies	Graph Information
PPV Maximum: 0.320 in/sec (6.6162 sec)	Duration: -0.500 s To: 12.000 s
Acoustic: 112 dBL 0.08 Mb 0.0012 psi 8 Pa @ 0.0 Hz (1.0324 sec)	Acoustic Scale: 40 Pa (10.0 Pa/Div)
Radial: 0.320 in/sec @ 7.3Hz (6.6162 sec)	Seismic Scale: 0.40 in/sec (0.100 in/sec/div)
Vertical: 0.200 in/sec @ 7.3Hz (6.5576 sec)	Time Intervals: 1.00 sec
Transverse: 0.220 in/sec @ 7.4Hz (6.5479 sec)	
Last Calibration Date: 6/8/2010	

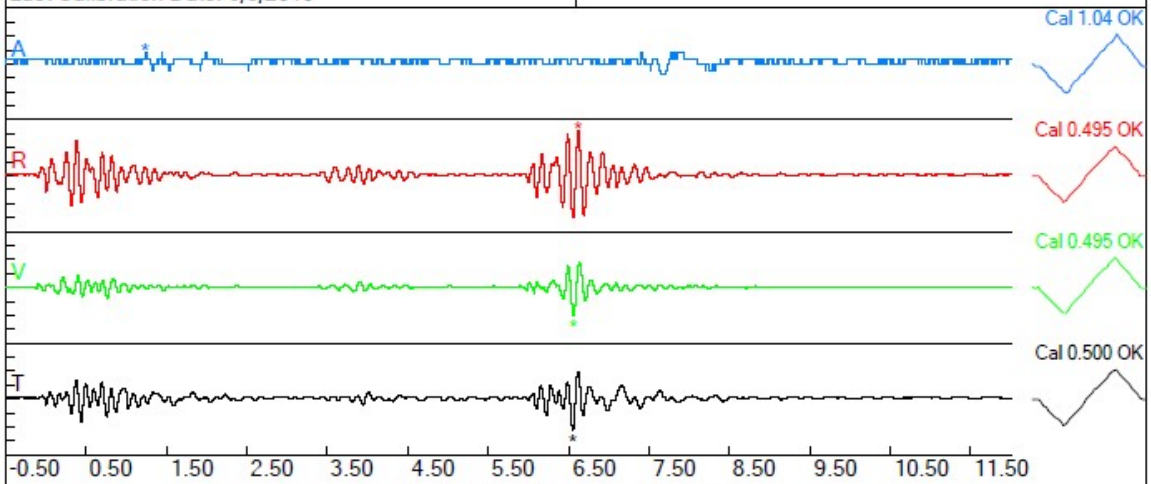

Fast Fourier Transform - Amplitude Spectrum

FFT Peak Frequencies	FFT Graph Information
Acoustic: 1.00 Hz (Amp = 60.59)	Range: 1 to 500 Hz
Radial: 6.88 Hz (Amp = 143.96)	Acoustic Scale: 60.59
Vertical: 6.56 Hz (Amp = 55.29)	Seismic Scale: 143.96
Transverse: 6.88 Hz (Amp = 94.94)	

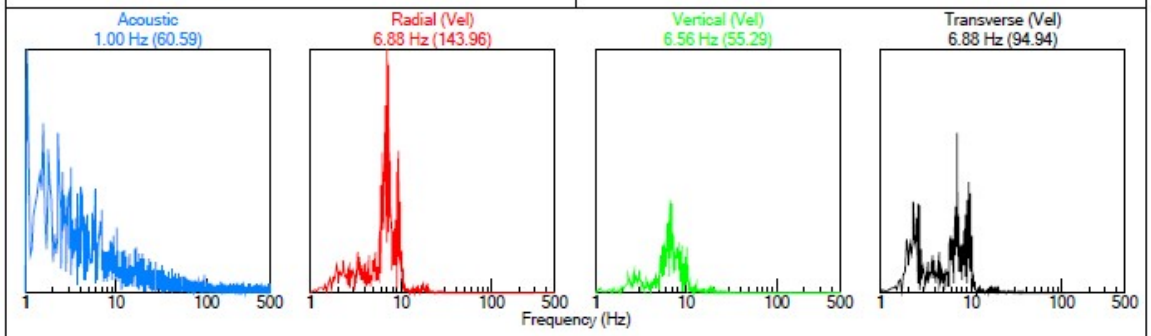

File: 4906201106291533001.dtb
Number: 001
Date: 6/29/2011
Time: 15:33
SN: 4906
Seis. Trigger: 0.050 in/sec
Air Trigger: 148
Sample Rate: 1024
Duration: 12.0 Seconds
Pre-Trigger: 0.50 Seconds
Gain: 2.0x
Voltage: 7.0

Peaks and Frequencies	Graph Information
PPV Maximum: 0.450 in/sec (0.4424 sec)	Duration: -0.500 s To: 12.000 s
Acoustic: 122 dBL 0.24 Mb 0.0035 psi 24 Pa @ 10.8 Hz (0.4134 sec)	Acoustic Scale: 40 Pa (10.0 Pa/Div)
Radial: 0.365 in/sec @ 10.0Hz (0.5010 sec)	Seismic Scale: 0.60 in/sec (0.150 in/sec/div)
Vertical: 0.235 in/sec @ 10.8Hz (0.4639 sec)	Time Intervals: 1.00 sec
Transverse: 0.450 in/sec @ 7.6Hz (0.4424 sec)	
Last Calibration Date: 12/13/2010	

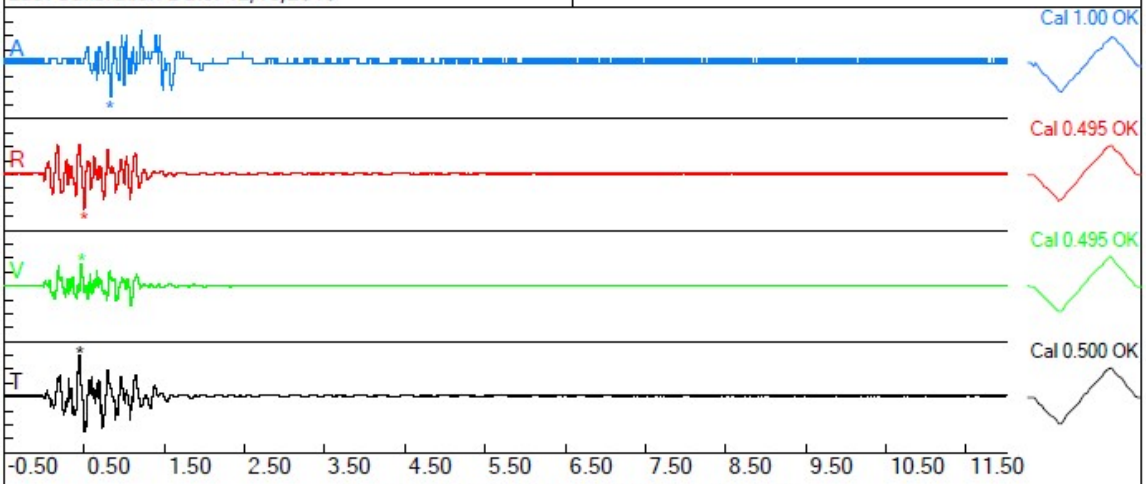

Fast Fourier Transform - Amplitude Spectrum

FFT Peak Frequencies	FFT Graph Information
Acoustic: 11.94 Hz (Amp = 41.74)	Range: 1 to 500 Hz
Radial: 8.19 Hz (Amp = 62.15)	Acoustic Scale: 41.74
Vertical: 6.25 Hz (Amp = 36.80)	Seismic Scale: 79.10
Transverse: 8.38 Hz (Amp = 79.10)	

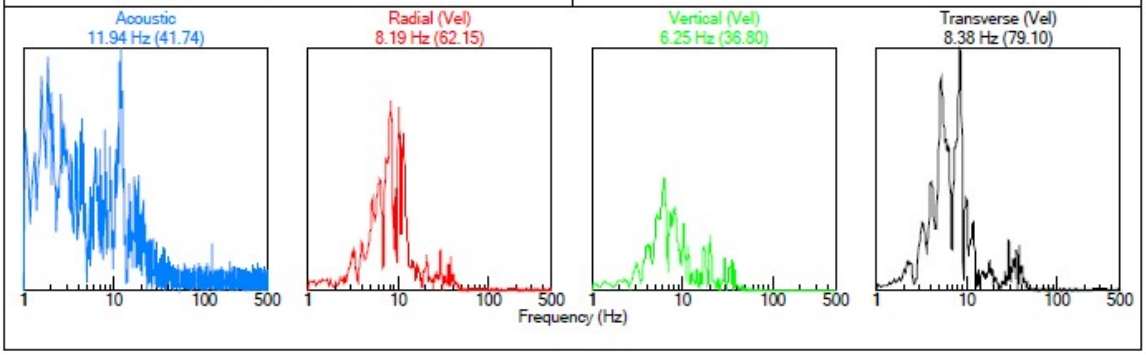

File: 4762201106291533001.dtb
Number: 001
Date: 6/29/2011
Time: 15:33
SN: 4762
Seis. Trigger: 0.100 in/sec
Air Trigger: 148
Sample Rate: 1024
Duration: 12.0 Seconds
Pre-Trigger: 0.50 Seconds
Gain: 2.0x
Voltage: 6.9

Peaks and Frequencies	Graph Information
PPV Maximum: 0.175 in/sec (0.0146 sec)	Duration: -0.500 s To: 12.000 s
Acoustic: 112 dBL 0.08 Mb 0.0012 psi 8 Pa @ 0.0 Hz (0.0000 sec)	Acoustic Scale: 40 Pa (10.0 Pa/Div)
Radial: 0.175 in/sec @ 7.5Hz (0.0146 sec)	Seismic Scale: 0.20 in/sec (0.050 in/sec/div)
Vertical: 0.095 in/sec @ 8.0Hz (0.0371 sec)	Time Intervals: 1.00 sec
Transverse: 0.105 in/sec @ 5.2Hz (1.1279 sec)	
Last Calibration Date: 6/8/2010	

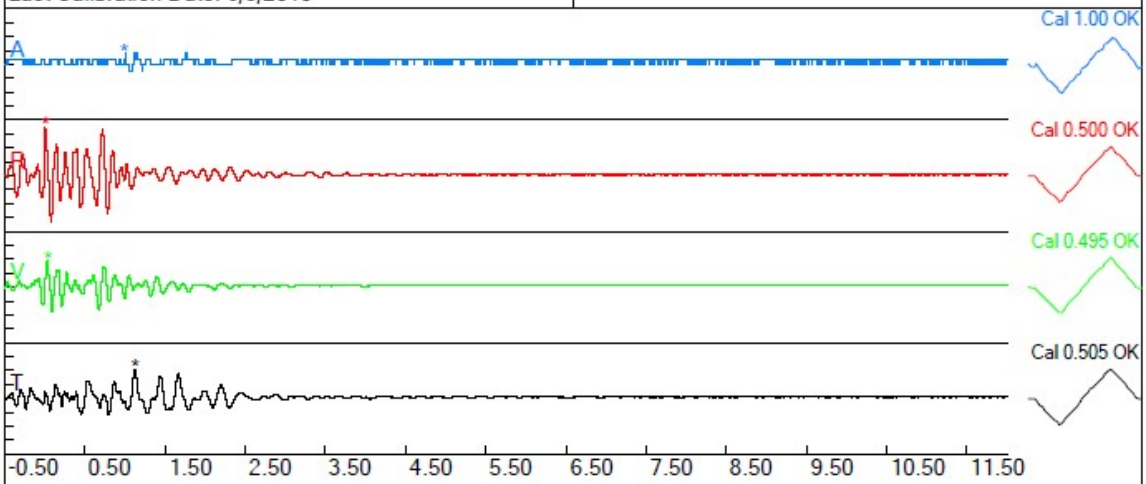

Fast Fourier Transform - Amplitude Spectrum

FFT Peak Frequencies	FFT Graph Information
Acoustic: 3.19 Hz (Amp = 25.78)	Range: 1 to 500 Hz
Radial: 7.13 Hz (Amp = 44.97)	Acoustic Scale: 25.78
Vertical: 8.81 Hz (Amp = 21.76)	Seismic Scale: 44.97
Transverse: 3.69 Hz (Amp = 39.51)	

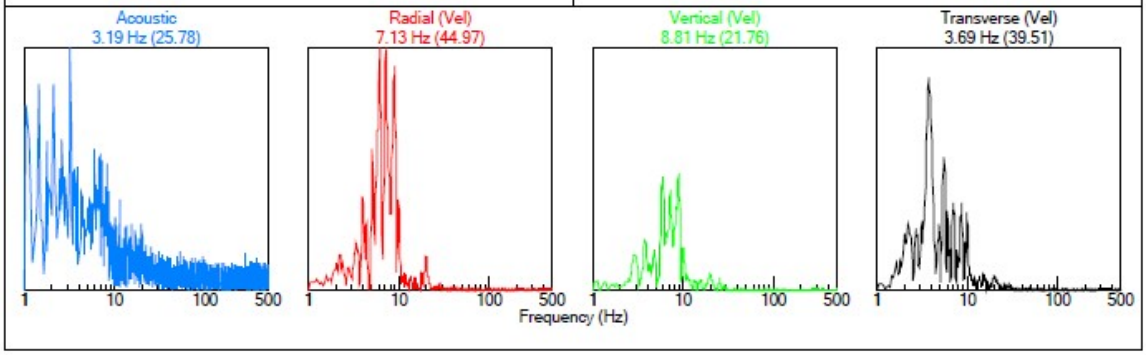

File: 3599201106291533007.dtb
Number: 007
Date: 6/29/2011
Time: 15:33
SN: 3599
Seis. Trigger: 0.010 in/sec
Air Trigger: 142
Sample Rate: 1024
Duration: 12.0 Seconds
Pre-Trigger: 0.50 Seconds
Gain: 2.0x
Voltage: 6.9

Peaks and Frequencies	Graph Information
PPV Maximum: 0.120 in/sec (1.0547 sec)	Duration: -0.500 s To: 12.000 s
Acoustic: 106 dBL 0.04 Mb 0.0006 psi 4 Pa @ 0.0 Hz (1.50M sec)	Acoustic Scale: 40 Pa (10.0 Pa/Div)
Radial: 0.115 in/sec @ 8.8Hz (0.7266 sec)	Seismic Scale: 0.20 in/sec (0.050 in/sec/div)
Vertical: 0.095 in/sec @ 7.1Hz (0.5049 sec)	Time Intervals: 1.00 sec
Transverse: 0.120 in/sec @ 8.8Hz (1.0547 sec)	
Last Calibration Date: 6/10/2011	

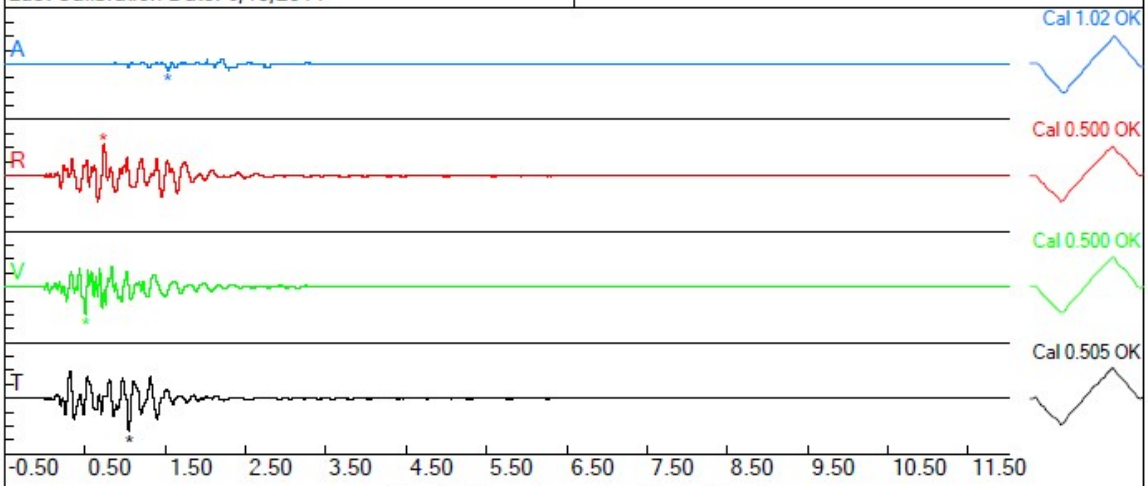

Fast Fourier Transform - Amplitude Spectrum

FFT Peak Frequencies	FFT Graph Information
Acoustic: 3.81 Hz (Amp = 7.24)	Range: 1 to 500 Hz
Radial: 4.88 Hz (Amp = 22.33)	Acoustic Scale: 7.24
Vertical: 5.06 Hz (Amp = 20.34)	Seismic Scale: 25.88
Transverse: 5.06 Hz (Amp = 25.88)	

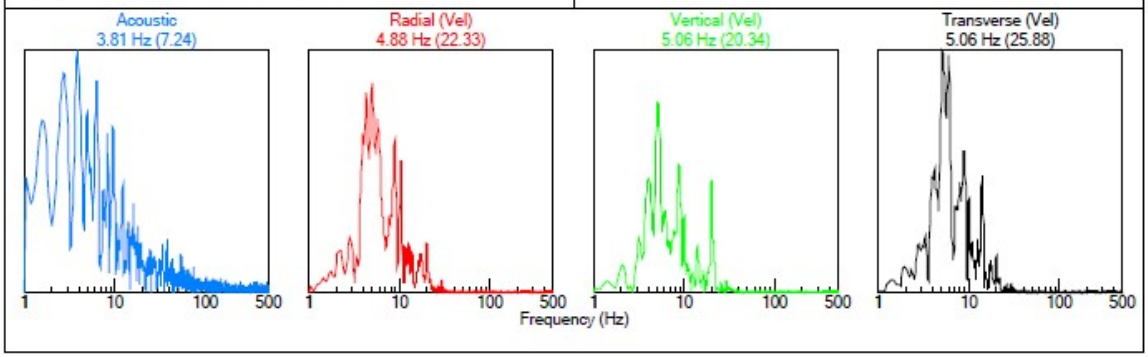

File: 4906201106291844002.dtb
Number: 002
Date: 6/29/2011
Time: 18:44
SN: 4906
Seis. Trigger: 0.050 in/sec
Air Trigger: 148
Sample Rate: 1024
Duration: 12.0 Seconds
Pre-Trigger: 0.50 Seconds
Gain: 2.0x
Voltage: 7.0

Peaks and Frequencies	Graph Information
PPV Maximum: 0.820 in/sec (1.2021 sec)	Duration: -0.500 s To: 12.000 s
Acoustic: 123 dBL 0.28 Mb 0.0041 psi 28 Pa @ 18.2 Hz (0.6608 sec)	Acoustic Scale: 40 Pa (10.0 Pa/Div)
Radial: 0.820 in/sec @ 8.6Hz (1.2021 sec)	Seismic Scale: 1.00 in/sec (0.250 in/sec/div)
Vertical: 0.600 in/sec @ 9.3Hz (1.1641 sec)	Time Intervals: 1.00 sec
Transverse: 0.600 in/sec @ 7.3Hz (1.2061 sec)	
Last Calibration Date: 12/13/2010	

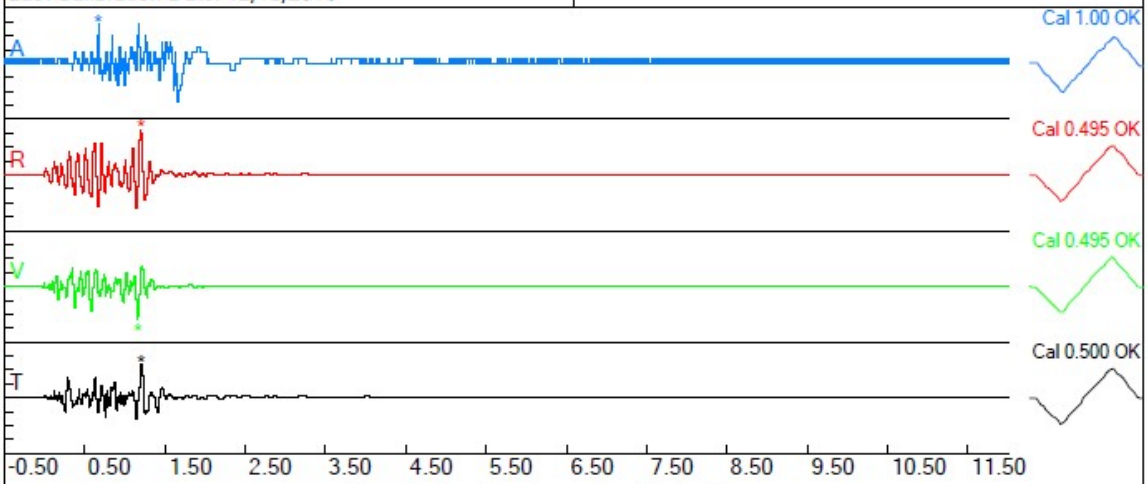

Fast Fourier Transform - Amplitude Spectrum

FFT Peak Frequencies	FFT Graph Information
Acoustic: 1.50 Hz (Amp = 70.31)	Range: 1 to 500 Hz
Radial: 10.25 Hz (Amp = 194.18)	Acoustic Scale: 70.31
Vertical: 10.13 Hz (Amp = 104.47)	Seismic Scale: 194.18
Transverse: 7.75 Hz (Amp = 84.80)	

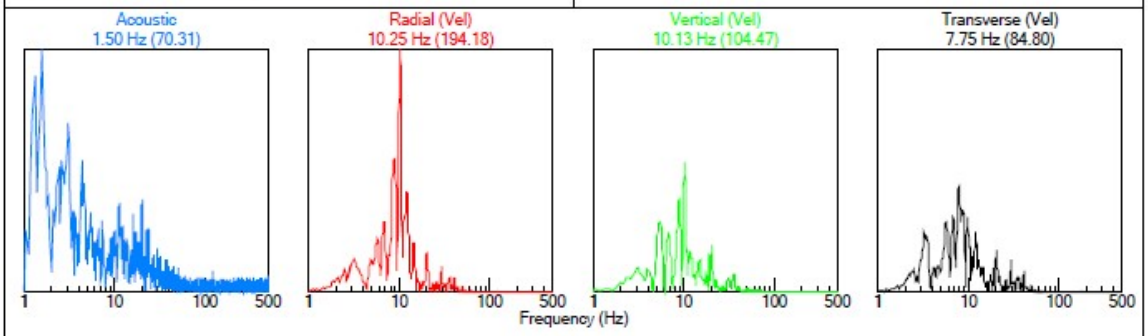

File: 3599201106291844009.dtb
Number: 009
Date: 6/29/2011
Time: 18:44
SN: 3599
Seis. Trigger: 0.010 in/sec
Air Trigger: 142
Sample Rate: 1024
Duration: 12.0 Seconds
Pre-Trigger: 0.50 Seconds
Gain: 2.0x
Voltage: 6.9

Peaks and Frequencies	Graph Information
PPV Maximum: 0.125 in/sec (1.3877 sec)	Duration: -0.500 s To: 12.000 s
Acoustic: 110 dBL 0.06 Mb 0.0009 psi 6 Pa @ 11.6 Hz (1.0009 sec)	Acoustic Scale: 40 Pa (10.0 Pa/Div)
Radial: 0.120 in/sec @ 9.1Hz (1.0107 sec)	Seismic Scale: 0.20 in/sec (0.050 in/sec/div)
Vertical: 0.095 in/sec @ 6.9Hz (1.0107 sec)	Time Intervals: 1.00 sec
Transverse: 0.125 in/sec @ 8.6Hz (1.3877 sec)	
Last Calibration Date: 6/10/2011	

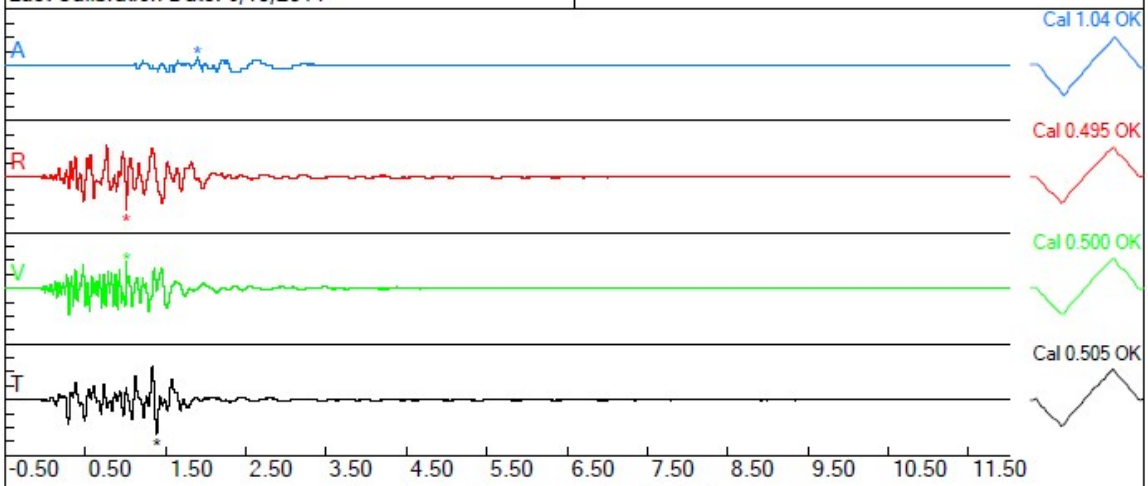

Fast Fourier Transform - Amplitude Spectrum

FFT Peak Frequencies	FFT Graph Information
Acoustic: 2.06 Hz (Amp = 18.57)	Range: 1 to 500 Hz
Radial: 5.06 Hz (Amp = 27.15)	Acoustic Scale: 18.57
Vertical: 20.31 Hz (Amp = 23.53)	Seismic Scale: 27.15
Transverse: 5.25 Hz (Amp = 18.34)	

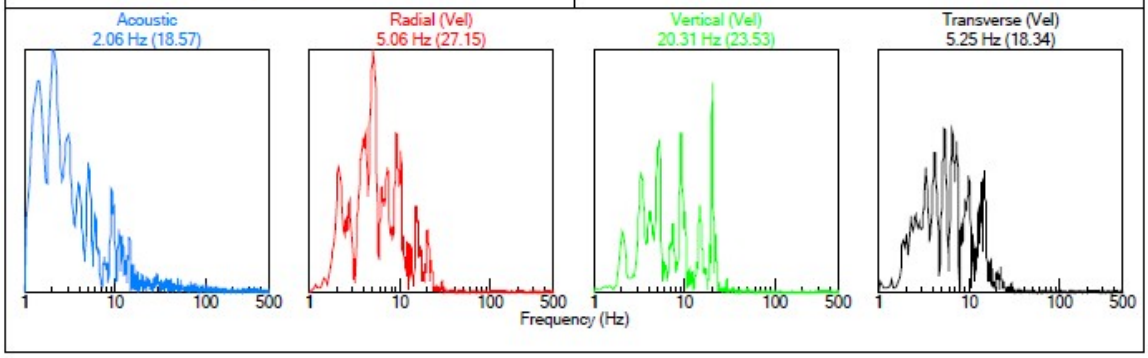

File: 4762201106291845003.dtb
Number: 003
Date: 6/29/2011
Time: 18:45
SN: 4762
Seis. Trigger: 0.100 in/sec
Air Trigger: 148
Sample Rate: 1024
Duration: 12.0 Seconds
Pre-Trigger: 0.50 Seconds
Gain: 2.0x
Voltage: 6.9

Peaks and Frequencies	Graph Information
PPV Maximum: 0.175 in/sec (0.8779 sec)	Duration: -0.500 s To: 12.000 s
Acoustic: 112 dBL 0.08 Mb 0.0012 psi 8 Pa @ 0.0 Hz (1.0734 sec)	Acoustic Scale: 40 Pa (10.0 Pa/Div)
Radial: 0.175 in/sec @ 6.7Hz (0.8779 sec)	Seismic Scale: 0.20 in/sec (0.050 in/sec/div)
Vertical: 0.095 in/sec @ 8.1Hz (1.2246 sec)	Time Intervals: 1.00 sec
Transverse: 0.120 in/sec @ 3.1Hz (1.4590 sec)	
Last Calibration Date: 6/8/2010	

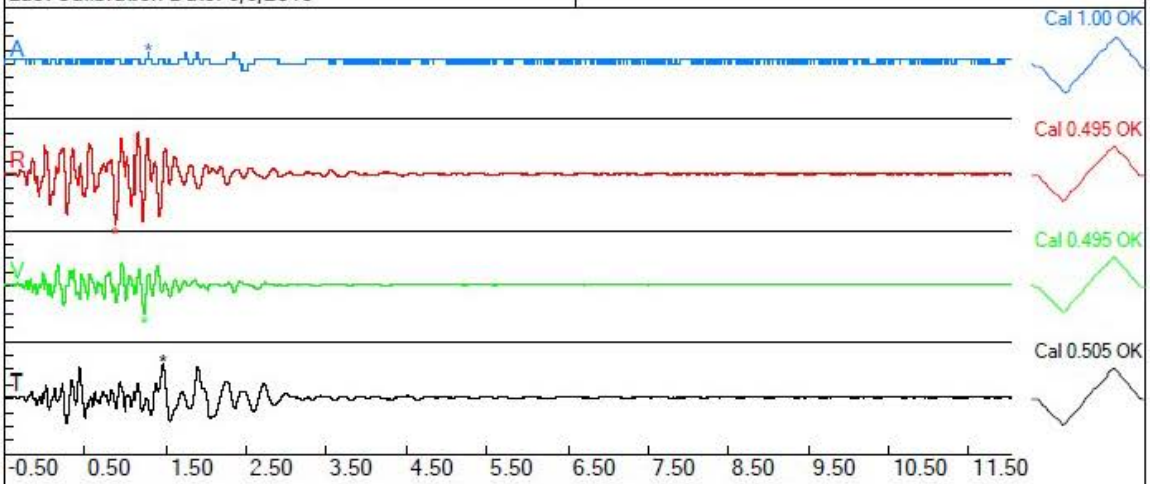

Fast Fourier Transform - Amplitude Spectrum
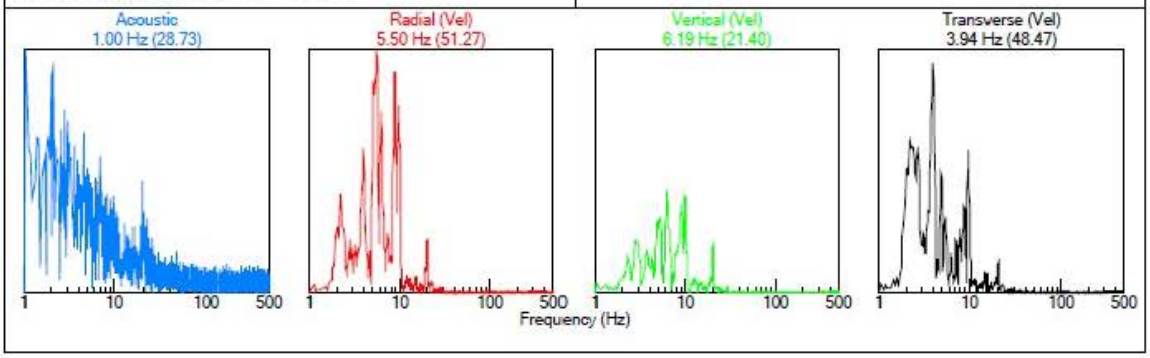
FFT Peak Frequencies	FFT Graph Information
Acoustic: 1.00 Hz (Amp = 28.73)	Range: 1 to 500 Hz
Radial: 5.50 Hz (Amp = 51.27)	Acoustic Scale: 28.73
Vertical: 6.19 Hz (Amp = 21.40)	Seismic Scale: 51.27
Transverse: 3.94 Hz (Amp = 48.47)